

eScholarship@UMassChan

Digital and Analog STAT5 Signaling in Erythropoiesis: A Dissertation

Item Type	Doctoral Dissertation
Authors	Porpiglia, Ermelinda
DOI	10.13028/xnva-0d81
Publisher	University of Massachusetts Medical School
Rights	Copyright is held by the author, with all rights reserved.
Download date	2026-03-07 18:07:27
Link to Item	https://hdl.handle.net/20.500.14038/31894

DIGITAL AND ANALOG STAT5 SIGNALING
IN ERYTHROPOIESIS

A Dissertation Presented

By

Ermelinda Porpiglia

Submitted to the Faculty of the
University of Massachusetts Graduate School of Biomedical Sciences, Worcester
in partial fulfillment of the requirements for the degree of

DOCTOR OF PHILOSOPHY

AUGUST 16, 2011

PROGRAM IN IMMUNOLOGY AND VIROLOGY

DIGITAL AND ANALOG STAT5 SIGNALING
IN ERYTHROPOIESIS

A Dissertation Presented
By
Ermelinda Porpiglia

The signatures of the Dissertation Defense Committee signifies completion and approval
as to style and content of the Dissertation

Merav Socolovsky, Ph.D., MBBS, Thesis Advisor

Roger Davis, Ph.D., Member of Committee

Rachel Gerstein, Ph.D., Member of Committee

Madelyn Schmidt, Ph.D., Member of Committee

Norbert Perrimon, Ph.D., Member of Committee

The signature of the Chair of the Committee signifies that the written dissertation meets
the requirements of the Dissertation Committee

Michelle Kelliher, Ph.D, Chair of Committee

The signature of the Dean of the Graduate School of Biomedical Sciences signifies that
the student has met all graduation requirements of the school

Anthony Carruthers, Ph.D.,
Dean of the Graduate School of Biomedical Sciences

Immunology and Virology Program (IVP)
August 16, 2011

Dedication

“Do not quench your inspiration and your imagination; do not become the slave of your model.” VINCENT VAN GOGH

This thesis is dedicated to my parents who taught me to be determined and follow my dreams. They supported me, despite the distance of an ocean is between us, and they helped me bring things in perspective when I was getting lost in the labyrinths of science. I would like to extend the dedication to all those who helped me nurture my passion for science and discovery and to a few special people who are not here anymore but inspired me and supported me through this journey.

Acknowledgements

First of all, I would like to thank my advisor, Merav Socolovsky, for giving me the great opportunity to perform my graduate thesis research in her laboratory, for helping me grow scientifically and personally, for encouraging me to be the best scientist I can be and for always being there when I needed help and support.

My laboratory mates played a very important role in my graduate student journey. They are like family to me, since I have spent with them days and nights in the laboratory. Thanks Ying for “initiating” me to the Socolovsky’s laboratory. Ramona, thanks for always answering my numerous questions and teaching me not only how to do science and be a good scientist but also how to persevere and be strong when things don’t go smoothly. Thanks for being supportive and encouraging during the hard times and for being a friend. Miro, thanks for making me laugh and for “annoying” me over and over again. Without you life in the lab would have never been the same. Also, thanks for all your help with graphics: you are very talented and you would always sit and help me design the most beautiful picture for my scientific models. Thanks Jeff and Shen, for being always helpful and supportive. Thanks Daniel, for being the best trainee I have ever had. You have always been excited about learning new things and also very understanding and encouraging. It has been fun working with you and seeing you grow scientifically. I hope your passion for science will keep increasing and I wish you a bright future ahead. I would like to thank Julie for keeping my sugar levels high, offering help when I needed the most and always keeping me informed about the most exciting events on the UMass campus. Thanks Josias for bringing some more international flavor to the lab.

I would like to thank the entire Cancer Biology Department: everybody has always been very helpful, sharing knowledge and reagents and creating an excellent working environment. A special thanks goes to Minakshi and Ding Ding for sharing with me the secrets of quantitative western blotting. Thanks Tina for being a colleague and friend. I am indebted to the members of the Flow Cytometry core. In particular, I would

like to thank Rich who has been a great teacher, always accessible to discuss a new experiment or answer my numerous questions and Ted who never complained about my heavy use of the LSR II machine, constantly offered help and support, and definitely contributed to the success of many of my experiments.

I would like to thank my previous advisor, Rossella Tupler for being always encouraging and supportive and for being a role model. I would like to thank Michael Green, for welcoming me to his laboratory as an international student during my Master Thesis Research: it has been a great experience. I would also like to thank past and current members of the Green Laboratory: Claude, Daniel, Stephan, Amy, and Glenn for being of constant help through my graduate career. I would like to thank Genevieve, Chris, Martin, Jason, Jack, Kavitha, for guiding me through graduate school. You have always being a great example to me and you helped me unconditionally. I wish you the best in your career. A special thanks goes to Eric, for being always very supportive and encouraging and for his wonderful career advices.

I would like to thank the members of my thesis research committee, Michelle Kelliher, Rachel Gerstein, Steven Grossman and Madelyn Schmidt. I have always received from you great scientific inputs and wonderful career advices. I am especially grateful to Michelle and Lyn for the enormous support. In addition, I would like to thank Norbert Perrimon for accepting to act as external examiner and Roger Davis for becoming a member of the Dissertation Examination Committee. I consider myself extremely lucky for having the opportunity to meet and interact with so many cutting-edge scientists. This journey has definitely made me stronger and has enhanced my passion for science.

I would like to thank my family for being very understanding and supportive through the tough times. Without your encouragement and support I would have never reached this goal. Thanks mom and dad, Hjlenia, Emanuela and Aberto, Guy and Sandro. Thanks to my grandmother, who always wish I would stop studying and start working. Thanks Grace for coming to this world: you brought joy to my life. Thanks to the

newcomers Alessia and Giorgia, which I didn't get a chance to meet yet. I apologize to all of you for being so far away and for missing so many family events.

I would like to thank my friends for making this journey more enjoyable, for sharing some great times and for constantly helping me to keep going during the hard times. Thanks Prerna, Megha, Ahmed, Kristen, Katerina, Tora, Mo, Minakshi, Dimitra, Connie, Jenny, Rachel, Bhavana, Ling: it has been great to support each other and I wish you the best for the future. Thanks Didi, Luca, Thomas, Dilja, Peter, Luanne, June, Kai, Malek, Ghassan, Tatiana: you have made my time in graduate school more enjoyable, supported me unconditionally and made me feel home away from home. Thanks Mina for the great times together. I would also like to thank my friends who live far away and who supported me through the entire journey: Stefania and Antonio, Vince, Giovanni, Rosalba, Laura and Matteo, Silvia and Matteo, Antonietta and Giuliano, Charity and Steven.

Last but not least I would like to thank my roommates, current and past, for sharing life experiences with me, for the good times and the infinite support.

Thank you all for helping me reach this goal!

Abstract

Erythropoietin (Epo) modulates red blood cell production (erythropoiesis) by binding to its receptor and activating STAT5, a Signal Transducer and Activator of Transcription (STAT) protein implicated in both basal and stress erythropoiesis. Epo concentration in serum changes over three orders of magnitude, as it regulates basal erythropoiesis and its acceleration during hypoxic stress. However, it is not known how STAT5 translates the changes in Epo concentration into the required erythropoietic rates. We addressed this question by studying STAT5 phosphorylation, at the single cell level, in developing erythroblasts.

We divided erythroid progenitors in tissue into several flow-cytometric subsets and found that each of them exhibited distinct modes of Stat5 activation, based on their developmental stage. STAT5 activation is bistable in mature erythroblasts, resulting in a binary (or digital), low-intensity STAT5 phosphorylation signal (p-Stat5). In early erythroblasts, and in response to stress levels of Epo, the low intensity bistable p-Stat5 signal is superseded by a high-intensity graded, or analog, signal.

The gradual shift from high-intensity graded signaling in early erythroblasts to low intensity binary signaling in mature erythroblasts is due to a decline in STAT5 expression with maturation. We were able to convert mature, digital transducing erythroblasts into analog transducers simply by expressing high levels of exogenous STAT5. We found that EpoR-HM mice, expressing a mutant EpoR that lacks STAT5 docking sites, generate the binary, but not the analog, STAT5 signal. Unlike Stat5-null

mice, which die perinatally, the EpoR-HM mice are viable but deficient in their response to stress, demonstrating that while binary STAT5 signaling is sufficient to support basal erythropoiesis, analog signaling is required for the stress response. Bistable systems contain a positive loop, which is important for flipping the switch between the two stable ‘on’ or ‘off’ states. We show that bistable activation is the result of an autocatalytic loop in which active STAT5 promotes further STAT5 activation. The isolated STAT5 N-terminal domain, which is not required for STAT5 phosphorylation, enhanced autocatalysis, converting a high intensity graded signal into a high intensity binary response. The N-terminal domain is known to participate in a radical conformational reorientation of STAT5 dimers inherent in STAT5 activation. We propose that the N-terminal domains of active STAT5 dimers facilitate the conformational reorientation of inactive dimers, in a prion-like autocatalytic interaction that underlies bistability and binary signaling. Together, bistable STAT5 activation, combined with a graded response allow erythropoietic rate to faithfully reflect a wide Epo concentration range, while preventing aberrant signaling.

Table of Contents

Signature Page	iii
Dedication	iv
Acknowledgements	v
Abstract	viii
Table of contents	x
List of Figures	xiii
List of Third Party Copyrighted Material	xv
CHAPTER I: Introduction	
Erythropoiesis	1
Identification of erythroid progenitors	2
Erythropoietin receptor signaling	7
<i>In vivo</i> study of EpoR distal domain in erythropoiesis	11
STAT biology	15
STAT structure and functional domains	17
Negative regulation of STAT activation	21
Conformational reorientation during STAT phosphorylation/dephosphorylation cycle	22
STAT5 and erythropoiesis	30
Erythropoietin mediated STAT5 activation in cell lines	31
Signaling dynamics in biology	32
Development of a novel flow cytometric method to study protein phosphorylation at the single cell level	40
STAT5 and cancer	42
Aims of the study	44
CHAPTER II: Autocatalytic activation of Stat5 underlies bistability and binary signaling	
Copyright notice	47
Introduction	48
Results	52
Flow cytometric measurements of phosphorylated-Stat5 (p-Stat5) in primary erythroblasts	52
Erythroid maturation determines the p-Stat5 response	53
Binary and graded Stat5 signaling coexist in developing erythroblasts	60
EpoR-HM erythroblasts generate only binary low-intensity p-Stat5 signal	67
The maximal p-Stat5 response (p-Stat5 _{max}) is linearly correlated with Stat5 expression levels	69

Exogenous Stat5 expression rescues graded high intensity p-Stat5 signaling in EpoR-HM erythroblasts and in wild-type S3 cells	79
Cellular Stat5 is limiting during Stat5 phosphorylation in erythroid cells	87
Distinct biological functions of the binary and graded signaling modes.....	89
The low intensity p-Stat5 signal shows hysteresis.....	95
A steep relationship between FLAG-Stat5 expression and Epo-independent, constitutive p-Stat5	96
p-Stat5 promotes phosphorylation of inactive Stat5 in trans	98
The time course of p-Stat5 is consistent with autocatalysis	103
The isolated ND amplifies the binary p-Stat5 signal	107
The isolated ND enhances hysteresis and constitutive p-Stat5 activation.....	114
Phosphorylation of a ND-truncated Stat5 molecules is amplified by coexpression of the isolated ND	118
The isolated Myc-ND coimmunoprecipitate with full length FLAG-Stat5 ND	118
ND dimerization surface mutations are deficient in p-Stat5 amplification but retain p-Stat5 suppressive effect.....	119
Discussion	123
Coexisting graded and binary Stat5 signaling allows for fidelity in signaling over a wide Epo range.....	123
Mechanism of bistability: p-Stat5-mediated positive feedback exerted at the Stat5 phosphorylation step	126
Hypothesis: an autocatalytic conformational switch	130
Sites of interaction of the ND with Stat5	132
Implications for STAT's role in disease	133
Material and methods	133
Mouse models	133
Erythropoietin injections in adult mice	133
Fetal liver cell preparation	134
Amaxa Biosystem Nucleofection	134
Pervanadate treatment.....	134
SOCS3 siRNA	135
Mouse Embryonic Fibroblasts (MEF) preparation.....	135
Flow cytometry	135
DNA constructs: cloning and mutagenesis	136
Quantitative Real-Time PCR	137
Denaturing Immunoprecipitation and Quantitative Western Blotting.....	137
Western Blot Analysis	138

CHAPTER III: Identification and analysis of mouse erythroid progenitors using the

CD71/Ter119 flow-cytometric assay

Copyright Notice	140
Introduction	141
Protocol	145
Representative results	151
Discussion	162
Differentiation stage of erythroblasts within the flow-cytometrically defined subsets	163
Intracellular antigens.....	164

Fetal liver CD71/Ter119 subsets	164
Interpretation of changes in the frequency of erythroid subsets	165
CHAPTER IV: Conclusions and Future directions	167
Conclusions	167
Significance of our findings	171
Biological functions of digital and analog signaling in erythroblasts.....	171
Studying the regulation of Stat5 expression.....	173
Investigating the mechanisms of the coexistence of digital and analog signaling.....	174
Structural studies to confirm our hypothesis on the positive feedback mechanisms.....	176
Stat5 and leukemia	178
APPENDIX I: Contrasting dynamic responses in vivo for the Bcl-x_L and Bim erythropoietic survival pathways	
Copyright Notice	180
Abstract	181
Introduction	182
Results	185
Erythroid developmental delay in Stat5 ^{-/-} embryos	185
Bcl-x _L and Bim expression in fetal liver is differentiation-stage and embryonic day dependent	186
Bcl-x _L and Bim expression in fetal liver are regulated by Stat5	187
Bcl-x _L is rapidly induced in adult early erythroblasts in response to a single Epo injection.....	196
Expression pattern of Bim in basal and stress adult erythropoiesis.....	201
The erythroblast response to reduced atmospheric oxygen	204
The response of erythroblast Bim, Fas and Bcl-x _L to reduced atmospheric oxygen	205
Response of Bim and Bcl-x _L pathways to chronic erythropoietic stress.....	212
The Bcl-x _L response to an “acute on chronic” stress stimulus	212
Stat5 activation <i>in vivo</i> undergoes adaptation.....	218
The Bcl-x _L and Bim stress responses in EpoR-H and EpoR-HM mice	223
The p-Stat5 response to an “acute on chronic” stress stimulus.....	227
Discussion	228
Regulation of Bim and Bcl-x _L expression in early versus late erythroblasts	228
Adaptation allows functional specialization of the Bcl-x _L response to the acute phase of stress.....	231
Mechanisms of adaptation in the Bcl-x _L response	231
Implications for myeloproliferative diseases	232
Material and methods	235
Mouse models	235
Erythropoietic stress.....	235
Flow Cytometry	235
Quantitative Real-Time PCR	238
CFU-e Colony Assay	238
Enzyme Linked Immunoabsorbent Assay (ELISA)	239
Data Analysis	239

Bibliography240

List of Figures

CHAPTER I

Figure 1.1 Identification of Erythroid progenitors by the traditional methods and flow cytometry	4
Figure 1.2 Negative regulation of erythropoietin receptor signaling.....	9
Figure 1.3 <i>In vivo</i> models of EpoR distal domain truncations.....	13
Figure 1.4 Structural and functional domains in STAT family members.....	18
Figure 1.5 Phosphorylated and unphosphorylated STAT conformation and structure	24
Figure 1.6 Model of STAT dephosphorylation by conformational reorientation.....	28
Figure 1.7 Summary of different types of signaling responses	34
Figure 1.8 Components of bistable systems	38

CHAPTER II

Figure 2.1 The p-Stat5 response in fetal liver	55
Figure 2.2 The p-Stat5 response in fetal liver and in adult tissue.....	58
Figure 2.3 Binary p-Stat5 signaling in EpoR-HM erythroblasts	62
Figure 2.4	65
Figure 2.5 SOCS3 regulation of Stat5 signaling.....	71
Figure 2.6 Stat5 signaling in Shp1 ^{-/-} fetal liver	73
Figure 2.7 The maximal p-Stat5 response (p-Stat5 _{max}) is linearly correlated with Stat5 expression levels.....	75
Figure 2.8 Analysis of Stat5 phosphorylation in Stat5 ^{+/-} and EpoR ^{+/-} embryos.....	77
Figure 2.9 High exogenous Stat5 levels rescue high intensity graded p-Stat5 signaling in EpoR-HM cells	82
Figure 2.10 High exogenous Stat5 levels rescue high-intensity graded p-Stat5 signaling in wild type S3 cells.....	85
Figure 2.11 Biological functions of binary and graded signaling.....	92
Figure 2.12 Hysteresis and positive feedback in Stat5 activation	100
Figure 2.13 Hysteresis and autocatalysis in Stat5 activation	104
Figure 2.14 The Stat5 ND enhances bistable Stat5 activation.....	110
Figure 2.15 The isolated Stat5 ND enhances hysteresis and constitutive p-Stat5 activation.....	115
Figure 2.16 Phosphorylation of a ND-truncated Stat5 molecule is amplified by coexpression of the isolated ND	121

CHAPTER III

Figure 3.1 Experimental strategy to study erythropoiesis using flow cytometry	143
Figure 3.2 The CD71/Ter119 erythroid subsets in mouse spleen.....	153
Figure 3.3 Cell cycle analysis of CD71 ^{high} Ter119 ^{high} erythroblasts in mouse bone marrow	155
Figure 3.4 CD71/Ter119 erythroid subsets in mouse fetal liver.....	158
Figure 3.5 Cell cycle analysis of fetal liver erythroid subsets	160

CHAPTER IV

Figure 4.1 Dimmer switch model of Stat5 signaling	169
---	-----

APPENDIX I

Figure A1.1 Delayed maturation and altered Bcl-x _L and Bim expression in Stat5 ^{-/-} fetal liver	189
Figure A1.2 Bim and Bcl-x _L in fetal liver erythroblasts	192
Figure A1.3 Fas suppression in E14.5 fetal liver erythropoiesis	194
Figure A1.4 Bcl-x _L induction in adult early erythroblasts in response to Epo injection	198
Figure A1.5 Transient Bcl-x _L induction contrasts with slower Bim suppression in response to Epo injection	202
Figure A1.6 A reduced oxygen environment elicits a rapid, transient Bcl-x _L induction and a slow persistent Bim suppression	207
Figure A1.7 The Bcl-x _L response to repeated Epo injections	210
Figure A1.8 The Bcl-x _L response to chronic stress and to ‘acute on chronic’ stress	214
Figure A1.9 Plasma Epo measurements in mice with β-thalassemia and in ts-VHL ^{-/-} mice	216
Figure A1.10 Adaptation in the Bcl-x _L and p-Stat5 responses is dependent on the EpoR C-terminal cytoplasmic domain	220
Figure A1.11 The Bcl-x _L and Bim responses in EpoR-H and EpoR-HM mice	224
Figure A1.12 Regulation of Bcl-x _L and Bim expression in erythropoiesis	233

List of Third party copyrighted material

Figure Number	Publisher	License Number
Figure 1.1A	Lippincott Williams & Wilkins, Inc.	2706271023732
Figure 1.2	Elsevier Ltd.	2706271474927
Figure 1.4A	Nature Publishing Group	2707891030950
Figure 1.4B	Cell Press	2707870774013
Figure 1.5A	Cell Press	2715090243923
Figure 1.5B	CSHL Press	Permission Granted
Figure 1.6	CSHL Press	Permission Granted
Figure 1.7	International Union of Biochem; Elsevier Publ	2711420335811
Figure 1.8A	Elsevier Ltd., Current Opinion Journals	2707891377271
Figure 1.8B	AAAS	2707891222056

CHAPTER I: Introduction

1. Erythropoiesis

Erythropoiesis, the production of red blood cells, is regulated by the glycoprotein hormone erythropoietin (Epo), whose production is modulated by tissue oxygen tension. Given the central role of red blood cells in oxygen transport, erythropoiesis is a tightly regulated process aimed at maintaining homeostasis as well as responding to changes in oxygen demand. Definitive erythropoiesis in mice occurs in the fetal liver, whereas basal adult erythropoiesis occurs primarily in the bone marrow and at low levels in the spleen. However, in conditions that cause hypoxic stress, such as moving to high altitude, blood loss or anemia, the spleen becomes the main erythropoietic organ and erythropoiesis can increase up to 10-fold its basal rate, in a process known as stress erythropoiesis.

Tissue oxygen tension modulates Epo secretion by the kidney peritubular cells through the Hypoxia-Inducible Factor (HIF) [1]. The transcription factor HIF-2, composed of an oxygen sensitive α subunit, HIF-2 α , and a constitutively expressed β subunit, HIF- β , regulates Epo induction by binding to hypoxia-response elements (HREs) in the promoter of the Epo gene [2, 3]. Under normal oxygen conditions, the HIF-2 α subunit is hydroxylated by oxygen- and iron-dependent prolyl-hydroxylases, allowing binding of the von Hippel-Lindau tumor suppressor (pVHL) and subsequent targeting of the HIF-2 α subunit for proteasomal degradation [4, 5]. Under conditions of hypoxia the α subunit is stabilized leading to the formation of an active HIF-2 $\alpha\beta$ heterodimer.

Epo levels can increase up to 1000 fold during severe tissue hypoxia [6]. High Epo, in combination with other factors, such as stem cell factor (SCF) [7],

glucocorticoids [8, 9] and bone morphogenetic protein 4 (BMP4) [10], promotes an increased erythropoietic rate. However, the details of Epo receptor (EpoR) signaling during basal and stress erythropoiesis are not yet known.

2. Identification of erythroid progenitors

Erythroid progenitors are generated from hematopoietic stem cells present in the fetal liver or in the bone marrow, via multipotential progenitors, such as the common myeloid progenitor (CMP) and the megakaryocytic/erythrocytic progenitor (MEP). Erythroid progenitors have been identified in the past using colony-forming assays in semisolid medium (Figure 1.1A). The earliest committed erythroid progenitor identified *ex vivo* by this method is the Burst Forming Unit-erythroid (BFU-e), that generates, in the presence of Epo, Stem Cell Factor (SCF) and Interleukin-3 (IL-3), about 500 cells in 6-10 days [11]. A more mature progenitor is the Colony Forming Unit-erythroid (CFU-e), that forms, in the presence of Epo, colonies of 8-32 cells in 2-3 days [12]. CFU-e gives rise to increasingly mature erythroblasts that are identified by their morphology and are classified into proerythroblasts, basophilic, polychromic and orthochromic erythroblasts.

Our laboratory has developed a flow-cytometric assay that allows identification and analysis of erythroblasts in freshly isolated hematopoietic tissue. By staining total fetal liver (Figure 1.1C), bone marrow or spleen cells (Figure 1.1B) with antibodies against the cell surface markers CD71, the transferrin receptor, and Ter119, an erythroid specific marker, we can identify erythroid subsets that form a developmental sequence [13, 14]. In the fetal liver we identify six subsets, S0 to S5 (Figures 1.1C and 3.4). As they progress in differentiation, they decrease in size, compact their chromatin and start

expressing hemoglobin (Figure 1.1C). Subsets S1 to S5 are Epo dependent *in vitro* and *in vivo* and entirely erythroid. The S0 subset, on the other hand, though still largely composed of early erythroid progenitors, also contains non-erythroid cells (30% of S0), which comprise cells of other hematopoietic lineages and earlier uncommitted progenitors. In the adult tissue, by combining the CD71/Ter119 staining with the forward scatter parameter (FSC), we resolve 4 subsets, ProE (Ter119^{med} CD71^{high} FSC^{high}), EryA (Ter119^{high} CD71^{high} FSC^{high}), EryB (Ter119^{high} CD71^{high} FSC^{low}), and EryC (Ter119^{high} CD71^{low} FSC^{low}) (Figure 1.1B). These subsets, which morphologically represent progressively mature erythroblasts, approximately correspond to proerythroblasts, basophilic erythroblasts, basophilic and polychromic erythroblast, polychromic and orthochromic erythroblasts, respectively.

EpoR is expressed in long term HSCs, cells with BFU-e potential [15, 16], as well as early erythroblasts (Figure 1.1A). In fetal liver cells, it is expressed in subsets S0 to S3. Mice that lack either Epo or EpoR die at embryonic day 13 (E13), due to severe anemia. The fetal liver of these knock-out mice can generate normal numbers of BFU-e and CFU-e progenitors but cannot produce mature red blood cells [17], indicating an essential role for EpoR signaling in erythropoiesis. Janus Kinase 2 (Jak2)^{-/-} mice die one day earlier than the EpoR^{-/-} mice and exhibit a decreased number of total fetal liver cells as well as erythroid progenitors, suggesting that JAK2 is required at earlier stages of erythroid development than the EpoR [18].

Figure 1.1 Identification of erythroid progenitors by traditional methods and flow cytometry.

(A) Hematopoietic stem cells in the fetal liver or bone marrow generate the common myeloid progenitor (CMP), which gives rise to the megakaryocytic/erythrocytic progenitor (MEP) that commits to the erythroid lineage. Cells in the same vertical position indicate the same differentiation stage. (Top panel) Traditional methods of identifying erythroid progenitors comprise: colony forming assays, used to identify the Burst Forming Unit-erythroid (BFU-e) and Colony Forming Unit-erythroid (CFU-e) (left); morphological assays (cytospins), used to identify erythroblasts (right). A recently developed flow cytometric assay (bottom panel), based on simultaneous staining for CD71 and Ter119, allows the identification of erythroblasts that form a developmental sequence (ProE, EryA, EryB, EryC) directly within adult hematopoietic tissue.

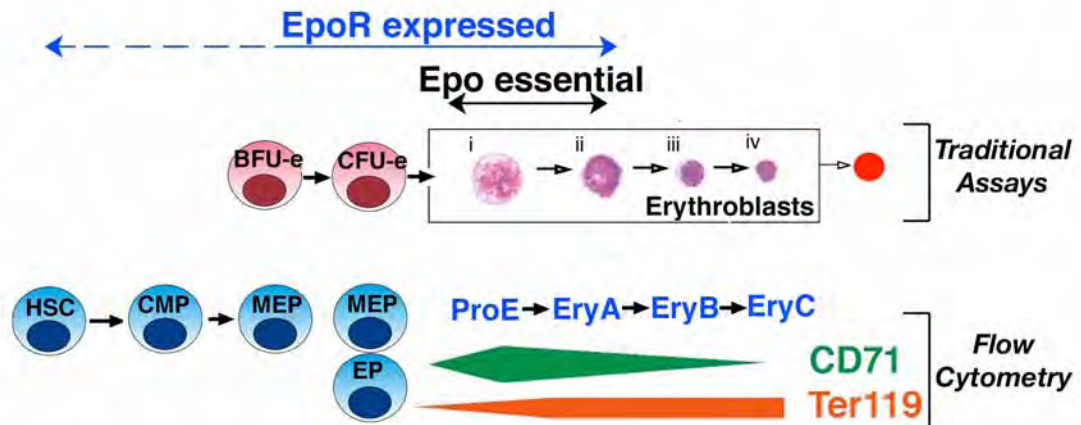
(B) Gating strategy for freshly explanted spleen erythroid subsets. Dead cells are excluded by staining with LIVE/DEAD fixable viability staining and gating on the negative population. CD71/Ter119 staining combined with forward scatter (FSC) analysis, resolves 4 subsets: ProE (Ter119^{med} CD71^{high} FSC^{high}), EryA (Ter119^{high} CD71^{high} FSC^{high}), EryB (Ter119^{high} CD71^{high} FSC^{low}), and EryC (Ter119^{high} CD71^{low} FSC^{low}). Same data as in figure A1.4.

(C) (Top) Gating strategy for freshly isolated fetal liver cells processed for intracellular staining. The gate drawn in the side scatter (SSC)/FSC dot plot serves to exclude small events like nuclei and debris. The diagonal gate identifies single cells, while excluding doublets or aggregates. The CD71/Ter119 staining in total fetal liver cells identifies

subsets S0-S4. S3 cells are subdivided, based on the FSC parameter in S3 large and S3 small. (Bottom) A cytopsin preparation of cells from individual subsets is shown. Decrease in cell size and hemoglobin expression is observed with maturation.

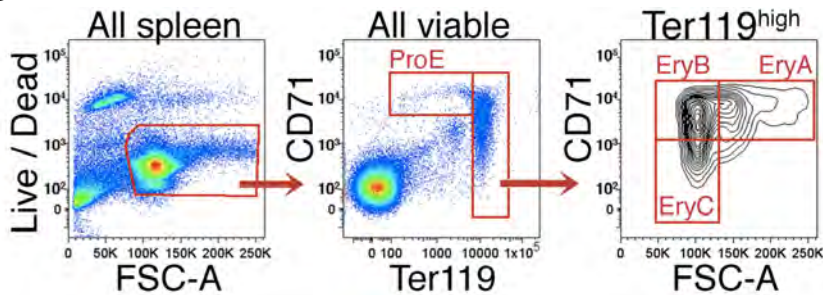
Figure 1.1

A

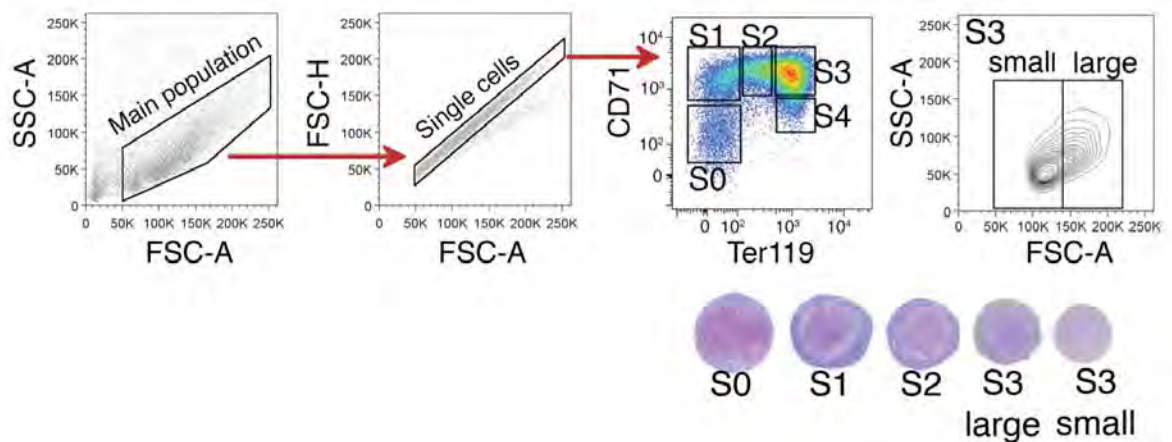


Reproduced with permission of LIPPINCOTT WILLIAMS & WILKINS, INC. Socolovsky M, Molecular insights into stress erythropoiesis, *Curr Opin Hematol*, 14: 215-24 [19], Copyright (2007).

B



C



3. Erythropoietin receptor signaling

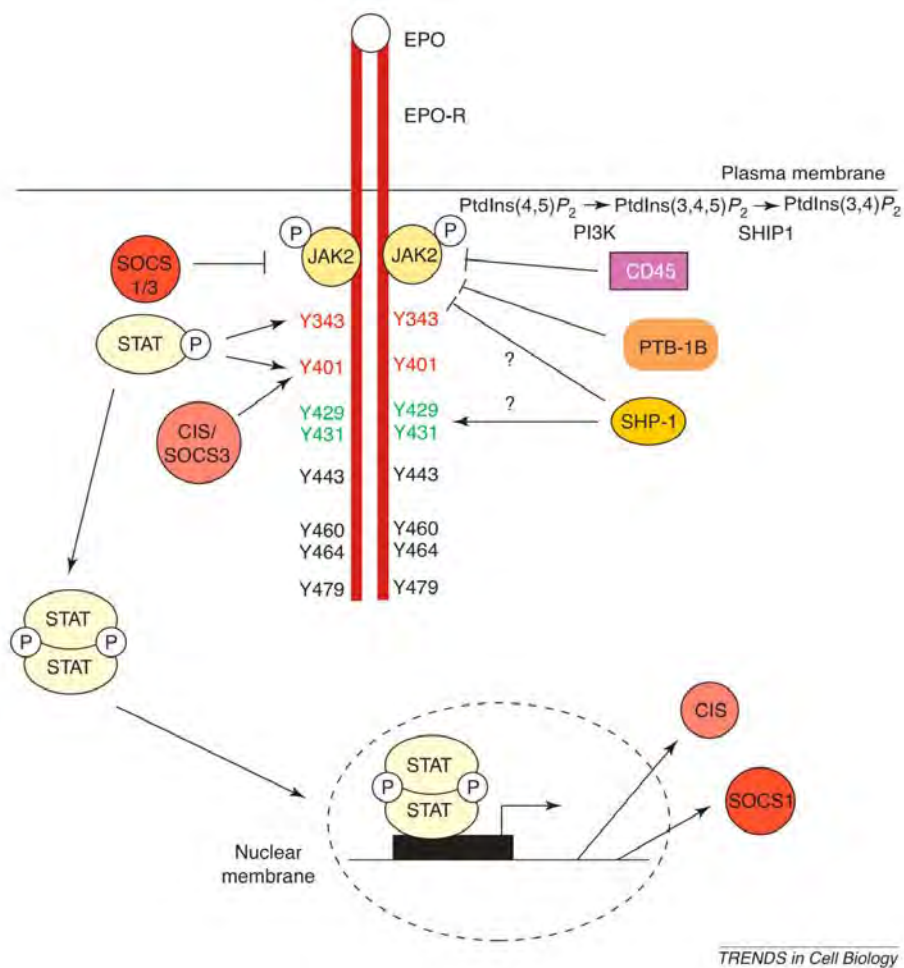
The EpoR, first identified in 1989 [20], is a class I cytokine receptor characterized by the presence of conserved regions in the extracellular domain, a cysteine motif (a set of four conserved cysteine residues) and a WSXWS motif in proximity of the transmembrane segment. The murine EpoR is a 507 amino acid protein that contains an extracellular domain, a transmembrane domain and a cytosolic domain lacking any kinase activity, but associated with JAK2 kinase. The inactive EpoR is present in the membrane as a homodimer [21, 22]. An EpoR mutant containing an intermolecular disulfide bond in proximity of the membrane, R129C, is constitutively active and is able to cause erythroleukemia in mice [23].

Upon ligand binding, the receptor undergoes a conformational change that leads to activation of the pre-associated kinase, JAK2, and subsequent phosphorylation of the cytoplasmic domain of the receptor at eight tyrosine residues. The phosphorylated tyrosines serve as docking site for several signaling molecules that contain Src-Homology 2 (SH2) domains, such as STAT5 (Signal Transducer and Activators of Transcription 5), PI-3 kinase, Mitogen Activated Protein Kinases (MAPKs) and several negative regulators. Upon binding to the phosphorylated receptor the signal transduction molecules are phosphorylated. They then dissociate from the receptor and deliver the signals directly to the nucleus, in the case of STAT5, or to downstream effectors. STAT5 primarily binds to Y343 and Y401 of the EpoR [24-26], whereas Y479 recruits the p85 subunit of PI-3 kinase [27, 28] and Y464 is bound directly by Grb2 [29]. Among the MAPKs, EpoR activates Erk1/2, SAP Kinase/Jun kinase and p38 [30-33].

Cytoplasmic negative regulators include tyrosine phosphatases and members of the Suppressor of Cytokine Signaling (SOCS) family, which bind to the phosphorylated tyrosines on the EpoR and prevent further signaling by competing with the signaling molecules for receptor binding (SOCS family members) or inactivating JAK2 or the receptor (Figure 1.2). Among the cytoplasmic phosphatases, SH-2 domain containing phosphatase-1 (SHP1) binds to Y429 and Y431 [34] and indirectly inactivates JAK2 [35], CD45 and protein-tyrosine phosphatase 1B (PTP1B) directly inhibit JAK2 [36, 37], whereas SHP2 and SH-2 domain containing inositol-5-phosphatase (SHIP-1) are recruited to Y401 [38]. The SOCS family members, CIS, SOCS1 and SOCS3, are transcriptionally induced upon Epo-mediated STAT5 activation and act by different mechanisms. CIS and SOCS-3 bind to Y401 and therefore compete with STAT5 for receptor binding [39-41], while SOCS1 and SOCS3 exert their action by N-terminal inactivation of JAK2 [41, 42].

Figure 1.2 Negative regulation of erythropoietin receptor signaling. Erythropoietin receptor cytoplasmic domain contains 8 tyrosines, which upon phosphorylation, serve as docking site for several signaling molecules, one of which is STAT5. STAT5 activation initiates a negative feedback loop, that leads to signal termination, by inducing the transcription of negative regulators of the SOCS family: CIS, SOCS1 and SOCS3. CIS and SOCS3 bind to Y401 on the EpoR, competing with STAT5 and therefore preventing further phosphorylation. SOCS1 and SOCS3 inhibit JAK2 by direct binding. Other negative regulators include the cytoplasmic tyrosine phosphatases SHP-1, PTP1-B and CD45, which negatively regulate JAK2.

Figure 1.2



Reprinted from [Trend in Cell Biology], Volume 15, Richmond TD et al., Turning cells red: signal transduction mediated by erythropoietin, Pages: 146-55 [43], Copyright (2005) with permission from Elsevier.

4. *In vivo* study of EpoR distal domain in erythropoiesis

Naturally occurring mutations in the C-terminal domain of human EpoR, to which negative regulators are recruited, have been associated with familial erythrocytosis [44, 45], a disorder of red blood cell production, characterized by an absolute increase in red cell mass, with elevated hematocrit and hemoglobin levels. These findings suggested that lack of negative regulation could be the cause of excessive red blood cell production. Moreover, studies in cell lines suggested a central role for Y343, a STAT5 docking site, in EpoR signaling and erythropoiesis (Chapter I-3 and I-10).

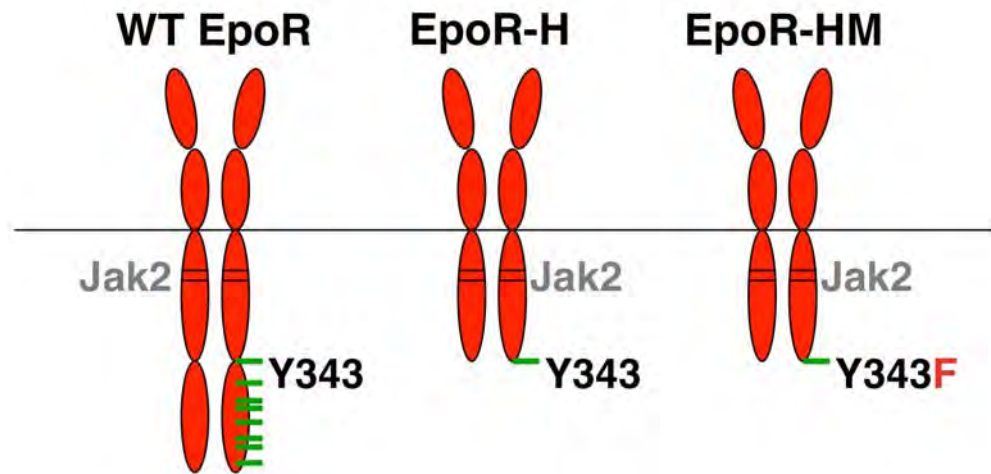
In order to study the role of the EpoR distal domain in erythropoiesis, two knock-in mice were generated, in which a C-terminally truncated EpoR was 'knocked-in' at the wild-type EpoR locus. EpoR-H mice retained Y343, whereas EpoR-HM mice contained, in addition to the truncation, a mutation of the residual tyrosine to phenylalanine (Y343F) (Figure 1.3). Both mice are viable and fertile. EpoR-H mice exhibit a slight increase in hematocrit levels, whereas the EpoR-HM mice show a slight decrease [46]. In addition, EpoR-HM mice showed increased renal Epo transcript levels, which were 1.9 fold higher than in wild type controls, while EpoR-H mice showed a decrease to levels that were about 60% of the wild type controls [47].

Several studies showed that EpoR-HM mice, despite normal basal erythropoiesis, are unable to respond to anemic stress induced by hemolysis, 5-fluorouracil treatment or bone marrow transplantation. Conversely, efficient stress erythropoiesis is rescued in EpoR-H mice, which are also hypersensitive to Epo [47, 48].

These findings suggest that an EpoR lacking any tyrosines is sufficient to support basal erythropoiesis *in vivo* and that EpoR tyrosines are required for the erythropoietic stress response.

Figure 1.3 Mouse models of EpoR distal domain truncation. EpoR-H and -HM mice are knock-in mice expressing a C-terminally truncated EpoR. The STAT5 docking site, Y343, is maintained in EpoR-H mice while is mutated to phenylalanine in EpoR-HM mice. JAK2 is activated upon Epo binding to the receptor, in both mouse models.

Figure 1.3



5. STAT Biology

The JAK-STAT pathway was first identified in the early 1990 during the study of interferon (IFN) signaling [49-51]. This new pathway could transduce signals from the cell surface directly to the nucleus, rapidly inducing new genes, through proteins with dual function in signal transduction and activation of transcription, STAT proteins.

STAT proteins are latent cytoplasmic transcription factors that become activated by phosphorylation of a single carboxy-terminal tyrosine in response to a variety of extracellular signals, such as cytokines, growth factors and hormones.

In the classical JAK/STAT pathway, ligand binding to the cytokine receptor, devoid of intrinsic tyrosine kinase activity, leads to receptor dimerization and activation of the pre-associated JAK kinase. The activated JAKs trans-phosphorylate the receptor cytoplasmic tyrosines generating docking site for the STAT proteins that then become substrates of the JAK. Upon tyrosine phosphorylation and nuclear translocation, STATs exert their function as transcriptional activators.

STAT activation also occurs downstream of other receptor families, such as receptors with intrinsic tyrosine kinase activity (for example, the Epidermal Growth Factor (EGF) receptor) [52] as well as seven-transmembrane receptors, associated to tyrosine kinases like Src [53].

The importance of the JAK-STAT pathway is highlighted by its evolutionary conservation. STAT molecules first emerged with multicellularity, and therefore, with intercellular signaling. For example, a STAT molecule required in the induction of pre-stalk cell differentiation, has been described in the slime mold, *Dictyostelium discoideum*

[54]. The *Drosophila melanogaster* genome only encodes for one STAT molecule, STAT92E (or D-STAT), which is essential for development [55, 56] and is very similar to murine STAT5. The *Drosophila* JAK/STAT pathway regulates eye development [57], sex determination [58, 59], germ cells self renewal [60, 61] and hemocyte proliferation and differentiation [62]. STAT molecules have been found in the African Malaria mosquito (*Anopheles gambiae*) [63], in zebrafish (*Danio rerio*) [64], frog (*Xenopus laevis*) [65] and the round spotted puffer fish (*Tetradon fluviatilis*) [66].

The identification of multiple mammalian STAT indicates that the genes encoding for STAT proteins have undergone duplication in the evolution of mammals. Seven mammalian STAT genes have been identified to date, Stat1, 2, 3, 4, 5A, 5B and 6. The generation of STAT knock out models has uncovered the essential function of individual STATs *in vivo*. Stat3^{-/-} mice are embryonic lethal [67], whereas Stat5a, b^{-/-} mice die perinatally [68]. The finding that not all STAT molecules are essential for life might reflect the specialized function of some of these proteins. While STAT3 is ubiquitously expressed and functions in a variety of biological processes, STAT5 role is more prominent in hematopoiesis, reproductive system development and mammary gland development (STAT5A) [69] as well as body growth (STAT5B) [70]. STAT1, 2, 4 and 6, on the other hand, have more specialized roles in the immune system. STAT1 plays a central role in IFN signaling (IFN α/β and IFN γ) [71, 72], STAT2 is important for IFN α/β signaling only [73], while STAT4 and 6 are involved in T cell signaling downstream of IL-12 and IL-4, respectively [71, 72, 74, 75].

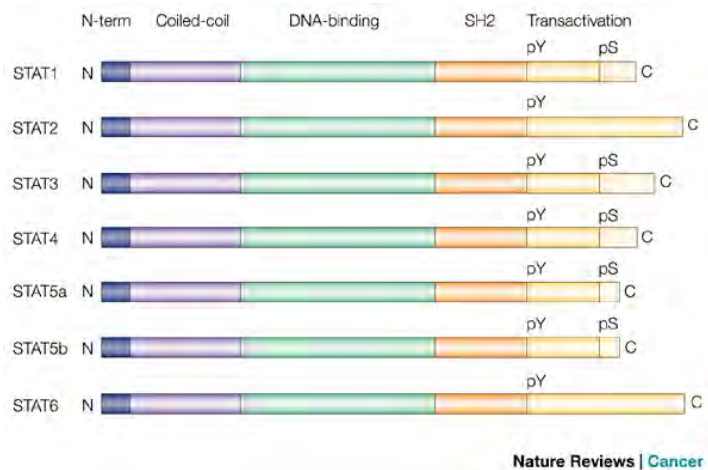
6. STAT structure and functional domains

The mammalian STAT proteins exhibit a 28% to 40% sequence identity in their first 700 amino acids. The sequence of the carboxyl-terminal region of the protein is the most divergent part among members of the STAT family. STAT2 and 6 are 850 amino acids long, while STAT1, 3, 4, 5A and 5B proteins contains between 750 and 795 amino acids. Sequence comparison and mutagenesis studies have revealed the presence of conserved functional domains within STAT proteins [76, 77]: N-terminal domain (ND), Coiled-coil domain (CCD), DNA binding domain (DBD), linker domain, SH2 domain and transactivation domain (Figure 1.4).

Figure 1.4 Structural and functional domains in STAT family members. (A) STAT family members share the following conserved domains: N terminal domain (N-term), Coiled-coil domain (CCD), DNA binding domain (DBD), Src homology 2 (SH2) domain and the transactivation domain (TAD). The C-terminal region of the protein is the most divergent among STAT family members. (B) Crystal structure of phosphorylated STAT1 core bound to DNA. ND and TAD were not part of the crystal structure. (Top Panel) Colored representation of the identified domains in a ribbon diagram: CCD (green), DBD (red), linker domain (orange), and SH2 domain (blue). A stick representation of the phosphotyrosine is shown. The DNA double helix is shown in grey. (Bottom Panel) Molecular surface of the STAT1 dimer: the colors indicate the electrostatic potential, with red representing positive and blue representing negative potential.

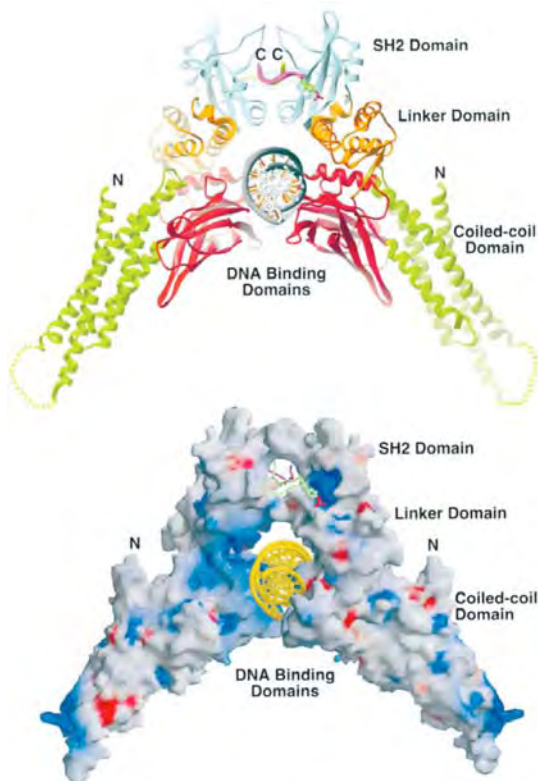
Figure 1.4

A



Reprinted by permission from Macmillan Publisher Ltd: [Nat Rev Cancer], Volume 4, Yu, H. and R. Jove, The STATs of cancer-new molecular targets come of age, Pages: 97-105 [78], Copyright (2004).

B



Reprinted from [Cell], Volume 93, Chen X et al., Crystal structure of a tyrosine phosphorylated STAT-1 dimer bound to DNA, Pages: 827-39 [76], Copyright (1998), with permission from Elsevier.

The crystal structure of tyrosine phosphorylated human STAT1 (Figure 1.4B) and mouse STAT3 dimers bound to DNA revealed a rigid hydrophobic core (residues 130-712) formed by the CCD, the DBD, the linker domain and the SH2 domain [76, 77]. The region containing the tyrosine phosphorylation site appeared flexible. The tyrosine-phosphorylated dimers were stabilized by interaction between the phospho-tyrosine of one monomer and the SH2 domain of the other.

The structure of the ND (amino acids 1-130) has been determined separately for STAT1 and STAT4 [79, 80]. The domain consists of 8 helices that are organized in a hook-like structure. The ND is connected to the molecule core by a flexible tether of approximately 20 amino acids. Functionally, the ND plays a crucial role in STAT dimerization, in the activation/inactivation cycle and in the formation of higher order molecular complexes, such as tetramers that can bind to adjacent DNA consensus sites. The DBD, which consists of several beta sheets, interacts with the DNA both in the major and minor groove, at consensus oligonucleotide palindromic sequences, 5'-TT(N₄₋₆)AA-3' [81]. The SH2 domain recognizes phospho-tyrosine residues specifically [82, 83] and is required for binding to activated receptors and for the formation of phosphorylated STAT dimers. All STAT molecules except STAT2 form homodimers upon tyrosine phosphorylation. Only a few heterodimeric complexes are formed, consisting of STAT1:3, STAT1:2 and STAT5A:5B [84]. In addition, the transactivation domain regulates transcription by interacting with several coactivators [85], undergoes serine phosphorylation and seems to regulate the stability of some STAT proteins [86].

7. Negative regulation of STAT activation

STAT activation is transient and tightly regulated since constitutive activation of several STAT molecules is oncogenic (Chapter I-13). Negative regulators of STAT signaling are present both in the nucleus and the cytoplasm.

The nuclear regulators of STAT signaling include nuclear phosphatases and Proteins that Inhibit Activated STATs (PIAS). The nuclear tyrosine phosphatase TC45, has been implicated in dephosphorylation of STAT1 and 3 [87]. PIAS proteins have been shown to interact with STAT1 and 3 in mammalian cells and block DNA binding, *in vitro* [88]. Moreover, genetic studies in *Drosophila* suggest that PIAS could modulate STAT activity *in vivo* [57].

The cytoplasmic regulators include phosphatases and SOCS family proteins. SHP1, SHP2, CD45 and PTP1B, promote tyrosine dephosphorylation of the receptor and the kinase, therefore preventing further STAT tyrosine phosphorylation [81, 89-91]. The SOCS family proteins, that include SOCS1-4 and CIS, are part of the negative feedback loop initiated by receptor signaling. They are transcriptionally induced upon STAT activation and act on the activated receptor, the JAK kinase and STATs [92]. The SOCS family proteins act through three different mechanisms: 1) ***N-terminal inactivation of JAKs*** by binding to their catalytic pocket [93, 94]; 2) ***Receptor association***. By binding to tyrosine phosphorylated receptors they compete with STATs and therefore prevent further STAT activation [95, 96]; 3) ***SOCS-box mediated proteasomal degradation***. SOCS proteins act as adaptors for E3 ubiquitin ligase complexes, mediating ubiquitination and degradation of JAKs [42, 97-99].

8. Conformational reorientation during STAT phosphorylation/ dephosphorylation cycle

STAT molecules were originally reported to be monomeric in their inactive form [100]. However, several studies indicated the presence of unphosphorylated STAT dimers in the cytoplasm of unstimulated cells. Unphosphorylated STAT3 was shown to form stable homodimers [101], as well as higher order complexes called the statosomes [102], by size exclusion chromatography. Unphosphorylated STAT1 could be coimmunoprecipitated with STAT2 and STAT3, in absence of cytokine stimulation [103, 104]. Moreover, studies using surface plasmon resonance and other methods demonstrated that inactive STAT1 was mainly dimeric [105].

Yeast two-hybrid analysis showed the formation of unphosphorylated STAT4 dimers in absence of cytokine stimulation [106]. Importantly, mutations in the ND dimerization interface of STAT4 impaired the formation of unphosphorylated STAT4 dimers and prevented cytokine-mediated phosphorylation, suggesting a role for ND-ND interactions in the formation of unphosphorylated STAT dimers. ND-ND interactions were found to be homotypic for all STATs except STAT2 [106]. The interaction between NDs was also supported by the observation that isolated STAT NDs are present in solution as homodimers [107, 108].

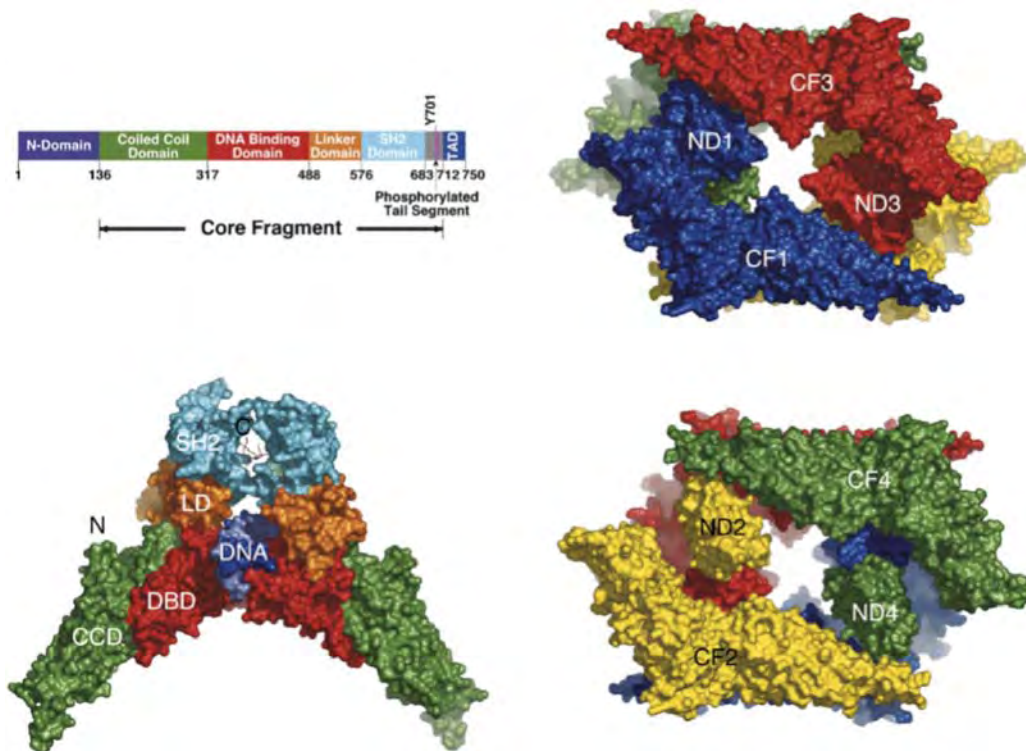
Comparison of the crystal structure of unphosphorylated STAT1 [80] and STAT5 [109] with the previously available structures of phosphorylated STAT1 and 3 (Chapter I-6), revealed that unphosphorylated dimers were rearranged differently in space than the phosphorylated ones, with the SH2 domains located at opposite ends of the dimer (Figure

1.5A). Unphosphorylated dimers were stabilized by interaction between the CCD of one monomer and the DBD of the other, as well as by reciprocal interaction between the NDs. The phosphorylated dimers were referred to as “parallel”, because the SH2 domains are at the same end of the tyrosine-phosphorylated structure, while the unphosphorylated dimers were referred to as “antiparallel” (Figure 1.5B).

Figure 1.5 Phosphorylated and unphosphorylated STATs conformation and structure. (A) Crystal structure of phosphorylated (bottom left) and unphosphorylated STAT1 (right). (B) Three potential dimerization interfaces between the two monomers have been identified: the reciprocal pY-SH2 interaction in the parallel, phosphorylated dimer and the ND-ND interaction as well as the CCD-DBD interaction in the antiparallel, unphosphorylated dimer. The white circle represents the unphosphorylated tyrosine, while the red circle indicate the phosphorylated tyrosine (PY).

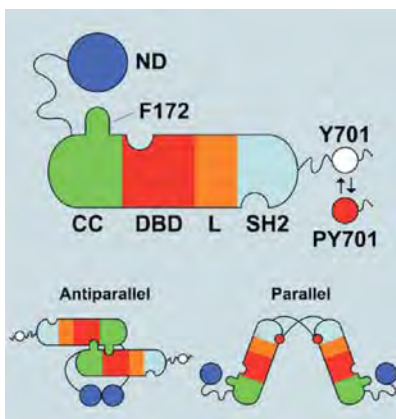
Figure 1.5

A



Reprinted from [Molecular Cell], Volume 17, Mao X et al., Structural bases of unphosphorylated STAT1 association and receptor binding, Pages: 761-71 [80] Copyright (2005), with permission from Elsevier.

B



Reprinted from [Genes & Development], Volume 20, Mertens C et al., Dephosphorylation of phosphotyrosine on STAT1 dimers requires extensive spatial reorientation of the monomers facilitated by the N-terminal domain, Pages 3372-81 [110], Copyright (2006), with permission from Cold Spring Harbor Laboratory Press.

Mutagenesis studies, performed to disrupt the interaction between the NDs (F77A and/or L78A) or the CCD and the DBD (F172W) in STAT1, showed absence of unphosphorylated dimers and a persistent STAT1 phosphorylation phenotype, characterized by prolonged phosphorylation in IFN γ -stimulated cells and resistance to TC45 phosphatase treatment *in vitro* [111]. A similar persistent phosphorylation phenotype was previously observed upon partial deletion of the ND of STAT1 [112] and following substitution of STAT1 ND with the ND of STAT2 or STAT5 in a STAT1 chimera [113], suggesting that the STAT ND plays a central role in the phosphorylation/dephosphorylation cycle. These findings led to the hypothesis that, upon DNA dissociation, phosphorylated STAT dimers undergo a conformational change from parallel to antiparallel, to expose the phosphorylated tyrosines to phosphatases for dephosphorylation.

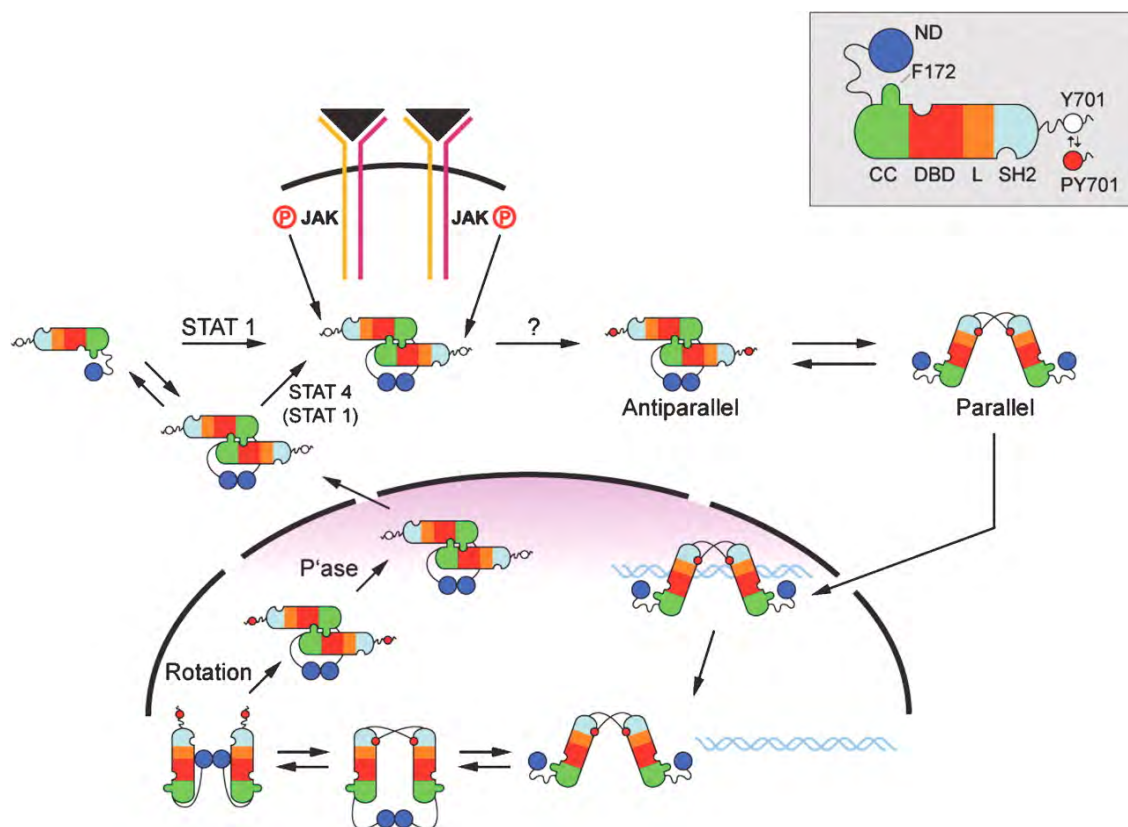
Experiments with differentially tagged monomers showed that there is no exchange of partners in a dimer during the phosphorylation/dephosphorylation cycle, suggesting that the conversion from parallel to antiparallel dimers must occur through reorientation, without dissociation of the monomers [110]. Moreover, shortening of the flexible tether that connects the ND to the core caused a persistent phosphorylation phenotype, indicating that the tether was required for the conformational reorientation. These findings led to the development of a mechanistic model for the conformational reorientation of the dimer in which following DNA dissociation, interacting NDs could disrupt the pY-SH2 interaction, possibly by binding to the body of the phosphorylated molecule. Subsequent rotation of the dimer, stabilized by the ND-ND interface, could

facilitate the interaction between the CCD of one monomer and the DBD of the other, stabilizing the antiparallel dimer and providing an accessible substrate for phosphatases (Figure 1.6).

Figure 1.6 Model of STAT dephosphorylation by conformational reorientation.

Three dimerization interfaces between the two monomers have been proposed: 1) reciprocal PY-SH2 interaction in the phosphorylated parallel dimer; 2) ND-ND interaction and 3) CCD-DBD interaction in the unphosphorylated antiparallel dimer. Upon dissociation from the DNA (surrounded by the nuclear membrane) phosphorylated (the red circle represents the phosphorylated tyrosine (PY)) parallel STAT dimers undergo a conformational reorientation, involving the contact between interacting NDs and the body of the molecule (aimed at disrupting the PY-SH2 interaction) followed by rotation. The reorientation leads to the formation of an antiparallel dimer that is accessible to phosphatase (P'ase) and can be dephosphorylated and exported to the cytoplasm.

Figure 1.6



Reprinted from [Genes & Development], Volume 20, Mertens C et al., Dephosphorylation of phosphotyrosine on STAT1 dimers requires extensive spatial reorientation of the monomers facilitated by the N-terminal domain, Pages 3372-81 [110], Copyright (2006), with permission from Cold Spring Harbor Laboratory Press.

9. STAT5 and erythropoiesis

STAT5 was first identified in mammary tissue from lactating sheeps as Mammary Gland Factor (MGF), a transcription factor activated by the prolactin receptor and responsible for the expression of milk protein genes in mammary epithelium [114]. The search for the mouse homolog led to the discovery of STAT5A and a closely related protein, STAT5B [115-117]. STAT5A and STAT5B are encoded by two genes, located next to each other in opposite orientation on chromosome 11 (in mice) and chromosome 17 (in humans), in the same locus as the Stat3 gene. STAT5A and STAT5B are highly homologous with 96% identity at the protein level. The three-dimensional structure of the unphosphorylated STAT5A core fragment showed similarity to other members of the STAT family [109]. STAT5 regulates hematopoiesis, reproductive system development and mammary gland development (STAT5A) as well as body growth (STAT5B) [68-70, 118-121]. Moreover, STAT5 is constitutively activated in many leukemias and myeloproliferative syndromes, and its constitutive activation is sufficient for hematopoietic cell transformation [122-125].

STAT5 is a central player in EpoR signaling and a critical regulator of erythropoiesis. Mice lacking STAT5 exhibit severe anemia and die perinatally [68], whereas mice hypomorphic for STAT5, in which the first exon of each STAT5 gene has been deleted ($Stat5^{\Delta N/\Delta N}$), survive to adulthood but show a defective response to erythropoietic stress [119, 126-129]. In erythroblasts, STAT5 is a key mediator of cell survival through induction of B-cell lymphoma-extra large (Bcl_{XL}) [130], an antiapoptotic molecule of the Bcl2 family. $Bcl_{XL}^{-/-}$ mice die at day E12.5 due to severe

anemia and brain defects, despite the fact that the number of BFU-e, CFU-e and erythroblasts is normal [131]. On the other hand, exogenous expression of human Bcl_{XL} in murine erythroblasts allows Epo-independent differentiation [132]. However, STAT5 is not the only transcription factor that mediates Bcl_{XL} induction in erythropoiesis: GATA1 also participates in the induction of Bcl_{XL} expression [133]. Moreover, it has recently been shown that STAT5 controls the induction of erythroblast CD71 in fetal liver tissue [119, 134].

10. Erythropoietin-mediated STAT5 activation in cell lines.

The current knowledge of STAT5 activation downstream of the EpoR is based on *in vitro* studies using cell culture systems. The ability of Epo to induce tyrosine phosphorylation of STAT5 via JAK2 was first shown in CTLL-2 cell lines transfected with EpoR [135]. The DNA binding activity of STAT5 in response to Epo has been reported in COS cells transfected with EpoR and STAT5 and in several hematopoietic cell lines [25, 136, 137]. Moreover, *in vitro* kinase assays and studies using EpoR mutants showed that Jak2 is required for STAT5 phosphorylation [138]. Transfection of several EpoR mutants in multiple cell lines demonstrated that STAT5 phosphorylation was mediated primarily through Y343, although other EpoR tyrosines could substitute for its absence [24-26]. Y401 of the EpoR was, in fact, sufficient to mediate maximal STAT5 activation (both phosphorylation and DNA binding activity) upon Epo stimulation, while Y429 and Y431 were shown to activate STAT5 to an intermediate level [25, 26]. On the other hand, cells transfected with the EpoR F8 mutant, in which all tyrosines were mutated to phenylalanine, activated STAT5 at low levels in response to high Epo

concentrations, suggesting that JAK2 could directly phosphorylate STAT5 in cells containing an EpoR without any tyrosine [24, 34].

Despite the numerous studies in cell lines, STAT5 phosphorylation at the single cell level, in primary erythropoietic tissue, has not yet been analyzed, due to technical limitations. Based on previous studies (Chapter I-11), the importance of analyzing signaling at the single cell level has emerged.

11. Signaling dynamics in biology

Previous studies have shown that a signal transduction pathway can specify multiple biological functions, in different cell contexts or within the same cell. For example, the Raf/Mek/Erk cascade can cause proliferation in tissue culture cells, differentiation or proliferation in PC12 cells [139, 140], activation of Cdc2-cyclinB complexes in oocytes [141], and fate determination in developing embryos [142]. However, it is still unknown how signaling specificity for a given downstream outcome is determined.

The dynamics of the signal, more precisely the way it varies with time and stimulus strength, could specify its function in situations where different stimuli that converge on the activation of an identical signaling molecule generate distinct functional outcomes within the same cell. For example, in PC12 cells EGF stimulation causes cell proliferation through transient Erk activation whereas NFG treatment leads to neurite outgrowth and differentiation through sustained Erk signaling [143-145]. Therefore, understanding signal dynamics could help us gain insights in the determinants of signaling specificity.

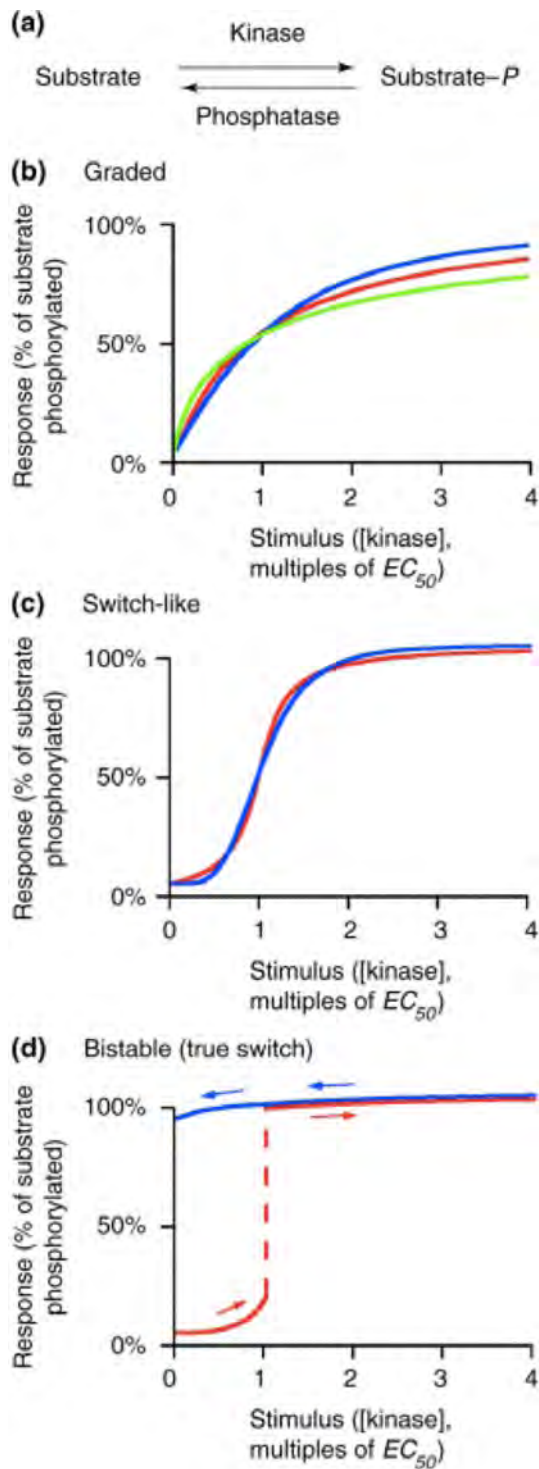
Signal characteristics can change with time (sustained versus transient signaling) and dose (graded versus switch-like response). For example, a phosphorylation/dephosphorylation reaction can exhibit a graded, switch-like or bistable response (Figure 1.7). The various types of signaling responses are described in more detail below.

A graded response is characterized by a hyperbolic stimulus response curve, described by the Michaelis-Menten equation: at low stimulus concentration the response increases linearly with the stimulus and then it levels off (Figure 1.7b). A switch-like response, on the other hand, is characterized by a sigmoidal stimulus response curve, described by the Hill equation, in which the Hill coefficient (n_H), that is bigger than 1, is an indicator of how switch-like the response is (Figure 1.7c).

A switch-like type of response has a built-in threshold: at low stimulus concentration there is almost no response, but once the threshold is reached the system flips from “off” to “on” over a very narrow range of doses (Figure 1.7d) [146]. In 1982, Goldbeter and Koshland proposed the term “ultrasensitivity” to describe systems that are characterized by a sigmoidal stimulus response curve [147]. Cooperative enzymes are the best example of an ultrasensitive system.

Figure 1.7 Summary of different types of signaling responses. (a) Scheme of the phosphorylation/dephosphorylation reaction. (b) Graded response: characterized by a hyperbolic stimulus response curve, described by the Michaelis-Menten equation. (c) Switch like response: characterized by a sigmoidal stimulus response curve, described by the Hill equation, with a Hill coefficient (n_H) bigger than one. It has a built-in threshold that determines the ultrasensitivity. Systems described by a sigmoidal response curves are defined as ultrasensitive. (d) Bistable response: characterized by ultrasensitivity and positive feedback.

Figure 1.7



Reprinted from [Trends in Biochemical Sciences], Volume 23, Ferrell JE, How regulated protein translocation can produce switch-like responses, Pages: 461-5 [148], Copyright (1998), with permission from Elsevier.

Similarly to a switch-like response, a bistable response exhibits ultrasensitivity. In addition, bistable systems are characterized by the presence of two stable states, hysteresis and a positive feedback loop [148]. Hysteresis is the memory for a transient stimulus (Figure 1.8A). When a system exhibits hysteresis, the stimulus history influences the response. In particular, the stimulus response curve varies based on whether the system was previously exposed to the stimulus or never stimulated before. In an hysteretic system it is easier to maintain the system in its stable state than to flip it from one state to the other [149]. A non-biological example of hysteresis is a light switch: once the switch is ‘on’ it is not going to switch itself ‘off’. By contrast, a non-hysteretic system, such as a doorbell, needs somebody to be continuously pushing at it, in order to be active. The positive feedback loop, which can be generated by multiple mechanisms, ensures that the system does not rest in intermediate states, and therefore contributes to the generation of two stable states.

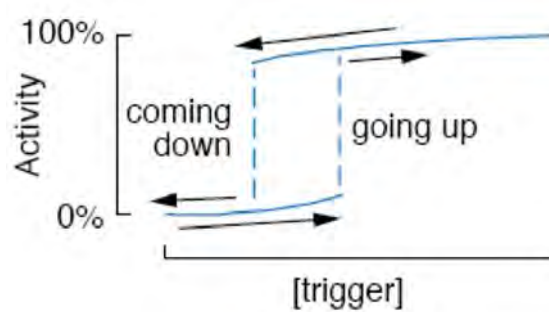
Xenopus laevis oocyte maturation is an example of a bistable system. In *Xenopus* oocytes, Erk2 activation converts a continuously variable stimulus, progesterone concentration, into an “all or none” biological response, oocyte maturation [150]. Intracellularly, Erk2 activation is bistable as a result of intrinsic ultrasensitivity and positive feedback [150-157]. Erk2 participate in the positive feedback by regulating the protein stability of its activator, Mos [158-161]. The ultrasensitivity of the cascade helps setting the threshold for the activation of the positive feedback, whose role is to ensure the oocyte does not dwell in intermediate states of Erk2 phosphorylation. A combination of ultrasensitivity and the presence of a positive feedback loop, often observed in bistable

systems, helps to filter out “noise” while allowing a decisive response (Figure 1.8B). Similar mechanisms underlie several ‘all or none’ phenomena, such the generation of action potential in neurons and the lysis-lysogeny switch in *E. Coli* infection by phage lambda [162].

Figure 1.8. Components of bistable systems. (A) Hysteresis: memory for a transient stimulus. Representation of the activity as a function of stimulus concentration: if the system has been stimulated before, it will stay on until the stimulus is decreased to a concentration that is well below (dotted line on the “coming down” curve) the one that set the system on initially (dotted line on the “going up” curve). (B) The combination of ultrasensitivity and positive feedback allows for a bistable response. The graph represents calculated stimulus response curves for MAPK phosphorylation assuming one of the two components is present, none is present or both are present. The x-axis represents the concentration of Mos, the progesterone-activated MAP kinase, which is upstream of Erk2. The y-axis represents the phosphorylation of Erk2. When none of the two components is present the response looks graded. When only ultrasensitivity is present the response is not decisive. When only positive feedback is present the system is activated by noise (lack of a threshold). When both components are present the response is decisive above a threshold of activation (set by the ultrasensitivity). The combination of the two characteristics leads to a true switch.

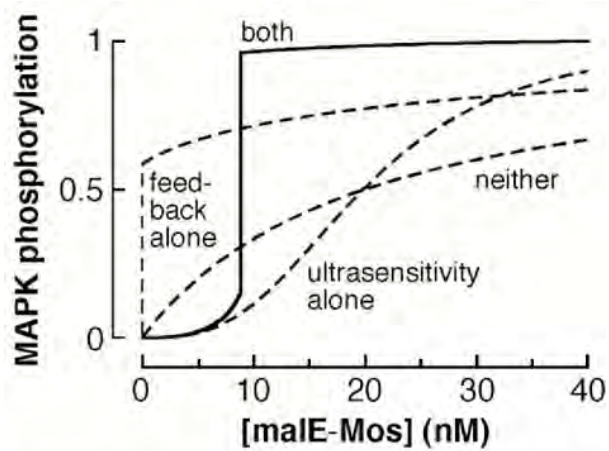
Figure 1.8

A



Reprinted from [Current Opinion in Cell Biology], Volume 14, Ferrell JE, Self-perpetuating states in signal transduction: positive feedback, double-negative feedback and bistability, Pages: 140-8 [148], Copyright (2002), with permission from Elsevier.

B



From Ferrell JE et al., The biochemical basis of an all-or-none cell fate switch in *Xenopus* oocytes, *Science*, 280: 895-8 [150], Copyright (1998). Reprinted with permission from AAAS.

The advantage of the *Xenopus laevis* oocyte system is the ability to study signal transduction at the single cell level. The response of a population of cells does not always reflect the response of individual cells, especially when the cells differ, for example, with respect to the threshold of activation. In the case of *Xenopus* oocyte maturation, at the level of the population the response to progesterone is graded, with the number of oocytes that undergo maturation being proportionally related to the amount of progesterone. However, within each oocyte the response is “all or none” [150, 163, 164].

Recent advances in flow cytometry led to the development of a new method to perform quantitative studies of cellular signaling within rare cell populations of primary cells, facilitating the study of signaling dynamics in biological systems (Chapter I.12).

12. Development of a new flow-cytometric method to study protein phosphorylation at the single cell level

The most commonly used methods to study protein phosphorylation are western blot and immunoprecipitation. However, these biochemical techniques suffer several limitations, such as requirement of a large number of cells, the inability to analyze heterogenous cell populations, and lack of single cell resolution.

The recent development of phospho-flow cytometry, a flow cytometric method used to study the phosphorylation status of signaling molecules in single cells, has revolutionized the study of cellular signaling [165-170]. This method offers several advantages compared to traditional biochemical approaches, such as 1) requirement of a small number of cells; 2) ability to discriminate cell subsets by simultaneous staining for

the cell surface markers and the phospho-protein of interest; 3) single cell resolution, which allows quantitative analysis of protein phosphorylation.

Cells are stimulated with the growth factor of interest, fixed to freeze the phosphorylation status of the signaling molecule, permeabilized to allow access of the phospho-antibody within the cell, and simultaneously stained with the phospho-antibody and antibodies against the cell surface markers of interest. One of the biggest challenges of this technique is to preserve the integrity of the cell surface markers during the fixation and permeabilization step. However, the benefits that this method offers definitely outweigh the efforts required for its optimization.

We adapted this technique to the flow cytometric method developed in our laboratory (Chapter I-2 and Chapter IV) to study STAT5 activation, at the single cell level, in freshly isolated erythropoietic tissue.

13. STAT5 and cancer

Among all the STAT molecules, STAT3 and STAT5 are frequently over-activated in cancer. STAT5 is constitutively activated in a variety of human solid tumors such as breast cancer [171, 172], head and neck cancer [173, 174]; in blood malignancies, such as chronic myeloid leukemia (CML) [175-177], acute myeloid leukemia (AML) [175, 178], acute lymphoblastic leukemia (ALL) [175, 178]; as well as in myeloproliferative disorders (MPD) [179-181]. The V617F mutation in JAK2, found in many patients with polycythemia vera (PV), has been associated with constitutive STAT5 activation [182-186].

Naturally occurring mutations in the Stat5 gene have not been identified. Constitutive STAT5 activation usually occurs downstream of over-active kinases that are the result of genetic or epigenetic abnormalities. In the *Drosophila* larvae, mutations responsible for constitutive activation of the JAK kinase hopscotch (hop^{Tum-1} and hop^{742}) allow the formation of melanotic tumors and cause a leukemia-like excessive proliferation of hemocytes [187, 188]. D-STAT, which is very similar to STAT5, is hyperactivated in hop^{Tum-1} larvae and is required for tumor formation [189, 190]. In mammals, an example of constitutively active kinase of which STAT5 is a target [122, 177, 191, 192], is the BCR-ABL kinase, a fusion protein consisting of Abelson leukaemia protein (ABL) kinase and the breakpoint-cluster region (BCR), that has been shown to cause CML [193]. The TEL-JAK fusion protein, that causes a myelo- and lympho-proliferative disease, also leads to constitutive STAT5 activation [194]. Moreover, STAT5 is constitutively activated by the FMS-like tyrosine kinase 3 (FLT3) receptor

tyrosine kinase in AML [195] and its activation is blocked by a FLT-3 specific inhibitor [196]. STAT5 is required for the BCR-ABL [197-200] and TEL-JAK mediated leukemogenesis [179]. Furthermore, a constitutively active STAT5 mutant is sufficient to cause leukemia in a bone marrow transplantation model [125, 179]. These findings suggest that STAT5 plays a very important role in leukemogenesis.

Therefore, understanding STAT5 signaling in a physiological context can help us gain insights into the regulation of its activity during malignant transformation and design targeted therapies. The currently available drugs aimed to inhibit STAT5 in leukemia are small molecule inhibitors of the upstream kinases [196, 201]. Targeting STAT proteins directly, ideally through small molecule inhibitors, will increase the treatment specificity, minimize the off-target effects and increase the efficacy.

Aims of the study

Epo concentration in serum spans three orders of magnitude from 10 milliunits/mL in the basal state, to 10 units/mL during hypoxic stress, when it drives a sharp increase in the rate of red blood cells formation (Chapter I-1). However, the mechanisms responsible for modulating the erythropoietic rate are largely unknown. Epo acts on erythroid progenitors by binding to the EpoR and initiating intracellular signaling. Among the several signaling molecules activated downstream of EpoR, STAT5 plays a central role in both basal and stress erythropoiesis (Chapter I-3 and I-9). Therefore, we hypothesized that dynamic changes in Stat5 signaling are responsible for modulating the erythropoietic rate within a broad range of Epo concentrations.

Our knowledge of STAT5 activation downstream of the EpoR, is mainly based on *in vitro* studies using cell culture systems (Chapter I-10). Previous studies exploring the dynamics of signaling in *Xenopus laevis* oocytes highlighted the importance of investigating signaling at the single cell level (Chapter I-11). However, due to technical limitations of the traditional biochemical approaches to study signal transduction (Chapter I-12) STAT5 phosphorylation at the single cell level, in primary erythropoietic tissue, has not yet been analyzed.

To understand how intracellular STAT5 signaling translates the wide range of Epo concentrations into the correct erythropoietic rate, we combined a flow-cytometric assay that allows identification of stage-specific erythroblasts in primary erythropoietic tissue (Chapter I-2 and Chapter III) with flow-cytometric measurements of STAT5 phosphorylation with single cell resolution (Chapter I-12). We aimed to define the

identity and spectrum of erythroblasts in which STAT5 is phosphorylated downstream of EpoR and to study the dynamics of STAT5 signaling during basal and stress erythropoiesis.

The significance of our study extends beyond erythropoiesis. STAT5 has been shown to play a central role in leukemogenesis (Chapter I-13). Therefore, studying the dynamics of STAT5 signaling in primary tissue could help us gain insights in the regulation of erythropoiesis as well as understand the mechanisms of malignant transformation.

The next chapter, Chapter II, represents the main body of work in this thesis. It describes the identification of two modes of STAT5 signaling in erythroblasts, digital and analog signaling, which are required for basal and stress erythropoiesis, respectively. Moreover, it investigates in detail the molecular mechanisms underlying the generation of these two modes of STAT5 signaling. The subsequent chapter, Chapter III, describes the flow cytometric method developed in our laboratory to identify erythroblasts within freshly isolated erythropoietic tissue. The last chapter summarizes the main findings and discusses future directions.

Appendix I describes the *in vivo* study of the dynamic responses of two survival pathways, the Bcl-x_L and Bim pathways, during erythropoietic stress. Moreover, it investigates the molecular mechanisms responsible for these dynamic behaviors. Bcl-x_L is a STAT5 target gene. In order to understand the molecular mechanism of Bcl-x_L response to erythropoietic stress, I investigated STAT5 signaling *in vivo* using models of acute and chronic erythropoietic stress, as well as two knock-in mice, EpoR-HM and

EpoR-H mice, which lack the cytoplasmic regulatory domain of the EpoR but differ by one essential tyrosine residue, Y343 (Chapter I-4). We found that the dynamics of STAT5 activation paralleled the one of Bcl-x_L response, although on two different time scales, indicating that STAT5 signaling behavior during erythropoietic stress dictates Bcl-x_L dynamics.

Chapter II Attributions and Copyright information

The material in this chapter has been submitted for publication in a modified format. This chapter represents original work by the authors.

Autocatalytic Activation of Stat5 Underlies Bistability and Binary Stat5 Signaling

Ermelinda Porpiglia¹, Daniel Hidalgo¹, A. Rami Tzafirri² and Merav Socolovsky^{1#}

¹Department of Pediatrics and Department of Cancer Biology, University of Massachusetts Medical School, Worcester MA 01605 USA

² Concord Biomedical Sciences and Emerging Technologies, Department of Science Services, 500 Patriot Way, Lexington, MA 02421 USA

Authorship Contributions:

EP designed and performed research, analyzed and interpreted data for all the experiments in this chapter and wrote the manuscript. DH designed and performed research. RT performed the kinetic analysis. MS designed research, analyzed and interpreted data and wrote the manuscript.

Disclosure of Conflicts of Interest:

None of the authors have any conflicts of interest to declare.

CHAPTER II: Autocatalytic activation of Stat5 underlies bistability and binary signaling

Introduction

Healthy individuals at sea level continuously generate red blood cells at a rate of 2.5 million per second, in a process known as ‘basal erythropoiesis’ that is essential to life. Erythropoiesis increases by up to 10 fold its basal rate in response to hypoxic stress, as may occur at high altitude, or in response to anemia or hemorrhage. The wide dynamic range of erythropoietic rates is regulated by the hormone Erythropoietin (Epo), whose concentration in blood spans a remarkable, three-orders of magnitude range, from ≈ 0.01 U/ml in the basal state to 10 U/ml in extreme stress. Epo exerts its effects by binding to its receptor, EpoR, a transmembrane homodimer of the cytokine receptor superfamily expressed by erythroid progenitors [20]. Epo binding to EpoR results in activation of Jak2, a cytoplasmic tyrosine kinase closely associated with the EpoR, and in phosphorylation of EpoR cytoplasmic-domain tyrosines that act as docking sites for Stat5 and other signaling molecules [202].

A key challenge lies in understanding how EpoR signaling encodes extracellular Epo concentration, specifying a given erythropoietic rate from within the wide range of rates spanning basal and stress erythropoiesis. Here we addressed this question by studying Stat5, which, as suggested by mouse genetic models, is a key mediator of both basal and stress erythropoiesis. Stat5-null mice die perinatally due to anemia, suggesting

an inability to sustain basal erythropoiesis; while mice hypomorphic for Stat5 are deficient in their response to erythropoietic stress [119, 126-128].

Stat5 functions are due to two highly homologous proteins, Stat5a and Stat5b, of the Signal Transducers and Activators of Transcription (STAT) family. STAT proteins are latent cytoplasmic transcription factors that become activated by phosphorylation of a C-terminal tyrosine in response to a variety of extracellular signals [84, 203]. Stat5 is a key mediator of cell survival in erythroblasts and other hematopoietic progenitors; it is also implicated in the regulation of the cell cycle and in leukemogenesis [119, 126-128].

Stat5 shares the conserved STAT protein domain structure. An N-terminal domain (ND) is connected via a flexible 'tether' to the molecule's core containing the DNA-binding (DBD) and a coiled-coil (CC) domains. A C-terminal SH2 domain binds to phosphorylated YXXL motifs on the activated EpoR, facilitating phosphorylation of Stat5's C-terminal tyrosine. The newly phosphorylated Stat5 (p-Stat5) dissociates from the EpoR, homodimerizes via reciprocal interactions between the C-terminal tyrosines and the C-terminal SH2 domains, and relocalizes to the nucleus where it activates transcription.

Although it has long been known that active STATs form 'parallel' homodimers, with both SH2 domains and both C-terminal tyrosines at the same end of the dimeric complex, recent crystallographic and functional studies show that inactive STATs also form dimers. However, inactive dimers are in an 'anti-parallel' conformation, with the two SH2 domains at opposite ends of the dimeric complex. The inactive anti-parallel dimers are held by reciprocal CCD and DBD interactions and by ND dimerization [80,

109]. STAT dimers do not dissociate during the phosphorylation/dephosphorylation cycle, which must therefore entail radical reorientations between the anti-parallel and parallel dimer conformations [110]. The functional implications of these conformational reorientations to the dynamics of STAT activation are not clear.

Here we set out to investigate whether the dynamic properties of the Stat5 signal, namely, the manner with which it varies with stimulus strength or with time, might somehow specify erythropoietic rate. Previously, distinct dynamic forms of both the ERK and the Ras signals have been shown to specify distinct cellular responses [204] [205]. The dynamic form of a signal, however, is often masked when measured in large populations of cells with inherently variable responses. Analysis of a signal's dynamic properties therefore requires measurement in single cells.

Here we combined a flow-cytometric assay that allows identification of differentiation-stage-specific erythroblasts in primary tissue [14, 127, 206] with single-cell flow-cytometric measurement of Stat5 phosphorylation in wild-type and mutant mice [207]. We found that Stat5 activation is bistable, a consequence of an autocatalytic interaction between active and inactive Stat5 that promotes Stat5 activation and that is mediated via the Stat5 N-terminal domain (ND). Bistable activation gives rise to a low-intensity binary Stat5 signal in mature erythroblasts, that is both necessary and sufficient for mediating Stat5 functions in basal erythropoiesis. By contrast, stress levels of Epo generate a much higher, graded Stat5 signal unique to early erythroblasts. We show that higher Stat5 expression is the key factor that allows p-Stat5 to increase beyond its low-intensity bistable activation level in early progenitors during stress. The combination of a

low-intensity but decisive, bistable signal in response to basal Epo, together with a further graded increase in p-Stat5 in response to stress, ensures high fidelity Stat5 signaling throughout the wide basal and stress range of Epo concentrations. Further, based on our results, we expand the previously proposed hypothesis suggesting STAT conformational reorientation during its phosphorylation/dephosphorylation cycle [110]. We propose that the ND of active Stat5 molecules facilitates this conformational reorientation *in trans*, underlying autocatalysis and bistability.

Results

Flow cytometric measurement of phosphorylated-Stat5 (p-Stat5) in primary erythroblasts

Murine erythropoiesis takes place in fetal liver between embryonic days 12 (E12) and 15, and in adult bone marrow and spleen. We used cell-surface markers CD71 and Ter119 to identify stage-specific erythroid progenitors directly within primary tissue [14, 206, 208]. The CD71/Ter119 epitopes are preserved following cell fixation and permeabilization, which are required in order to measure intracellular p-Stat5 (Figure 2.1A). This allowed us to sub-divide fetal liver into several erythroid differentiation subsets, labeled S0 to S3 (Figure 2.1A left panel). The earliest erythroid progenitors are found in the S0 subset, where they form $\approx 70\%$ of all S0 cells. Subsets S1 to S3 are composed entirely of Epo-dependent erythroblasts, with the least mature in S1 and the most mature in S3; the S3 subset is further divided into earlier, large cells and later, small cells (Figure 2.1A). Intracellular Stat5 activation was measured following cell fixation and permeabilization with an AlexaFluor 647-conjugated antibody directed against the tyrosine-phosphorylated Stat5. An Epo-dependent p-Stat5 signal was obtained in wild-type, but not in Stat5^{-/-}, fetal liver (Figure 2.1B, upper panels). Further, the p-Stat5 signal was lost if, following Epo stimulation, fixed cells were incubated with λ phosphatase (Figure 2.1B, lower panels). Therefore, the p-Stat5 signal is specific to the active, phosphorylated-Stat5. Work below (Figure 2.9A) also confirmed, with the use of a Stat5 mutant, that the signal is specific to the phosphorylated, C-terminal Y694 residue.

Erythroid maturation determines the p-Stat5 response

We stimulated freshly isolated fetal liver cells with Epo and examined the resulting p-Stat5 response (Figures 2.1C-E, 2.2A). Specifically, we measured three aspects of the p-Stat5 fluorescence signal (Figure 2.1C). First, ‘total p-Stat5’ corresponds to the p-Stat5 median fluorescence intensity (MFI) of the entire cell population in a subset; the total p-Stat5 MFI of all the S3 cells in the red histogram, upper panel of Figure 2.1C, is 1200 fluorescence units. This measure includes both signaling and non-signaling cells in the subset. Second, we measured the number of ‘p-Stat5 positive’ (p-Stat5⁺) cells, or the fraction within the p-Stat5⁺ gate (Figure 2.1C, lower panel), as an estimate of the number of signaling cells within the subset. The placement of the p-Stat5⁺ gate was determined by reference to the baseline, pre-stimulation histogram (black histogram, Figure 2.1C lower panel), which was closely similar to that of cells stained with an AlexaFluor 647-conjugated isotype-control antibody in place of the anti-p-Stat5 antibody. Last, we measured the ‘p-Stat5 in p-Stat5⁺ cells’, which estimates the p-Stat5 MFI in signaling cells only (Figure 2.1C lower panel, where p-Stat5 in p-Stat5⁺ cells is 1700 fluorescence units).

We examined the p-Stat5 response to Epo at 15 minutes post stimulation, when a peak response is attained and persists for 15-30 minutes (see time course of activation, Figure 2.2B). The p-Stat5 signal intensity was clearly dependent on erythroblast maturation stage, being highest in S1, and decreasing with erythroid maturation through subsets S2 and S3. In the earliest, S0 subset, only ~25% of cells responded to Epo, suggesting that the p-Stat5 response to Epo is enabled with the onset of Epo dependence at the transition

from S0 to S1 (Figures 2.2A, 2.2C; [208]). We contrasted the detailed responses of earlier, S1 cells with those of more mature, S3 cells. Figure 2.1D shows the p-Stat5 response, measured as delineated in Figure 2.1C, to Epo concentrations spanning the physiological (<0.05 U/ml) and hypoxic-stress range (0.05 to 10 U/ml). S1 cells generated a graded increase in total p-Stat5 (Figure 2.1D, upper panel), which reflected a graded increase in both the number of signaling cells (p-Stat5⁺ cells, Figure 2.1D middle right panel) as well as in the MFI of signaling S1 cells (Figure 2.1D, lower right panel). By contrast, the highest total p-Stat5 MFI attained by ‘S3 large’ (=‘S3’) cells was ≈4 fold lower than in S1. Although S3 cells also showed a graded increase in total p-Stat5 MFI with Epo stimulation, this was principally a result of a graded increase in the number of p-Stat5⁺ cells, while the p-Stat5 MFI of signaling p-Stat5⁺ cells showed relatively little variation (Figure 2.1D lower panel). A summary of five independent experiments for all erythroid subsets shows that these dose/response characteristics are reproducible, and that the decrease in total p-Stat5 signal intensity from S1 to S3 occurs gradually as cells mature (Figure 2.1E).

Figure 2.1 The p-Stat5 response in fetal liver.

(A) Flow cytometric method of identifying differentiation-stage-specific erythroblasts directly in freshly isolated fetal liver. Fetal livers from E13.5 embryos were fixed and permeabilized in preparation for intracellular p-Stat5 measurements, and labeled with antibodies directed at cell-surface CD71 and Ter119. Subsets S0 to S4 (left histogram) contain erythroblasts of increasing maturation, as seen from the morphological appearance of cytopsin cell preparations from each subset (stained with Giemsa and diaminobenzidine). The right histogram shows the further division of S3 cells into small and large subsets based on the flow-cytometric ‘forward scatter’ parameter.

(B) Specificity of the Alexa 647-conjugated anti-p-Stat5 antibody (BD Biosciences # 612599). Upper panels: response of S1 cells from either wild-type or Stat5^{-/-} fetal livers to Epo stimulation (2 U/ml) for 15 minutes (red histograms). Blue histograms are baseline fluorescence in the absence of Epo. Lower panels: Epo-stimulated (2 U/ml; 15 minutes, red histograms) or unstimulated (blue histograms) S1 cells in wild-type fetal liver, either treated or untreated with λ-phosphatase prior to p-Stat5 staining. Numbers in all panels indicate the fraction (%) of p-Stat5⁺ cells within the indicated horizontal gates.

(C) Illustration of the three measures used to analyze the p-Stat5 response to Epo stimulation (9 U/ml, 15 minutes, red histogram) in S3-subset erythroblasts. The black histogram corresponds to pre-stimulation cells of the same subset.

(i) ‘total p-Stat5 median fluorescence intensity (MFI)’ (upper panel): the p-Stat5 MFI of the entire S3-subset population, represented by the shaded red histogram. This measure does not distinguish between signaling and non-signaling cells. The black histogram corresponds to the unstimulated S3 subset population.

(ii) ‘p-Stat5⁺ cells(%)’ (lower panel): cells within the p-Stat5⁺ gate, shaded in red, expressed as a fraction (percent) of all cells in the Epo-stimulated S3 subset. This is an estimate of the number of signaling cells. The placement of the p-Stat5⁺ gate was determined by reference to the baseline, pre-stimulation histogram (in black), so that no more than 1% of the unstimulated population is included within the p-Stat5⁺ gate.

(iii) '*p-Stat5* in *p-Stat5*⁺ cells' (lower panel): estimates the p-Stat5 MFI in signaling cells only.

(D) Response of cells in subsets S1 and S3 to stimulation with Epo. Freshly isolated fetal liver cells were deprived of Epo for 90 minutes and were then stimulated with a range of Epo concentrations as indicated, from 0.004 to 9 U/ml, for 15 minutes. Colored flow-cytometry histograms correspond to Epo-stimulated cells, black histograms in each panel correspond to unstimulated cells (Epo=0). An overlay of the responses is shown in the two lowest panels.

For each Epo concentration, three measures of the p-Stat5 response, as illustrated in 'C', are noted next to each flow-cytometry histogram in blue, black and green, corresponding to the total p-Stat5 MFI, to the p-Stat5⁺ cells (%), and to the p-Stat5 in p-Stat5⁺ cells, respectively. Each of these measures is then plotted as a function of Epo concentration (right panels); the color of each symbol in these plots corresponds to the color of the respective flow-cytometry histogram for the same Epo concentration.

(E) The p-Stat5 response to a range of Epo concentrations at 15 minutes post stimulation. Summary of five independent experiments similar to 1D. Data (mean ± SE) for each experiment were normalized by expressing each p-Stat5 MFI reading as a ratio to the p-Stat5 MFI in p-Stat5⁺ cells of the 'S3 large' subset following stimulation with 1 U/ml Epo for 15 minutes. Data in the upper two panels were fitted with Hill curves.

Figure 2.1

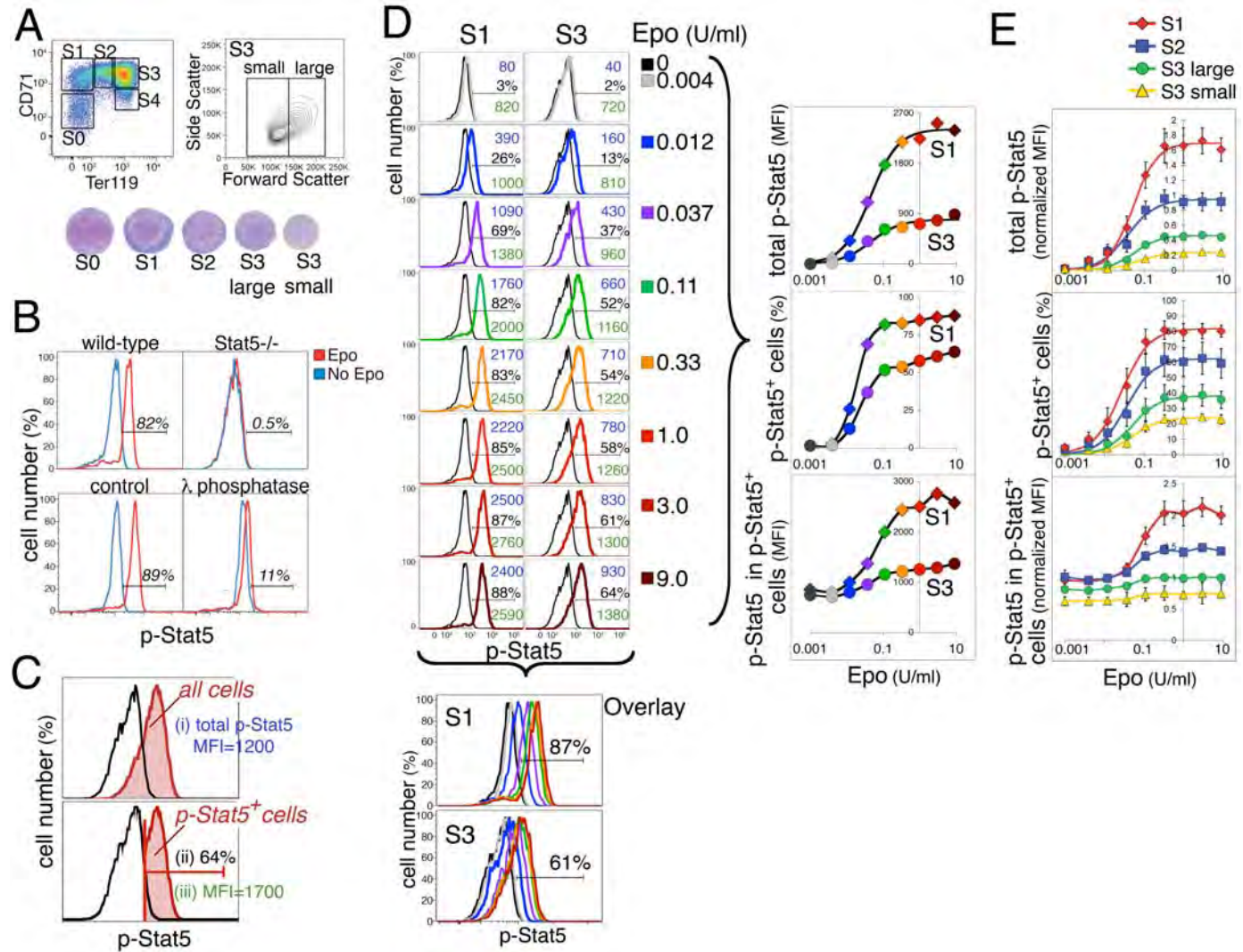


Figure 2.2: The p-Stat5 response in fetal liver and in adult tissue.

(A) The p-Stat5 response of fetal liver subsets S0 to S3 to Epo (2 U/ml, 15 minutes). Freshly isolated fetal liver cells were deprived of Epo for 90 minutes and were then stimulated. Cells were labeled for CD71, Ter119 and p-Stat5.

(B) Time-course of the p-Stat5 response to Epo (2 U/ml for up to 6 hours). Each of the three measures used to assess the p-Stat5 response (Figure 2.1C) is plotted versus time. Representative of 5 similar experiments.

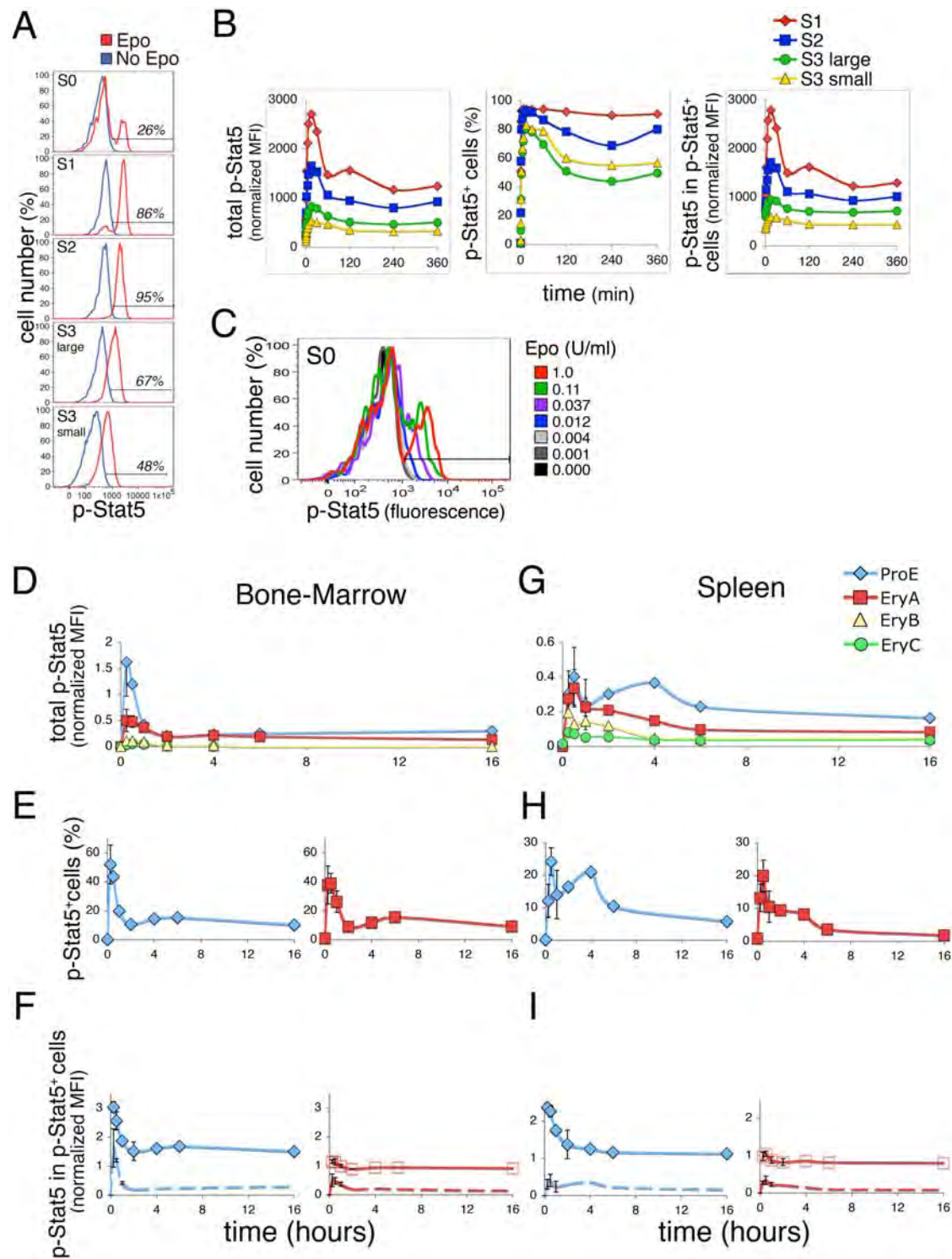
(C) Representative responses of S0 cells to stimulation with a range of Epo concentrations for 15 minutes. Flow-cytometry histogram overlay is shown. Even at the highest Epo concentrations, only 20 to 30% of S0 cells are responsive to Epo. For responding cells, the p-Stat5 MFI increases with Epo concentration, in the manner seen for S1 cells.

(D-I) Time course of the p-Stat5 response to Epo stimulation *in vivo*, in adult mouse bone-marrow and spleen. Mice were injected with Epo (300U/25g mouse subcutaneously). Bone marrow and spleen were harvested at the indicated time points for up to 16 hours following injection, and cells were immediately fixed, permeabilized and labeled for CD71, Ter119 and p-Stat5. Erythroid subsets in adult mouse bone-marrow or spleen may be defined by flow cytometry using cell surface Ter119 and CD71 (Figures 1.1B, 3.2A; [14]). Cells in subsets ProE→EryA→EryB→EryC contain cells of increasing maturity. The maturation stage of ProE resembles that of S2 in fetal liver and the maturation stage of EryA resembles that of S3.

(D-F) Bone-marrow subsets; **(G-I)** Spleen subsets; **(D)**, **(G)** total p-Stat5 response; **(E)**, **(H)** p-Stat5⁺ cells; **(F)**, **(I)** p-Stat5 in p-Stat5⁺ cells (solid lines). For comparison, the dashed lines show the total p-Stat5 response data from **(D)**, **(G)**, respectively.

Data is pooled from four independent experiments. Each time point is the mean \pm sem of data from two to four mice. MFI data is normalized as follows: background MFI in the absence of Epo is subtracted, and the remainder MFI is expressed as a ratio to MFI of p-Stat5⁺ cells in bone-marrow EryA at time=1 hour for each experiment.

Figure 2.2



Binary and Graded Stat5 signaling coexist in developing erythroblasts

The intensity of the p-Stat5 signal within signaling S3 cells (p-Stat5 MFI in p-Stat5⁺ cells) remained relatively constant in spite of wide variation in the number of responding cells (Figure 2.1E, lower panel). We found similar behavior in maturation-stage equivalent cells in adult tissue (Figure 2.2 D-I). These observations raised the possibility that S3 cells may be generating a binary p-Stat5 response. Under this hypothesis, individual S3 cells would either express their maximal p-Stat5 levels regardless of Epo concentration (and be ‘on’), or fail to respond and remain ‘off’; they would not assume intermediate levels of p-Stat5 stably. A binary p-Stat5 response in single cells may nevertheless result in a graded response at the population level. This is illustrated in Figure 2.3A, which contrasts three hypothetical cases of signaling cells. In the first case (Figure 2.3A left panels), there is a graded increase in signal within individual cells in response to increasing Epo concentration, resulting in a graded increase in the total p-Stat5 MFI at the population level. The two hypothetical cases of binary signaling (Figure 2.3A, middle and right panels) differ only in the Epo threshold at which cells respond with a p-Stat5 signal. In the ‘variable threshold’ example, individual cells vary substantially with respect to the Epo concentration at which they switch from ‘off’ to ‘on’. At the population level, this results in a graded p-Stat5 response to increasing Epo concentration. The corresponding flow-cytometry histograms at each Epo dose (in color) are a composite of two underlying histograms, of non-signaling cells (in grey) and signaling cells (in black). Only the amplitudes of the black and grey histograms change with Epo concentration, while their MFI remains constant. However, the MFI of

the composite, color histogram, representing the total p-Stat5 response for all subset cells, increases gradually with Epo dose. In the second binary signaling example (Figure 2.3A, right panels), cells have a similar threshold to Epo stimulation, so that the entire cell population switches from ‘off’ to ‘on’ within a narrow range of Epo concentrations. This results in the population response resembling the binary responses of individual cells, with a much steeper Epo dose/p-Stat5 response curve that is characterized by a high Hill coefficient ($n_H > 1$).

The graded p-Stat5 response of the S3 population does not therefore preclude the possibility that individual S3 cells have binary responses that are masked by variable response thresholds (as in Figure 2.3A, middle panel). We found, however, that binary p-Stat5 signaling became apparent at the population level, in a manner resembling the ‘similar threshold’ example, when we examined p-Stat5 signaling in the EpoR-HM mutant mouse (Figure 2.3 B-E).

Figure 2.3. Binary p-Stat5 signaling in EpoR-HM erythroblasts.

(A) Contrasting graded and binary signaling responses: three hypothetical examples.

In a graded signaling response (left panels), increasing Epo concentration results in a graded increase in p-Stat5 in individual cells, represented by increasingly darker shades of grey. Simulations of the corresponding flow-cytometric profiles show that increasing Epo concentration causes a gradual shift of the p-Stat5 fluorescence histogram to the right. A plot of the total p-Stat5 median fluorescence intensity (MFI) vs. Epo concentration has Michaelian kinetics with a Hill coefficient (n_H) of 1 (lower left panel, please note a log scale was used for the x-axis).

In binary signaling (middle and right panels), the p-Stat5 signal in individual cells can only assume two states, either ‘off’ (white) or ‘on’ (black), but intermediate states (shades of grey) are unstable. Two distinct cases of binary signaling are illustrated, that differ in their threshold responses.

In ‘variable threshold’ (middle panels), the threshold at which Epo causes a cell to switch from ‘off’ to ‘on’ varies substantially between cells of the population. Consequently, increasing Epo concentration causes a gradual increase in the number of cells that are p-Stat5⁺ (‘on’). The simulated flow-cytometric histograms at each Epo concentration (in color) are each the sum of two histograms, corresponding to cells that are ‘off’ (light grey histograms) and cells that are ‘on’ (black histograms). The median fluorescence of the ‘on’ and ‘off’ histograms remain unaffected by Epo concentration, but as Epo increases, the number of cells in the ‘on’ histogram, reflected by its height, increases, with a corresponding decrease in the height of the ‘off’ histogram. Although individual cells have binary responses, there is a graded increase in the MFI of colored histogram representing the whole population. Therefore, a plot of total p-Stat5 MFI vs. Epo concentration shows a graded response and has a low Hill coefficient (here, $n_H=1$).

In the case of cells with binary responses and similar threshold (right panels), cells switch from ‘off’ to ‘on’ within a much narrower Epo concentration range. Consequently, the response of the whole population reflects the response of individual cells more closely. Flow-cytometric histograms representing the population tend to be in

one of two principal positions, corresponding to the ‘on’ or to the ‘off’ states. A plot of total p-Stat5 MFI vs. Epo concentration is steep, reflected by a high Hill coefficient (n_H , > 1).

(B) Representation of the cytoplasmic domains of wild-type EpoR, or its truncated mutants, EpoR-H and EpoR-HM. Tyrosine residues are represented by red lines. Tyrosine 343 is the only remaining tyrosine in EpoR-H, and is mutated in EpoR-HM.

(C) The p-Stat5 response to Epo (2 U/ml, 30 minutes) in S1 cells from wild-type (WT), EpoR-H (H) or EpoR-HM (HM) fetal livers on E13.5. Percentage of cells in the p-Stat5⁺ gate is indicated.

(D) Fluorescence p-Stat5 histogram overlay of S1 cells from E13.5 wild-type (top) or EpoR-HM (bottom), stimulated with a range of Epo concentrations for 30 minutes. Representative of 3 similar experiments. S1 cells in each case are pooled from several fetal livers of the same genotype.

(E) Top left panel: plots of ‘p-Stat5 MFI vs. Epo concentration’, in wild-type or EpoR-HM S1 cells; the p-Stat5 MFI data corresponds to the histograms shown in ‘D’. Data is fitted with Hill curves.

Top right panel: Hill curves that were fitted to the data in ‘D’ as in the top left panel, but shown as a fraction of the maximal p-Stat5 response ($p\text{-Stat5}_{\max}$). The $p\text{-Stat5}_{\max}$ was calculated from fitting the Hill equation to the experimental ‘total p-Stat5’ data. Hill coefficients (n_H) are indicated.

Lower panel: table summarizing the Hill coefficients (n_H) obtained by fitting the Hill curve to plots of ‘total p-Stat5 vs Epo concentration’, for each of subsets S1 to S3, in each of three independent experiments. Fetal liver cells were pooled from 3 or 4 embryos of each genotype in each experiment. Differences between n_H for EpoR-HM and WT are significant at $p=0.01$, paired t test. ‘ r^2 ’ is Pearson’s product moment correlation coefficient, correlating experimental data with values predicted by the Hill equation for the corresponding Epo concentrations.

Figure 2.3

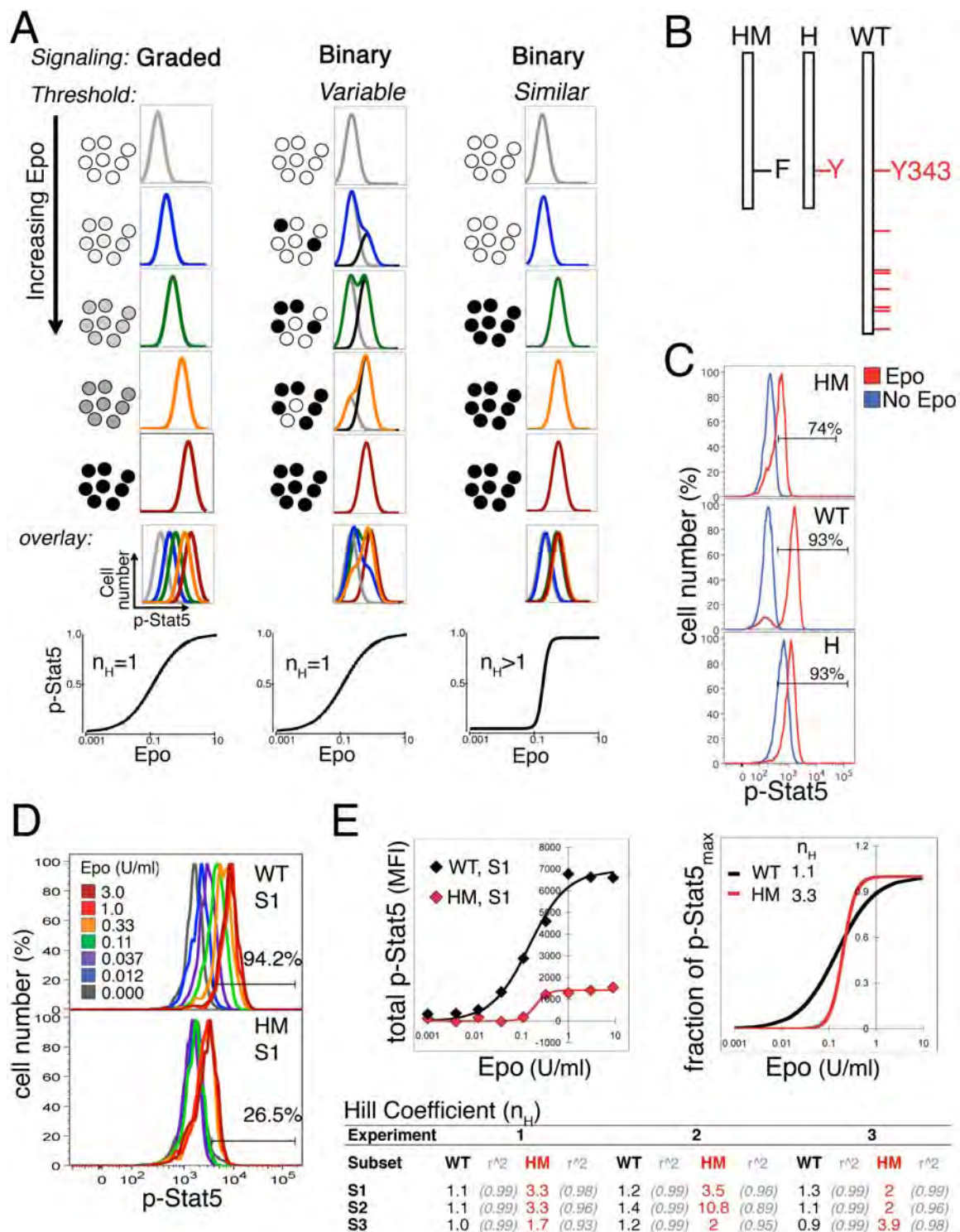


Figure 2.4: Binary p-Stat5 signaling in EpoR-HM erythroblasts.

(A) Representative plots of ‘total p-Stat5 versus Epo concentration’ for subsets S1 to S3 in wild-type (left panel) and EpoR-HM (right panel) fetal liver. This experiment was also illustrated in Figure 2.3D.

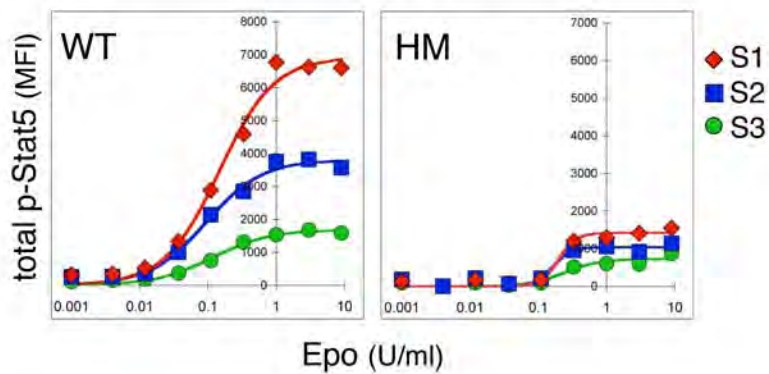
(B) Values for p-Stat5_{max} and apparent K_m obtained by fitting Hill curves to plots of ‘total p-Stat5 MFI vs. Epo concentration’ of the type illustrated in ‘A’. The Hill equation was used as follows:

$$\text{p-Stat5} = \frac{(\text{p-Stat5}_{\text{max}})S^n}{(K_m)^n + S^n}$$

Where S = Epo concentration in U/ml, and ‘p-Stat5’ is the total p-Stat5 fluorescence; best fit was obtained by varying n (= Hill coefficient), K_m (=the apparent K_m) and p-Stat5_{max} (=the maximal p-Stat5 response to high Epo), using the solver function of Microsoft Excel. ‘r²’ is Pearson’s product moment correlation coefficient, correlating experimental data with values predicted by the Hill equation for the corresponding Epo concentrations. The Hill coefficients and r² values for this analysis are shown in Figure 2.3E. Differences between K_m and p-Stat5_{max} were all significant (paired t-test, p=0.003 and 0.023, respectively).

Figure 2.4

A



B

Experiment	1			2			3		
K_m (apparent)									
Subset	WT	HM	Fold change	WT	HM	Fold change	WT	HM	Fold change
S1	0.15	0.2	1.3	0.11	0.32	2.9	0.06	0.4	6.7
S2	0.09	0.16	1.8	0.08	0.3	3.8	0.06	0.53	8.8
S3 large	0.1	0.24	2.0	0.1	0.34	3.5	0.1	0.68	9.1
$pStat5_{max}$									
	WT	HM	Fold change	WT	HM	Fold change	WT	HM	Fold change
S1	6943	1422	4.9	6870	1833	3.7	1828	554	3.3
S2	3810	1042	3.7	3535	1124	3.1	1206	417	2.9
S3 large	1685	729	2.3	2032	957	2.1	585	168	3.5

EpoR-HM erythroblasts generate only binary low-intensity p-Stat5 signal

We studied p-Stat5 signaling in the EpoR-H and EpoR-HM mouse strains, in which the respective EpoR truncation mutants are ‘knocked-in’ at the wild-type EpoR locus, replacing wild-type EpoR (Figure 2.3B, [46]). EpoR-H lacks seven of the eight cytoplasmic domain tyrosines. The remaining tyrosine, Y343, a Stat5 docking site, is mutated to phenylalanine in EpoR-HM, which therefore lacks tyrosine docking sites for Stat5.

S1 cells from EpoR-H fetal livers generated a p-Stat5 signal equivalent to that of wild-type cells, but had a high background of p-Stat5 in the absence of Epo stimulation, consistent with a previously-identified negative regulatory function for the carboxy-terminal domain (Figure 2.3C, lower panel; [209]). S1 cells from EpoR-HM fetal liver, by contrast, generated only a low intensity p-Stat5 response to Epo, consistent with previous studies (Figure 2.3C, upper panel; [25]). A full Epo dose/p-Stat5 response analysis revealed that the maximal p-Stat5 signal generated by S1 cells in EpoR-HM was \approx 3-4 fold lower than in wild-type S1, resembling in intensity p-Stat5 signals generated by more mature, wild-type S3 cells (Figures 2.3D, 2.3E upper left panel, 2.4A). Strikingly, in addition to their lower p-Stat5 intensity, the EpoR-HM S1 response was binary, resembling the hypothetical example of binary signaling in a population of cells with similar Epo thresholds (Figure 2.3A, right panels). Thus, unlike wild-type S1, the p-Stat5 fluorescence histograms in EpoR-HM S1 are in one of two clusters, either ‘off’ or ‘on’ (Figure 2.3D, lower panel). This binary behavior was reflected in the steep Epo dose/ p-Stat5 response curve for EpoR-HM S1 cells (Figure 2.3E upper panels). In each of 3

independent experiments, the Hill coefficients found for each of the EpoR-HM subsets were consistently higher than in wild-type controls (Figure 2.3E, lower panel), with n_H for S1 cells ranging between 2 and 3.5. Taken together, S1 cells in EpoR-HM have lost the high intensity graded signaling mode characteristic of this subset. The residual signal is of low intensity, similar to that of S3 cells, and is binary in nature.

The maximal p-Stat5 response (p-Stat5_{max}) is linearly correlated with Stat5 expression levels

We investigated factors that might account for the gradual decrease in the p-Stat5 response as cells mature (Figure 2.1E). The transition from subset S1 to ‘S3 small’ takes 24 to 48 hours *in vivo* [206, 208] and entails large changes in gene expression. We examined the potential role of established Stat5 regulators, and found that neither SOCS3 (Figure 2.5) nor SHP1 [210] (Figure 2.6) regulate the peak intensity of the p-Stat5 response. We also examined the potential role of changes in EpoR or Stat5 expression during erythroblast maturation. To this end we investigated embryos heterozygous for either Stat5 or EpoR (Figure 2.7). An Epo dose/ p-Stat5 response analysis in fetal liver cells from Stat5^{+/-} embryos showed a clear decrease in the p-Stat5 signal across the entire Epo concentration range compared with wild-type controls (see representative example in Figure 2.7A; data from the entire dataset of 7 Stat5^{+/-} and 6 wild-type littermates embryos is summarized in Figure 2.7B). Fitting Hill curves to the dose/ response data yielded the apparent K_m, the maximal p-Stat5 signal at high Epo concentrations, defined as ‘p-Stat5_{max}’, and the Hill coefficient, n_H (Figure 2.8A). In addition to the clear decrease in p-Stat5_{max} in all subsets of the Stat5^{+/-} fetal liver (Figures 2.7A and B, 2.8A), the p-Stat5 response curve was steeper, reflected in a higher Hill coefficient (Figure 2.7B).

We also examined the Epo dose/p-Stat5 response in fetal livers derived from EpoR^{+/-} embryos and their littermate controls (Figure 2.7C). We found an approximately 2-fold decrease in EpoR mRNA in EpoR^{+/-} fetal livers (Figure 2.8B). Unlike the Stat5^{+/-} embryos, there was no change in p-Stat5_{max} in EpoR^{+/-} fetal liver, suggesting that cell-

surface EpoR is not limiting for the maximal p-Stat5 response. Instead, the EpoR^{+/-} dose/response curves were shifted to the right, with a 2-fold increase in the apparent K_m (Figures 2.7C, 2.8C), suggesting that a doubling in Epo concentration compensated for the reduced expression of EpoR.

To assess the relation between Stat5 expression and the maximal p-Stat5 response more precisely, we measured total Stat5 protein levels in individual cells within each of the Stat5^{+/-} and wild-type embryos, using anti-Stat5 antibodies and flow cytometry (Figures 2.7D, 2.8D). Stat5 expression decreased with maturation, being highest in S1 and 4 fold lower in 'S3 large' cells (Figure 2.7D, closed symbols). A similar pattern was observed in Stat5^{+/-} embryos, but for each corresponding subset, Stat5 expression was approximately halved compared with wild-type cells (Figure 2.7D open symbols). There was a linear correlation ($R^2=0.85$) between Stat5 expression levels and the maximal p-Stat5 response (p-Stat5_{max}) across all subsets in both wild-type and Stat5^{+/-} embryos (Figure 2.7E; p-Stat5_{max} was determined by fitting a Hill curve to data from each embryo). These findings suggested that decreased Stat5 expression caused the decrease in the p-Stat5 response with cell maturation, as well as the reduced p-Stat5_{max} in Stat5^{+/-} embryos.

Figure 2.5 SOCS3 regulation of Stat5 signaling.

(A) Real time PCR for SOCS3 in sorted S0-S3 subsets from wild type embryos (E13-E14.5). The left graph shows SOCS3 mRNA relative to β actin (mean \pm SE), calculated from 3 independent experiments. The right graph shows the Δ Ct \pm SE for each individual experiment.

(B) Fetal liver cells were electroporated with SOCS3 siRNA or with 'scrambled' control siRNA. Four hours later the cells were stimulated with Epo and collected at different time points. The time course of the p-Stat5 response is shown (two independent experiments (top and bottom)).

(C) Fetal liver cells were treated as in 'B'. Real time PCR for SOCS3 mRNA at the indicated times is shown (mean \pm SE).

Figure 2.5

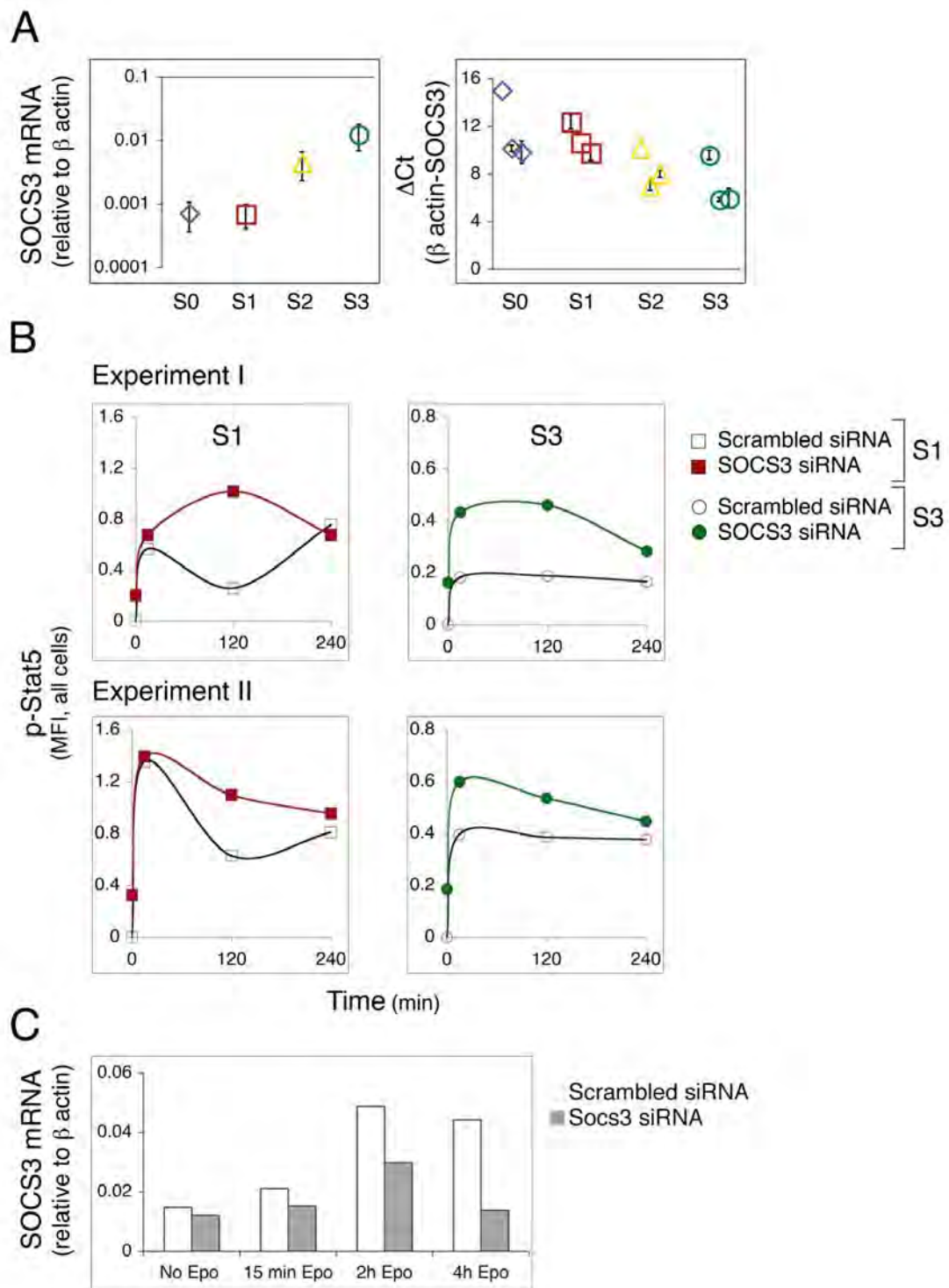


Figure 2.6 Stat5 signaling in Shp1^{-/-} fetal liver.

(A) Real time PCR for Shp1 in sorted S0-S3 subsets from wild type embryos (E12.5-E13.5). The left graph shows Shp1 mRNA relative to β actin (mean \pm SE), calculated from 3 independent experiments. The right graph shows the Δ Ct \pm SE for each individual experiment.

(B) Epo dose/p-Stat5 response analysis in Shp1^{-/-} fetal liver fitted with Hill curves. Data (mean) from 2 independent experiments each with one embryo of each genotype.

(C) Time course of p-Stat5 response to Epo stimulation with 0.2U/ml, in Shp1^{-/-} embryos (n=5) and in matched controls (n=3). Data points are measurements in individual embryos.

Figure 2.6

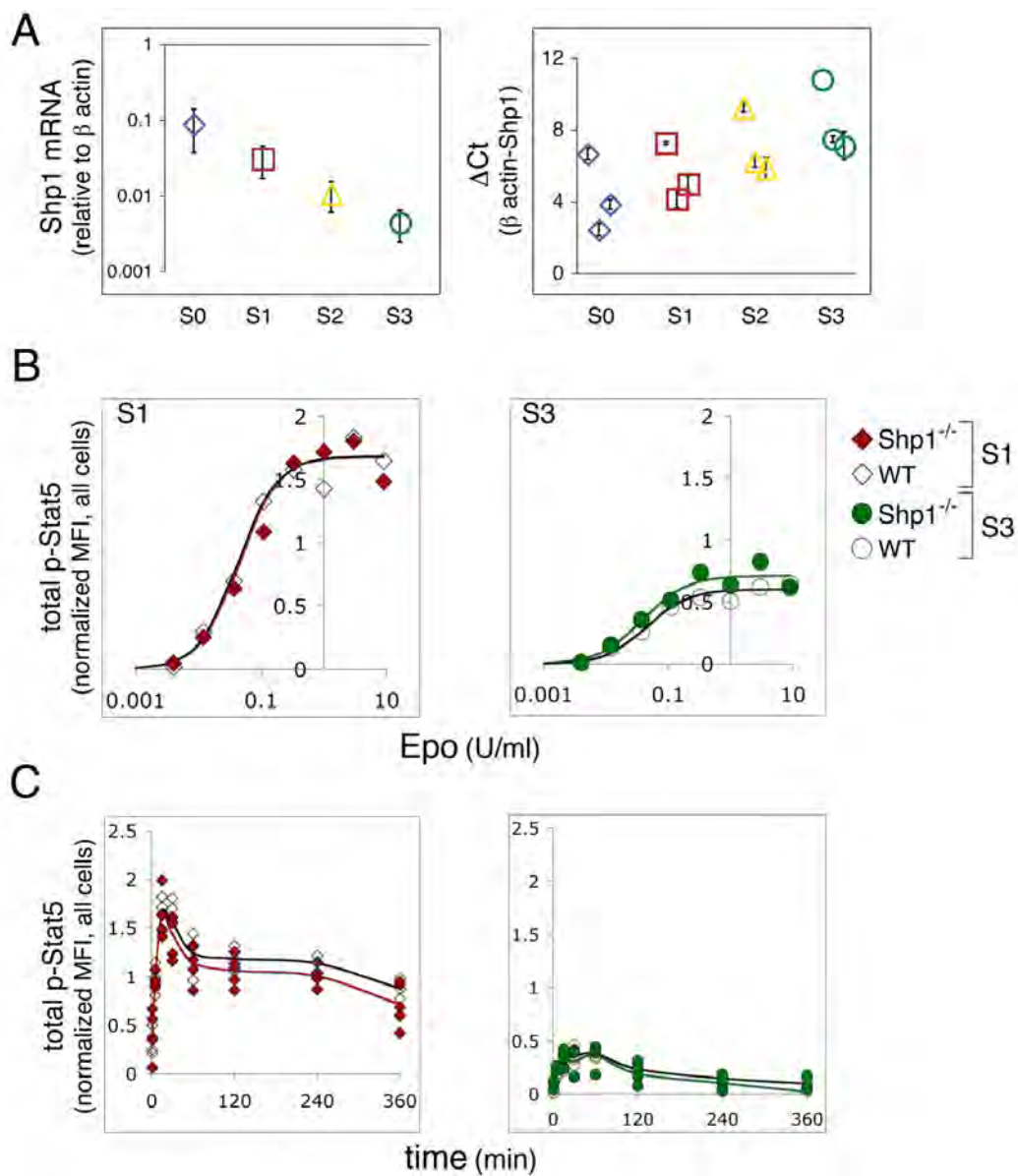


Figure 2.7 The maximal p-Stat5 response ($p\text{-Stat5}_{\max}$) is linearly correlated with Stat5 expression levels.

(A) The p-Stat5 response of S1 cells from Stat5^{+/-} fetal liver and from littermate wild-type controls. Representative p-Stat5 fluorescence histograms are shown for the indicated Epo concentrations.

(B) Plots of ‘total p-Stat5 vs. Epo concentration’ in Stat5^{+/-} and in wild-type littermate fetal livers in experiments similar to ‘A’, fitted with Hill curves. Data (mean \pm SE) from n= 7 Stat5^{+/-} embryos and 6 littermate controls, each analyzed separately. p-Stat5 MFI was normalized as in Figure 2.1E. Parameter values used for fitting the Hill curves and goodness of fit information are in Figure 2.8A.

(C) Plots of ‘total p-Stat5 vs. Epo concentration’ in EpoR^{+/-} and in wild-type littermate fetal livers, fitted with Hill curves. Data (mean \pm SE) from n=4 EpoR^{+/-} embryos and 3 littermate controls, each analyzed separately. p-Stat5 MFI was normalized as in Figure 2.1E. Parameters values used for fitting the Hill curves and goodness of fit information are in Figure 2.8C.

(D) Stat5 protein expression in subsets S1, S2 and S3 in wild-type or Stat5^{+/-} embryos. Individual data points correspond to data from individual embryos. Stat5 protein was measured by flow-cytometry, and is expressed as a ratio to the average fluorescence signal for S1 cells in all wild-type embryos. The assay was verified using Stat5^{-/-} embryos, see Figure 2.8D.

(E) Linear correlation between Stat5 protein expression and $p\text{-Stat5}_{\max}$, across all subsets in Stat5^{+/-} and wild-type embryos ($R^2=0.85$). Data points correspond to individual embryos. Stat5 protein expression as in ‘D’. $p\text{-Stat5}_{\max}$ was determined by fitting Hill curves to individual embryo ‘total p-Stat5 vs. Epo concentration’ analyses, with p-Stat5 normalized as in Figure 2.1E.

Figure 2.7

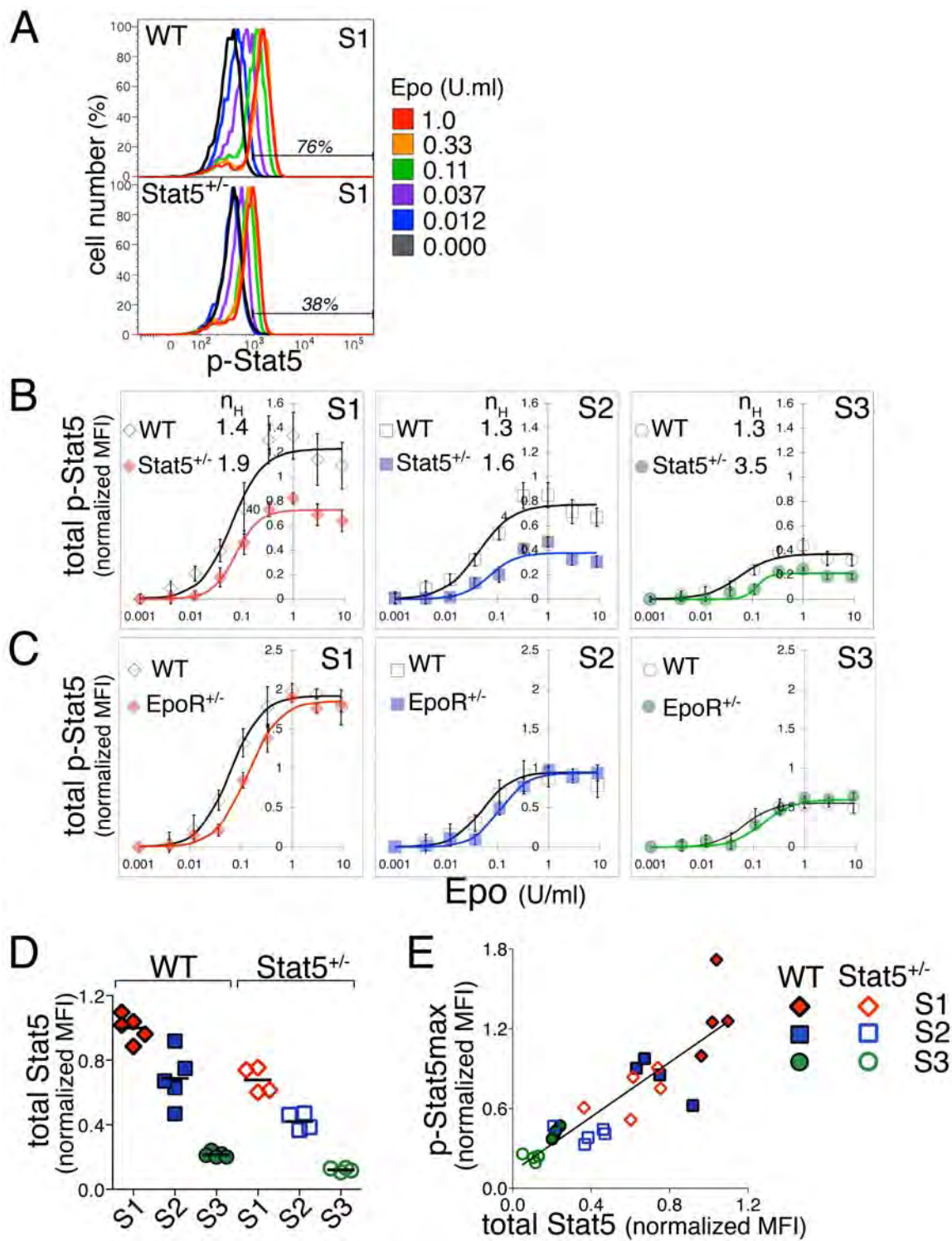


Figure 2.8 Analysis of Stat5 phosphorylation in Stat5^{+/-} and EpoR^{+/-} embryos.

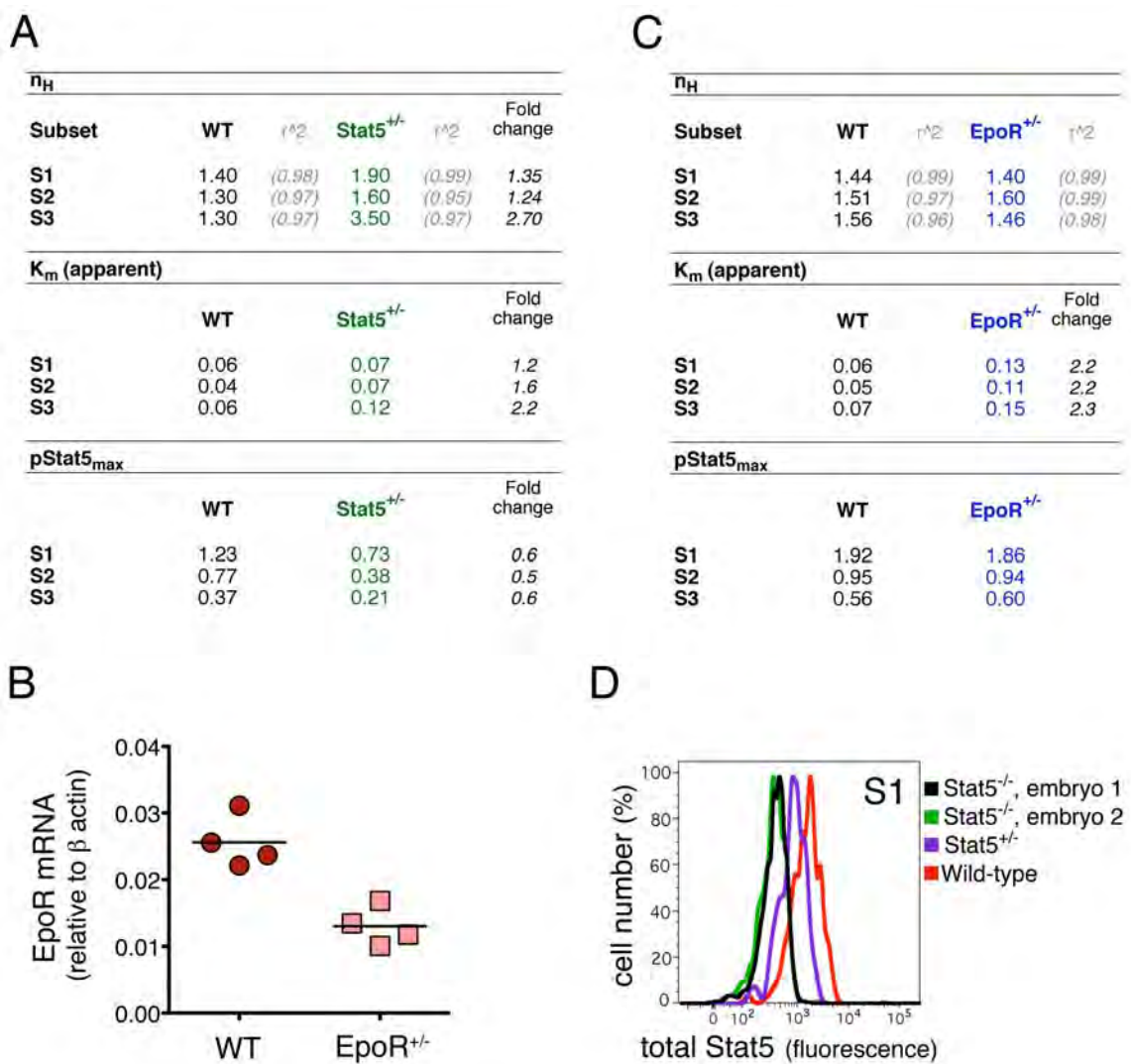
(A) Values for the Hill coefficients, p-Stat5_{max}, and apparent K_m, obtained by fitting Hill curves (see legend to Figure 2.4B) to the plots of ‘total p-Stat5 MFI vs. Epo concentration’ shown in Figure 2.7B. Note a substantially lower p-Stat5_{max} in Stat5^{+/-} embryos. Data is derived by fitting the Hill curve through the mean values obtained from the means of a total of 7 Stat5^{+/-} and 6 control embryos, analyzed independently. ‘r²’ is Pearson’s product moment correlation coefficient, correlating experimental data with values predicted by the Hill equation for the corresponding Epo concentrations.

(B) EpoR mRNA was measured using quantitative RT-PCR in fetal livers of wild type (red circles) or EpoR^{+/-} (pink squares) embryos (E13.5). Data points represent measurements in individual embryos, and are expressed relative to β actin mRNA. Mean values for each genotype are denoted with a black line.

(C) Values for the Hill coefficients, p-Stat5_{max}, and apparent K_m, obtained by fitting Hill curves (see legend to Figure 2.4B) to the plots of ‘total p-Stat5 MFI vs. Epo concentration’ shown in Figure 2.7C. Note doubling of the apparent K_m in EpoR^{+/-} embryos. Data is derived by fitting the Hill curve through the mean values obtained from the means of a total of 4 EpoR^{+/-} and 3 control embryos, analyzed independently. ‘r²’ is Pearson’s product moment correlation coefficient, correlating experimental data with values predicted by the Hill equation for the corresponding Epo concentrations.

(D) Measurements of Stat5 protein using flow-cytometry. Fixed and permeabilized fetal liver cells were labeled with CD71, Ter119, and with a rabbit polyclonal antibody which recognizes Stat5 regardless of its state of activation, and with a secondary anti-rabbit IgG antibody conjugated to APC. Flow cytometry histograms reflecting total Stat5 protein expression (as APC fluorescence) are shown for two Stat5^{-/-} embryos (these provide the non-specific background fluorescence); and for one wild-type and one Stat5^{+/-} embryo. Stat5 expression in Figure 2.7D, E was determined as Stat5 MFI, with background fluorescence subtracted, and expressed as a ratio to the average Stat5 MFI of S1 cells.

Figure 2.8



Exogenous Stat5 expression rescues graded high intensity p-Stat5 signaling in EpoR-HM erythroblasts and wild-type S3 cells

To test whether the loss of the high-intensity p-Stat5 response in mature, S3 cells is indeed due to their decreased Stat5 expression (Figure 2.7E), we asked whether we could rescue high-intensity Stat5 signaling in these cells by exogenously expressing Stat5. In parallel, we also examined the effect of exogenous Stat5 expression in EpoR-HM erythroblasts, which signal exclusively via the low-intensity binary signaling mode (Figure 2.3 D-E). We electroporated FLAG-tagged Stat5a constructs ('FLAG-Stat5'), control FLAG-tagged Stat5aY694F ('FLAG-Stat5Y694F') lacking the C-terminal tyrosine, or 'empty vector' control ('pcDNA3'), into freshly isolated wild-type or EpoR-HM fetal liver. Cells were incubated overnight in the presence of Epo (0.2 U/ml), to allow expression of the transduced constructs. Cells were deprived of Epo for 3 hours prior to their stimulation with a range of Epo concentrations (0.004 to 9 U/ml). Cells were then fixed and labeled with both anti-FLAG and anti-p-Stat5 antibodies. A single electroporation contained cells with a spectrum of FLAG expression levels, allowing us to determine how FLAG-Stat5 expression affected the p-Stat5 response (Figures 2.9, 2.10). We noted that in the absence of Epo stimulation, cells expressing the highest levels of FLAG-Stat5 nevertheless contained p-Stat5 (Figure 2.9A, top left panel, double-headed arrows). This constitutive p-Stat5 signal was specific, since it was absent in cells expressing equivalent levels of FLAG-tagged Stat5Y694F, which cannot be tyrosine phosphorylated (Figure 2.9A, middle left panel). This phenomenon is further addressed below (Figure 2.12). In response to stimulation with Epo, there was an increase in p-

Stat5, with the highest response in cells expressing the highest levels of FLAG-Stat5 (Figure 2.9A, top middle panel). To analyze the p-Stat5 response quantitatively for each FLAG-Stat5 expression level, we sub-divided the ‘p-Stat5 vs. FLAG-Stat5’ dot plots for EpoR-HM into narrow vertical gates, each of which contained cells with similar FLAG-Stat5 expression (Figure 2.9B, left panels). Three of these vertical gates, numbered 10 to 12, are color coded in red, green and blue respectively, in three examples of cells stimulated with Epo concentrations of 0 U/ml (top left panel), 0.33 U/ml (middle left panel) or 9 U/ml (bottom left panel). Panels to the right show an overlay of responses to the three Epo concentrations in each of the red, green or blue vertical gates. The entire p-Stat5 response data set to nine Epo concentrations in each of 4 vertical gates (9 to 12) for EpoR-HM is plotted in the lower panel of Figure 2.9B, fitted with Hill curves. A similar analysis for wild-type S3 cells is shown in Figure 2.10A.

Inspection of the Epo dose/p-Stat5 response curves for wild-type (Figure 2.10A) and EpoR HM erythroblasts (Figure 2.9B) shows that they are altered by exogenous FLAG-Stat5 in two ways. First, the maximal response ($p\text{-Stat5}_{\text{max}}$) in a given vertical gate was positively and linearly correlated with the level of FLAG-Stat5 expression in that gate (Figures 2.9C, 2.10B). Second, as FLAG-Stat5 expression increased, there was a decrease in the steepness of the p-Stat5 response curves, as reflected by decreasing Hill coefficients (Figures 2.9B, lower right panel for EpoR-HM, and 2.10A, lower right panels for wild-type S3 cells). As examples, the high FLAG-Stat5 expression (MFI=1700) in gate 12 gave rise to a higher $p\text{-Stat5}_{\text{max}}$ (MFI=1100) and a lower Hill

coefficient ($n_H=1.4$) than in gate 9, where a lower FLAG-Stat5 expression (MFI=340) resulted in a lower p-Stat5_{max} (MFI=120) and a high Hill coefficient ($n_H=2.5$).

Therefore, by varying the level of exogenous Stat5 expression in a single cell type (wild-type S3 cells, or EpoR-HM S3 cells), we were able to generate the entire spectrum of Stat5 signaling responses encountered in the erythroblast maturation series (Figure 2.1E). Taken together, the data in Figures 2.7, 2.9 and 2.10 show that decreasing Stat5 expression with erythroblast maturation is the cause of the gradual shift from high-intensity, graded signaling in early erythroblasts to low intensity, binary signaling in mature erythroblasts.

The loss of high-intensity Stat5 signaling in EpoR-HM shows that, in addition to high Stat5 expression, this mode of signaling also requires Stat5 docking sites on the EpoR. Exogenous expression of Stat5 successfully compensated for the EpoR-HM mutation, however, rescuing high-intensity graded signaling in these cells (Figure 2.9).

The linear dependence of p-Stat5_{max} on Stat5 expression levels, whether endogenous (Figure 2.7E) or exogenous (Figures 2.9C, 2.10B), indicates that Stat5 is limiting for Stat5 phosphorylation in erythroid cells. A theoretical analysis of this finding is provided below.

Figure 2.9 High exogenous Stat5 levels rescue high-intensity graded p-Stat5 signaling in EpoR-HM cells.

(A) The p-Stat5 response to Epo in S3 cells expressing exogenous FLAG-Stat5. Wild-type fetal liver cells were electroporated with either FLAG-tagged Stat5a (=FLAG-Stat5, C-terminal tag, top panels), FLAG-tagged Stat5Y694F (middle panels) or ‘empty vector’ (pcDNA3, lower panels). Following overnight incubation in the presence of Epo (0.2 U/ml), cells were deprived of Epo for 3 hours, and then either left unstimulated (left panels) or were stimulated with Epo for 30 minutes (response to 9 U/ml is shown here, middle panels; altogether 9 different Epo concentrations were examined, ranging from 0.04 to 9 U/ml, and are shown in panel B and in Figure 2.10). Double-headed arrows indicate Epo-independent p-Stat5, seen only in cells expressing high levels of FLAG-Stat5.

(B) Analysis strategy for the experiment described in panel ‘A’; results for EpoR-HM S3 erythroblasts are shown here; results for wild-type S3 are in shown Figure 2.10. Dot plots of the p-Stat5 response vs. FLAG-Stat5 expression are shown for 3 of the nine Epo concentrations examined (left panels; Epo= 0, 0.33 or 9 U/ml). For analysis, these dot plots were sub-divided into narrow vertical gates, each containing cells of similar FLAG-Stat5 expression. Three of these gates, numbered 10 to 12, are highlighted in red, green and blue. Data from each of the three red gates (gate 10) were overlaid in a single histogram (top right histogram, highlighted in red). This histogram therefore contains the p-Stat5 responses to a range of Epo concentrations, of cells expressing similar FLAG-Stat5 levels (580 ± 13 , $\text{MFI} \pm \text{SE}$). A similar analysis was carried out for each of the nine Epo concentrations for cells in gate 10, and the ‘total p-Stat5 response’ to each Epo concentrations were plotted and fitted with a Hill curve (red symbols and curve, lowest right panel). A similar analysis was carried out for each of the other vertical FLAG-Stat5 gates; Hill coefficients are indicated next to the Hill curve for each gate. Data points in the ‘total p-Stat5 vs. FLAG-Stat5’ plots are mean \pm sem for cells in each gate. Each of the ‘total p-Stat5’ MFI measurements was corrected by subtracting background

fluorescence, given by the ‘total p-Stat5’ MFI of cells expressing FLAG-Stat5Y694F in the same gate.

(C) Linear correlation between FLAG-Stat5 expression and p-Stat5_{max} in EpoR-HM S3 cells ($R^2=0.998$); analysis is of data shown in ‘B’. p-Stat5_{max} is the maximal p-Stat5 response to Epo, defined by the Hill equation in Figure 2.4 and obtained by fitting Hill curves to data in ‘B’, lower right panel, for each of the indicated vertical FLAG expression gates.

Figure 2.9

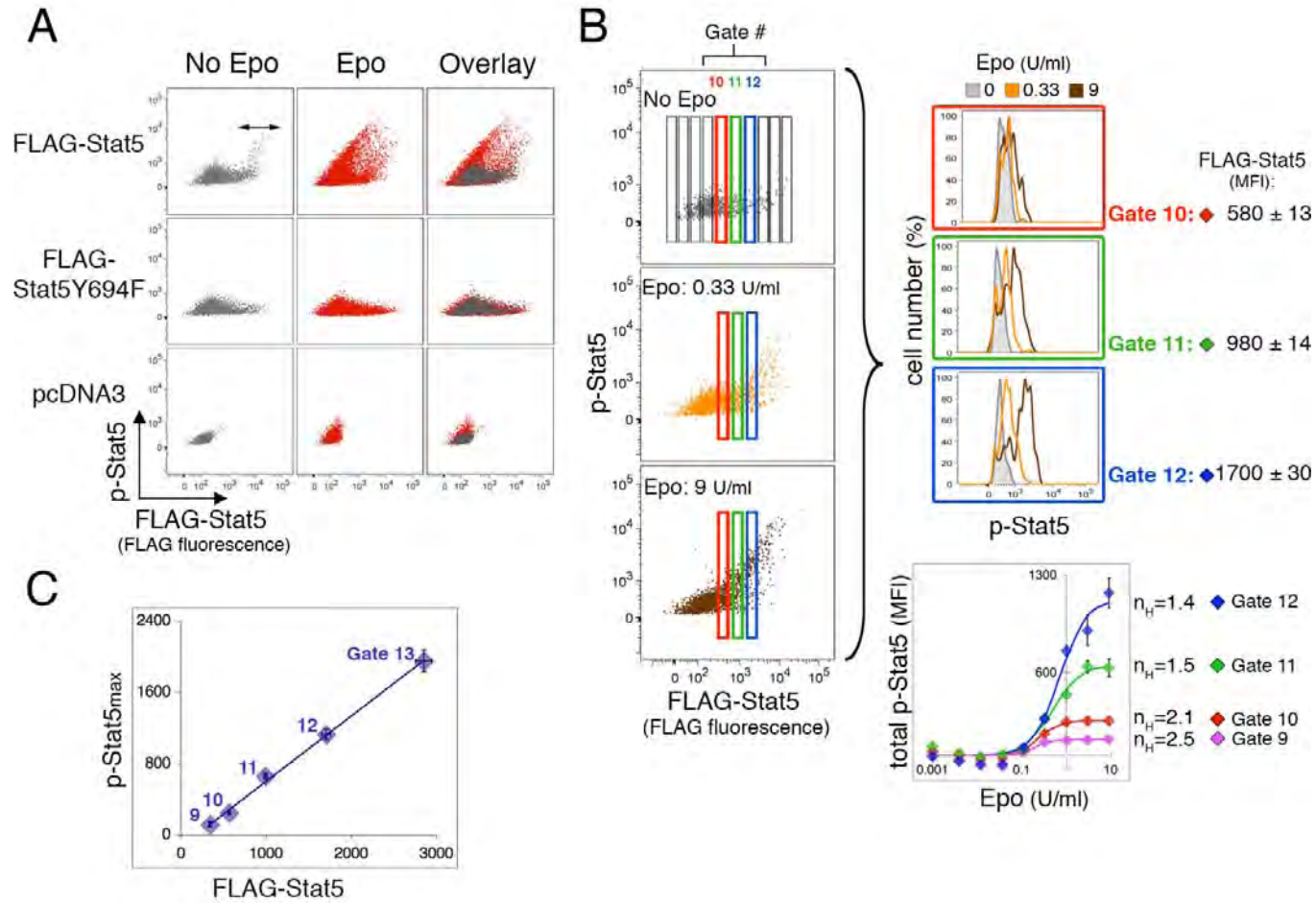


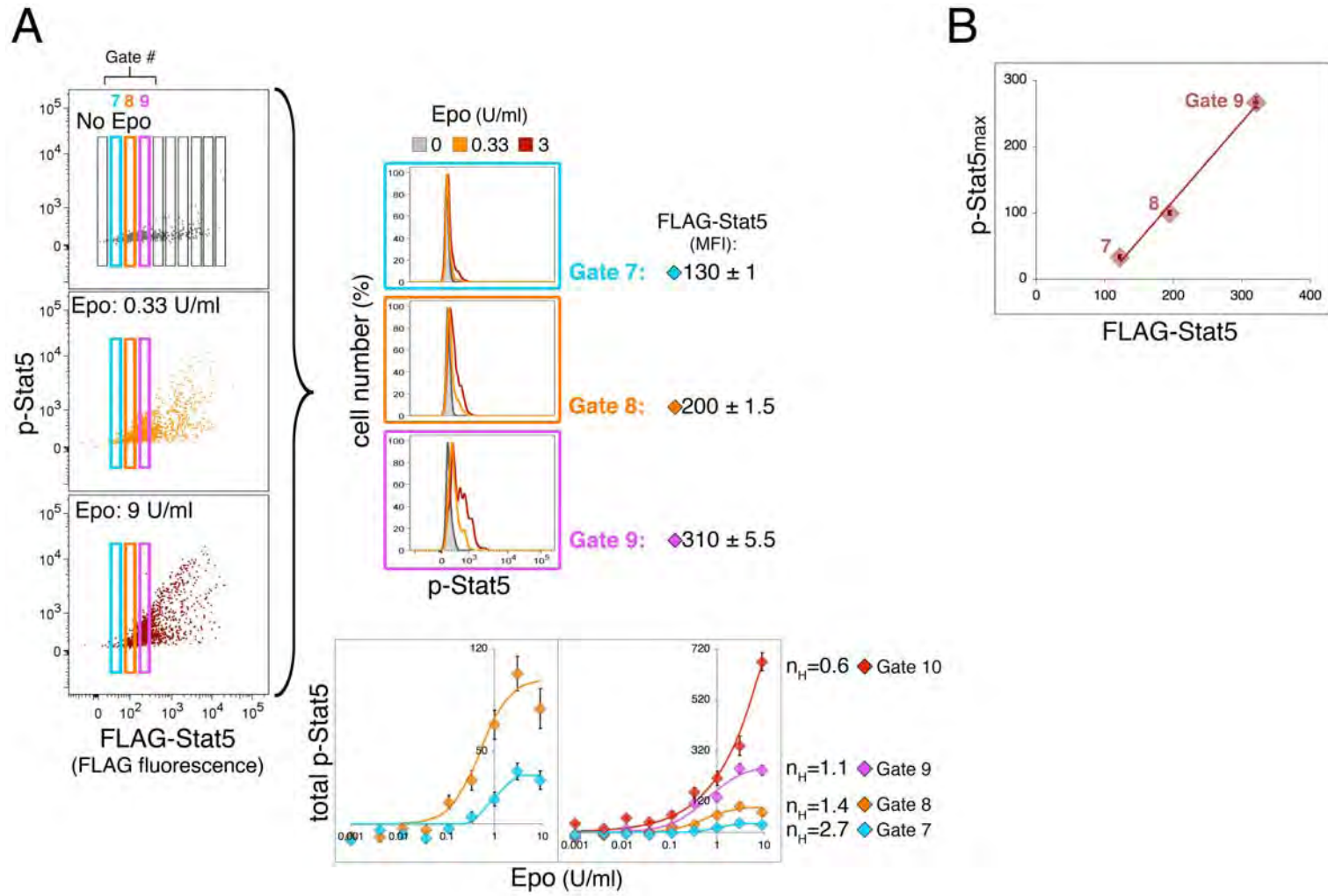
Figure 2.10: High exogenous Stat5 levels rescue high-intensity graded p-Stat5 signaling in wild-type S3 cells.

Experiment as described in Figure 2.9A.

(A) The p-Stat5 response of wild type S3 cells expressing exogenous FLAG-Stat5, to three Epo concentrations. Vertical gate analysis as described for EpoR-HM erythroblasts in Figure 2.9B. Hill plots for cells in vertical FLAG-Stat5 gates numbered 7 and 8 are shown twice, with different y-axis scales. Data points in Hill plots are mean \pm sem for cells in each gate.

(B) Linear correlation between FLAG-Stat5 expression and p-Stat5_{max} in wild-type S3 cells ($R^2=0.96$); analysis is of data shown in 'A'. p-Stat5_{max} is the maximal p-Stat5 response to Epo, defined by the Hill equation in Figure 2.4 and obtained by fitting Hill curves to data in 'A', lower right panel, for each of the indicated vertical FLAG expression gates.

Figure 2.10



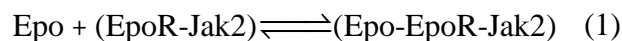
Cellular Stat5 is limiting during Stat5 phosphorylation in erythroid cells

Our data shows that maximal p-Stat5 produced in response to Epo dosing (= 'p-Stat5_{max}') is linearly related to total cellular Stat5 (Figures 2.7E, 2.9C, 2.10B). This linear relationship is maintained across all erythroid progenitor stages and over a wide range of cellular Stat5 expression levels, whether endogenous, or exogenously introduced into cells. By contrast, p-Stat5_{max} is not affected by the reduced number of cell-surface EpoRs in EpoR^{+/-} cells (Figure 2.7C). It is also apparently unaffected by the decrease in cell-surface EpoRs known to occur with progenitor differentiation [13], since introduction of exogenous Stat5 into late erythroid progenitors increases p-Stat5_{max} linearly with cellular Stat5.

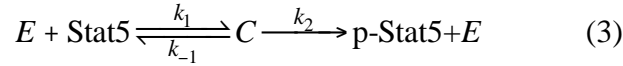
These findings suggest that the limiting parameter for p-Stat5_{max} is cellular Stat5, rather than the number of cell-surface EpoRs. Therefore, conditions of substrate excess, required for Michaelis-Menten kinetics, do not apply to Stat5 phosphorylation in erythroid cells. Instead, the analysis below shows that our results are consistent with conditions of enzyme excess. Under such conditions, maximal product formation is linearly related to initial substrate concentration [211, 212].

Analysis:

Epo binds a pre-formed complex of EpoR and Jak2, to form an active enzyme complex, or 'E':



The activated enzyme complex ‘ E ’ binds Stat5, to form an enzyme-substrate complex ‘ C ’, which phosphorylates Stat5:



Let initial Stat5 concentration be denoted as ‘ S_0 ’ and the concentration of the product, p-Stat5, as ‘ P ’. From reaction (3), the rate of p-Stat5 formation, dP/dt , is provided by

$$\frac{dP}{dt} = k_2 C \quad (4)$$

If the active enzyme concentration is in great excess of ‘ S_0 ’, that is, $E \gg S_0$, then reaction (1) is essentially independent of reaction (3). Namely, the binding of Stat5 to E will not appreciably decrease E from its value as set by reaction:

$$E \approx E_0 \quad (5)$$

where E_0 is the initial active enzyme concentration¹. More generally, this assumption holds whenever the fraction of substrate-bound enzyme is negligible: $\frac{C}{E} \ll 1$; such

conditions arise not only at pure enzyme excess, $E \gg S_0$, but also under the weaker

requirement that, $E + K_m \gg S_0$, where $K_m = \frac{k_{-1} + k_2}{k_1}$ is the Michaelis-Menten constant

of reaction (3) [212].

Under these conditions,

$$C = \frac{E_0(S_0 - P)}{K_m + E_0} \quad (6)$$

¹ Note that strictly speaking E_0 is not the initial active enzyme concentration, but the equilibrium concentration implied by reaction (1).

From (4), (5) and (6), the rate of formation of p-Stat5 ($=P$) is given by

$$\frac{dP}{dt} = k_2 \frac{E_0(S_0 - P)}{K_m + E_0} \quad (7)$$

If we let $K = \frac{k_2 E_0}{K_m + E_0}$, equation (7) now becomes

$$\frac{dP}{dt} = K(S_0 - P). \quad (8)$$

From (8), and the initial condition $P = 0$, the concentration of the product, p-Stat5 increases with time as

$$P = S_0(1 - e^{-Kt}) \quad (9)$$

Equation (9) is in agreement with our observations in Figures 2.7E and 2.9C, that the maximal value for P , 'p-Stat5_{max}', obtained by fitting the Hill equation to the Epo dose/p-Stat5 response data (when a relative steady state is reached, ≈ 15 minutes after the onset of Epo stimulation), is independent of E_0 and K_m and is a linear function of the initial Stat5 substrate concentration, S_0 . Therefore, our observations are consistent with the initial assumption of this analysis that the active enzyme complex is in excess of cellular Stat5 concentration.

Distinct biological functions of the binary and graded Stat5 signaling modes

Mice lacking Stat5 die perinatally of severe anemia [68, 119, 126]. By contrast, EpoR-HM mice, which retain only the low-intensity binary p-Stat5 signal, are viable with near-normal basal erythropoiesis. Therefore, the low intensity binary p-Stat5 signal is sufficient to support essential Stat5 functions in basal erythropoiesis. EpoR-HM mice are, however, deficient in their response to erythropoietic stress, a deficit that, by comparison

with the normal stress phenotype of the EpoR-H mouse (Figure 2.3B), was attributed to the absence of the Y343 Stat5 docking site on the mutant EpoR-HM receptor [47]. Therefore, the high intensity Stat5 signal absent in EpoR-HM may be specifically required during stress. We examined these possibilities by studying two established Stat5 functions: its anti-apoptotic effect in erythroblasts, required in both basal and stress erythropoiesis [126, 127, 213]; and its induction of the transferrin receptor (CD71), which transports iron for hemoglobin synthesis [134, 214].

We first examined the role of Stat5 signaling in erythroblast survival, by incubating freshly isolated fetal liver cells from either EpoR-HM, Stat5^{-/-}, or strain-matched wild-type embryos, in the absence of Epo for 90 minutes. We then labeled the cells with Annexin V, to detect cells undergoing apoptosis. A large fraction (40%) of Stat5^{-/-} S1 cells, but only 1-2% of wild-type controls, were Annexin V positive, confirming that Stat5 is essential to erythroblast survival. The level of apoptosis of EpoR-HM cells, however, was low and similar to that of wild-type controls (Figure 2.11A, representative examples in left panels, summary of several experiments in right panels). Therefore, the low-intensity, binary Stat5 signal is sufficient for mediating Stat5's anti-apoptotic function in EpoR-HM erythroblasts, and for maintaining basal erythropoiesis.

To examine the erythropoietic stress response, we administered adult EpoR-HM mice, or wild-type control mice, with a single subcutaneous injection of Epo (100U/ 25 g mouse) that generates stress-levels Epo concentrations *in vivo*. As previously reported [46], the EpoR-HM mice failed to increase their hematocrit (Figure 2.11B, left upper panel). The erythropoietic response to high Epo entails upregulation of erythroblast cell-

surface CD71 [14], a Stat5 target [134, 214]. We found that Epo injection caused a 2 to 3-fold increase in cell surface CD71 of wild-type Ter119^{high} CD71^{high} spleen erythroblasts, but failed to generate an increase in erythroblasts from EpoR-HM mice (Figure 2.11B, duplicate experiments in upper right panel, flow-cytometry contour plots in lower panels). We have found above that the high intensity Stat5 signal, missing in EpoR-HM erythroblasts, can be rescued in these cells by high exogenous Stat5 expression (Figure 2.9B). We therefore asked whether rescue of the high-intensity Stat5 signal might also restore high CD71 expression to EpoR-HM erythroblasts. EpoR-HM or wild-type fetal liver cells were electroporated with either FLAG-Stat5 or with control FLAG-Stat5Y694F, as illustrated in Figure 2.9A. Cell-surface CD71 was measured by flow cytometry following overnight culture in the presence of stress Epo levels (0.2 U/ml). We found that rescue of high-intensity p-Stat5 signaling to EpoR-HM erythroblasts by exogenous FLAG-Stat5 (Figure 2.9B), also restored their high CD71 expression (Figure 2.11C). There was no change in CD71 expression as a result of exogenous expression of the inactive, FLAG-Stat5Y694F mutant. These findings strongly suggest that CD71 upregulation by Stat5 is a function specifically mediated by the high-intensity graded Stat5 signal during the erythropoietic response to stress.

Figure 2.11 Biological functions of binary and graded Stat5 signaling.

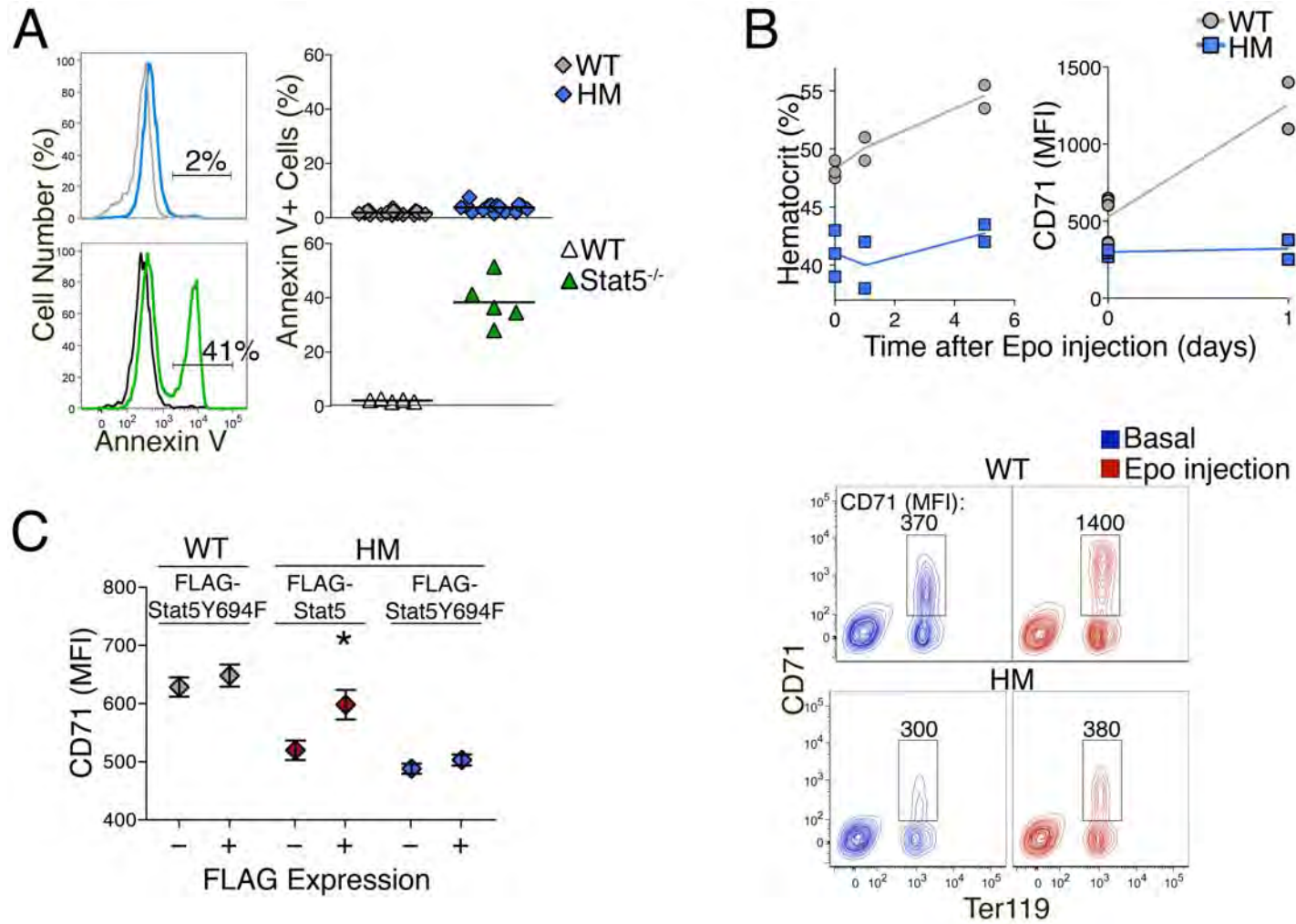
(A) Increased erythroblast apoptosis in Stat5^{-/-} but not in EpoR-HM fetal liver. Freshly harvested fetal livers from E13.5 Stat5^{-/-} or from EpoR-HM embryos and from matched controls were incubated in the absence of Epo for 90 minutes. Cells were then labeled with 7-AAD to exclude dead cells, and with Annexin V, CD71 and Ter119 to assess apoptosis. Representative histograms are shown for S1 cells in EpoR-HM (top left panel) or Stat5^{-/-} (bottom left panel) fetal liver: cells shown have preserved membrane impermeability to the DNA dye 7-AAD. Summary of Annexin-V⁺ cells in 3 independent experiments is shown in right panels; each data point corresponds to an individual embryo, black line represents the mean for all embryos of a given genotype. Number of embryos analyzed: EpoR-HM=15, strain and age matched controls= 20; Stat5^{-/-}=5, littermate controls=5. No statistically significant difference was detected between EpoR-HM and control embryos; the difference between Stat5^{-/-} and control embryos is significant (p=0.0007, 2 tailed t test, unequal variance).

(B) Adult EpoR-HM mice fail to generate an erythropoietic stress response. Adult EpoR-HM mice or strain-matched wild-type mice were injected with Epo (100 U/ 25g mouse). Hematocrit measurements are shown in top left panel. Expression level of CD71 (expressed as MFI) in CD71^{high}Ter119^{high} splenocytes are summarized in the top right panel. Each data point represents an individual mouse. A representative example of flow-cytometric CD71 measurement one day post-injection is shown in the contour plots in the lower panel. Numbers in lower panel are the CD71 MFI of cells in the indicated CD71^{high}Ter119^{high} gate.

(C) Rescue of stress-induced CD71 upregulation in EpoR-HM fetal liver cells after rescue of high-intensity graded p-Stat5 signaling by transduction with high levels of FLAG-Stat5. EpoR-HM or wild-type fetal liver erythroblasts were transduced with either FLAG-Stat5 or FLAG-Stat5Y694, as described in Figure 2.9A. Cells were incubated overnight in the presence of stress-levels of Epo (0.2 U/ml; this is 6 to 10 fold the Epo basal levels), and were then labeled and analyzed for CD71, Ter119 and FLAG expression by flow-cytometry. CD71 (MFI) is compared in cells negative for FLAG

expression (FLAG gate 6 or lower, Figure 2.9B) with cells expressing high levels of FLAG (FLAG gate 10 or higher, Fig 2.9B), in the same electroporation sample. Data points are mean \pm sem of 9 replicates; differences in CD71 expression between EpoR-HM cells expressing high or low levels of FLAG-Stat5 are significant at $p=0.020$ (two-tailed t-test, unequal variance).

Figure 2.11



The low-intensity p-Stat5 signal shows hysteresis

The binary nature of the low-intensity p-Stat5 signal, reflected in its steep Epo dose/p-Stat5 response relationship, may arise from either a monostable or a bistable system [149, 215]. A monostable binary system is analogous to a doorbell: its response reflects the current stimulus. It is described by a single, continuous stimulus/response curve, where a given stimulus always elicits a similar response regardless of stimulus history. By contrast, a bistable system is analogous to a toggle-switch. Its stimulus/response curve is discontinuous, since the response is either 'off' or 'on', but intermediate states are unstable. The response of bistable systems is dependent on both the current stimulus and on stimulus history, namely, whether the system was previously 'on' or 'off'. This phenomenon, known as hysteresis, endows the system with memory [149, 215, 216]. Thus, a stimulus that is insufficient to generate a response in resting cells may nevertheless be sufficient for maintaining the 'on' response in cells that are already 'on' as a result of a previous, stronger stimulus.

To determine whether the p-Stat5 response in fetal liver cells was bistable or monostable we stimulated cells with Epo at either 0.2 U/ml, or a ten-fold lower concentration (0.02 U/ml) (Figure 2.12A). At 30 minutes, when p-Stat5 reached a relative steady state, cells that were initially stimulated at the higher Epo concentration (0.2 U/ml) were switched to a ten-fold lower concentration (0.02 U/ml). The consequent changes in p-Stat5 were followed for several hours, and compared with those of cells that were subject to either high (0.2 U/ml) or low (0.02 U/ml) Epo throughout.

In S3 (Figure 2.12 A upper panels), a ten-fold reduction in Epo did not alter total p-Stat5 for the first 90 minutes, compared with cells remaining in high Epo. By 6 hours after the switch to lower Epo, total p-Stat5, though lower than in cells remaining in high Epo, was higher than in cells confined to low Epo throughout. Therefore, S3 cells had ‘memory’ for the initial 30-minute period of high Epo, 6 hours previously. By contrast, the high-intensity signal in S1 declined rapidly after the switch to low Epo, with kinetics that were the reverse of the onset of response at $t=0$ (Figure 2.12A, lower panels). By 15 minutes, p-Stat5 in S1 declined to a low intensity, stable signal that resembled the intensity of the hysteretic signal in S3. Hysteresis was also observed in a second experimental strategy, where Epo was completely withdrawn from the culture medium (Figure 2.13A, B). We therefore concluded that the low-intensity, binary signal in S3 was generated by a bistable system.

A steep relationship between FLAG-Stat5 expression and Epo-independent, constitutive p-Stat5

A bistable response suggests the presence of a positive feedback interaction or its equivalent. Such an interaction is responsible for the steep stimulus/response curve, amplifying low but supra-threshold signals to their full ‘on’ state and making intermediate states unstable [149, 215]. The hysteresis in the p-Stat5 response of S3 cells indicated bistability, and therefore raised the possibility that a positive feedback interaction, or its equivalent, may be promoting p-Stat5 formation. There were two broad possibilities regarding such an interaction. First, p-Stat5 might itself participate in a positive feedback interaction that contributes to further Stat5 phosphorylation.

Alternatively, a positive feedback interaction may be present at any of the upstream steps that are required for, and precede, the Stat5 phosphorylation step. These included the binding of Epo to EpoR, Jak2 activation and/or EpoR phosphorylation. Several lines of evidence discussed below, while not discounting other steps as possible contributors to the bistable p-Stat5 response, nevertheless suggest that p-Stat5 itself is responsible for a positive feedback interaction that contributes to bistable Stat5 activation.

The first line of evidence comes from analysis of Epo-independent p-Stat5 activation in cells expressing high FLAG-Stat5 (constitutive p-Stat5; Figures 2.9A upper left panel, 2.12B upper panel, double-headed arrows). We also found constitutively active p-Stat5 in non-erythroid cells that express high Stat5 levels, including Stat5-null mouse embryonic fibroblasts (MEFs) infected with high-titer retrovirus encoding Stat5 (Figure 2.13C). To analyze this finding quantitatively, we measured total p-Stat5 in a series of vertical gates containing cells of increasing FLAG fluorescence, as illustrated in Figure 2.9B. This analysis showed that the appearance of p-Stat5 occurs reproducibly above an abrupt FLAG-Stat5 expression threshold (Figure 2.12B, lower panel). The level of p-Stat5 then rises steeply with increasing FLAG-Stat5 expression, delineating a steep, non-Michaelian sigmoidal curve with a Hill coefficient of 2.4. This high Hill coefficient suggests that inactive, FLAG-Stat5 participates in a cooperative or positive feedback interaction during its phosphorylation reaction. Since this reaction occurs in the absence of Epo stimulation, cooperativity or positive feedback must involve FLAG-Stat5 directly, rather than be due solely to upstream components of EpoR signaling.

We hypothesized that the FLAG-Stat5 threshold at which constitutive p-Stat5 first appears is determined by the balance between the background levels of kinase and phosphatase activities within resting (unstimulated) erythroblasts. This was supported by the response of unstimulated erythroblasts to treatment with pervanadate, a broad-spectrum phosphatase inhibitor. We found a time-dependent decrease in the FLAG-Stat5 threshold for constitutive p-Stat5, with the curves describing the dependence of p-Stat5 on FLAG-Stat5 shifting to the left (Figure 2.13D).

p-Stat5 promotes Stat5 phosphorylation *in trans*

The second line of evidence suggesting that p-Stat5 promotes phosphorylation of as yet inactive Stat5 comes from biochemical experiments in which we asked whether two populations of Stat5 molecules, distinguished by a tag, might affect each other's phosphorylation state. Specifically, we asked whether a population of activated, untagged, p-Stat5 molecules could alter the phosphorylation level of a second, FLAG-tagged population of Stat5 molecules. In the absence of an interaction between active and inactive Stat5, phosphorylation of the FLAG-tagged Stat5 molecules should be unaffected by the presence of the untagged p-Stat5. Figure 2.12C illustrates the expected result of such an experiment if, however, p-Stat5 promotes the phosphorylation of as yet unphosphorylated Stat5 *in trans*. In the latter case, the phosphorylation level of the FLAG-tagged Stat5 molecules might increase as a result of the presence of untagged, p-Stat5 molecules in the same cell.

We transfected 293T cells with FLAG-tagged Stat5, in the presence or absence of untagged Stat5 constructs that give rise to constitutive p-Stat5 *in vivo*. As untagged

constructs, we used either the constitutively phosphorylated Stat5 mutant, Stat5 1*6 [217], or alternatively, the untagged wild-type Stat5, since we found it to be constitutively active when expressed at high levels (Figure 2.12B). We assessed the phosphorylation level of the FLAG-tagged Stat5 by specifically immunoprecipitating FLAG-tagged protein under denaturing conditions, followed by quantitative blotting using infra-red imaging, for p-Stat5 (Figure 2.12D, E). Control cells were transfected with FLAG-Stat5Y694F, in the presence or absence of Stat5 1*6. Similar levels of FLAG-tagged protein were immunoprecipitated from these cells as from cells expressing FLAG-Stat5, but immunoblotting showed no p-Stat5 signal (Figure 2.12D, E), confirming that Stat5 1*6 was not co-immunoprecipitated with the FLAG-tagged protein.

In five independent immunoprecipitation experiments, we found that the presence of untagged, phosphorylated Stat5 in cells caused a 2 to 4 fold increase (mean \pm SE = 2.7 \pm 0.4, $p < 0.020$) in the phosphorylation level of FLAG-Stat5, compared with its baseline phosphorylation level when present in cells not containing the untagged constructs. FLAG-Stat5 expression in both groups of cells was similar (mean \pm SE = 1.2 \pm 0.1, Figure 2.12D, E).

These results suggest that p-Stat5 promotes the phosphorylation of as yet inactive, unphosphorylated Stat5.

Figure 2.12 Hysteresis and positive feedback in Stat5 activation.

(A) Stat5 signaling in freshly isolated fetal liver S3 cells shows hysteresis. Fetal liver cells were stimulated with Epo at 0.2 U/ml (dark blue or red symbols) or at 0.02 U/ml (grey symbols). At 30 minutes post stimulation (marked with arrows), Epo concentration was diluted ten fold from 0.2 to 0.02 U/ml for some of the cells (light blue or orange). The time course of the total p-Stat5 response is shown for S3 (upper panel) and S1 (lower panel) cells. Left panels show a magnified x-axis for the first 60 minutes. Representative of 3 similar experiments. See also Figure 2.13A, B.

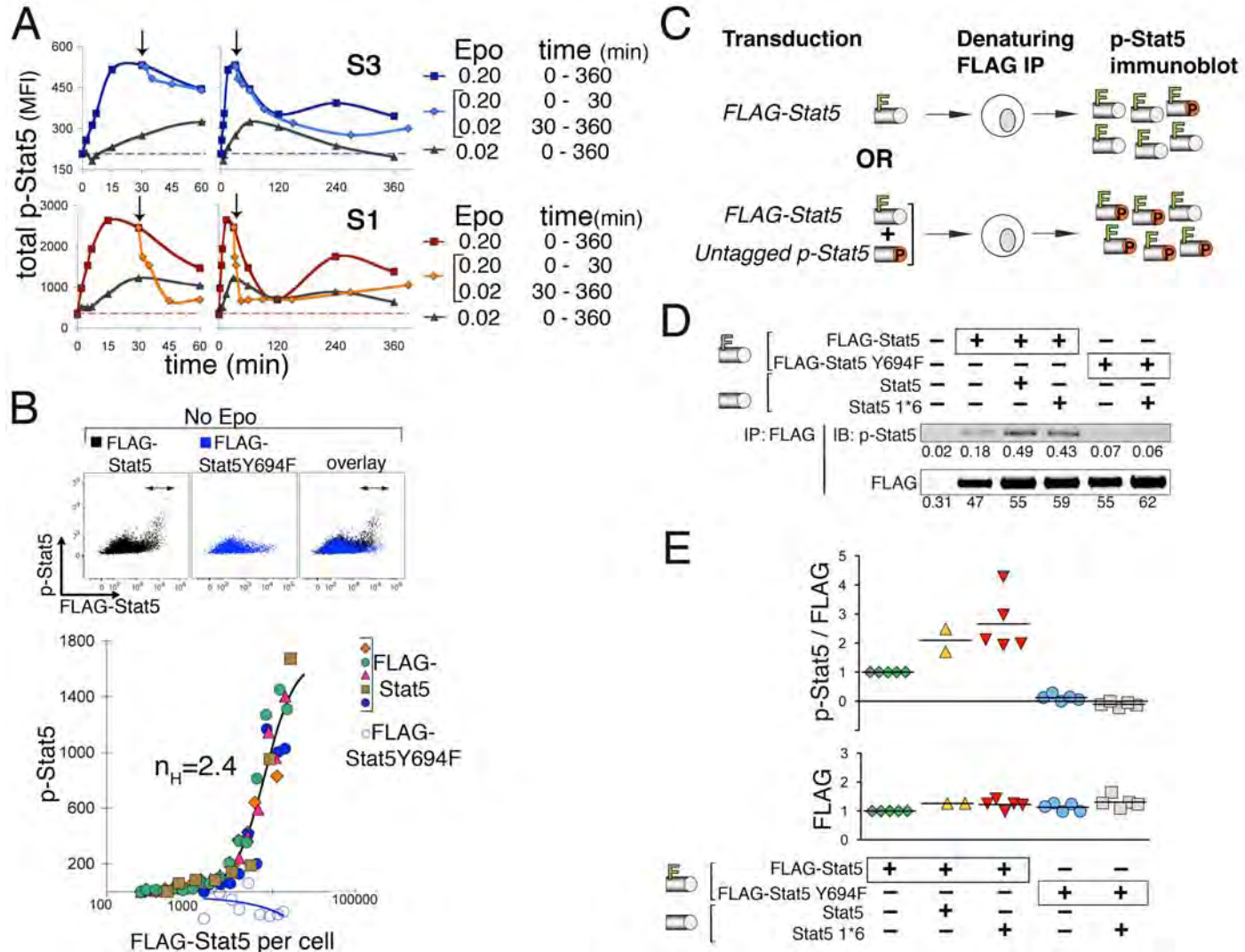
(B) Constitutive (Epo-independent) p-Stat5 in cells expressing high levels of FLAG-Stat5. Cells were electroporated with FLAG-Stat5 or with control, non-phosphorylatable FLAG-Stat5Y694F, incubated overnight in Epo (0.2U/ml) and then deprived of Epo for three hours, as described in Fig 2.9A. Upper panels: p-Stat5 may be seen in cells with high FLAG-Stat5, indicated by the double arrow; no p-Stat5 is seen in cells expressing equivalent levels of FLAG-Y694F. Lower panel: analysis of 5 independent electroporations in 3 independent experiments similar to that shown in the upper panels. Each symbol corresponds to the FLAG and p-Stat5 MFIs of cells in one vertical gate in a p-Stat5 vs FLAG dot plot from one electroporation. The background p-Stat5 MFI for cells expressing FLAG-Stat5Y694F is also shown. Data was fitted with a Hill curve, $n_H=2.4$.

(C) Design of an experiment to examine whether p-Stat5 promotes Stat5 phosphorylation *in trans*. Cells were electroporated with FLAG-tagged Stat5 (top), or with a combination of both FLAG-tagged Stat5 and a non-tagged Stat5 construct that would give rise to constitutive p-Stat5 *in vivo*. The level of phosphorylation of the FLAG-tagged Stat5 in both these cell populations is examined using denaturing FLAG immunoprecipitation to dissociate Stat5 dimers, followed by quantitative western blotting for both p-Stat5 and FLAG. The illustrated outcome corresponds to the case when p-Stat5 promotes Stat5 phosphorylation, so that an increased proportion of the FLAG-Stat5 molecules is phosphorylated when the cells also contained non-tagged p-Stat5; the alternative outcome would have been that the FLAG-Stat5 phosphorylation is similar

whether or not cells also express non-tagged p-Stat5. The FLAG tag is represented by the green letter 'F'; phosphorylation is indicated in red and by the letter 'P'.

(D), (E) Constitutively-active non-tagged p-Stat5 facilitates phosphorylation of FLAG-Stat5 *in trans*. Experimental design as in panel 'C'. 293T cells were transfected with either FLAG-Stat5 or with control, FLAG-Stat5Y694F. Some cells were also electroporated with a non-tagged Stat5 construct that would give rise to constitutive (Epo-independent) p-Stat5 *in vivo*: either non-tagged wild Stat5, or non-tagged Stat5 1*6. FLAG-tagged protein was immunoprecipitated 48 hours post transfection, under denaturing conditions, followed by quantitative blotting using infrared imaging for p-Stat5 and for FLAG. Panel 'D' shows a representative western blot; the numbers below each lane correspond to the infra-red fluorescence reading from each band, corrected for background. Panel 'E' shows a summary of 5 independent experiments (only two experiments also had samples of cells with non-tagged wild type Stat5; all experiments had samples of cells expressing non-tagged Stat5 1*6). Data points in 'E' refer to fluorescence readings for each lane in individual experiments, normalized to the fluorescence reading in cells expressing FLAG-Stat5 only in the same experiment. Mean for all 5 experiments is shown (black line). Increase in p-Stat5 relative to FLAG-Stat5, in FLAG-Stat5 cells that also express non-tagged Stat5 1*6, was significant (mean \pm sem: 2.7 ± 0.4 , $p < 0.020$, paired t test). There was no significant difference in FLAG-Stat5 expression in both groups of cells (mean \pm sem: 1.2 ± 0.1).

Figure 2.12



The time course of p-Stat5 activation is consistent with autocatalysis

Our findings suggested that p-Stat5 is a product of a reaction it promotes. We therefore asked whether Stat5 phosphorylation obeys autocatalytic reaction kinetics. Autocatalytic reactions are characterized by an initial latent period or slow phase, accelerating into a rapid phase when the accumulating product feeds back to accelerate the reaction. The reaction may eventually slow down as the reactants become limiting, giving rise to a sigmoidal time course [218, 219].

We examined a detailed time course of p-Stat5 formation in response to stimulation with a low Epo concentration, or alternatively, in response to pervanadate, a non-specific phosphatase inhibitor (Figure 2.13E, F). In both cases, the time course for p-Stat5 formation was in good agreement with an autocatalytic time course. Phosphatase inhibition was performed on cells expressing FLAG-Stat5. This showed the lag phase that precedes the accelerated phase of p-Stat5 accumulation to be shorter in cells expressing higher FLAG-Stat5 (Figure 2.13E).

Figure 2.13: Hysteresis and positive feedback in Stat5 activation.

(A), (B) Stat5 signaling in S3 cells shows hysteresis. Freshly isolated fetal liver cells were stimulated with Epo (0.2U/ml; dark blue or red symbols). At 30 minutes post stimulation, Epo was removed from some of the cells (light blue or orange) by washing them three times in non-Epo containing medium; the time of wash is indicated with arrows. The time course of the total p-Stat5 response to S3 (upper panels) and S1 (lower panels) is shown in panel 'A'; a magnified x-axis is shown for the first 60 minutes in the left panel. The number of p-Stat5⁺ cells, and the p-Stat5 MFI in p-Stat5⁺ cells over the same time period in the same experiment are shown in panel 'B'. Dashed lines mark the pre-stimulation level of total p-Stat5. Representative of 3 similar experiments.

(C) Constitutive p-Stat5 in non-erythroid cells expressing high levels of Stat5. Stat5^{-/-} mouse embryonic fibroblasts (MEFs) were infected with retrovirus (MSCV) encoding wild-type Stat5 (upper panel), or alternatively were infected with retrovirus encoding FLAG-tagged Stat5 or FLAG-Stat5Y694F (lower panel); control cells were infected with MSCV only. The dilution of the retroviral supernatant for each construct are indicated above each lane. Western blotting for p-Stat5, FLAG or Stat5 protein is shown.

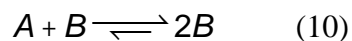
(D) The FLAG-Stat5 threshold for constitutive p-Stat5 is sensitive to phosphatase inhibition. Fetal liver cells were electroporated with FLAG-Stat5 as described in Figure 2.9A and incubated overnight in 0.2 U/ml Epo. Cells were then incubated in the absence of Epo for over 3 hours prior to the addition of pervanadate. p-Stat5 was measured at the indicated time points following pervanadate addition; control cells were incubated for similar time periods in the absence of pervanadate. Individual symbols correspond to the total p-Stat5 in individual vertical FLAG gates as illustrated in Figures 2.9B and 2.10A. Representative of 3 similar experiments.

(E) The time course of p-Stat5 formation following phosphatase inhibition by pervanadate is consistent with autocatalysis. Data is from the experiment presented in panel 'D'. Each curve corresponds to the time course of total p-Stat5 formation in a specific FLAG- gate (the FLAG MFI for each gate is indicated in the legend). An initial slow phase of p-Stat5 accumulation is followed by a faster phase, consistent with an

autocatalytic reaction. The slow phase is shorter in gates with higher FLAG-Stat5 levels. Each data point is the mean of duplicate samples.

(F) The time course of p-Stat5 activation by Epo is consistent with autocatalysis. Fresh fetal liver cells were stimulated with a low concentration of Epo (0.02 U/ml). The time course of the total p-Stat5 response is shown for S1 and S3 cells; two independent experiments are shown, colored blue and red, respectively. Data was fitted by the curve corresponding to a second order autocatalysis [Equation (11) below].

The second order autocatalysis reaction is defined as (1) [218]:

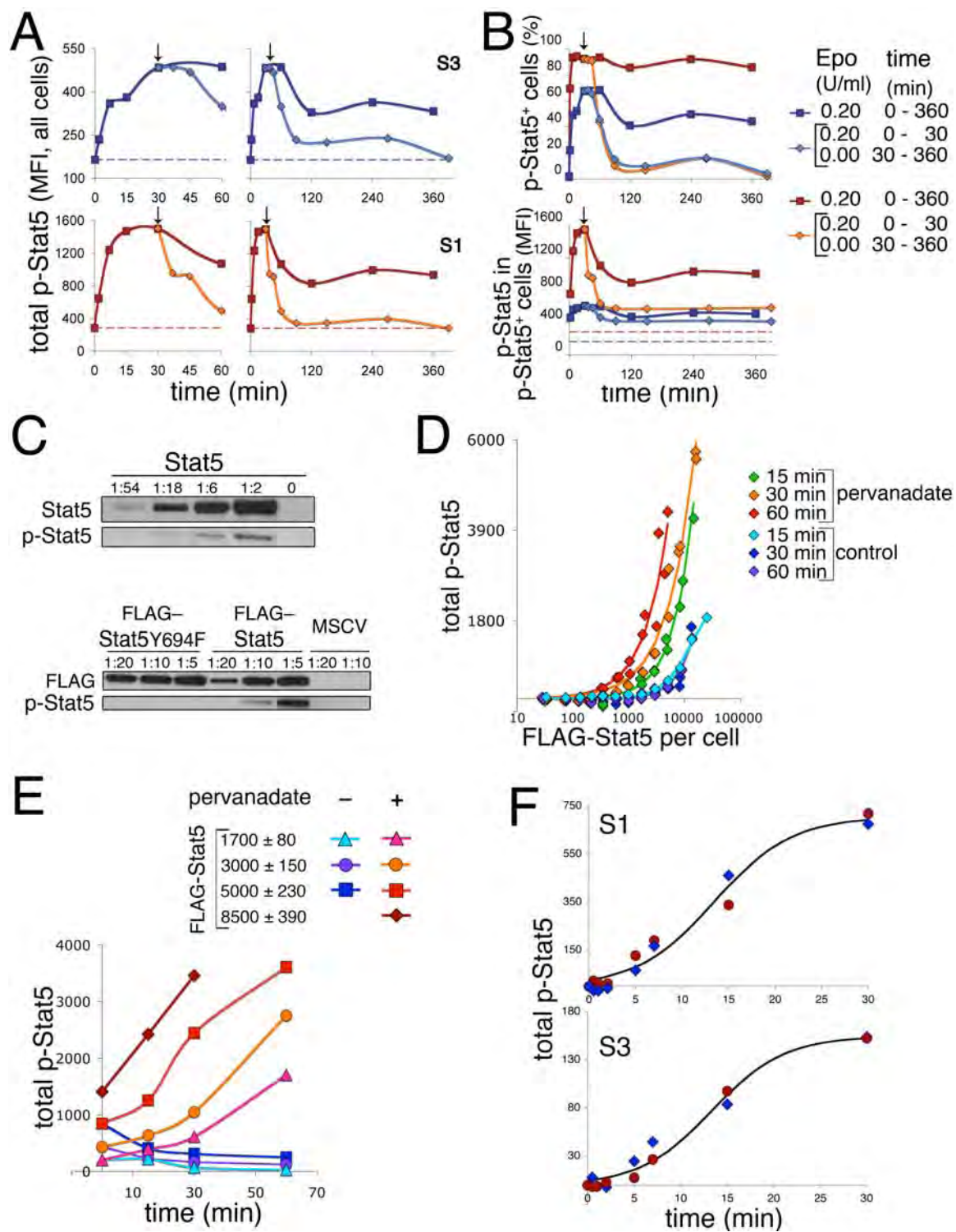


Here, $A = \text{Stat5}$, and $B = \text{p-Stat5}$

The concentration of the product B at time t , B_t , is given by:

$$B_t = \frac{A_0 + B_0}{1 + \frac{A_0}{B_0} e^{-k(A_0 + B_0)t}} \quad (11)$$

Figure 2.13



The isolated Stat5 N-terminal domain (ND) amplifies the binary p-Stat5 signal

The ND is connected to the core of the Stat5 molecule by a flexible tether (Figure 2.14A) and is not essential for phosphorylation of the Stat5 C-terminal tyrosine. It is thought to play a role in the formation of Stat5 tetramers [125, 220]. In addition, intradimer ND dimerization was recently suggested to stabilize the anti-parallel, inactive Stat5 dimer, dissociating upon Stat5 phosphorylation [80, 109].

We examined the effect of exogenous expression of the isolated Stat5 ND on the dynamics of Stat5 phosphorylation. We electroporated fetal liver cells with a construct encoding the full-length FLAG-Stat5 molecule, either alone, or together with a construct encoding the isolated Myc-tagged ND (Figure 2.14A-D). Following overnight incubation to allow expression of the transduced constructs, we assessed the effect of the isolated ND on the phosphorylation of the co-expressed FLAG-Stat5 in response to Epo stimulation. To analyze the effect of Myc-ND on FLAG-Stat5 phosphorylation quantitatively, we used a two-dimensional gate matrix where the position of each rectangular gate is denoted by (x,y) coordinates (Figure 2.14B). All gates with the same 'x' coordinate contain cells with similar FLAG fluorescence, and therefore, with similar FLAG-Stat5 expression. Similarly, all gates with the same 'y' coordinate have similar Myc fluorescence and contain cells with similar Myc-ND expression. In samples that were electroporated with a FLAG-Stat5 but not with a Myc-ND construct, coordinates are indicated as (x,-). Control cells were electroporated with either empty vector (pcDNA3, response as shown in Fig 2.9A), FLAG-Stat5 alone or Myc-ND alone (Figure 2.14B).

As shown previously (Figures 2.9, 2.10) in the absence of the Myc-ND, an increase in FLAG-Stat5 expression, from gate (8,-) to gate (11,-), results in increased p-Stat5 MFI (Fig 2.14C, compare green and blue histograms). The p-Stat5 signal intensity in FLAG-gate 11, however, increased further in cells that also expressed Myc-ND (Figure 2.14C, compare red and blue histograms). A similar amplification of the Epo response as a result of Myc-ND expression was found for other FLAG expression gates (Figure 2.15A). Similar amplification was also seen when non-tagged ND was expressed.

An inspection of the p-Stat5 histograms (Figures 2.14C, 2.15A) showed a qualitative difference in the pattern of p-Stat5 signal amplification by FLAG-Stat5 and by Myc-ND. An increase in FLAG-Stat5 expression from FLAG gate (8,-) to (11,-) increased both the fraction of p-Stat5⁺ cells within the population, as well as their range of p-Stat5 signal intensities, in agreement with our previous results, in which the level of FLAG-Stat5 expression determined maximal p-Stat5 signal intensity (Figures 2.9B, 2.10A). However, addition of Myc-ND to cells resulted principally in an increased number of p-Stat5⁺ cells, without increasing maximal p-Stat5 (compare flow cytometric histograms for cells in gate (11,3) with cells in gate (11,-) and see overlay of blue and red histograms, Figure 2.14C; see also Figure 2.15A).

We therefore examined the effect of Myc-ND on the entire Epo dose/p-Stat5 response curve (Figure 2.14D). As found previously (Figure 2.10A) S3 cells expressing very low levels of FLAG-Stat5, in gate (6,-), responded to Epo stimulation with a low-intensity, steep (binary) p-Stat5 signal, characterized by a high Hill coefficient ($n_H=3$). Cells expressing higher levels of FLAG-Stat5, in gate (10,-), responded in a graded

fashion to increasing Epo concentrations, evident from the low Hill coefficient ($n_H=0.6$), but the response reached high p-Stat5 signal intensities. By contrast, cells in gate (10,3), expressing the same high level of FLAG-Stat5, but that in addition also expressing Myc-ND, responded with a steep (binary) high-intensity p-Stat5 signal, reflected in a high Hill coefficient ($n_H=4.8$).

The precise change in p-Stat5 was dependent on the expression level of Myc-ND relative to FLAG-Stat5. For a given level of FLAG-Stat5, low levels of Myc-ND (gates with coordinates (x,3) or (x,4)) amplified the p-Stat5 response (Figure 2.15B, red histograms), whereas higher levels of Myc-ND (gates with coordinates (x,5) or (x,6)) resulted in lower amplification, and potentially in inhibition, of the p-Stat5 response (Figure 2.15B, blue histograms).

Figure 2.14 The Stat5 ND enhances bistable Stat5 activation.

(A) Representation of the Stat5 structural domains and of tagged Stat5 constructs (not to scale). ND: N-terminal domain; CC: coiled-coil domain; DBD: DNA binding domain; SH2: SH2 domain; Y694: C-terminal tyrosine targeted in the activating phosphorylation reaction. Stat5Y694F is a non-phosphorylatable mutant. Stat5 Δ ND is missing the first 129 N-terminal amino acids. Stat5, Stat5 Δ ND and Stat5Y694F are FLAG-tagged at the C-terminal end. The isolated ND was expressed with a C-terminal Myc tag.

(B) Gating strategy for the analysis of fetal liver cells transduced with both FLAG-Stat5 and Myc-ND constructs. Fluorescence measurements were made simultaneously for FLAG, Myc, p-Stat5, CD71 and Ter119 expression. FLAG and Myc fluorescence are shown for S3 cells transduced with either Myc-ND only, FLAG-Stat5 only, or both constructs (left, middle and right histograms respectively). To analyze the effects of Myc-ND and FLAG-Stat5 expression on the p-Stat5 response, we sub-divided the Myc vs. FLAG dot plots using a two-dimensional gate matrix. Each rectangular gate has coordinates (x, y). The 'x' coordinate denotes the horizontal position of the gate, which increases with increasing FLAG expression. Gates with the same 'x' coordinates contain cells with similar levels of FLAG expression. The 'y' coordinate denotes the vertical position of the gate and increases with increasing Myc expression; all gates with the same 'y' coordinate contain cells with similar 'Myc' expression.

(C) Effect of the isolated Stat5 ND on the p-Stat5 response to Epo. Fetal liver cells were transduced with FLAG-Stat5 only, or with both FLAG-Stat5 and Myc-ND, as in panel 'B'. After overnight incubation, cells were stimulated with Epo (2 U/ml) for 30 minutes. The p-Stat5 response is shown for cells in three FLAG and Myc expression gates (see panel 'B'): cells transduced with FLAG-Stat5 only, expressing low levels of FLAG-Stat5, in gate (8,-) (green histogram); cells transduced with FLAG-Stat5 only, expressing high levels of FLAG-Stat5, in gate (11,-) (blue histogram); and cells transduced with both constructs, expressing the same high levels of FLAG-Stat5, but in

the presence Myc-ND, in gate (11,4) (red histogram). Black histograms show the pre-stimulation p-Stat5 signal for each corresponding gate.

(D) Low levels of the isolated Myc-ND increase the steepness of the p-Stat5 response to Epo. Cells were transduced with FLAG-Stat5 alone or with both FLAG-Stat5 and Myc-ND. Following overnight incubation, cells were stimulated with a range of Epo concentrations, as described in Figures 2.9A, B and 2.10. The 'total p-Stat5 vs. Epo concentration' plot is shown for the indicated expression gates (see panel 'B'): cells transduced with FLAG-Stat5 only, expressing low levels of FLAG-Stat5, in gate (6,-) (green); cells transduced with FLAG-Stat5 only, expressing higher levels of FLAG-Stat5, in gate (10,-) (blue); and cells transduced with both constructs, expressing the same high levels of FLAG-Stat5, but in the presence Myc-ND, in gate (10, 3) (red). An overlay of all three responses is shown. Data points are MFI \pm sem of the p-Stat5 response for all cells within a gate. Data is fitted with Hill curves.

(E) Low levels of the isolated Myc-ND increase the p-Stat5 response of fetal liver S3 cells electroporated with FLAG-Stat5 Δ ND. Fetal liver cells were electroporated with FLAG-Stat5 Δ ND in the presence or absence of Myc-ND; responses of cells transduced with control FLAG-Stat5 in the same experiment are also shown. Responses are shown for gates with FLAG coordinate 9, and where applicable, Myc coordinate 3. Representative of 2 experiments.

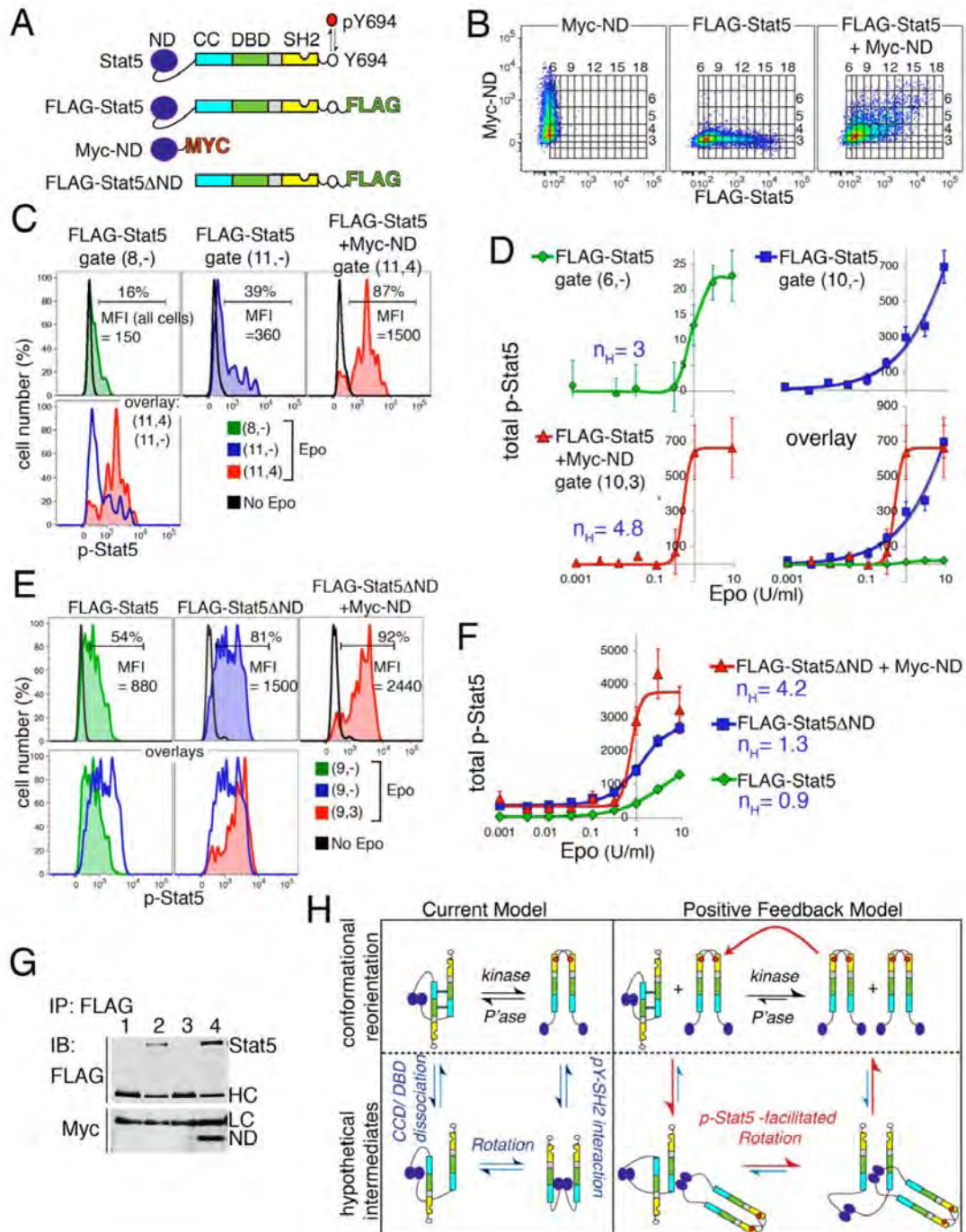
(F) Epo dose/p-Stat5 response curves for fetal liver cells expressing FLAG-Stat5 Δ ND in the presence or absence of Myc-ND; responses of cells transduced with control FLAG-Stat5. Response of FLAG-Stat5 constructs in the presence or absence of Myc-ND correspond to expression gates (11,3) or (11-), respectively. Hill coefficients are indicated. Data are MFI \pm sem. Representative of two experiments.

(G) Co-immunoprecipitation of the Myc-ND with wild-type Stat5. 293T cells were electroporated with either vector alone (pcDNA3, lane 1), FLAG-Stat5 (lane 2), Myc-ND (lane 3), or with both FLAG-Stat5 and Myc-ND (lane 4). Whole cell lysate was immunoprecipitated with FLAG-specific antibody and western blotting of the same membrane was carried out with either an anti-FLAG antibody (upper gel) or with an anti-

Myc antibody (lower gel). The position of Stat5, the isolated ND, and IgG heavy and light chains (HC and LC respectively) is shown.

(H) Pictorial representation of the current model (top left panel) and the proposed positive feedback model (top right panel) for the Stat5 phosphorylation/dephosphorylation cycle. The Stat5 domains correspond to the key in panel 'A'. Hypothetical intermediates are based on [110]. The positive feedback model is based on a second-order autocatalytic reaction. See 'Discussion' section, 'Hypothesis: an autocatalytic conformational switch' for details.

Figure 2.14



The isolated Stat5 ND enhances hysteresis and constitutive p-Stat5 activation

The finding that the isolated Stat5 ND amplified the p-Stat5 response and generated a steep dose/response curve suggested that p-Stat5-mediated positive feedback is mediated via the Stat5 ND. We hypothesized above that the hysteresis in p-Stat5 signaling (Figures 2.12A, 2.13A,B), as well as the Epo-independent (constitutive) p-Stat5 in cells expressing high levels of FLAG-Stat5 (Figure 2.12B), are both outcomes of the p-Stat5-mediated positive feedback. We therefore examined the effects of the isolated Stat5 ND on these phenomena. We found that constitutive p-Stat5 was enhanced in cells that, in addition to expressing high FLAG-Stat5, also expressed Myc-ND (Figure 2.15C). Further, co-expression of Myc-ND with FLAG-Stat5 enhanced the hysteresis of the p-Stat5 response to Epo (Figure 2.15D). At a given level of FLAG-Stat5 expression, following a ten-fold Epo dilution, cells expressing Myc-ND had a p-Stat5 response similar to that of cells lacking Myc-ND, from which Epo was not removed (Figure 2.15D; compare orange and black curves and histograms, respectively).

Figure 2.15 The isolated Stat5 ND enhances hysteresis and constitutive Stat5 activation.

(A) The isolated Stat5 ND enhances the p-Stat5 response to Epo. Experiment as described in Figure 2.14B, C. The p-Stat5 response of cells expressing FLAG-Stat5 only is shown in blue, and of cells expressing both FLAG-Stat5 and Myc-ND is shown in red; each histogram corresponds to cells in the indicated gate; histograms on the same horizontal row have the same level of FLAG-Stat5 expression. Black histogram show the p-Stat5 signal pre-stimulation for the corresponding gate. The percentages indicate the number of p-Stat5⁺ cells.

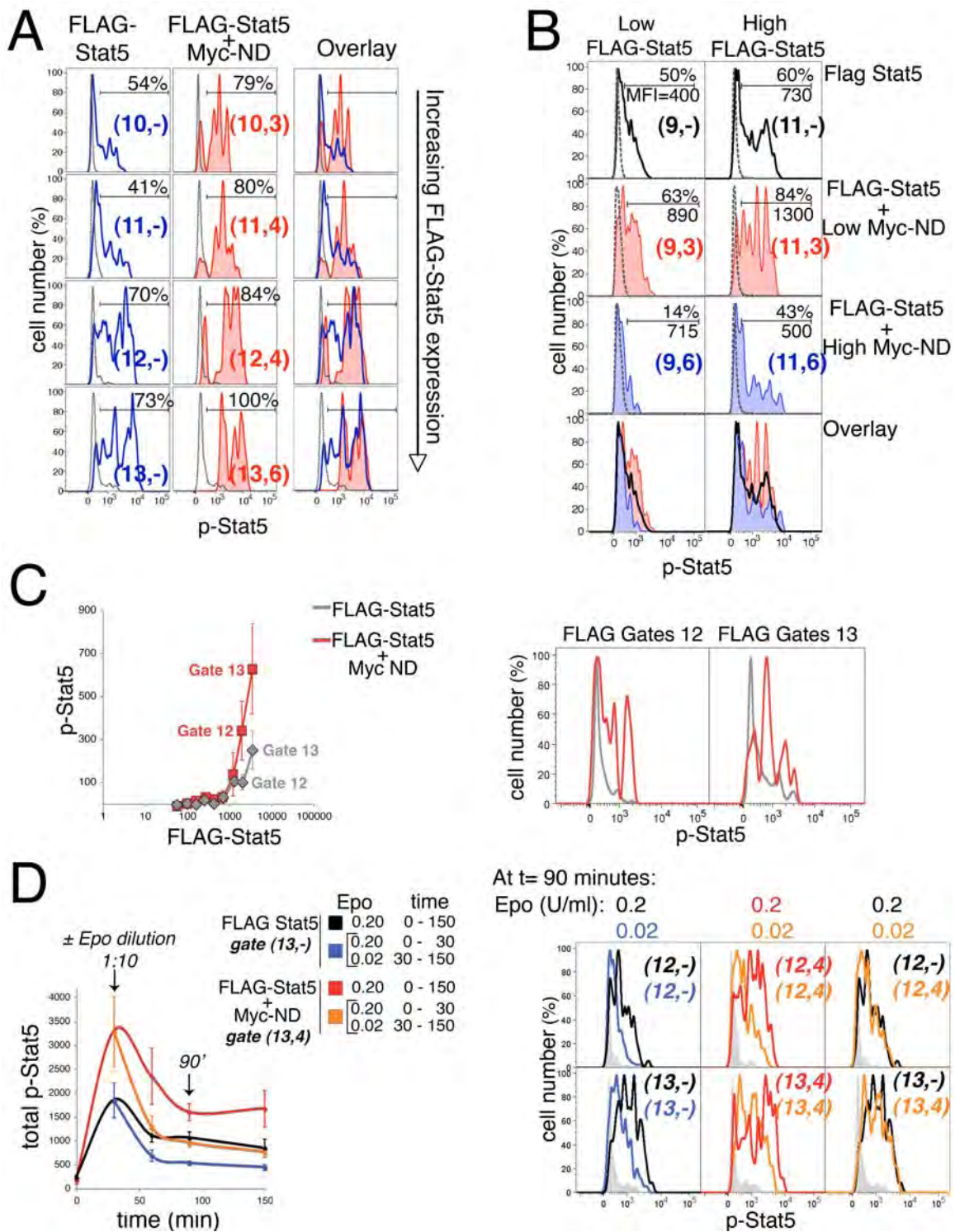
(B) Effect of different levels of Myc-ND expression on the p-Stat5 response to Epo. Experiment as described in Figure 2.14B. Cells expressing FLAG-Stat5 at two different levels, corresponding to gate 9 (left histograms) and gate 11 (right histograms) are shown as examples. Response in the absence of Myc-ND is shown in black; response in cells that also express, in addition to FLAG-Stat5, low levels of Myc-ND (Myc-ND gate 3), is shown in red; response in cells that express high levels of Myc-ND (Myc-ND gate 6) is shown in blue. The coordinates for each gate are indicated; percentages correspond to the number of p-Stat5⁺ cells; MFI values are for total p-Stat5 (for all cells in the gate).

(C) Effect of Myc-ND expression on constitutive p-Stat5, in cells expressing FLAG-Stat5. Fetal liver cells were electroporated with either FLAG-Stat5 alone or with both FLAG-Stat5 and Myc-ND, as described in Figure 2.14B. After overnight incubation, cells were deprived of Epo for 3 hours. Cells expressing high levels of FLAG-Stat5 contain p-Stat5 in the absence of Epo stimulation, as shown in Figure 2.12B. Data was analyzed as in Figure 2.12B; cells in FLAG-gates 12 and 13 contain p-Stat5, which reaches higher levels if the cells also express Myc-ND. Data is mean \pm sem for cells in each gate; the flow-cytometry histograms for gates 12 and 13 is shown on the right.

(D) Effect of Myc-ND expression on the hysteresis of the p-Stat5 response to Epo. Fetal liver cells expressing either FLAG-Stat5 alone, or both FLAG-Stat5 and Myc-ND, were prepared as described in Figure 2.12B. Cells were stimulated with 2 U/ml Epo. At 30 minutes, Epo concentration in the medium of some cells was diluted ten-fold to 0.2

U/ml. The p-Stat5 response was followed for an additional 2 hours. At $t = 90$ min (60 min after Epo dilution), cells in the diluted Epo medium expressing both FLAG-Stat5 and Myc-ND (orange curve and histograms) had p-Stat5 levels equivalent to cells in the non-diluted medium that expressed FLAG-Stat5 alone (black curve and histogram). Thus, the expression of the Myc-ND was sufficient to compensate for a ten-fold dilution in Epo, over extended periods of time. Time course is shown for cells in FLAG gates 13 (data points are mean \pm sem for cells in each gate), histograms are shown for $t = 90$ minutes for cells in FLAG gates 12 and 13.

Figure 2.15



Phosphorylation of an ND-truncated Stat5 molecule is amplified by co-expression of the isolated ND

We investigated the properties of a Stat5 mutant in which the ND is absent, Stat5 Δ ND, and the effect of exogenous ND on this mutant. As previously reported [125], the Stat5 Δ ND has a higher level of constitutive activity than wild-type Stat5 (Figure 2.16A, upper panels). In addition we found that at equivalent FLAG expression levels, the Stat5 Δ ND p-Stat5 response to Epo was higher than that of wild-type Stat5 (Figures 2.14E, compare green and blue histograms; 2.16A, lower panels). Co-expression of relatively low levels of Myc-ND with the FLAG-Stat5 Δ ND resulted in further amplification of the p-Stat5 signal, beyond the already higher signal generated by this mutant (Figure 2.14E, compare blue and red histograms). Co-expression of the Myc-ND also rendered the Epo dose/p-Stat5 response relationship of FLAG-Stat5 Δ ND steeper, as reflected by a higher Hill coefficient (Figure 2.14F, compare red and blue Hill curves). In contrast to the effect of low Myc-ND expression, high expression of the Myc-ND either failed to amplify, or had a suppressive effect on the p-Stat5 signal (Figure 2.16B, black Hill curve). Taken together, these findings are similar to the effects exerted by the isolated ND on wild-type Stat5, suggesting that amplification of the p-Stat5 signal by the isolated ND, and the steeper dose/response curve it generates, do not require an interaction between the isolated ND and the Stat5 ND domain.

The isolated Myc-ND co-immunoprecipitates with full-length FLAG-Stat5

We examined whether the isolated Myc-ND interacts with the full-length unphosphorylated Stat5 dimers. We transfected 293T cells with either FLAG-Stat5 or

with Myc-ND, or co-transfected the cells with both constructs. Whole cell lysates were subjected to immunoprecipitation with a FLAG-specific antibody, and immunoprecipitates were examined by western blotting (Figure 2.14G). The same membrane was first blotted for the Myc epitope, and then stripped and blotted for the FLAG epitope. In cells co-transfected with both Myc-ND and FLAG-Stat5, the FLAG antibody immunoprecipitated both FLAG and Myc epitopes, indicating an interaction between Myc-ND and FLAG-Stat5. No Myc-ND was seen in immunoblots of cells transfected with either construct alone.

ND dimerization surface mutations are deficient in p-Stat5 amplification but retain p-Stat5 suppressive effect

Mutations of L78 in STAT4, or the homologous F77 and/or L78 in STAT1, disrupt the homodimerization of their respective ND domains [106, 111]. An alignment of STAT1, STAT4 and STAT5a suggests that these residues are conserved in the STAT5a ND (Figure 2.16C). We mutated the equivalent residues in the STAT5 ND domain, to generate several isolated ND domain mutants, with mutations NDL82S or NDF81A/L82A. We also generated a full length Stat5 molecule bearing the F81A/L82A mutations, and found that it was similar in its behavior to the Stat5 Δ ND mutant, showing increased constitutive activity and an amplified response to Epo.

Co-expression of the mutant Myc-ND molecules with FLAG-Stat5 suggested that they were deficient in amplifying the p-Stat5 response when expressed at lower levels, though they were still able to suppress the p-Stat5 response when expressed at high levels (Figure 2.16D, E). Thus, expression of the Myc-NDL82S failed to amplify the p-Stat5

response of FLAG-Stat5 (Figure 2.16D, compare blue and green histograms), while within the same FLAG/Myc expression gates, the wild-type Myc-ND generated substantial amplification (Figure 2.16D, compare blue and red histograms; equivalent levels of Myc-ND and Myc-NDL82S are expressed within the (10,4) gates, see Figure 2.16D lower panels). Similar results were obtained with the Myc-NDF81A/L82A mutant (Figure 2.16E, F), which failed to amplify the p-Stat5 signal. Of note, high expression levels of the mutant Myc-NDF81A/L82A, like high expression of Myc-ND, suppressed the p-Stat5 response (Figures 2.16E, 2.15B). Therefore, mutations at the F81/L82 residues of the ND uncouple its amplifying activity, exerted at low expression levels, from its suppressive activity, exerted at high expression levels.

Figure 2.16 Mutations of the Stat5 ND domain.

(A) Constitutive activity (upper panels) and Epo responsiveness (lower panels) of a Stat5 molecule missing its N-terminal 129 amino acids, 'Stat5 Δ ND'. Wild-type fetal liver cells were electroporated with FLAG-tagged Stat5 Δ ND, or control FLAG-Stat5 or FLAG-Stat5Y694F, and examined 18 hours later. The response of S3 cells is shown. Representative of 3 experiments

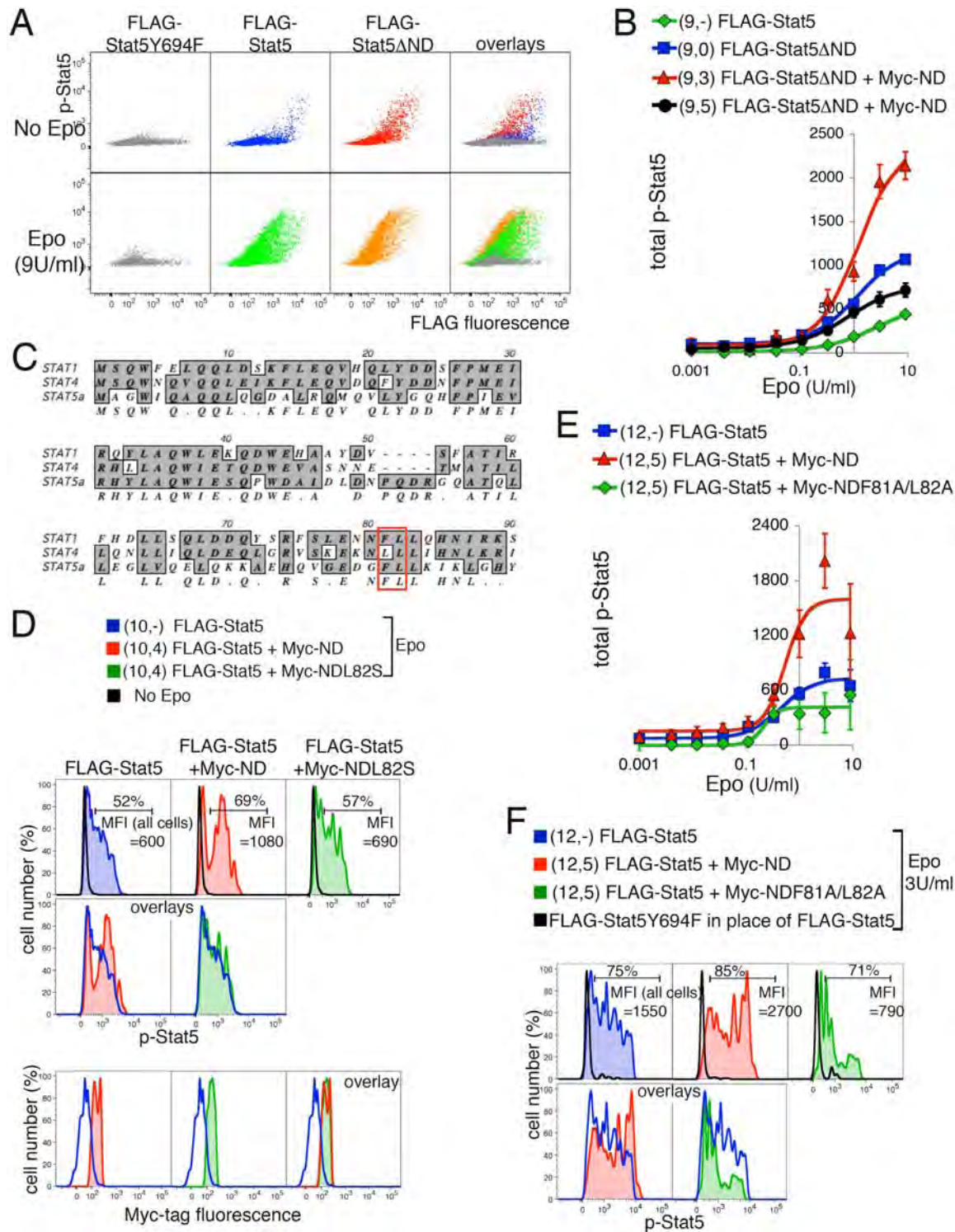
(B) Epo dose/p-Stat5 response of fetal liver S3 cells electroporated with FLAG-Stat5 Δ ND in the presence or absence of Myc-ND; responses of cells transduced with control FLAG-Stat5 in the same experiment are also shown. Responses are shown for gates with FLAG coordinate 9, and where applicable, Myc coordinates 3 (low expression) or 5 (high expression). Data points are MFI \pm SEM. Representative of 2 experiments.

(C) Alignment of the N-terminal portion of the STAT1, STAT4 and STAT5a NDs. The red rectangle marks conserved F81 and L82 residues, previously shown to be in the dimerization interface of the STAT1 and STAT4 NDs [106, 108].

(D) Fetal liver cells were electroporated with FLAG-Stat5 in the absence (blue histogram) or presence of either Myc-ND (red histogram) or its mutant, Myc-NDL82S (green histogram). p-Stat5 response histograms are shown for expression gates with (10,4) coordinates (upper panels). Myc expression for Myc-ND and Myc-NDL82S in gates (10,4) is very similar (lower panels).

(E), (F) Fetal liver cells were electroporated with FLAG-Stat5 in the absence (blue histogram and curve) or presence of either Myc-ND (red histogram and curve) or its mutant, Myc-NDF81A/L82A (green histogram and curve). p-Stat5 response histograms are shown in 'F' for expression gates with (12,5) coordinates. The entire Epo dose/p-Stat5 response curve for the same gates is shown in 'E'. Hill coefficients are 1.44 for FLAG-Stat5, 2.2 for FLAG-Stat5 + Myc-ND, and 3.2 for FLAG-Stat5 + Myc-NDF81A/L82A. Data points are MFI \pm SEM.

Figure 2.16



Discussion

Stat5 signaling in erythroblasts combines a low-intensity bistable signal with a high intensity graded response. Together, these allow fidelity in signal transduction in the low-basal Epo range, with the ability to generate a graded response over the wide range of stress Epo concentrations. High intensity, graded Stat5 signaling in early erythroblasts gradually transitions to a low intensity binary response in mature erythroblasts. This shift in signaling mode is caused by the gradual loss in Stat5 expression with erythroblast maturation. By restoring high Stat5 expression to mature S3 erythroblasts, we were able to reverse this shift and endow them with a high intensity graded p-Stat5 response.

Using Stat5^{-/-} and EpoR-HM mice, we show that the binary and graded p-Stat5 signaling modes are required in basal and stress erythropoiesis, respectively.

Further, we investigate the mechanism of bistability in Stat5 activation and show that it is caused by an autocatalytic positive feedback exerted by active p-Stat5 on inactive Stat5, that promotes Stat5 phosphorylation. Strikingly, the isolated Stat5 ND dramatically enhances the bistability, converting a graded, high intensity signal into a high-intensity bistable response. These data, together with biochemical and kinetic data, lead us to propose a model in which the ND of active p-Stat5 molecules promotes the Stat5 phosphorylation reaction.

Co-existing graded and binary Stat5 signaling allows for fidelity in signaling over a wide Epo range

Theoretical analysis and synthetic models have shown that a given signaling network may generate either binary (digital) or graded (analog) responses, depending on

the value of key parameters [149, 221, 222]. Recent reports suggest that both modes may coexist in cells [205, 223]. Thus, Ras signaling in lymphocytes is of a low-intensity, analog form, but can assume a high intensity, digital form when a SOS positive feedback loop is activated. Hence, distinct ways of juxtaposing binary and graded signaling modes have evolved that increase the information content of transduced signals.

A key feature of the erythropoietic system is its wide dynamic range. The precise erythropoietic rate generated by erythroid progenitors is dependent on Epo concentration, which varies from basal to stress erythropoiesis through three orders of magnitude. Our aim at the outset was to understand how Stat5 signaling reflects this vast Epo range. A graded signal transduction system would have made it possible for downstream responses to be augmented incrementally throughout the Epo range. However, a drawback of the graded mode of signaling is that, at low Epo concentrations, such as those that sustain basal erythropoiesis (<0.05 U/ml), the ratio of signal to noise would be low, reducing signaling fidelity. By contrast, a binary signaling mode, while generating a decisive signal, would not be able to respond to incremental changes in Epo concentration during increasing levels of stress.

Here we found that Stat5 signaling bridges this conundrum by combining bistable activation in response to low Epo in the basal range, with the capacity for a further, graded increase in Stat5 signal intensity in response to stress levels of Epo. The bistable activation of Stat5 results in a decisive signaling threshold, transducing with fidelity the low Epo concentrations that support basal erythropoiesis. In response to high Epo, the p-

Stat5 signal can be increased further, in a graded incremental manner that reflects the level of stress.

By comparing mouse genetic models that either completely lack Stat5 function (the Stat5^{-/-} mouse), or that specifically lack the graded, high intensity signal (the EpoR-HM mouse), we found that the binary, low-intensity signal is both necessary and sufficient for erythroblast survival and for maintenance of basal erythropoiesis (Figure 2.11A). By contrast, the high intensity graded p-Stat5 signal is required for the response to erythropoietic stress, as seen from the inability of EpoR-HM mice to respond to stress. Further, exogenous Stat5 expression in EpoR-HM erythroblasts, which rescued their ability to signal via the graded high-intensity mode, also rescued high CD71 expression, a Stat5-dependent response specific to stress (Figure 2.11C).

The binary form of the p-Stat5 signal in S3 erythroblasts is a result of bistable Stat5 activation in cells where Stat5 expression is low. In earlier S1 erythroblasts, however, the presence of higher levels of Stat5 permits high Epo concentrations to generate a higher-intensity graded signal beyond that generated through bistable activation. Several lines of evidence suggest that the high intensity response in S1 may mask an initial, low-intensity bistable activation of Stat5: 1) In EpoR-HM S1 cells, lacking high intensity Stat5 signaling, the residual signaling mode is binary. 2) There is a persistent, or hysteretic, low-intensity p-Stat5 signal in S1 cells following Epo wash or dilution, similar in intensity to that found in S3 cells (Figure 2.13B). 3) We found similar autocatalytic reaction kinetics in both S1 and S3 cells in response to Epo stimulation (Figure 2.13F).

It is unclear what confines bistable activation to a low-intensity response. Why is it that, in cells such as S1, which are capable of a high intensity response, autocatalysis does not continue until the maximal p-Stat5 response is obtained? We were able to artificially provoke such a binary, high intensity response in cells expressing high FLAG-Stat5 by also co-expressing low-levels of the isolated Stat5 ND (Figure 2.14D). Whatever the mechanism that prevents such a high-intensity binary response under physiological conditions, it is clearly essential for the unique way in which bistable activation co-exists with graded p-Stat5 signaling in erythroblasts.

Mechanism of bistability: p-Stat5-mediated positive feedback exerted at the Stat5 phosphorylation step

We found a steep p-Stat5 response to Epo stimulation, with Hill coefficients in the range of 2 to 4, in fresh EpoR-HM erythroblasts (Figure 2.3D, E), and in electroporated wild-type S3 expressing low-levels of FLAG-Stat5 (Figures 2.14D, 2.10A). The potential mechanisms of such a binary response fall into two broad categories, monostable, or bistable. We found that the p-Stat5 response in S3 cells showed hysteresis, persisting well beyond either removal or dilution of the Epo stimulus (Figures 2.12A, 2.13A, B). This therefore indicated that the binary response resulted from bistable Stat5 activation.

A key requirement for bistability is the presence of a positive loop, containing a positive feedback interaction and/or an even number of negative feedback links [149, 224]. Such a loop ensures that the system ‘flips’ between two states without resting in intermediate states. In principle, any step in the Epo-mediated signaling pathway upstream of Stat5 phosphorylation, including Epo binding to its receptor and Jak2

activation, may be the site of such a positive loop. Below we list evidence suggesting that inactive Stat5 is the target of positive feedback exerted by p-Stat5, and that this positive feedback is primarily responsible for bistable Stat5 activation:

(a) A steep dependence of constitutive p-Stat5 on FLAG-Stat5 expression

($n_H=2.4$). In the absence of Epo stimulation, S3 erythroblasts expressing high levels of FLAG-Stat5 contain Epo-independent (constitutive) p-Stat5 (Figure 2.12B). There is a steep dependence of constitutive p-Stat5 on FLAG-Stat5 expression, with a Hill coefficient of 2.4. Therefore, inactive Stat5 is a reactant in a phosphorylation reaction that involves either cooperativity or a positive loop. Since this reaction takes place in the absence of Epo stimulation, cooperativity or positive feedback must involve Stat5 directly, and cannot be accounted for by upstream components of EpoR signaling.

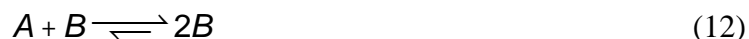
(b) p-Stat5 promotes phosphorylation of inactive Stat5 *in trans*.

We expressed two distinct populations of Stat5, distinguished by the presence or absence of a FLAG-tag, in the same cells. We found that the presence of a population of untagged p-Stat5 molecules in the cell caused an increase in the level of phosphorylation of the second, tagged population (Figure 2.12D, E). Therefore, p-Stat5 promotes *in trans* the phosphorylation of as yet inactive Stat5 molecules. In principle, p-Stat5 may promote Stat5 phosphorylation by either accelerating the forward, phosphorylation reaction, or alternatively, by retarding the reverse, dephosphorylation reaction.

(c) The time course of p-Stat5 accumulation obeys autocatalytic reaction

kinetics. Evidence in **(a)** above suggests that inactive Stat5 is the target of cooperativity or positive feedback, whereas evidence in **(b)** suggests that it is p-Stat5 that exerts

positive feedback on this phosphorylation reaction; taken together, these findings suggest that the Stat5 phosphorylation reaction is accelerated by its own product, p-Stat5. Therefore, Stat5 phosphorylation is an autocatalytic reaction. Autocatalysis is a type of positive feedback in which the product accelerates (or catalyzes) the reaction in which it is formed. Second order autocatalytic reactions are defined as



where substrate A is converted to the product B [218]. As a result of B 's interaction with A , the rate of reaction (12) is faster than the rate of the non-autocatalytic, first order reaction:



The observations noted in **(a)** and **(b)** therefore suggest that the Stat5 phosphorylation reaction may be represented as an autocatalytic reaction similar to reaction (12):



Support for this comes from the reaction kinetics of Stat5 activation. The time course of an autocatalytic reaction is characterized by an initial latent period or slow phase, accelerating into a rapid phase when the accumulating product feeds back to accelerate the reaction. We observed this pattern for the time course of p-Stat5 accumulation in response to phosphatase inhibition, as well as in response to Epo stimulation (Fig 2.13E, F).

As noted above, the finding that p-Stat5 promotes phosphorylation of Stat5 *in trans* does not, by itself, allow us to determine whether it does so by accelerating the forward, phosphorylation reaction, or by inhibiting the reverse, dephosphorylation

reaction. However, the finding that p-Stat5 accumulation accelerates with time in a manner consistent with autocatalysis, even in the presence of phosphatase inhibition by pervanadate (Figure 2.13E), makes it less likely that p-Stat5 accelerates its own accumulation through phosphatase inhibition. We noted that the length of the slow phase for p-Stat5 accumulation in response to pervanadate is dependent on the concentration of inactive Stat5, being shorter in cells expressing higher FLAG-Stat5 (Figure 2.13E). This further supports our earlier conclusion (see **(a)** above) that inactive Stat5 participates directly in the positive feedback interaction.

(d) The isolated Stat5 ND enhances bistability. In the physiological setting, the low-intensity p-Stat5 signal was bistable, whereas the high intensity signal was graded. The graded property of the high intensity signal was radically modified by the expression of the isolated Stat5 ND, which converted it into a high-intensity binary response (Figure 2.14D). The isolated ND therefore uncouples the otherwise clear link between high intensity p-Stat5 signaling, and reduced steepness of the Epo dose/p-Stat5 response curve (Figures 2.3, 2.7, 2.9, 2.10). The ability of the isolated ND to break this link and generate a high intensity binary signal suggests that it is the ND that mediates the interaction responsible for the binary nature of the p-Stat5 response. In addition to increasing the Hill coefficient of the p-Stat5 response to Epo, the isolated ND increased constitutive p-Stat5 for a given FLAG-Stat5 expression level (Figure 2.15C) and enhanced the hysteretic p-Stat5 signal following Epo wash or dilution (Figure 2.15D). These findings support the hypothesis that the Stat5 ND is responsible for mediating the positive loop that gives rise to bistable Stat5 activation. They add to the kinetic and biochemical evidence in **(a)-(c)**

above, suggesting that autocatalytic p-Stat5 phosphorylation is a principal mediator of bistable Stat5 activation.

Hypothesis: an autocatalytic conformational switch

We hypothesize that the ND may, in some way, either increase the likelihood of phosphorylation by the kinase, or alternatively, decrease the likelihood of the phosphatase reaction. The ND is connected to the core STAT molecule via a long flexible tether that is thought to provide it with mobility and therefore with the ability to interact with various domains within the STAT dimer [110]. In the inactive dimer conformation, reciprocal NDs are dimerized in an interaction that is thought to stabilize the inactive anti-parallel dimer [106]. Our finding that the FLAG-Stat5 Δ ND has an amplified response to Epo stimulation is consistent with decreased stability of the inactive, anti-parallel dimer, as a result of the absence of the ND domains. Structural data and FRET experiments show that STAT activation results in separation of the two NDs [109]. Therefore, the Stat5 ND, which mediates an *intra*-dimer interaction within inactive dimers, becomes available for other interactions once Stat5 is phosphorylated. Consistent with this, the ND is required for the formation of tetramers of active STATs, through *inter*-dimer interactions [125, 220, 225]. The ND-mediated positive feedback may therefore be mediated by the newly-available NDs of p-Stat5, through *inter*-dimer interactions. Consistent with this, we coimmunoprecipitated inactive Stat5 with the isolated ND domain (Figure 2.14G).

In recent years, a new role had emerged for the ND, as an essential component in the radical reorientation between the parallel and anti-parallel conformations that STAT

molecules undergo during the phosphorylation/dephosphorylation cycle. Thus, ND-truncated STAT1, STAT4, or STAT5 are deficient in this cycle, with STAT dimers either persisting in the phosphorylated, parallel conformation, in the case of STAT1 and STAT5 [109, 110], or unable to form the parallel dimer conformation, in the case of STAT4 [106]. Of interest here, the isolated STAT1 ND could complement the persistently phosphorylated, ND-truncated Stat1, allowing its dephosphorylation. This and other data suggested that the ND is required for facilitating the reorientation of parallel Stat1 dimers into the anti-parallel conformation [110]. The assumption had been that the STAT1 ND exerts this function '*in cis*', from within the dimer undergoing reorientation.

The role of the ND in dimer reorientation, together with the availability of the p-Stat5 ND for *inter*-dimer interactions, suggests a mechanism for the positive feedback mediated by p-Stat5 in Stat5 phosphorylation. We propose that the reorientation of inactive Stat5 from the anti-parallel to the parallel conformation is relatively inefficient or energetically unfavorable, and may require a chaperone. The NDs of parallel, active dimers may chaperone this conformational switch, promoting the formation of parallel dimers (Figure 2.14H). The resulting parallel dimers have a higher likelihood of becoming phosphorylated, either because they may be better kinase substrates, or else they may be poorer phosphatase substrates; the latter is likely due to the masking of the phosphotyrosine within the SH2 domain.

The resulting reaction, in which parallel dimers catalyze the conversion of anti-parallel dimers to the parallel conformation, would result in self-replication of the parallel

structure, giving rise to a prion-like, autocatalytic process [226] that would form the basis for bistability and binary signaling.

Site of interaction of the ND with Stat5

Co-expression of FLAG-Stat5 Δ ND with low-levels of the isolated Myc-ND resulted in a high-intensity binary p-Stat5 response, similar to that obtained when Myc-ND was co-expressed with wild-type Stat5 (Figure 2.14D, F). Similarly, expression of the FLAG-Stat5 Δ ND with high levels of the Myc-ND promoted dephosphorylation (Figure 2.16B) in the way it promoted the dephosphorylation of wild-type Stat5 (Figure 2.15B). The latter findings are similar to those reported for Stat1, where the isolated ND promoted the dephosphorylation of the ND-truncated Stat1 [110]. Together, these findings suggest that the inter-dimer ND-mediated interaction does not occur via an inter-dimer ND dimerization. The ND therefore interacts *in trans* with a non-ND, core domain of the STAT molecule.

We found that NDs bearing mutations at F81 or L82, two residues in the ND dimerization interface, were deficient in amplification of the p-Stat5 response (Figure 2.16D-F). Given that ND dimerization does not play a part in the inter-dimer interaction, these findings raise the possibility that that the dimerization interface may, in addition to ND dimerization, also interact with the Stat5 core domain. An alternative possibility is that the ND domains of active Stat5 dimers may need to be in a homodimeric form in order to mediate inter-dimer interactions.

Implications for STAT's role in disease

Our work raises the possibility that activation of other STATs may also be bistable, since all STAT family members share highly conserved structural motifs. Further, many STATs are believed to undergo a similar conformational reorientation during their activation/deactivation cycle.

STAT proteins are implicated in a variety of disease processes, and in particular, Stat3 and Stat5 have causal roles in cell transformation. The finding that Stat5 activation is bistable is relevant to leukemogenesis, where constitutively active Stat5 is an essential component of cell transformation downstream of many oncoproteins. Therefore, an understanding of the mechanisms that contribute to bistable activation would aid in designing novel therapeutic approaches.

Materials and Methods

Mouse models

BALB/c ByJ and C57BL/6J and C57BL/6J-Ptpn6^{me-v}/J strains were purchased from the Jackson Laboratory (Maine). Stat5-null were supplied by Dr. Lothar Hennighausen, NIDDK, Bethesda, MD, and EpoR-H and EpoR-HM by Dr Jim Ihle, St. Jude Children's Research hospital, Memphis, TN. Mice were matched for the same background strain and embryonic age in all experiments.

Erythropoietin injections in adult mice

Adult mice were injected with a single dose of Epo (3-10 IU/gram sub-cutaneously). Mice were sacrificed at different time points, as described in the animal protocol, and the erythropoietic tissues, spleen and bone marrow, were collected in phosphowash, as

described previously [168]. The tissues were processed in phosphowash, fixed with paraformaldehyde, permeabilized with acetone and stored at -80C until the staining was performed.

Fetal liver cell preparation

Fetal livers were isolated at E12.5-E14.5, dissociated mechanically, and deprived of Epo for 90 minutes in the presence of 20% serum prior to Epo stimulation. Cells were then stimulated with different doses of Epo for a fixed time (dose response curve) or with a single dose of Epo at multiple time points (time course).

Amaxa Biosystem Nucleofection

Fresh fetal liver cells were prepared for electroporation using the Mouse ES Cell Nucleofector Kit (VPH-1001, Amaxa Biosystem) according to the manufacturer's instructions. Electroporations were performed using the Amaxa Biosystem Nucleofector (program X-001). Following electroporation, cells were incubated for 18 hours in Epo (0.2 U/mL), Stem Cell Factor (100 ng/mL) and Interleukin-3 (10 ng/mL), washed 3 times and incubated in 20% serum for 3 hours prior to Epo stimulation.

Pervanadate treatment

Cells were electroporated with a pcDNA3 vector expressing pcDNA3-FLAG-Stat5, pcDNA3-FLAG-Stat5Y694F or pcDNA3 vector alone and cultured overnight in the presence of SCF (100 ng/ml), IL3 (10 ng/ml) and Epo (0.5 U/ml). 18 hours after electroporation cells were washed 3 times, starved of growth factors for 3 hours and treated with pervanadate for different times as described [227]. Cells were collected, washed with phospho-wash buffer, fixed, permeabilized and frozen at -80C. Cells were subsequently analyzed for p-Stat5 by flow cytometry.

SOCS3 siRNA

Fetal liver cells were electroporated with 2 μ g of SOCS3 (L-040626-01, Dharmacon) or control (D-001810-10, Dharmacon) siRNA. Cells were recovered in 20% serum for 4 hours and subsequently stimulated with Epo (0.2 U/ml) in a time course experiment

Mouse Embryonic Fibroblasts (MEFs) Infection

Stat5^{-/-} MEFs were seeded at 30% confluency. Cells were incubated with retroviral supernatant dilutions, in the presence of polybrene (4 μ g/mL), for 6 hours. The retroviral supernatant was removed and cells were collected at 48 hours post infection for western blotting.

Flow cytometry

Epo-stimulated cells were harvested in phosphowash (PBS, 1mM sodium orthovanadate, 1mM β -glycerol phosphate, 1 μ g/mL microcystin), fixed in 1.6% paraformaldehyde, permeabilized in 80% acetone and stored at -80°C. Thawed cells were stained in PBS/3% milk with AF647-conjugated anti-phospho Stat5 (612599, BD Biosciences), for Ter119 and CD71 as described [14], and where indicated, for Stat5 (ab 7969, Abcam followed by anti-rabbit-APC, Jackson ImmunoResearch Laboratories), FLAG (F4049, Sigma Aldrich) and Myc (2272, Cell Signaling Technology). In all electroporation experiments, cells were stained with LIVE/DEAD Fixable Blue Dead Cell Stain Kit for UV excitation (L-23105, Invitrogen), prior to fixation and permeabilization in order to exclude dead cells from analysis. λ -phosphatase treatment was for 15 minutes at 37°C on fixed and permeabilized cells (1,000 units, New England Biolabs).

Apoptosis assays were done on fresh fetal livers that were deprived of Epo for 90 minutes and then stained for CD71, Ter119 and Annexin V according to the manufacturer's instructions (BD Biosciences). Spleen and bone marrow cells isolated from adult mice were immediately stained with CD71 and Ter119 as described [14]. Cells were analyzed on an LSRII cytometer (BD Biosciences). Data were analyzed with FlowJo software (Tree Star, Stanford University, Stanford, CA).

DNA constructs: cloning and mutagenesis

pcDNA3-Flag Stat5a, pcDNA3-Flag Stat5 1*6 were generated by cloning the FLAG-Stat5 (wild type or mutant), provided by Dr. T. Kitamura, in the pcDNA3 construct (Invitrogen). Retroviral constructs were previously described (Socolovsky et al, 1999, Cell, 98: 181-91). pcDNA3-Flag Stat5a-Y694F was generated by mutagenesis using the QuickChange Site-Directed Mutagenesis Kit (Stratagene) according to the manufacturer's instructions. pcDNA3-Myc Stat5 N-terminal domain construct was generated by cloning the sequence corresponding to Stat5a amino acid 1-130 into a pcDNA3 vector, subsequent mutagenesis to remove the stop codon and cloning into a pcDNA3 vector containing a triple Myc tag (gift of Dr. Ralph Scully, Harvard Medical School). Stat5 Δ ND was generated by removal of the first 129 amino acids of wild-type Stat5. The NDL82S and NDF81A/L82A mutants were generated by site-directed mutagenesis.

Quantitative RT-PCR

RNA was extracted, using the AllPrep DNA/RNA Micro Kit (80284, Qiagen), from FACS-sorted fetal liver cells. Taqman real time PCR (Applied Biosystems) was performed on cDNA prepared using the SuperScript First-Strand kit (Invitrogen). The

following probes were used for SHP-1, SOCS3 and EpoR respectively (Mm 00469148_g1, Mm 01249143_g1, Mm 01175895_g1, Applied Biosystems).

Denaturing Immunoprecipitation and Quantitative Western Blotting

Denaturing immunoprecipitation was performed on 10^7 cell equivalents of each protein lysate. Cells were boiled for 5 minutes in 200 μ L of a buffer containing 50 mM Tris-HCl (pH 8.0), 0.5% SDS, 1mM DTT, 10 mM NaF, 1 mM Na_3VO_4 , and 1 mM PMSF. Then, 800 μ L of a buffer containing 50 mM Tris-HCl (pH 8.0), 150 mM NaCl, 1% sodium deoxycholate, 1% NP-40, 2mM EDTA, 10 mM NaF, 1 mM Na_3VO_4 and 1 mM PMSF, were added. The samples were rotated for 5 minutes in the cold room and then centrifuged at maximum speed for 15 minutes. The lysate was incubated with 10ul of Dynabeads Protein G (100.04D, Invitrogen) for 1h in the cold room. The beads were removed and the remaining lysate was incubated overnight with 100ul of Dynabeads Protein G that were precoated with the FLAG antibody (F1804, Sigma-Aldrich) in the cold room. The Dynabeads-Ip-Antigen complexes were washed 4 times with lysis buffer, resuspended in 2X sample buffer and boiled for 10 minutes. The eluate was loaded on a 4-12% gradient polyacrylamide gels (Invitrogen). The gel was transferred onto a nitrocellulose membrane by semidry transfer method (Biorad), for 45 minutes at room temperature, according to the manufacturer instructions. After transfer the blot was analyzed using the Odyssey infrared imaging system (LI-COR, Biosciences, NE, USA). In summary, for FLAG staining, the membrane was incubated in Odyssey blocking buffer for 1 hour at room temperature. The membrane was then stained for 30 min in Odyssey blocking buffer in the presence of 1:1000 dilution of anti-FLAG antibody

(F1804, Sigma-Aldrich). The membrane was washed 4 times for 5 minutes in Tris-Buffered Saline with Tween 20 (TBST) buffer (50 mM Tris.HCl, pH 7.4, 150 mM NaCl, 0.2% Tween 20). Subsequently the membrane was incubated with 1:10000 dilution of anti-Mouse-IRDye 800CW secondary antibody (926-32210, LI-COR) for 1 hour at room temperature, in the dark. The membrane was finally washed 4 times for 5 minutes in TBST. For phospho-Stat5 staining the membrane was incubated in blocking buffer (5% milk in TBS) for 1 hour at room temperature. The membrane was then stained overnight in blocking buffer in the presence of 1:1000 dilution of anti phospho-Stat5 antibody (611964, BD Biosciences). The membrane was washed 4 times for 5 minutes in TBST. Subsequently the membrane was incubated with 1:10000 dilution of anti-Mouse-IRDye 800CW secondary antibody (926-32210, LI-COR) for 1h at room temperature, in the dark. The membrane was finally washed 4 times for 5 minutes in TBST. The membranes were scanned using the Odyssey infrared imaging system (LI-COR, Biosciences, NE, USA) and the images were analyzed using the Odyssey software.

Western Blot Analysis

Cell lysates were loaded on a 4-12% gradient polyacrylamide gels (Invitrogen). The gel was transferred onto Polyvinylidene fluoride (PVDF) membrane by semidry transfer method (Biorad), for 45 minutes at room temperature, according to the manufacturer instructions. After transfer the membrane was incubated in blocking buffer (5% milk in TBST) for 1 hour at room temperature. The membrane was stained overnight in blocking buffer with anti-FLAG (F1804, Sigma-Aldrich), anti-Myc (2272, Cell Signaling), anti-p-Stat5 (611964, BD Biosciences) or anti-Stat5 (610191, BD Biosciences) antibodies. The

membrane was washed 5 times for 7 minutes in TBST. The membrane was incubated with secondary antibody (anti-Rabbit HRP 1:5000 or anti-Mouse HRP 1:5000, Jackson ImmunoResearch laboratories, Inc.) in 5% milk TBST for 1 hour at room temperature. Immunodetection was performed by enhanced chemiluminescence (12015196001, Roche) for phospho-Stat5 and regular chemiluminescence (NEL104, Perkin Elmer) for Stat5, Myc and FLAG.

Chapter III Attributions and Copyright Information

The work in this chapter has been accepted for publication in Journal of Visual Experiments in a modified format.

Identification and analysis of mouse erythroid progenitors using the CD71/Ter119 flow-cytometric assay

Miroslav Koulis*, Ramona Pop*, Ermelinda Porpiglia*, Jeffrey R. Shearstone*, Daniel Hidalgo and Merav Socolovsky

Department of Pediatrics and Department of Cancer Biology, University of Massachusetts Medical School, Worcester MA USA

*contributed equally to this work.

Specific contributions to figures:

Figure 3.3: EP

Disclosure of Conflicts of Interest:

None of the authors have any conflicts of interest to declare.

Additional disclosures:

Figure 3.1 represents original art work by MK

CHAPTER III: Identification and analysis of mouse erythroid progenitors using the CD71/Ter119 flow-cytometric assay

Introduction

The study of erythropoiesis aims to understand how red cells are formed from earlier hematopoietic and erythroid progenitors. Specifically, the rate of red cell formation is regulated by the hormone erythropoietin (Epo), whose synthesis is triggered by tissue hypoxia. A threat to adequate tissue oxygenation results in a rapid increase in Epo, driving an increase in erythropoietic rate, a process known as the erythropoietic stress response. The resulting increase in the number of circulating red cells improves tissue oxygen delivery. An efficient erythropoietic stress response is therefore critical to the survival and recovery from physiological and pathological conditions such as high altitude, anemia, hemorrhage, chemotherapy or stem cell transplantation.

The mouse is a key model for the study of erythropoiesis and its stress response. Mouse definitive (adult-type) erythropoiesis takes place in the fetal liver between embryonic days E11.5 and E15.5, in the neonatal spleen, and in adult spleen and bone marrow. Classical methods of identifying erythroid progenitors in tissue rely on the ability of these cells to give rise to red cell colonies when plated in Epo-containing semi-solid media. Their erythroid precursor progeny are identified based on morphological criteria. Neither of these classical methods allow access to large numbers of differentiation-stage-specific erythroid cells for molecular study. Here we present a flow-cytometric method of identifying and studying differentiation-stage-specific erythroid

progenitors and precursors, directly in the context of freshly isolated mouse tissue (Figure 3.1). The assay relies on the cell-surface markers Ter119, CD71, and on the flow-cytometric ‘forward-scatter’ parameter, which is a function of cell size. The CD71/Ter119 assay can be used to study erythroid progenitors during their response to erythropoietic stress *in vivo*, for example, in anemic mice or mice housed in low oxygen conditions. It may also be used to study erythroid progenitors directly in the tissues of genetically modified adult mice or embryos, in order to assess the specific role of the modified molecular pathway in erythropoiesis.

Figure 3.1 Experimental strategy to study erythropoiesis using flow cytometry.

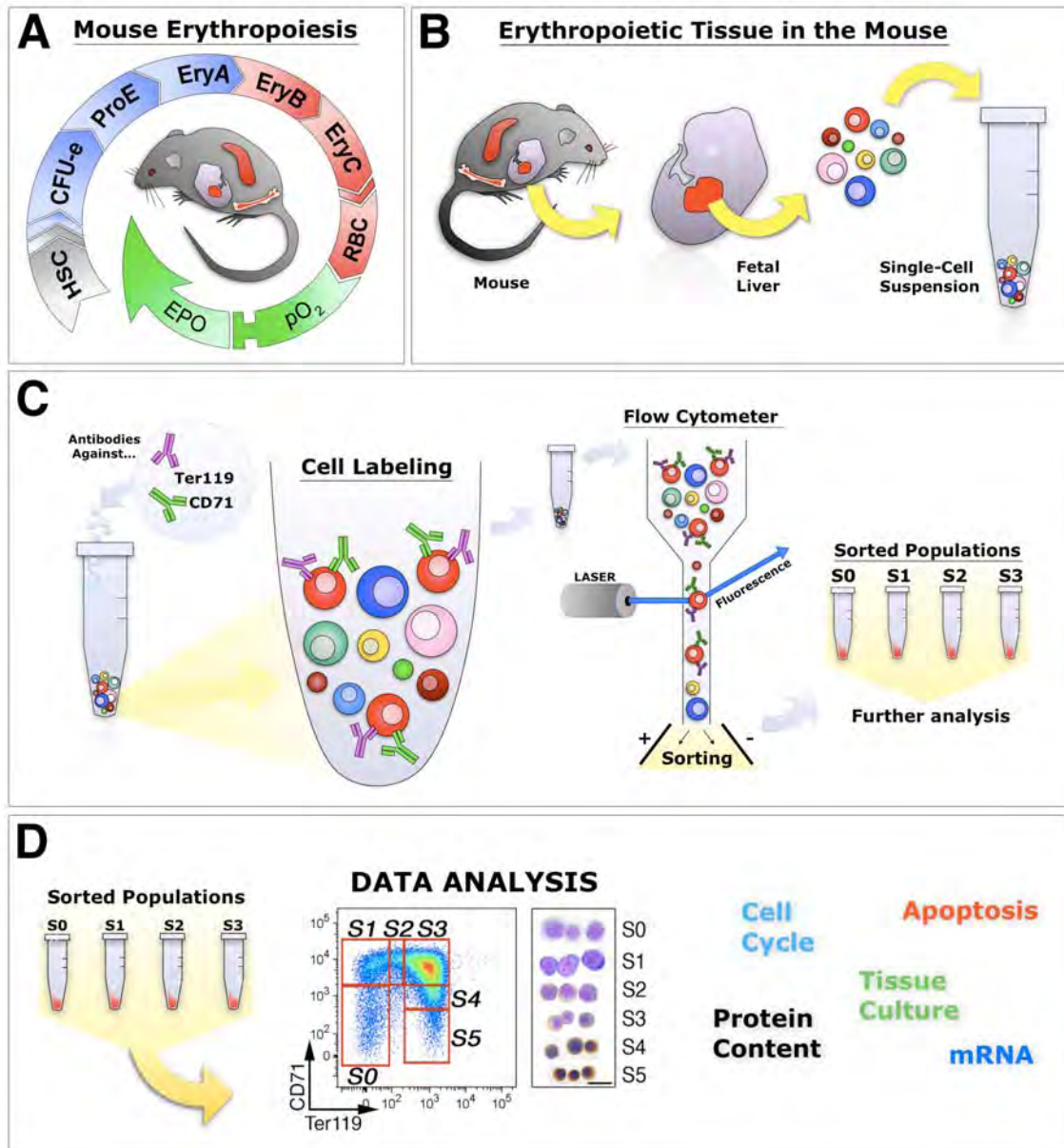
(A) The mouse is a key model for the study of erythropoiesis and its stress response. Mouse erythropoiesis occurs in the spleen, bone marrow, and in the fetal liver (middle). In these tissues, hematopoietic stem cells (HSC) are restricted to the erythroid lineage (blue and red stages), which in turn gives rise to red blood cells. Proper number of red cells maintains tissue oxygen (green) normal and negatively regulates Epo. Not enough red cells leads to tissue hypoxia. In turn, high Epo (green) increases erythropoiesis to correct the deficit.

(B) To study erythroid cells, we first isolate total cells from hematopoietic tissues (e.g. fetal liver).

(C) Freshly-isolated cells are labeled with fluorescent markers directed against erythroid, or any additional membrane or intracellular, antigens. Fluorescence data of the labeled sample is collected using flow-cytometer. Cells can be physically sorted using a cell sorter into separate tubes.

(D) Sample data is then analyzed using Flowjo analysis for erythroid markers, apoptosis and cell cycle. Representative analysis of fetal liver is shown in the middle panel. Sorted populations can be cytopun onto microscope slides (cytopins shown), analyzed for their protein and mRNA content, or cultured for further analysis.

Figure 3.1



Protocol

1. Harvesting of tissues:

- 1.1** Prepare tubes containing 2 to 5 ml cold staining buffer (phosphate-buffered saline (PBS) with added 0.2% BSA and 5mM glucose). Keep tubes on ice prior to tissue harvest.
- 1.2** Cull mice according to appropriate approved protocol (e.g. CO₂ inhalation followed by cervical dislocation).
- 1.3** Draw blood by cardiac puncture into EDTA or heparin blood-collection tubes for later analysis (e.g. hematocrit, reticulocyte count or CBC analysis).
- 1.4** Harvest the spleen and bones, placing tissues from each mouse in a separate tube, prepared in step 1. Easy access to spleen is from the left side. For the bone marrow, harvest one or both femurs. Keep tubes with harvested tissue on ice.
- 1.5** If desired, weigh the spleen. Mice undergoing an erythropoietic stress response are likely to show a significant increase in spleen weight.

2. Preparation of spleen cells:

- 2.1** Using a pre-moistened 3 ml syringe plunger, gently push the spleen, or part of the spleen (ideally, 0.1 gram or less, equivalent to approximately 10⁸ cells) through a 40 mm sterile cell strainer (Fisherbrand catalog number 22363547 or other) placed on top of a 50 ml conical tube. Keep the tube on ice during this procedure. Wash the cells through the strainer with a total of 2 ml staining buffer.

- 2.2 Gently pipette the strained cell suspension to break up any small clumps. If necessary, re-strain the cells.
- 2.3 Wash the cells twice by centrifugation and resuspend in cold buffer. For centrifugation, spin for 3' to 5' at approximately 1400 RPM at 4°C.
- 2.4 Count the cells using a hemocytometer. Typical yields are $1-2 \times 10^8$ cells/spleen. For flow cytometry analysis, aliquote 1 to 2×10^6 cells per sample, either into FACS staining tubes (BD Falcon polystyrene round-bottom tubes, 352008) or U-bottom 96 well plate (BD Falcon 353910). Sample staining volume is 200 μ l, to a final cell concentration 0.5 to 1×10^7 cells/ml or $1-2 \times 10^6$ cells/ 200 μ l sample.

3. Preparation of bone marrow cells:

- 3.1 Prepare 1 or 3 ml syringes with an attached 26G needle, pre-filled with cold staining buffer.
- 3.2 Remove muscles attached to the femur so as to visualize the bone clearly.
- 3.3 Using sharp surgical scissors, snip off both ends of the femur, as close as possible to the ends of the bone. This should reveal a small hole at each cut end, leading into the bone-marrow cavity, which runs through the length of the femur.
- 3.4 Using the pre-filled syringe in step 1, insert the needle through one of these holes, and gently flush the marrow out through the hole at the other end into a tube.

- 3.5 Dissociate the flushed cells by gentle pipetting, and strain through a 40 mm strainer as for the spleen above (see section 2.1).
- 3.6 Wash cells twice by centrifugation in cold staining buffer.
- 3.7 Count the cells and resuspend as in section 2.4. Typical yields are approximately 10^7 cells per femur.

4. Preparation of fetal liver cells:

- 4.1 To prepare timed-pregnant female mice, set up mice for mating in the evening; examine for vaginal plugs before 10 am the following day; the day on which the vaginal plug is detected is considered day 0.5. Veterinary staff may be able to assist investigators who are unfamiliar with this technique to identify pregnant females.
- 4.2 Timed-pregnant female mice are culled on days E11.5 to 14.5 of pregnancy. The uterine horns are removed into a Petri-dish containing ice-cold culture medium or staining buffer.
- 4.3 Embryos are removed from each uterus and the fetal liver is dissected. A dissecting microscope is required for E12.5 embryos or younger.
- 4.4 Livers may be dissociated mechanically by pipetting in buffer, and are processed either individually in 96-well plates, or pooled together, depending on experimental requirements.
- 4.5 A fetal liver at E13.5 has $\sim 10^7$ cells. Cells are washed twice in staining buffer and resuspended at $1-2 \times 10^6$ cells/ 200 μ l sample for flow-cytometric analysis.

5. Antibody staining for flow cytometry:

5.1 Prepare a primary antibody staining pre-mix to be used for all samples, except for control samples, containing the following:

- ChromePure Rabbit IgG (Jackson, 015-000-003), to a final concentration of 200 $\mu\text{g/ml}$. Check the stock concentration on the bottle (it can vary). This is used to block Fc receptors in mouse cells; alternative species that may be used for this are mouse IgG or rat IgG. Species choice is determined by the potential presence in the staining protocol of secondary antibodies directed against primary rat/mouse/rabbit antibodies, in which case those species cannot be used as blocking antibodies. Alternatively, 5% rabbit serum may also be used in place of purified IgG. A further alternative is the use of monoclonal antibodies or Fab fragments directed at the mouse Fc receptors. The basic protocol below does not include any secondary antibodies and so IgG of any of the three species may be used.
- CD71-FITC, diluted 1:200 (stock 0.5mg/ml, BD-Biosciences, 553266)
- Ter119-PE, diluted 1:200 (stock 0.2mg/ml, BD-Biosciences, 553673)
- Any additional antibodies directed at surface epitopes of interest, e.g. antibodies directed at Fas or FasL (final concentration 5 $\mu\text{g/mL}$) (see [14, 206]). Mix the antibody solution gently by inverting the tube 2-3 times.

5.2 Add 200 μl of the pre-mix to each cell sample and gently resuspend the cells.

5.3 Prepare control cell samples as follows:

- ‘Unstained’: these cells are left in staining buffer and provide the background autofluorescence of the cells.
 - ‘Single color’ controls: one such control is required for each antibody/color used in the protocol. The cells in these controls are stained either with a directly conjugated primary antibody, or with both a primary antibody and a conjugated secondary antibody. These controls are used to correct for spectral overlap between channels.
 - ‘Fluorescence minus one’ (FMO) controls: one such control is required for each antibody/color in the protocol: cells are stained with all the colors/antibodies in the protocol except for the color/antibody for which this is the FMO control. The FMO control for a particular channel provides the true background for that channel. It may include non-specific antibody of the same isotype, and conjugated with the same fluorescence mark as the test antibody (isotype control).
- 5.4** Incubate samples and relevant controls in the primary antibody stain on ice for 45’ to 1 hour in the dark (put aluminum foil cover on ice-bucket).
- 5.5** At the end of incubation, wash the cells by adding 3 ml of staining buffer to each sample tube and spin for 3’ to 5’ at approximately 1400 RPM at 4°C. If using 96 well plates, wash the cells three times in a volume of 200 µl.
- 5.6** If relevant, apply secondary antibody stain. Apply and wash as for the first antibody stain.

- 5.7** If relevant, a stain with Annexin V (apoptosis marker) is applied at the end of incubation, using a HEPES buffer as in the manufacturer's instructions. This stain is applied for 15 minutes at room-temperature, or for 1 hour on ice.
- 5.8** Cells are resuspended for flow cytometry analysis in staining solution containing a cell-impermeable DNA dye, to exclude dead cells. Several DNA dyes are available, including Propidium Iodide, 7-amino-actinomycin D (7AAD), or DAPI. The choice from amongst these depends on the available flow-cytometer channels, given the channels taken up for specific antibody staining, and channels available on the flow-cytometer. 7AAD is obtained from BD-Biosciences (559925) and used according to the manufacturer's instructions. For DAPI staining, make a stock of 1mg/ml in dimethylformamide (DMF) from powder (Roche, 236276), keep at -20°C, and dilute 1:10,000 to 1:15,000 in staining buffer.

6. Flow-cytometric sorting:

- 6.1** Cells are labeled with CD71, Ter119, and a viability dye as described for flow-cytometric analysis (section 5). Cell concentration during labeling may be increased to 5×10^7 /ml.
- 6.2** Antibody labeling for lineage-positive non-erythroid cells may be added with the primary antibody stain, if required, as follows:

Mix an equal volume of each of the following antibodies to make the lineage master mix:

FITC Rat Anti-Mouse CD41 MWRReg30, BD Pharmingen 553848

FITC Rat Anti-Mouse CD45R/B220 RA3-6B2, BD Pharmingen 553087

FITC Hamster Anti-Mouse CD3e 145-2C11, BD Pharmingen 553061

FITC Rat Anti-Mouse CD11b/Mac-1 M1/70, BD Pharmingen 557396

FITC Rat Anti-Mouse Ly-6G and Ly-6C (Gr-1) RB6-8C5, BD Pharmingen
553126

Use the master mix at 1:80 (This is equivalent to 1:400 dilution of each individual antibody stocks, which are all 0.5 mg/ml).

- 6.3** Use low-pressure sorting conditions and wide nozzles. For the Aria (BD Biosciences) we use 100 μ m nozzle, 20 psi pressure.
- 6.4** Collection buffer: PBS with added 20% Fetal Bovine Serum.
- 6.5** To check the purities of the sorted populations, re-run a small aliquot from each sample in a buffer that contains a viability dye (7AAD or similar).

Representative Results

CD71/Ter119 staining of adult bone marrow or spleen identifies a developmental sequence of four subsets, labeled ProE, EryA, EryB and EryC (Figure 3.2)[14]. Morphologically, these correspond to increasingly mature erythroblasts. Figure 3.2 illustrates the gating sequence at the data analysis stage, which discards very small event (including nuclei, red cells), aggregated cells and dead cells.

Expression of cell-surface proteins may be measured simultaneously for each of these subsets, by adding the relevant antibodies at the same time as Ter119 and CD71 staining. Figure 3.2 shows an example of cell-surface expression of the death receptor Fas [14]. This measurement was carried out in mice injected with Epo, or in control mice

injected with saline. It is apparent that Epo suppresses Fas expression in the EryA population *in vivo* [14]. Expression of intracellular proteins or cell cycle status may also be measured for cells in each subset. Figure 3.3 illustrates representative cell cycle analysis of freshly harvested bone-marrow cells. These measurements require, in addition to cell-surface staining with CD71 and Ter119, the fixation and permeabilization of cells for intracellular labeling (see Discussion section).

Figure 3.2 The CD71/Ter119 erythroid subsets in mouse spleen.

(A) Gating strategy: Spleen cells were processed and labeled with antibodies directed at CD71 and Ter119. This figure shows the analysis strategy following the data acquisition step. Dot-plot I shows all acquired events. The diagonal gate represents events that are likely to be single cells/events, excluding doublets or larger aggregates. Cells in this gate are further analyzed in dot-plot II. Here, very small events, likely nuclei or debris, are excluded. The gated cells are shown in dot-plot III, where DAPI-positive cells, that are likely membrane-permeable apoptotic cells, are excluded from further analysis. Dot-plot IV shows the resulting population of viable spleen cells. The ProE gate contains CD71^{high}Ter119^{intermediate} cells. Ter119^{high} cells are further analyzed in dot-plot V. Here CD71^{high} cells are subdivided into less mature, large ‘EryA’ erythroblasts (CD71^{high}Ter119^{high}FSC^{high}) and smaller, more mature ‘EryB’ erythroblasts (CD71^{high}Ter119^{high}FSC^{low}). The most mature erythroblast subset is EryC (CD71^{low}Ter119^{high}FSC^{low}). Dot-plot VI shows cell-surface Fas expression, specifically in the EryA subset, in mice in the basal state (injected with saline), and mice injected with a single dose of Epo. Staining with Fas was carried out simultaneously with the CD71/Ter119 staining.

(B) Cytospin preparations of cells sorted from each of the indicated subsets. Cells were stained with Giemsa and with Diaminobenzidine, the latter generates a brown stain with hemoglobin. (Cytospin data was originally published in [14]).

Figure 3.2

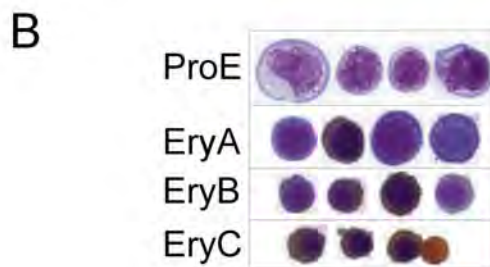
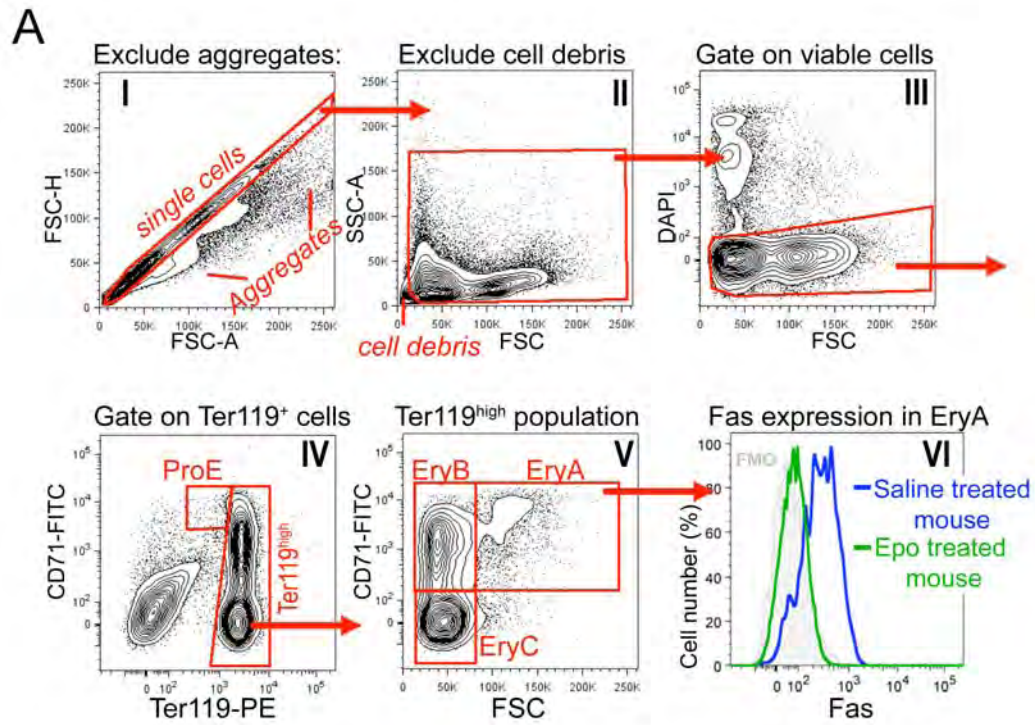
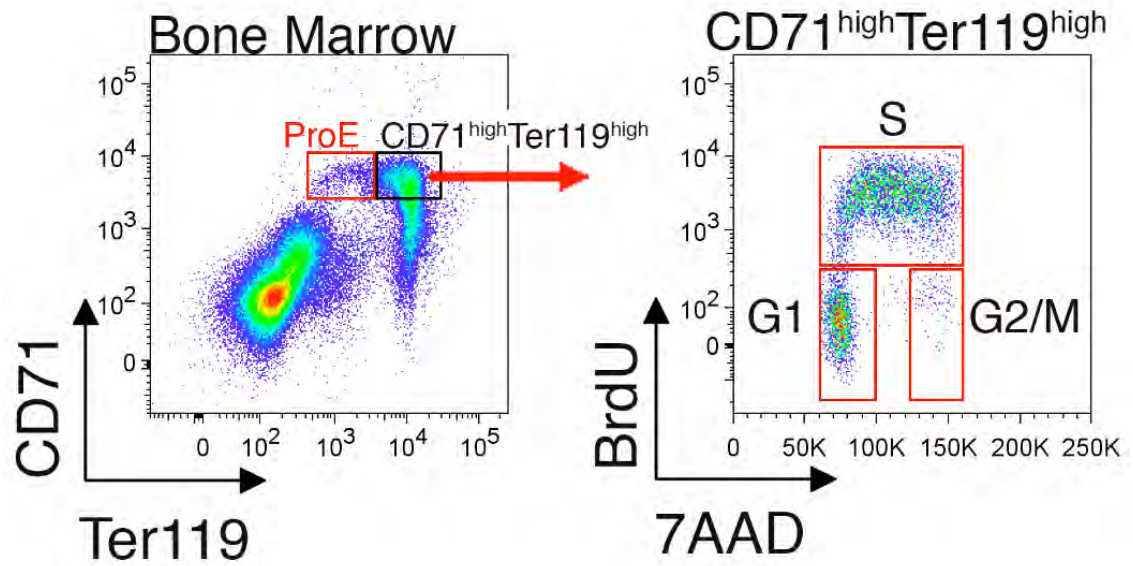


Figure 3.3 Cell cycle analysis of CD71^{high}Ter119^{high} erythroblasts in mouse bone marrow. Mice were injected intraperitoneally with BrdU, and spleen and bone marrow were harvested 30 to 60 minutes later. Bone marrow cells were fixed and permeabilized, and in addition to being stained for CD71 and Ter119, were stained for BrdU incorporation into their replicating DNA with a monoclonal antibody directed at BrdU (fixation, permeabilization and BrdU-staining protocol was according to manufacturer's instruction). BrdU-positive cells are in S-phase of the cycle. Interphase cells are BrdU-negative and may be resolved into G1 or G2/M phases using the DNA dye 7AAD.

Figure 3.3



In fetal liver, non-erythroid cells are first excluded by gating on 'Lin⁻' cells that are negative for CD41, Mac-1, Gr-1, B220 and CD3 (Figure 3.4). The remaining cells are sub-divided into 6 subsets, S0 to S5. The precise pattern of cells in fetal liver is dependent on embryonic age (see Discussion section). A representative cell cycle analysis of the S3 subset in E13.5 fetal liver is shown (Figure 3.5).

Figure 3.4 CD71/Ter119 erythroid subsets in mouse fetal liver.

(A) Gating strategy: Fetal liver cells were labeled for CD71, Ter119, and a cocktail of FITC-labeled antibodies directed at non-erythroid lineage markers ('Lin'). Viable cells (7AAD-negative) were analyzed for Lin expression, and the Lin⁻ cells were further subdivided into the S0 to S5 erythroid subsets. Compared to E14, E13 fetal liver is composed of less mature erythroblasts, shown by the near absence of cells in the mature S4/S5 subsets.

(B) Cytospin preparations of cells sorted from each of the indicated subsets. Cells were stained with Giemsa and with Diaminobenzidine, the latter generates a brown stain with hemoglobin. (Cytospin data was originally published in [208]).

Figure 3.4

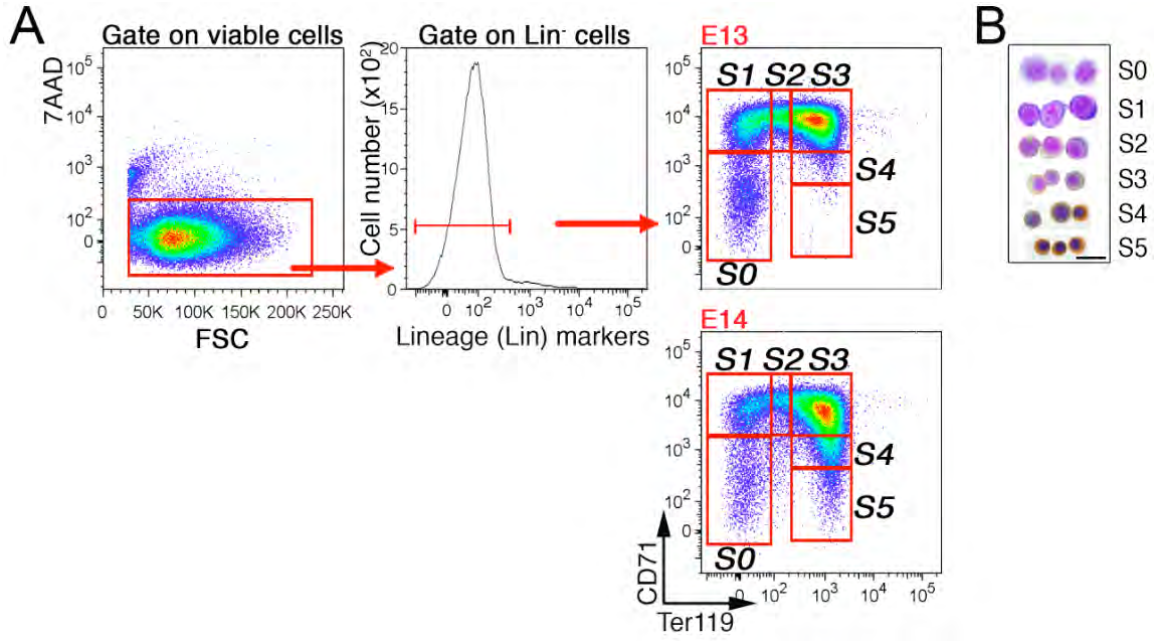
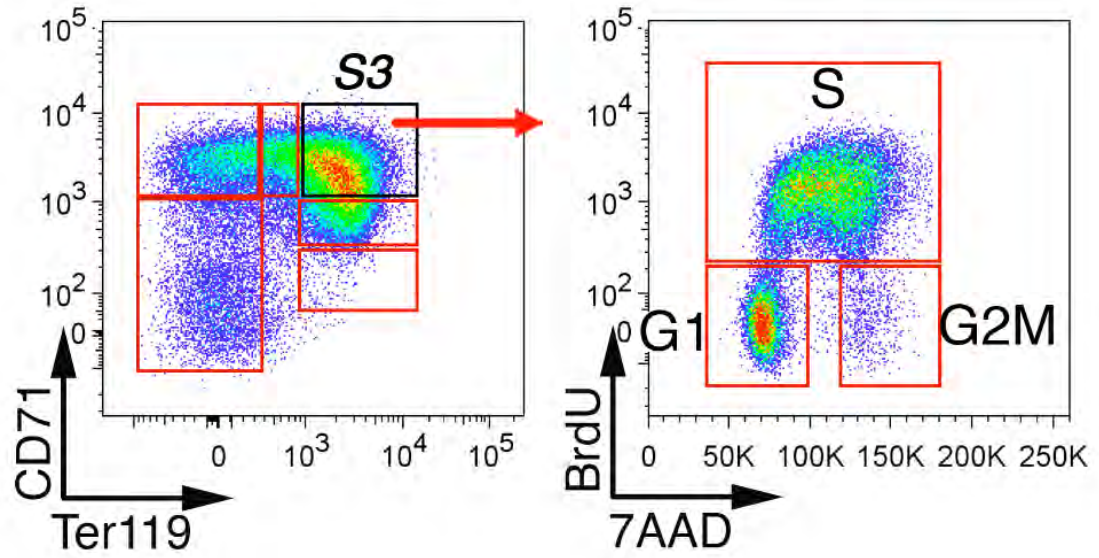


Figure 3.5 Cell cycle analysis of fetal liver erythroid subsets.

Pregnant mice were injected with BrdU, and fetal livers were harvested 30 to 60 minutes later, fixed, permeabilized and stained with antibodies against CD71, Ter119 and BrdU. Cell cycle status of S3 cells is shown.

Figure 3.5



Discussion

The flow-cytometric methodology allows simultaneous investigation of any cellular function that may be detected with a fluorescence-conjugated specific antibody or ligand, including cell-surface markers, protein expression, cell survival, cell signaling using phospho-specific antibodies [169], and cell cycle status. These measurements may be made in each of a number of differentiation-stage specific subsets, in the context of freshly isolated erythropoietic tissue. This method therefore allows assessment of functional and molecular changes at different levels of the erythropoietic system, in response to a wide range of erythropoietic stimuli or as a result of genetic mutations.

No antibody is without cross-reactivity, and cross-reactivity may be tissue-specific. It is therefore important to verify, even for previously tested antibodies, their specificity in the context of erythropoietic tissue, using either a null or a knock-down cell model.

Cells from specific erythroid subsets may be sorted for RNA or transcriptome analysis. Sort experiments should use low sorting pressures and wide nozzles, in order to minimize the shear stress on the cells. We recommend checking cell purity and viability following each sorting experiment. Of note, in the case of multiparameter flow cytometry, the true background for each color is its 'FMO' control (see 5.3), which includes, in addition to autofluorescence, the background due to spectral overlap from all other colors. At the analysis stage, a subset-specific 'FMO' control needs to be used.

Differentiation stage of erythroblasts within the flow-cytometrically defined subsets

The flow-cytometric ProE/EryA/EryB/EryC subsets are defined in terms of cell-surface marker expression and forward scatter. While it is likely that each of these subsets corresponds to approximately the same morphological erythroblast differentiation stage in a wide variety of mouse models, we recommend verifying this when examining a new mouse model. Cells from each of the flow-cytometrically-defined subsets should be sorted and cyospin preparations examined for morphological staging of erythroblasts.

Although the CD71/Ter119 subsets each contain erythroblasts of similar differentiation stage, there remains a degree of heterogeneity within each subset. In the first application of the CD71/Ter119 method, we divided Ter119⁺ cells into regions I to IV based on their CD71 expression. The precise borders between these regions were determined arbitrarily [127]. We subsequently added cell size information to the analysis, in the form of the forward scatter parameter. This allowed us to divide Ter119^{high} cells into subsets by following natural population contours [14] (Figure 3.2). This approach resulted in populations of more uniform maturation and in more reproducible results, and has been recently adapted by other investigators [228-230]. The EryA subset may be subdivided further where desired [230]. One group suggested the use of CD44 in place of CD71 [231]. Although CD44 is less useful in resolving early erythroblast stages, it may resolve later erythroblast subsets with more precision. Both markers may therefore be used, or alternatively, their choice may depend on the specific subsets of interest.

An alternative strategy employs multispectral imaging using the ImageStream technology (Amnis Corporation, Seattle, WA) [232]. It allows the simultaneous and rapid

acquisition of both morphological and flow-cytometric data on many thousands of cells. It is likely to become the 'gold standard' with respect to molecular analysis of stage-specific erythroblasts, since the morphological criteria by which differentiation stage is defined may be measured directly. However, at the present time this technology is less widely available than conventional flow cytometry, and suffers from two drawbacks: it does not allow cell sorting; and it is limited to a smaller number of flow-cytometric parameters.

Intracellular antigens

Detection of intracellular proteins or BrdU requires cell fixation and permeabilization. The precise fixation and permeabilization procedure depends on the intracellular antigen in question. We use the LIVE/DEAD Fixable Dead Cell Stain (Molecular Probes) during the fixation procedure, to distinguish viable from dead cells. Of note, permeabilization with detergents usually impacts the Ter119 signal, which is partially detergent soluble. We overcome this difficulty by using gentle detergents (such as the saponin-based 'perm/wash' buffer from BD Biosciences). We also stain for Ter119 both prior to, and following, the fixation & permeabilization procedure, in order to optimize the Ter119 signal. Alternatively, it is possible to sort viable cells from each of the CD71/ Ter119 subsets first, and carry out fixation and permeabilization separately on purified cells from each subset e.g. see the cell cycle analysis in fetal liver [208].

Fetal liver CD71/Ter119 subsets

The CD71/Ter119 staining pattern in fetal liver is dependent on embryonic age [206] (Figure 3.4). We subdivide fetal liver cells into 6 subsets, S0 to S5 [208]. At the

onset of definitive erythropoiesis in fetal liver on embryonic day 11 (E11), cells are concentrated in subsets S0 and S1 and are largely erythroid colony-forming cells (CFU-e). With embryonic development, CFU-e cells differentiate into proerythroblasts and maturing erythroblasts, and gradually populate subsets S2 to S5 (Figure 3.4).

Subsets S1 to S5 are composed almost entirely of erythroid cells of the definitive lineage. These subsets are absent in the EpoR^{-/-} fetal liver. A small number of Ter119⁺ cells in fetal liver correspond to the primitive (yolk sac) erythroid lineage. These cells are apparent in EpoR^{-/-} fetal liver, where no definitive lineage erythroblasts arise, but by E13.5 form less than 1% of Ter119⁺ cells in wild-type fetal liver [208].

The S0 subset is heterogeneous. At E13.5, 70% of S0 cells are erythroid cells at the CFU-e stage, just prior to the onset of EpoR dependence [208]. The remainder are earlier progenitors as well as cells of other hematopoietic lineages, principally megakaryocytes and macrophages; these cells may be sorted or gated out [208] (Figure 3.4).

Interpretation of changes in the frequency of erythroid subsets

Changes in the frequency of erythroid subsets should be interpreted with care. A change in frequency of cells in any given subset may be due to their altered apoptotic rate, altered transit time through that subset, or alternatively may be due to changes in the number of cells in other subsets. A common cause for increased frequency of early erythroblast subsets ProE and EryA is erythropoietic stress of multiple etiologies [14]. Similar findings have been noted in the 1960's by inspecting erythroblast morphologies during the stress response [233]. The precise reason for the increase in the relative

frequency of earlier precursors during stress is not clear, but in part may be due to the improved survival of these precursors during stress [14].

CHAPTER IV: Conclusions and future directions

1. Conclusions

We explored the dynamics of Stat5 activation in basal and stress erythropoiesis by using a novel flow-cytometric method that allowed us to measure Stat5 phosphorylation at the single cell level, in freshly isolated mouse erythropoietic tissue. We discovered two distinct modes of Stat5 signaling in erythroblasts of different developmental stages. Digital (or binary), low intensity Stat5 signaling was characteristic of mature erythroblasts, and early erythroblasts in response to physiological Epo doses, and was sufficient for basal erythropoiesis. An analog (or graded), high intensity Stat5 signaling was observed in early erythroblasts in response to stress levels of Epo, and was required for stress erythropoiesis. A gradual decrease in Stat5 expression with maturation, characterized the shift from high-intensity to low-intensity Stat5 signaling in developing erythroblasts.

We showed that digital Stat5 signaling is bistable and that bistability is the result of an autocatalytic loop. The isolated Stat5 N-terminal domain, which has been implicated in a radical conformational reorientation of Stat5 dimers required for Stat5 activation, enhanced autocatalysis. We propose that the N-terminal domain of p-Stat5 facilitates the reorientation of inactive dimers during the phosphorylation step, driving autocatalysis and binary signaling.

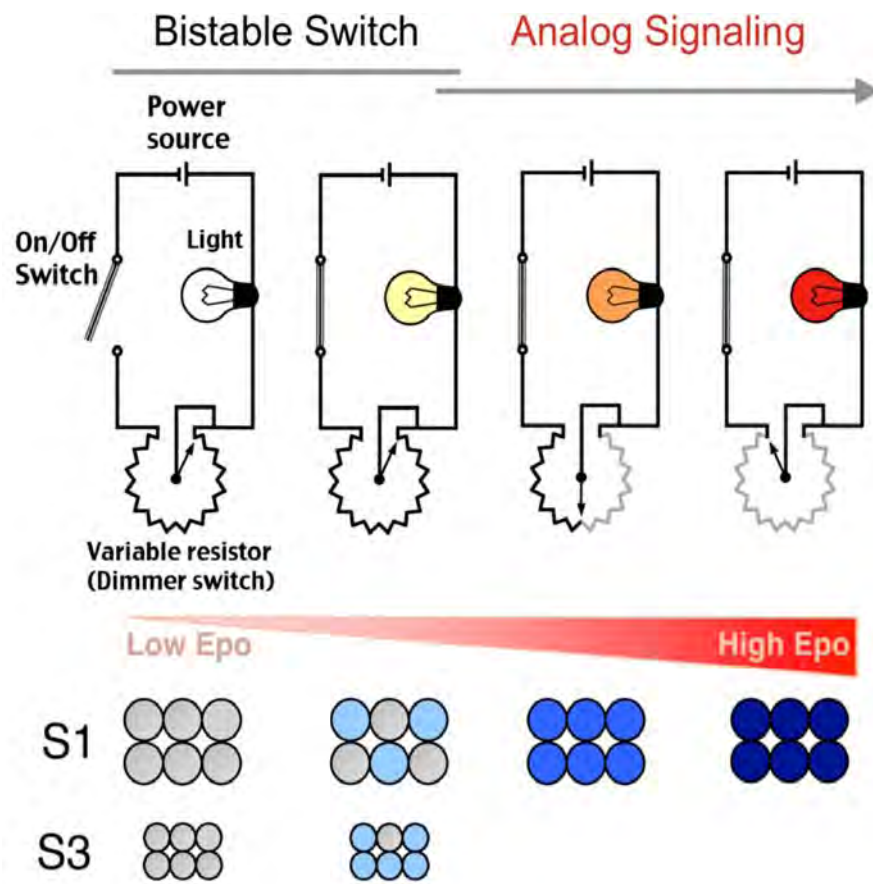
Interestingly, digital (binary) and analog Stat5 signaling combine in early erythroid progenitors in a manner reminiscent of a dimmer light switch: a bistable switch

generates a low intensity but decisive p-Stat5 signal; in response to stress levels of Epo, the amplitude of the signal increases further in a graded manner. Our findings indicate that this bimodal Stat5 activation system ensures a faithful regulation of the erythropoietic rate over a wide range of Epo concentrations. We predict that the dynamic characteristics of Stat5 signaling are likely to impact its function in hematopoiesis and leukemogenesis.

Figure 4.1 Dimmer switch model of Stat5 signaling.

The illustrated dimmer circuit contains a toggle switch that turns the light to a dim, 'on' level and is analogous to the bistable system that generates the digital low intensity p-Stat5 signal. The switch is connected in series to a variable resistor that generates a graded increase in light output, analogous to the high intensity analog p-Stat5 signal. The scheme at the bottom of the figure summarizes the modes of Stat5 activation in early (S1 cells) and late (S3 cells) erythroblasts. Stat5 activation is through a bistable switch that generates a low-intensity binary signal. Further increase in stimulus results in an analog, or graded, increase in the signal amplitude, but only in early, S1 cells expressing high Stat5 levels.

Figure 4.1



2. Significance of our findings

The identification of digital and analog Stat5 signaling modes in erythroblasts has implications for hematopoietic stem cells as well as for hematopoietic lineages in which Stat5 is activated during development, or in adult life, such as myeloid and lymphoid lineage [68, 118-121]. Studies in hematopoietic stem cells showed that different levels of Stat5 activity play an important role in stem cell maintenance versus lineage commitment [121, 234-236], supporting the hypothesis that different Stat5 signaling modes might be modulating these processes. In addition, it has been shown that Stat5 is essential for lymphoid development and differentiation [118, 237]. Therefore, it would be interesting to examine whether digital and analog modes of Stat5 signaling are implicated in developmental decisions or functional specification in other hematopoietic lineages.

Most important, our findings likely apply to other STAT molecules and therefore unravel a new level of regulation of STAT mediated biological processes. The ability to study cell signaling at the single cell levels opens the door to a new signaling universe. It is likely that future studies will uncover the dynamic features of many signaling molecules and their role in the regulation of biological systems. It is an exciting research area that holds potential for understanding the mechanisms of human diseases.

3. Biological function of digital and analog signaling in erythropoiesis

Stat5 activation culminates in the induction of gene expression. We hypothesize that digital and analog Stat5 signaling lead to differential gene expression in fetal liver early erythroblasts (S1 cells). To identify genes that are target of the two modes of

signaling we could perform gene expression profiling on S1 cells from wild type (exhibit digital and analog signaling) and EpoR-HM mice (only exhibit digital signaling), upon stimulation with Epo doses that are within the physiological or hypoxic stress range. The results of these experiments will help us gain insights in the mechanisms responsible for the biological functions of digital and analog signaling.

We have presented some evidence on the biological function of analog Stat5 signaling. EpoR-HM mice, which lack analog signaling, are unable to mount an erythropoietic stress response: upon Epo injection they fail to increase their hematocrit and upregulate CD71 expression (Figure 2.11). However, exogenous expression of Stat5 in fetal liver cells from these mice is able to rescue analog signaling (Figure 2.9B) and CD71 expression (Figure 2.11C). Analog signaling requires EpoR tyrosines. We think that in EpoR-HM mice high Stat5 expression levels are able to compensate for the lack of Stat5 docking sites and therefore rescue analog signaling, by increasing the local concentration of Stat5 molecules in proximity of the activated receptor. To prove *in vivo* the hypothesis that Stat5 analog signaling is required for stress erythropoiesis we will have to perform a bone marrow transplantation experiment in which bone marrow from EpoR-HM mice will be infected with a Stat5-expressing retrovirus and transplanted in irradiated EpoR-HM mice. Mice expressing high levels of Stat5 will be subjected to erythropoietic stress and hematocrit and CD71 expression will be measured. If our hypothesis is correct we will be able to rescue the erythropoietic stress response in EpoR-HM mice upon transplantation.

4. Studying the regulation of Stat5 expression

The finding that Stat5 levels modulate digital and analog signaling and, especially, are limiting for the production of p-Stat5 (Figures 2.7, 2.10), highlights the importance of understanding the regulation of Stat5 expression during erythroid maturation. In erythroblasts, Stat5 expression decreases with differentiation, both at the protein (Figure 2.7) and mRNA level (preliminary data), and cells that express low Stat5 levels (S3 cells) lack analog signaling (Figures 2.7, 2.10). Moreover, our findings that exogenous high-level Stat5 expression leads to constitutive Stat5 activation (Figure 2.12B), suggest that understanding the regulation of Stat5 expression, could help us gain insights into some of the mechanisms of leukemogenesis.

It has been shown that the C-terminal region of Stat5 mediates proteasome-dependent degradation of active Stat5 in cell lines [86, 238, 239]. However, it is not known whether post-translational regulation of Stat5 expression occurs during development. It would be interesting to explore this research direction and to understand the interplay between different mechanisms that control Stat5 expression.

Several mechanisms could regulate Stat5 post-transcriptionally. Importantly, Stat5 expression could be modulated by microRNAs, which are able to fine-tune gene expression to a level that is essential for developmental processes to occur. One microRNA, microRNA-222, has been reported as regulator of Stat5A expression in human endothelial cells [240]. This microRNA has also been shown to be downregulated during *in vitro* expansion of erythroid progenitors [241] and its overexpression is able to inhibit erythropoiesis [242]. However, further studies are required to prove its regulation

of Stat5A expression outside of the vascular system. Identifying microRNAs that are responsible for Stat5 regulation could uncover signaling pathways that are essential for the modulation Stat5 expression in our system as well as in related biological and developmental processes.

5. Investigating the mechanisms responsible for the coexistence of digital and analog signaling

It is noteworthy that a single molecule can exhibit different modes of signaling in the same cell (Figure 4.1). However, it is still unclear what are the factors that allow the co-existence of digital and analog signaling in early erythroblasts. The generation of distinct modes of signaling within the same cell has been reported for Ras in T cells, where initial receptor activation leads to a low intensity, analog Ras signaling, whereas full receptor activation gives rise to high intensity digital Ras signaling upon induction of a positive feedback loop [205, 243, 244].

Our findings raise an important question: what are the molecular mechanisms that limit the digital Stat5 signaling to a low intensity signal? Modulation of the positive feedback loop could be a mechanism. We were able to convert a high intensity graded into a high intensity digital response by expressing exogenous Myc-ND in the presence of FLAG-Stat5 in fetal liver cells (Figure 2.14D). These findings suggest that the availability of free Stat5 ND might be the limiting factor in the generation of a high intensity digital signal. The ND of multiple STAT proteins has been implicated in the formation of tetrameric or higher order molecular complexes [225, 245-249]. Therefore, sequestration of the ND of active Stat5 into multimeric Stat5 complexes could be a

mechanism to interrupt the Stat5-mediated positive feedback loop and therefore limit digital signaling to low intensity. It would be interesting to test this hypothesis in the future by studying the formation of Stat5 complexes under native conditions, in response to changes in the levels of Epo. Moreover, these studies could also be performed in the presence of exogenous wild-type or mutant ND.

A possible mechanism for the coexistence of digital and analog signaling is the generation of semi-phosphorylated Stat5 dimers (in which only one monomer is phosphorylated) at low Epo doses. They might be able to mediate the positive feedback but once fully phosphorylated they could lose that property. Semi-phosphorylated Stat5 dimers could be responsible for digital signaling at low Epo doses, whereas at Epo doses that are above physiological levels, an increase in fully-phosphorylated dimers or higher order molecular complexes, could lead to a graded increase of p-Stat5. Alternatively, an increase in the stability of phosphorylated Stat5 complexes could explain the emergence of analog Stat5 signaling with increasing Epo doses. For example it has been reported that STATs can form tetramers, which result in more stable DNA binding complexes compared to dimers and seem to regulate gene expression selectively [225, 245-248]. Moreover, the formation of high order molecular structures, which are more resistant to phosphatases compared to dimers, has been recently proposed for STAT1 [249].

Stat5 can form homodimers (Stat5A/Stat5A, Stat5B/Stat5B) as well as heterodimers (Stat5A/B), raising the possibility that different type of complexes could participate in digital versus analog Stat5 signaling. It is possible that Stat5A and Stat5B regulate each other, bind to the EpoR with different affinities, form complexes that are

semi- or fully-phosphorylated or that have different half-lives. To determine whether the ratio of Stat5 hetero- to homo-dimers is different in digital and analog Stat5 signaling, studies of Stat5 complexes under native conditions could be performed. Moreover, to determine the contribution of individual Stat5 proteins to the two modes of signaling, the p-Stat5 response to Epo in Stat5a^{-/-} or Stat5b^{-/-} mice could be investigated.

In addition to tyrosine phosphorylation, STATs undergo several post-translational modifications, such as serine phosphorylation [250-252], dephosphorylation by phosphatases [87, 90, 253, 254], arginine methylation [255, 256], acetylation/deacetylation [257], SUMOylation [258-260] and ubiquitination [86, 261]. It is not well understood how these distinct modifications are integrated and contribute to STAT function. Some of them might have a role in the regulation of the Stat5-mediated positive feedback and it would be interesting to investigate this possibility in future studies.

6. Structural studies to confirm our hypothesis on the mechanisms of positive feedback

We showed that low doses of Stat5 ND amplifies constitutive Stat5 activation (Figure 2.15C), enhances the p-Stat5 response to Epo (Figure 2.14C) and converts a high intensity analog response into a high intensity digital response (Figure 2.14D). Based on these findings we proposed that the ND of active Stat5 drives the Stat5 mediated autocatalytic loop by facilitating the conformational reorientation of antiparallel dimers to parallel dimers, during the phosphorylation step (Figure 2.14H).

Several future directions stem from our hypothesis:

- 1) **Mathematical modeling** of the “antiparallel to parallel conformational reorientation reaction”, which will take into account the presence of a Stat5 mediated positive feedback loop. Integration of our data with the mathematical model will allow us to test whether our positive feedback model (Figure 2.14H) is consistent with the data.
- 2) **Domain mapping studies.** Based on our findings that the isolated ND is able to enhance the phosphorylation of an N-terminally truncated Stat5 (Stat5 Δ ND), we hypothesize that Stat5 ND is able to interact with other domains within the Stat5 molecule, than just the ND. If our hypothesis is correct we should be able to co-immunoprecipitate a Stat5 Δ ND with a Stat5 ND, using purified proteins. If an interaction occurs, mutagenesis studies could be performed to identify the sites of interaction between the ND and the rest of the Stat5 molecule (Stat5 core). We predict that mutants NDs that do not interact with the Stat5 core will not be able to promote autocatalysis.
- 3) **Live cell Fluorescence Resonance Energy Transfer (FRET) measurements in the presence of isolated Stat5 ND.** Previous studies have shown that Stat5 molecules fused to YFP or GFP at their N-terminus were able to generate a FRET signal prior to cytokine stimulation, supporting the structural data according to which unphosphorylated STAT dimers are stabilized by ND-ND interaction. Upon prolactin stimulation the FRET signal was not detectable confirming the separation of NDs following activation [109]. It would be interesting to perform similar studies in our system in the presence of different concentration of isolated

ND and under different stimulation conditions, to define the role of the Stat5 ND in the conformational reorientation of Stat5 dimers.

4) **Crystallographic studies of the Stat5 core in the presence of the isolated ND.**

Structural studies are required to prove our hypothesis. First of all it is not clear how unphosphorylated Stat5 dimers approach the receptor, whether they are in the antiparallel or parallel form. Studying the details of this interaction is really important for understanding the molecular mechanisms of the positive feedback. Determining the crystal structure of the full length dimers in different conformations and understanding the interaction between the ND and the rest of the molecule will help us understand the dynamics of the interaction and will allow the design of small molecules that can inhibit the positive feedback. These drugs could be used for the treatment of leukemia that exhibit constitutively active Stat5 (Chapter IV-7). On the other hand being able to modulate the stability of the phosphorylated dimers and therefore the duration of the signal could be useful for the treatment of genetic conditions responsible for anemia.

7. Stat5 and leukemia

Stat5 is constitutively activated downstream of over-active kinases involved in the development of a variety of cancers [122, 123, 192, 194, 262-265]. Moreover, expression of a constitutively active Stat5 mutant is sufficient to cause multilineage leukemia in mice [125], indicating a central role for active Stat5 in leukemogenesis (Chapter I-13). We observed constitutive Stat5 activation in mouse fetal liver cells that expressed high-levels of exogenous Stat5. Constitutive Stat5 activation occurred abruptly once a

threshold of Stat5 expression was reached. This was observed in a sigmoidal relationship between FLAG-Stat5 expression and constitutive p-Stat5, suggesting that constitutive Stat5 activation occurred as the result of a cooperative interaction (Figure 2.12B).

We showed that digital Stat5 signaling is bistable and that bistability is the result of an autocatalytic loop in which active Stat5 promotes further Stat5 activation (Figure 2.12). The intrinsic ultrasensitivity observed in bistable systems helps setting the threshold for the activation of the positive feedback, so that it doesn't get set off by "noise", or in our case by background kinase levels (Chapter I-12). We think that high Stat5 levels are able to lower this threshold and therefore allow activation of the Stat5-mediated positive feedback loop in the presence of background kinase levels, leading to constitutive Stat5 phosphorylation. Therefore, we hypothesize that in tumor cells that lack a constitutively active kinase but still exhibit constitutively active Stat5, selection for Stat5 overexpression could be the mechanism leading to constitutively active Stat5. In support of our hypothesis, an unexplained increase in Stat5 expression has been reported in patients with myeloproliferative diseases [266, 267]. In order to test the hypothesis that Stat5 overexpression can be oncogenic we plan to perform a bone marrow transplantation experiment using cells infected with a Stat5-expressing retrovirus. We predict that infected stem cells expressing high levels of Stat5 will be transformed and will give rise to leukemia.

Understanding the regulation of Stat5 expression together with the mechanisms of its bistable activation could help us gain insights into the mechanisms of Stat5 mediated

oncogenesis. In the long run, our findings will lead to the development of targeted therapies not only for the treatment of red blood cell diseases but also for cancer.

Appendix I Attributions and Copyright information

The material in this chapter has been submitted for publication in a modified format. This chapter represents original work by the authors.

Contrasting Dynamic Responses *in vivo* of the Bcl-x_L and Bim Erythropoietic Survival Pathways

Miroslav Koulis^{1#}, Ermelinda Porpiglia^{1#}, Alberto Porpiglia¹, Ying Liu¹, Kelly Hallstrom¹ and Merav Socolovsky¹

¹Department of Pediatrics and Department of Cancer Biology, University of Massachusetts Medical School, Worcester MA USA

authors contributed equally

Authorship Contributions:

MK, EP designed and performed research, analyzed and interpreted data and wrote the manuscript. AP, KH and YL designed and performed research, analyzed and interpreted data. MS designed research, analyzed and interpreted data and wrote the manuscript.

Specific contributions to figures:

Figure A1.10: EP, MK

Disclosure of Conflicts of Interest:

None of the authors have any conflicts of interest to declare.

APPENDIX I: Contrasting Dynamic Responses *in vivo* of the Bcl-x_L and Bim Erythropoietic survival pathways

Abstract

Survival signaling by the erythropoietin (Epo) receptor (EpoR) is essential for erythropoiesis and for its acceleration in hypoxic stress. A number of apparently redundant EpoR survival pathways were identified *in vitro*, raising the possibility of their functional specialization *in vivo*. Here we used mouse models of acute and chronic stress, including a hypoxic environment and β -thalassemia, to identify two markedly different response dynamics for two early erythroblast survival pathways *in vivo*. Induction of the anti-apoptotic protein Bcl-x_L is rapid but transient, whilst suppression of the pro-apoptotic protein Bim is slower but persistent. Similar to sensory adaptation, however, the Bcl-x_L pathway ‘resets’, allowing it to respond afresh to acute stress superimposed on a chronic stress stimulus. Using ‘knock-in’ mouse models expressing mutant EpoRs, we found that adaptation in the Bcl-x_L response is due to adaptation of its upstream regulator Stat5, both requiring the EpoR distal cytoplasmic domain. We conclude that survival pathways show previously unsuspected functional specialization for the acute and chronic phases of the stress response. Bcl-x_L induction provides a ‘stop-gap’ in acute stress, until slower but permanent pathways are activated. Further, pathological elevation of Bcl-x_L may be the result of impaired adaptation, with implications for myeloproliferative disease mechanisms.

Introduction

Hypoxic stress accelerates the production of red cells by up to ten fold [268]. Erythropoietin (Epo) is essential for both basal and stress erythropoiesis. Epo exerts its effect by activating its receptor, EpoR, on the surface of erythroid progenitors [210]. Colony-forming unit-erythroid (CFU-e) progenitors and their immediate proerythroblast and basophilic erythroblast progeny are Epo-dependent [269]. Until recently, the rarity of these cells within hematopoietic tissue confined their biochemical study to *in vitro* culture systems, where they were found to undergo apoptosis when deprived of Epo [270]. It was therefore suggested that Epo regulates erythropoietic rate through the number of erythroid progenitors it rescues from apoptosis [270].

Recently, we [14] and others [231, 271] made use of cell-surface markers to identify maturation-specific erythroblast subsets directly within freshly isolated mouse hematopoietic tissue [14], including the Epo-responsive ProE (proerythroblasts, CD71^{high}Ter119^{medium}) and EryA (early basophilic erythroblasts, CD71^{high}Ter119^{high}FSC^{high}). This approach confirmed the central role of apoptosis in the erythropoietic stress response, showing that a substantial fraction of the early erythroblast compartment, particularly splenic ProE and EryA, undergo apoptosis *in vivo* in the normal basal state. Stress-induced high Epo levels suppress apoptosis and consequently promote early erythroblast expansion and an increase in erythropoietic rate [14].

Although a number of EpoR-activated survival pathways have been identified [47, 130, 272-274], relevance to erythropoiesis *in vivo* was documented for only a few, largely through gene ‘knockout’ studies revealing abnormal basal or stress erythropoiesis

[130, 228, 275-277]. Importantly, it is unknown how multiple survival pathways integrate *in vivo* to provide a coherent erythropoietic stress response, and whether the large number of survival pathways represents redundancy or functional specialization. The study of these pathways *in vivo*, now made possible with the advent of flow-cytometric techniques (Chapter III)[14, 231, 271], may assist in answering this question.

We recently investigated the role of the death receptor Fas, and its ligand, FasL, which are co-expressed by early erythroblasts and suppressed by EpoR signaling *in vivo* [14, 206, 278]. We found that, in addition to regulating cell survival, this pathway stabilizes basal erythropoiesis and accelerates its response to stress [279]. Therefore, anti-apoptotic pathways may have system-level functions that are not immediately apparent from their anti-apoptotic effects in culture. Here we set out to investigate two apoptotic regulators of the bcl-2 protein family that are targeted by EpoR signaling, the anti-apoptotic protein Bcl-x_L, and the pro-apoptotic Bim protein. Bcl-x_L induction is a major survival pathway in erythroblasts [280, 281], where it is regulated by EpoR-activated Stat5 [130, 213] synergistically with GATA1 [133]. Bcl-x_L^{-/-} mice die *in utero* of anemia, and Bcl-x_L^{-/-} ES cells do not contribute to erythropoiesis in chimeric mice [282]. In a Stat5-deficient mouse [129], reduced Bcl-x_L in early erythroblasts results in ineffective erythropoiesis and anemia [275]. Severe ineffective erythropoiesis in adult erythroblasts conditionally-deleted for Bcl-x_L [277] is corrected if mice are also deleted for the pro-apoptotic proteins Bax and Bak [283], suggesting that the requirement for Bcl-x_L in erythropoiesis is due to its anti-apoptotic effect.

In spite of the clear role for Bcl-x_L in basal erythropoiesis, it is not known

whether erythroblast Bcl-x_L levels increase further during stress, contributing to enhanced erythroblast survival. Elevated levels of erythroblast Bcl-x_L have been implicated in polycythemia vera [284, 285], suggesting that Bcl-x_L-mediated enhanced erythroblast survival has the potential to increase erythropoiesis above the basal rate [285]. It is not, however, known if this happens physiologically.

We contrasted Bcl-x_L with Bim, a BH3-only pro-apoptotic Bcl-2 family protein [286]. Bim downregulation is a key component of survival signaling by cytokines and oncoproteins such as Bcr-Abl or Jak2V617F in hematopoietic progenitors [287, 288]. EpoR survival signaling *in vitro* was recently shown to be in part due to decreased Bim mRNA [273, 289] and to ERK-mediated phosphorylation and degradation of the Bim protein [289]. Further, Bim^{-/-} mice have normal red cell numbers but these arise from a smaller pool of progenitors with enhanced survival [289]. Like Bcl-x_L, in addition to EpoR signaling, Bim suppression is also mediated by GATA-1, via its transcriptional target LRF [290]. LRF^{-/-} mice, which die in utero secondary to severe erythroblast apoptosis and anemia, were partly rescued by Bim deletion [290]. In spite of the clear role of Bim suppression in erythroblast survival, it is not known whether this pathway participates in the stress response.

Here we used intracellular multiparameter flow cytometry to measure Bcl-x_L and Bim in stage-specific erythroblasts directly in erythropoietic tissue of fetal and adult mice as they are undergoing differentiation and responding to stress *in vivo*. We found a similar, highly dynamic activation of the Bim and Bcl-x_L survival pathways in the fetus that was dependent on both developmental day and erythroblast differentiation stage.

These pathways diverge, however, in the adult, where their contrasting dynamic responses suggest a clear segregation of function during the acute and chronic phases of the stress response.

Results

Erythroid developmental delay in Stat5^{-/-} embryos

The definitive erythropoietic lineage generates enucleated red cells and first begins in the murine fetal liver on embryonic day 11.5 (E11.5). Using cell surface markers CD71 and Ter119, we divided fresh fetal liver into a developmental sequence of increasingly mature subsets S0 to S5 [208] (Figure A1.1A). Most S0 cells ($\geq 70\%$) are erythroid progenitors at the colony-forming unit stage (CFU-e), just preceding the onset of Epo/EpoR dependence that takes place at the transition from S0 to S1 [208]. Subsets S1 to S5 contain increasingly mature Epo-dependent CFU-e, proerythroblasts and erythroblasts [208]. Between E11.5 and E14.5, fetal liver cell number increases 1000 fold, and the majority shift in maturational stage from earlier erythroid progenitors and precursors (S0/S1/S2) at E11-E12, to late erythroblasts at E13-E14 [206] (Figure A1.1A). We previously showed that these dynamic changes are associated with an apoptosis rate that is dependent on both differentiation stage and developmental day [206]. Apoptosis is seen principally in CFU-e and early erythroblasts (S1-S2), where it is highest on E11.5, decreasing to a low value on E12-E12.5 and rising again on E13-E14 [206].

Given this dynamic picture, we set out to characterize the developmental and maturation-stage-specific expression of Bcl-x_L and Bim in wild-type and in Stat5^{-/-} mice (Figure A1.1). The Stat5^{-/-} mice [68] are anemic *in utero* leading to perinatal death, a

similar but more severe phenotype to that of the hypomorphic Stat5 mouse in which only the first Stat5 exon is deleted [129, 130]. We first analyzed the CD71/Ter119 profiles on sequential developmental days and found that erythroblast maturation in the Stat5^{-/-} embryos was delayed, as seen by their delayed progression from the S1 to S3 (Figure A1.1A, B). Specifically, on E12.5, the S1 subset contained only 10% of wild-type fetal liver cells, but 35% of the Stat5^{-/-} fetal liver cells (p<0.005); by contrast, the more mature S3 subset contained ≥60% of wild-type, but only 20% Stat5^{-/-} fetal liver (p=0.005). This pattern was not simply due to delayed expression of the cell surface markers Ter119 or CD71, as evident from cell size analysis of the S1 and S3 subsets using the flow-cytometric forward scatter parameter, which was unaltered for cells in each respective subset (not shown).

Bcl-x_L and Bim expression in fetal liver is differentiation-stage and embryonic-day dependent

We assessed Bcl-x_L and Bim protein expression using intracellular flow cytometry (Figure A1.1C, D), employing an anti-Bcl-x_L antibody that we previously verified for its specificity [275], and an anti-Bim antibody whose specificity we verified using Bim^{-/-} splenocytes (Figure A1.2A). We found that, consistent with previous findings *in vitro* [213, 281], Bcl-x_L is expressed at very low levels in the early S0-S2 compartment and increases with erythroblast differentiation (Figure A1.1C, D, upper panels). However, in addition, Bcl-x_L expression was highly dependent on developmental day, with high levels in the early S0-S2 subsets of E11.5 embryos, decreasing rapidly in the same subsets with embryonic age (Figure A1.1D upper panel).

Expression of the anti-apoptotic Bim protein is also dependent on both differentiation stage and embryonic day. We found a highly significant increase in both the long (Bim_L) and extra-long (Bim_{EL}) transcripts (Figure 3.S1B, $p < 0.0001$) and in the Bim protein (Figure A1.1D lower panel, $p < 0.0001$) with the transition from S0 to S1, a transition that marks the onset of erythroid progenitor dependence on EpoR [208]. This raised the possibility that induction of the pro-apoptotic Bim protein at the S0/S1 transition may be the cause of EpoR dependence. However, we found no significant differences in Epo dependence or in the sensitivity of Bim^{-/-} fetal liver erythroid progenitors to Epo using a CFU-e assay *in vitro* (Figure A1.2C).

Bim protein expression peaks in S1 and is gradually suppressed with erythroid differentiation, reaching its lowest values in mature erythroblasts (Figure A1.1D lower panel). Similar to Bcl-x_L, Bim expression was also a function of developmental day. For a given maturation subset, Bim expression is lowest on E11.5, peaking on E12.5, and decreasing in older embryos (Figure A1.1D). The changing fetal liver Bcl-x_L and Bim during embryonic days E11.5-E12.5 match our previous findings of large changes in apoptosis, cell number and Fas expression at this time [206].

Bim and Bcl-x_L expression in fetal liver are regulated by Stat5

The rapidly changing expression of Bim and Bcl-x_L during E11.5-E12.5 (Figure A1.1D), and the developmental delay in the Stat5^{-/-} fetal liver (Figure A1.1A, B), together impede our ability to assess the role of Stat5 in regulating Bim and Bcl-x_L expression at this time. However, the CD71/Ter119 profiles and Bim and Bcl-x_L expression begin to stabilize at E13.5, and the Stat5^{-/-} fetal liver profile approaches that of wild-type embryos

(Figure A1.1A, B, D). We therefore compared Bim and Bcl-x_L expression in Stat5^{-/-} fetal liver and wild-type littermates on E13.5-E14.5 (Figure A1.1E, Figure A1.2D, E).

Bcl-x_L expression in the Stat5^{-/-} fetal liver was 1.5 to 2 fold lower in the early erythroblast subsets S1 (p=0.01), S2 (p=0.03) and S3 (p=0.002). Bim levels in Stat5^{-/-} fetal liver were 30% and 40% higher, respectively, in the S3 and S4/5 subsets (p<0.01), suggesting Stat5 regulates its expression. For comparison, we also assessed expression of the erythroblast apoptotic regulators Fas and FasL in the Stat5^{-/-} fetal liver. We found no significant difference in Fas expression between Stat5^{-/-} embryos and wild-type littermates (Figure A1.3).

Figure A1.1 Delayed maturation and altered Bcl-x_L and Bim expression in Stat5^{-/-} fetal liver.

(A) Representative CD71/Ter119 profiles of Stat5^{-/-} fetal livers and wild-type littermates freshly isolated on consecutive embryonic developmental days (E11.5 to E14.5). S0 to S4/5 are increasingly differentiated erythroid progenitors and precursors subsets [208]. Dead cells were excluded using LIVE/DEAD viability dye.

(B) Summary statistics for analysis performed as in 'A', on 5 to 21 embryos per data point (mean ±SEM). Pooled from 3 independent experiments with multiple litters. Stars indicate statistically significant difference between wild-type and Stat5^{-/-} subsets with the following p values: For S1, E12.5 *p=0.002, E13.5 *p=0.00001. E14.5 *p=0.014. For S3, E12.5 *p=0.005, E13.5 *p=0.00004. E14.5 *p=0.010 (two-tailed t-test, unequal variance).

(C) Intracellular flow cytometry for Bcl-x_L and Bim proteins, in the indicated fetal liver subsets. Representative histograms are shown. Freshly isolated wild-type E14.5 fetal liver cells were stained with CD71, Ter119 and the LIVE/DEAD viability dye as in 'A'. Cells were then fixed, permeabilized and stained intracellularly: with an anti-Bcl-x_L antibody, an anti-Bim antibody or with an IgG isotype control.

(D) Bcl-x_L and Bim protein expression profiles, measured as in panel 'C', in fresh wild-type fetal liver cells at the indicated embryonic days, in each of the indicated differentiation subsets S0 to S4/5. Expression is measured as median fluorescence intensity (MFI), from which non-specific background fluorescence, defined as the MFI of the corresponding subset when binding an isotype control antibody, was subtracted. Data points are mean ± SEM.

For Bcl-x_L: n=5 to 14 wild-type embryos per datapoint, pooled from 3 independent experiments with multiple litters. Statistical significance values: S1, E11.5 vs. E14.5, *p<0.05 (two-tailed t-test, unequal variance). E14.5 S2 vs. S3, and E14.5 S3 vs. S4-5, *p<0.0002 (paired t-test).

For Bim: n=6 wild-type Balb/C embryos per datapoint. Statistically significance values: E13.5 S0 vs. E13.5 S1, *p<0.0001; E12.5 S1 vs. E12.5 S3, *p<0.0001; E11.5 S1 vs.

E12.5 S1, * $p < 0.0001$ (two-tailed t-test, unequal variance). Similar developmental pattern were observed in C57BL/6 and Balb/C backgrounds.

(E) Lower Bcl-x_L and higher Bim protein expression in E14.5 Stat5^{-/-} embryos compared with wild-type littermate controls, at the indicated differentiation subset.

For Bcl-x_L: n=11 to 21 embryos per genotype, with each symbol type representing median expression for one litter. Means \pm SEM for the population are indicated. Statistical significance values: S2, * $p = 0.03$. S3, * $p = 0.002$ (paired t test).

For Bim: data points are individual embryos. Mean \pm SEM for the population is shown. Statistical significance values: S3 and S4-5, * $p < 0.01$, two-tailed t-test, unequal variance.

See also Figure A1.2D, E.

Figure A1.1

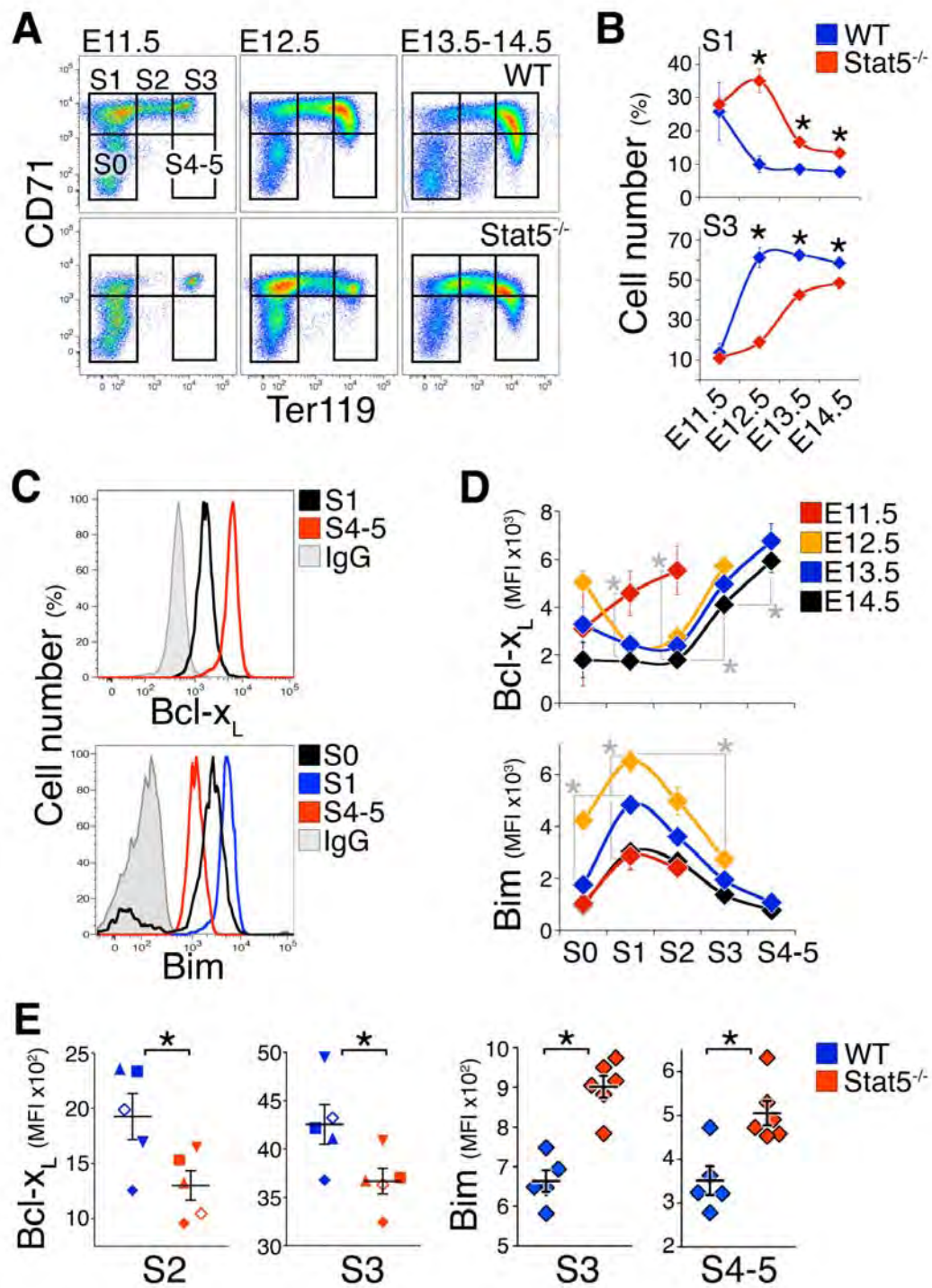


Figure A1.2 Bim and Bcl-xL in fetal liver erythropoiesis.

(A) Bim protein measurement by intracellular flow cytometry. Freshly explanted spleen cells from wild-type (blue) and $Bim^{-/-}$ (red) mice were stained with the LIVE/Dead viability dye, fixed, permeabilized, and stained with an anti-Bim antibody (Cell Signaling, #2819) or isotype control IgG, as described in materials and methods. Dead cells were excluded from analysis.

(B) Quantitative real-time PCR for the Bim isoforms Bim_{EL} and Bim_L in sorted S0 and S1 subsets from freshly harvested wild-type fetal liver. Data was expressed as a ratio to β -actin mRNA in each sample and normalized to the levels measured in S0 cells. Differences between S0 and S1 are statistically significant, Bim_{EL+L} , * $p=0.0003$; Bim_L , * $p=0.0000004$ (two-tailed t-test, unequal variance).

(C) CFU-e assay performed on wild-type and $Bim^{-/-}$ fetal livers. CFU-e colonies per whole fetal liver are shown for each genotype. Data are mean \pm SEM of 6 individual fetal livers per genotype from the same E13.5 litter. Grey bars are a pool containing one Bim wild-type embryo and five $Bim^{+/-}$ embryos. No significant (NS) difference in CFU-e numbers between the genotypes was observed ($p>0.05$, two-tailed t-test, unequal variance). Similar results were obtained when data were expressed as CFU-e colonies per 1×10^6 plated cells. Representative of two similar experiments.

(D) Lower $Bcl-x_L$ expression in $Stat5^{-/-}$ embryos compared with wild-type littermate controls, at the indicated embryonic day and differentiation subset. $n=11$ to 21 embryos per genotype, with each symbol type representing median expression for one litter. Means \pm SEM for the population are indicated. Statistical significance values: E13.5 S1, * $p=0.012$ (paired t-test).

(E) Higher Bim protein expression in $Stat5^{-/-}$ embryos compared with wild-type littermate controls: data points are individual embryos. Mean \pm SEM for the population is shown. Statistical significance values: E13.5 S3 and S4-5, * $p<0.01$, two-tailed t-test, unequal variance.

Figure A1.2

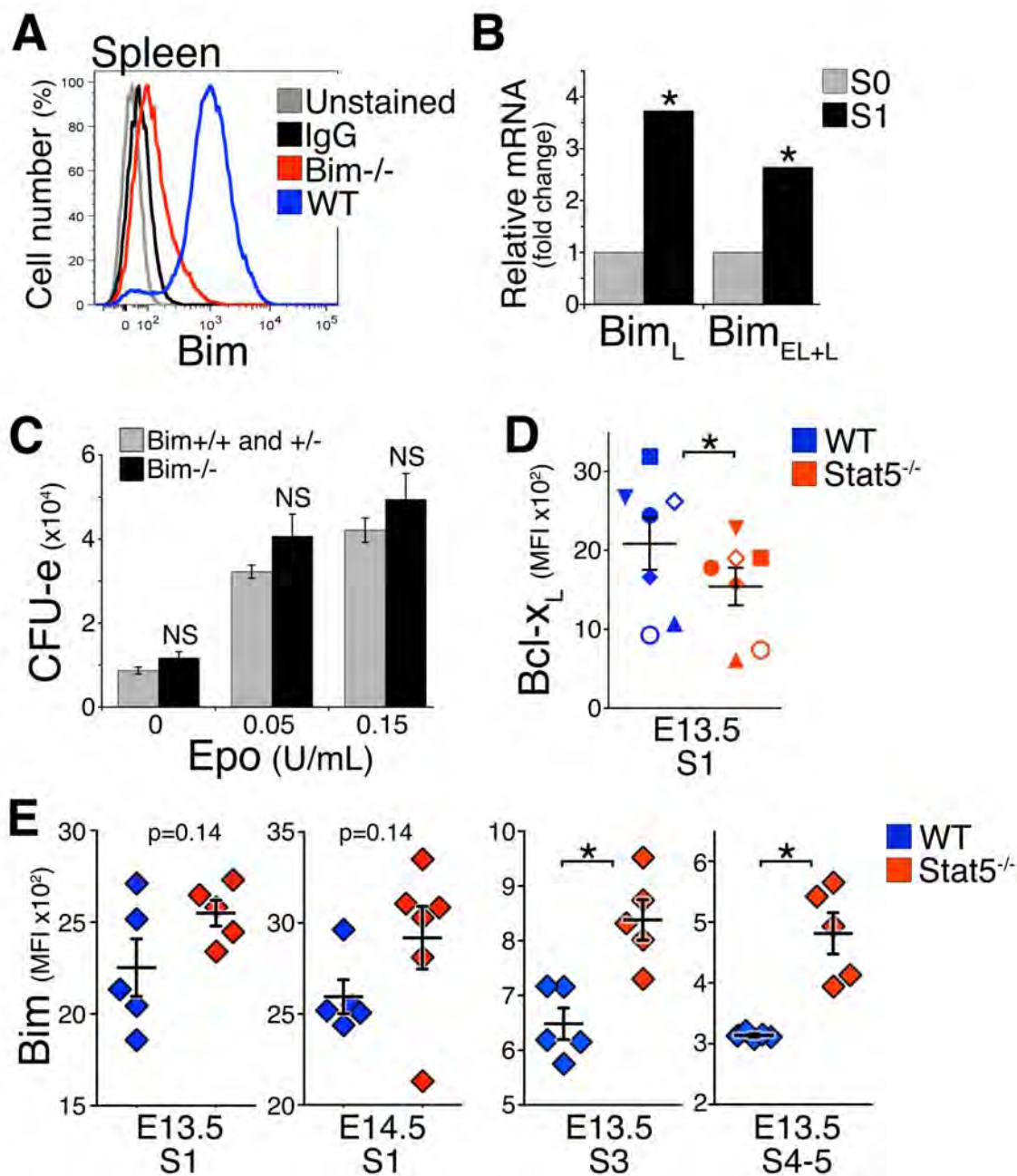
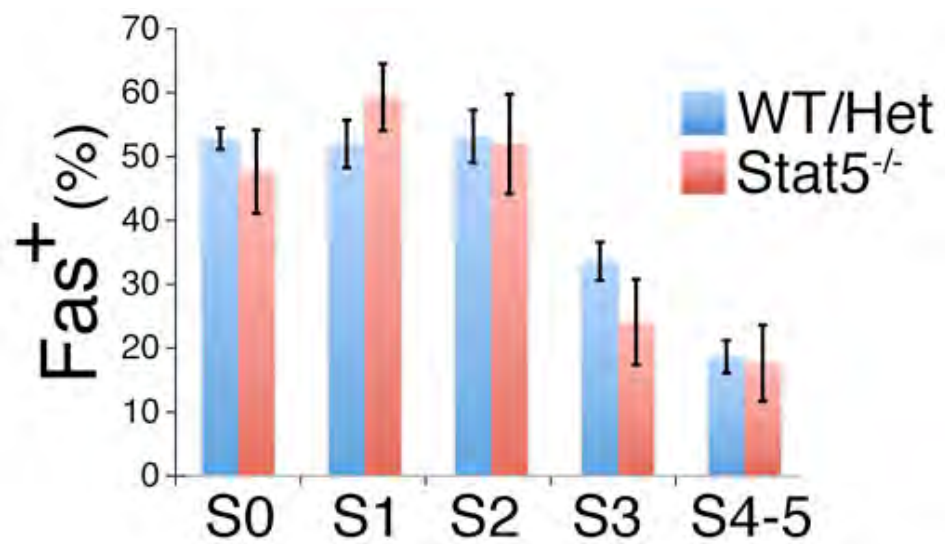


Figure A1.3 Fas expression in E14.5 fetal liver erythroblasts.

Cell-surface Fas was measured on freshly explanted fetal livers from wild-type or Stat5 heterozygous embryos (n=6) and from Stat5^{-/-} embryos (n=3). No significant differences were detected between the genotypes. (two-tailed t-test, unequal variance).

Figure A1.3



Bcl-x_L is rapidly induced in adult early erythroblasts in response to a single Epo injection

We examined Bcl-x_L expression in response to a single dose of Epo, the principal mediator of the stress response. A single subcutaneous injection (300 U/25 g) results in a rapid increase in serum Epo, peaking by 6 hours, persisting for 24 hours and declining to baseline by 36 hours (Figure A1.4A). We measured Bcl-x_L expression by intracellular flow cytometry, in each of the adult flow-cytometric erythroblast subsets ProE, EryA, EryB and EryC [14] (Chapter III and Figure A1.4B), in freshly explanted bone-marrow and spleen at the indicated time points (Figure A1.4C-E). In control, saline-injected mice, Bcl-x_L expression increases 6 fold with differentiation from ProE to EryC in both bone-marrow and spleen, a pattern similar to that of fresh fetal liver (representative histograms in Figure A1.4C, summary of several experiments in Figure A1.4E). Injected Epo caused a further induction of Bcl-x_L expression in all erythroblast subsets (Figure A1.4C, E). Proportionally, this increase was largest and most rapid in the earliest subsets, where basal Bcl-x_L levels are lowest, and where it peaked 5 fold its basal level within 16 hours of Epo injection in splenic ProE (p=0.0006) and 3 fold by 18 hours in splenic EryA (p=0.0009) (Figure A1.4C, E).

To assess the sensitivity of the Bcl-x_L pathway to injected Epo, we carried out a dose/response curve *in vivo*, injecting mice with the indicated Epo dose and examining peak Bcl-x_L expression at 18 hours in splenic EryA (Figure A1.4D). This analysis shows that half the maximal response is obtained with the injection of 3 U/25 g, estimated to result in a serum concentration of 0.3 U/ml, approximately a ~10 fold increase above

basal serum Epo. This response is more sensitive than that of the Fas-suppression pathway, where we found a half-maximal response with an injection of 10 U/25 g [279].

Induction of the Bcl-x_L protein is associated with an increase in the Bcl-x_L mRNA that follows a similar time course (Figure A1.5A).

Figure A1.4 Bcl-x_L induction in adult early erythroblasts in response to Epo injection.

(A) Time course of plasma Epo, assayed by ELISA, following a subcutaneous injection of 300 U/ 25 g. Two mice (identified as either circles or triangles) were assayed per time point.

(B) Gating strategy for freshly explanted ProE, EryA, EryB and EryC spleen erythroid subsets [14]. Live cells were selected, and subsets gated based on Ter119, CD71 expression and forward scatter (FSC).

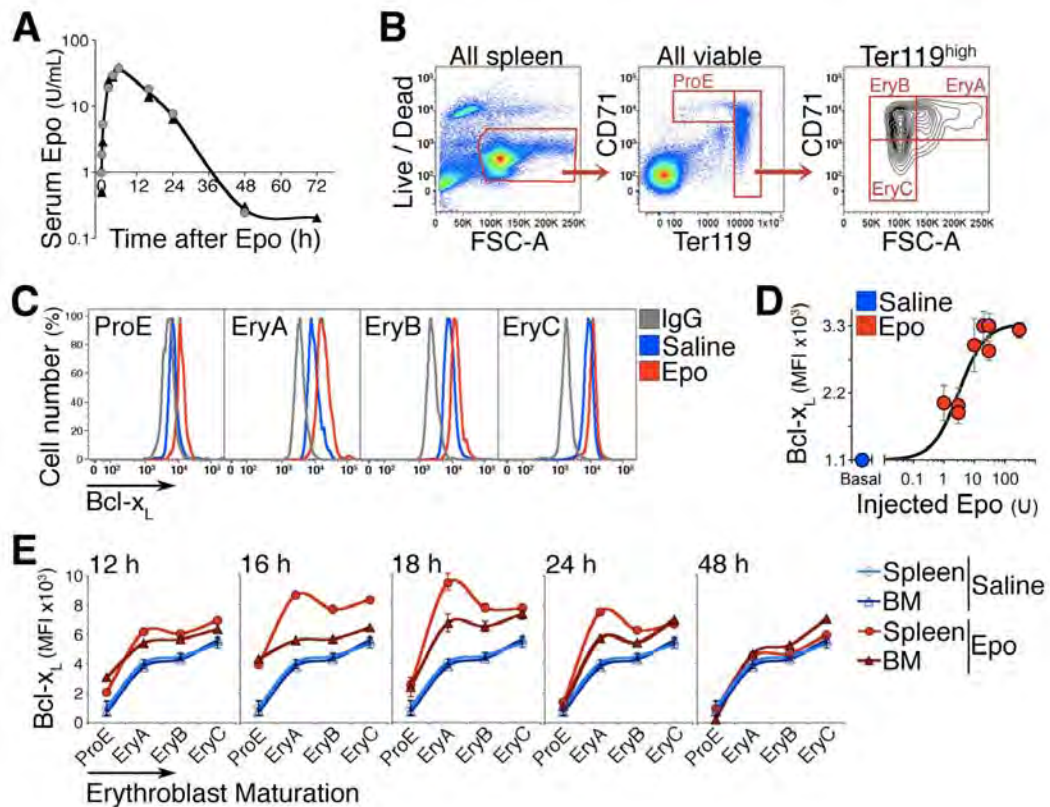
(C) Representative flow-cytometric histograms of intracellular Bcl-x_L protein in the indicated spleen erythroblast subsets. Anti-Bcl-x_L antiserum was used to stain erythroblasts from a saline-injected mouse (blue histograms), or an Epo-injected mouse (300 U/ 25 g, red histograms) in freshly explanted spleen at 18 hours post injection. An isotype control antibody was used to measure the non-specific binding in each subset (grey histograms).

(D) Epo dose/ Bcl-x_L response *in vivo* in spleen EryA. Wild-type Balb/C mice were injected subcutaneously with either saline (=basal, blue circle) or a single, increasing dose of Epo (1, 3, 10, 20, 30, or 300 U/ 25 g, red circles). Bcl-x_L was measured by flow cytometry as in panel 'C' at 18 hours post-injection, with the non-specific fluorescence reading subtracted for each subset. Data from two independent experiments was pooled and normalized. Datapoints were fitted with a Hill curve. Each datapoint represents mean \pm SEM of n=3 to 4 mice.

(E) Bcl-x_L expression measured as in panel 'C' in freshly explanted spleen, in each erythroblast subset at each of the indicated time-points following a single Epo injection (300 U/ 25 g). Each data point for Epo-injected mice is mean \pm SEM of n=4 mice for t=16, 18, 24, 48 hours; and mean of 2 mice for t=12 hours. Blue curves are mean \pm SEM of n=14 saline-injected mice pooled from all time-points. The same blue curves are reproduced for comparison with Epo-injected mice at each time-point). Statistical significance values: ProE at t=16h, in bone-marrow *p=0.005, in spleen *p=0.0006. EryA in spleen, *p=0.0009 at 16h, *p=0.0009 at 18h. EryA in bone-marrow, *p=0.013 at

16h, * $p=0.015$ at 18h. The induction of Bcl-x_L in splenic EryA was significantly higher than in bone-marrow EryA (* $p=0.021$). Two-tailed t-test with unequal variance used for all comparisons.

Figure A1.4



Expression pattern of Bim in basal and stress adult erythropoiesis

We used intracellular flow cytometry in adult spleen and bone-marrow, freshly explanted at the indicated time points following either saline or Epo injection (300 U/25g), to examine Bim expression. Bim is expressed at its highest levels in the early, ProE subset, declining gradually in subsequent differentiation subsets and reaching a quarter of its ProE level in EryC (Figure A1.5B). In response to an Epo injection Bim levels decreased further in all subsets (Figure A1.5B, C), with the largest decline in the early bone-marrow and spleen ProE progenitors, where they fell ~2 fold ($p < 0.0001$).

Importantly, the time course of Bim suppression in response to Epo injection was much slower, and more prolonged, than the Bcl-x_L response. Maximal Bim suppression was reached at 72 hours post injection in most subsets, a time when the Bcl-x_L induction had already peaked and returned to baseline (Figure A1.5C).

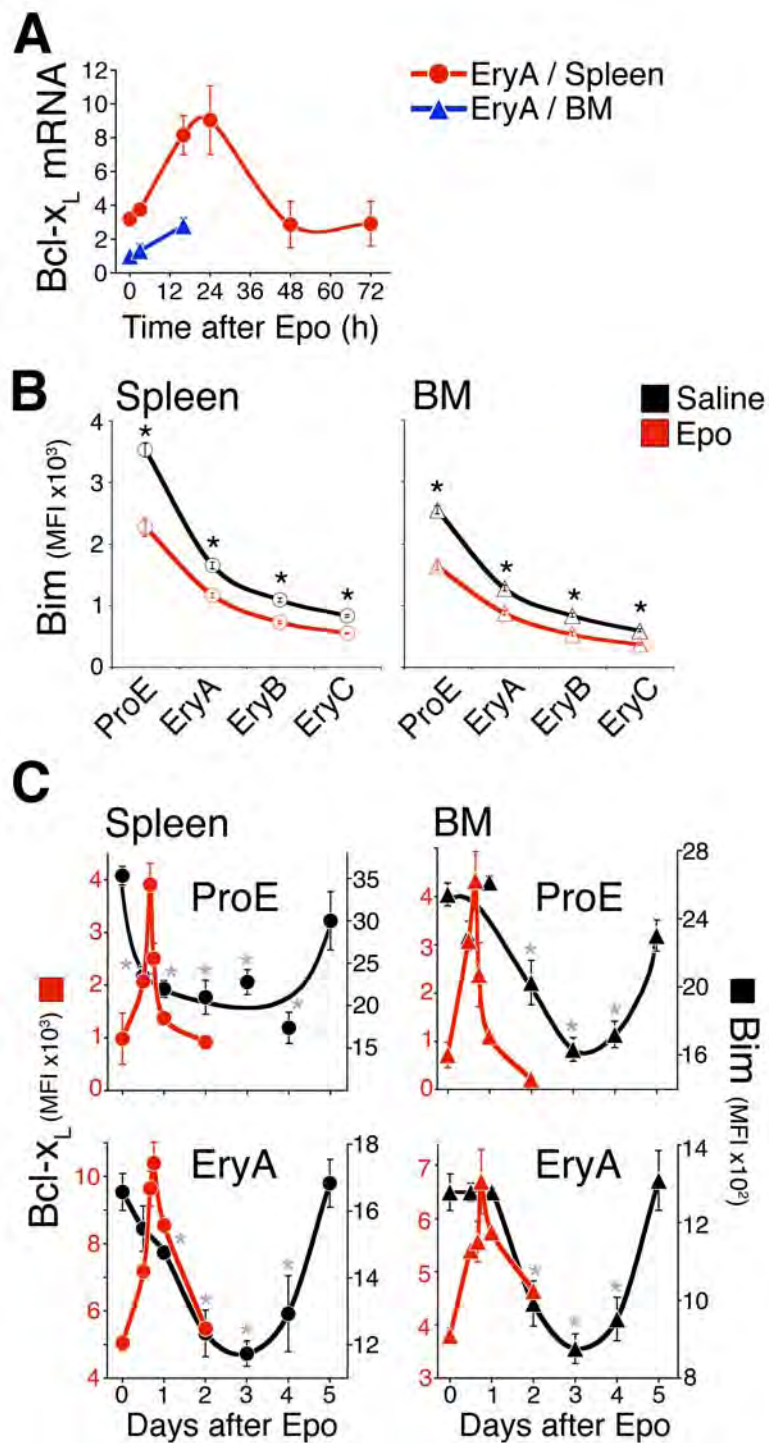
Figure A1.5 Transient Bcl-x_L induction contrasts with slower Bim suppression in response to Epo injection.

(A) Time course of Bcl-x_L mRNA expression following a single Epo injection (300 U/ 25g), in freshly isolated and sorted spleen and bone-marrow EryA. Quantitative real-time PCR, data points are mean \pm SEM of 3 independent experiments. Data is expressed relative to the β -actin mRNA and normalized to the value in bone-marrow EryA in saline-injected mice.

(B) Bim protein expression in adult erythroid differentiation subsets 3 days following a single injection of either Epo (red, 300 U/ 25 g) or saline (black). Bim was measured by flow cytometry in freshly explanted tissue, as illustrated in Figure A1.2A. Data are mean \pm SEM of n=21 mice for saline injection, and n=10 mice for Epo injection. *p<0.000005 (two-tailed t-test, unequal variance) for differences between Epo-injected and saline-injected mice.

(C) Time course of Bcl-x_L upregulation (red symbols, plotted on the left, red-numbered y-axis) and Bim suppression (black symbols, plotted on the right-numbered y-axis) in spleen (circles) and bone-marrow (BM, triangles) in response to a single Epo injection (300 U/ 25 g) on day 0. Includes a subset of the data plotted in panel 'B' (for Bim) and Figure A1.4E (for Bcl-x_L). For Bim, 5 experiments were normalized together. Bim data are mean \pm SEM of n=21 mice for day 0, and n=3 to 10 mice for days 1 to 5. Bim ProE curves (black lines) for spleen and bone-marrow were hand-drawn. Statistical analysis was performed by comparing Bim readings on day 0 with readings on the following days. Where indicated, spleen ProE: *p<0.005. Spleen EryA: *p<0.025. BM ProE: *p<0.02; BM EryA: *p<0.01. For all statistical tests, two-tailed t-test with unequal variance was used.

Figure A1.5



The erythroblast response to reduced atmospheric oxygen

The modulation of erythroblast Bim and Bcl-x_L levels by an Epo injection *in vivo* suggested that these pathways are likely to play a role in the physiological stress response. To test this, we placed mice in a reduced oxygen environment in which atmospheric partial oxygen pressure was reduced to 11% for up to 5 days (Figure A1.6). Epo levels in blood plasma rose rapidly in the first 24 hours, from a basal level of 12 mU/ml, to a peak of 29 mU/ml (p=0.001). This high Epo level was sustained until day 3. On days 4 and 5 Epo began to decline to a new lower plateau of 18 mU/ml (Figure A1.6A).

The hematocrit response was rapid, rising from 51.5% to 56% in the first 24 hours, and reaching a sustained plateau of 57% (Figure A1.6B). The rapid initial increase in hematocrit is likely in part to be the result of plasma volume adjustment in response to hypoxia [291, 292].

We examined the response of individual flow-cytometric erythroblast subsets in freshly explanted tissue at the indicated time points (Figure A1.6C-I). The results shown are from 23 pooled experiments, with at least 6 mice per time point. To evaluate the various responses in relation to the plasma Epo levels, the Epo response in Figure A1.6A is replicated as a gray line in subsequent panels (Figure A1.6E-I).

The absolute numbers of spleen ProE and EryA erythroblasts increased over the initial 3 days, reaching new plateaus that were 4 and 3 fold higher than basal values, respectively (Figure A1.6C, D). This increase in cell number was associated with a marked and significant reduction in apoptosis, with the number of Annexin V⁺ cells

declining from 55% to 32% ($p=0.002$) and 42% to 30% ($p=0.001$) in the ProE and EryA subsets, respectively (Figure A1.6E).

The response of erythroblast Bim, Fas and Bcl-x_L to reduced atmospheric oxygen

Given the clear changes in ProE and EryA apoptosis, we investigated their expression of the apoptotic regulators Fas, Bim and Bcl-x_L. We previously showed that cell surface Fas on spleen ProE and EryA decreases in response to a number of acute and chronic erythropoietic stress conditions. Maximal Fas suppression is reached within 24 to 48 hours and is maintained for the duration of the stress stimulus (Figure A1.6F) [14, 279].

The Bcl-x_L response was rapid and transient, its expression peaking by 18 hours in both ProE and EryA, and then rapidly dipping below baseline by 24 hours, in spite of the persisting high Epo levels (Figure A1.6G). The response of Bim, by contrast, was slower, reaching maximal suppression at 48 hours, with low levels maintained for the duration of high Epo levels (Figure A1.6H, I).

We examined the possibility that the transient increase in Bcl-x_L may be due to the relatively modest increase in plasma Epo generated by the hypoxic environment. We injected mice with Epo (300 U/ 25 g) daily for 3 consecutive days, which generates increasingly high plasma Epo equivalent to that of maximal stress conditions [268] (Figure A1.1A). We measured the Bcl-x_L response 18 hours following each injection (Figure A1.7). The amplitude of the Bcl-x_L response was larger in response to this higher Epo dose than in the response to the hypoxic environment, as expected from the Epo dose/Bcl-x_L response curve (Figure A1.4). However, the response to the second and third

Epo injections was smaller or absent (Figure A1.7), suggesting that the transience of the Bcl-x_L response is unrelated to Epo dose.

Figure A1.6 A reduced oxygen environment elicits a rapid, transient Bcl-x_L induction and a slow, persistent Bim suppression.

(A – I) Mice were placed in a low oxygen chamber (11%) on day 0, for the numbers of days indicated.

(A) Endogenous plasma Epo, assayed by ELISA. Data are mean \pm SEM. Difference relative to day 0 (n=27 mice) were significant at the following levels: day 1 (n=6) *p=0.001; day 3 (n=6), *p=0.006; day 4 (n=12), *p<0.0001; day 5 (n=3), *p=0.0000005. This Epo time course is drawn as a grey line in panels E to I.

(B) Daily hematocrit (HCT) measurement on blood collected immediately post euthanasia. Data are mean \pm SEM of n \geq 6 mice per time-point. Differences from day 0 are significant at the following levels: 12h, *p=0.019; 18h to day 5, *p<0.0002.

(C-D) Absolute number of spleen ProE and EryA per gram body weight. Data pooled from 23 independent experiments. Each datapoint is mean \pm SEM of n \geq 6 mice. Differences from day 0 (n=82 mice) are significant at the following levels: Spleen ProE day 1, *p=0.005; day 2, *p=0.047; days 3 to 5, *p \leq 0.005. Spleen EryA day 2, *p=0.034; days 3 to 5, *p \leq 0.001.

(E) Annexin V binding in spleen ProE (blue) and EryA (black). Data points are mean \pm SEM of 33 mice for day 0 and 3 to 7 mice for subsequent days, pooled from 2 to 5 independent experiments per day. Differences from day 0 are significant at the following values: Spleen ProE days 3 to 5, *p \leq 0.002. Spleen EryA day 1, *p=0.001; day 3, *p=0.03; day 4, *p=0.02; day 5, *p=0.001.

(F) Fas-positive cell frequency in spleen ProE (blue) and EryA (black), measured by flow cytometry in freshly explanted tissue. Data are mean \pm SEM of n=26 mice, pooled from 4 experiments (day 0) or n=3 mice for subsequent days. Differences from day 0 are significant at the following values: Spleen ProE day 1, *p=0.024; day 3, *p<0.00001; day 5, *p=0.001. Spleen EryA day 5, *p=0.04.

(G) Bcl-x_L protein expression in spleen ProE and EryA measured by flow cytometry in freshly explanted tissue. Data pooled from three independent experiments. Each data point is mean \pm SEM of n \geq 3 mice. Differences from day 0 (n=17) are significant at the

following levels: Spleen ProE 18h (n=3), *p<0.001; 24h (n=7), *p=0.019; day 2 (n=5), *p<0.0005. Spleen EryA 12h, *p=0.046; 18h, *p<0.0001; day 2, *p=0.02

(H-I) Bim protein expression in spleen (H) and bone-marrow (I) ProE and EryA, measured by flow cytometry in freshly explanted tissue. Data are mean \pm SEM of $n \geq 3$ mice. Differences from day 0 are significant at the following levels: Spleen ProE day 4, p=0.04. Spleen EryA day 3, p=0.04; day 4, p=0.02. Bone-marrow ProE day 2, p=0.007; day 3, p<0.00001; day 4, p<0.001; day 5, p=0.04. Bone-marrow EryA day 1, p=0.002; day 2, p=0.0001; day 3, p=0.05.

For all statistical tests, two-tailed t-test with unequal variance was used.

Figure A1.6

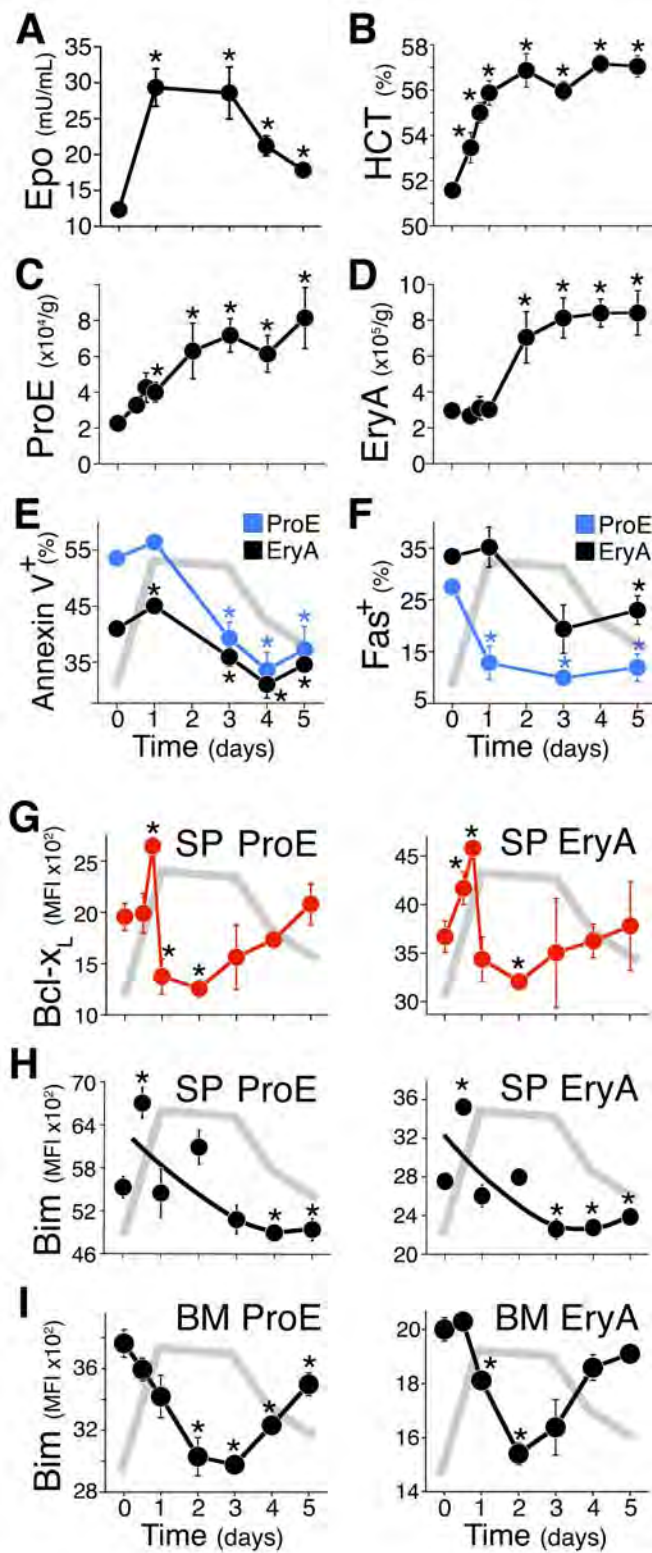
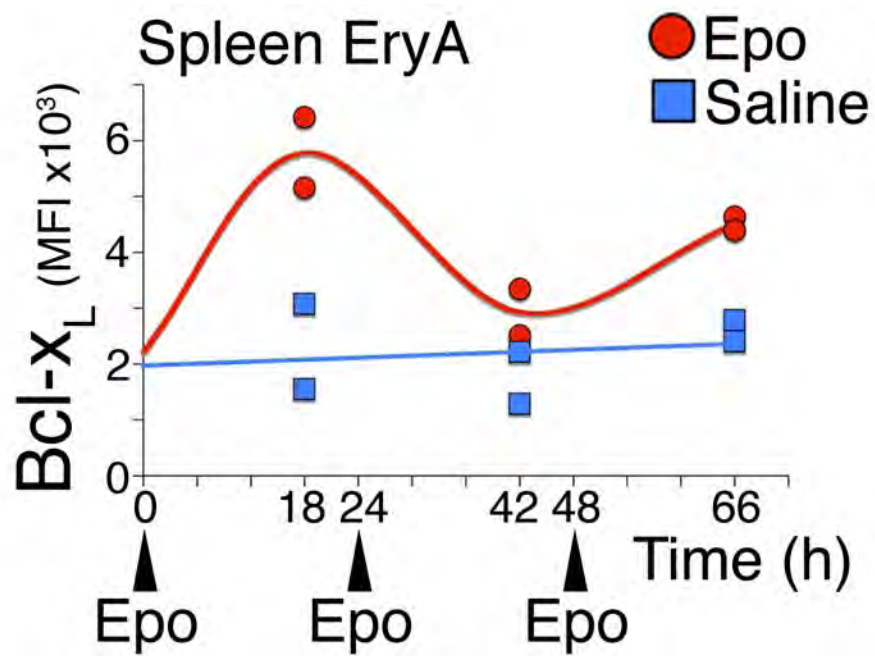


Figure A1.7 The Bcl-x_L response to repeated Epo injections.

Bcl-x_L expression following consecutive Epo injections. Wild-type mice were injected at time-points 0, 24 and 48 hours with either Epo (300 U/25g, indicated with arrowheads) or with saline. Bcl-x_L expression was assayed by flow cytometry in 2 mice for each treatment, 18 hours following each injection.

Figure A1.7



Response of the Bim and Bcl-x_L pathways to chronic erythropoietic stress

We went on to assess the Bim and Bcl-x_L response to chronic erythropoietic stress. The Bcl-x_L expression profiles in the ProE/ EryA-C subsets in either spleen or bone-marrow was unaltered by 3 distinct erythropoietic stress conditions: pregnancy at mid-gestation, chronic anemia due to β -thalassemia [293], and chronic erythrocytosis due to tissue-specific deletion of the von Hippel-Lindau gene that results in elevated Epo (ts-VHL^{-/-}) [294] (Figure A1.8A). Plasma Epo is elevated to 30 mU/ml and 220 mU/ml in the ts-VHL^{-/-} and β -thalassemia mice, respectively (Figure A1.9), a concentration range in which Bcl-x_L induction was seen in acute stress (Figure A1.6). Further, we have previously shown that cell surface Fas and FasL are downregulated in the same chronic stress models [14].

Unlike Bcl-x_L, Bim expression in the β -thalassemia mice was suppressed in all erythroblast subsets (Figure A1.8B), to levels similar to those seen in response to an acute Epo injection (Figure A1.5B).

The Bcl-x_L response to an ‘acute on chronic’ stress stimulus

The transience of the Bcl-x_L response to stress is reminiscent of sensory systems that undergo adaptation, such as neutrophil chemotaxis or sensory neural adapting systems. These systems respond to a change in the stimulus, rather than to absolute stimulus levels [215]. We therefore asked whether the desensitization of the Bcl-x_L pathway to chronic stress was permanent, or whether an acute change in the level of stress, superimposed on a chronic stress stimulus, would re-stimulate Bcl-x_L induction.

We injected β -thalassemia mice with a single Epo dose of 300 U/25 g, and examined their Bcl-x_L response at 18 hours post injection. We found a clear induction in Bcl-x_L in all erythroblast subsets in the β -thalassemia mice, closely resembling that of control mice in the bone-marrow, and only a little short of the wild-type response in the spleen (Figure A1.8C). This experiment suggests that while the Bcl-x_L response desensitizes to chronic stress, it rapidly responds to new changes in stress superimposed on the chronic stress levels.

Figure A1.8 The Bcl-x_L response to chronic stress and to ‘acute on chronic’ stress.

(A) Bcl-x_L expression in each of the three indicated mouse models of erythropoietic stress (red symbols) and matched controls (blue symbols), measured in freshly explanted tissue. Each data point is mean \pm SEM of 2 to 4 mice. There were no statistically significant differences between chronic stress and control mice.

(B) Representative experiment showing Bim expression in β -thalassemia mice in spleen (top) and bone-marrow (bottom). Two wild-type (black symbols) and one β -thalassemia mouse (red symbols) are shown.

(C) The Bcl-x_L response to an ‘acute on chronic’ stimulus. Bcl-x_L expression in spleen and bone-marrow erythroblasts in β -thalassemia mice and matched controls, 18 hours following a single injection of either Epo (300 U/ 25g, red symbols) or saline (blue symbols). Datapoints are mean \pm SEM of n=3 to 4 mice. Representative of 4 independent experiments. Statistically significant differences in Bcl-x_L between Epo and saline injections in each mouse model were seen in wild-type spleen ProE, *p=0.025; EryA, *p=0.0009; EryB, *p=0.01; EryC, *p=0.006; β -thalassemia spleen EryA, *p=0.0004; EryB, *p=0.004; EryC, *p=0.03; Wild-type BM EryA, EryB and EryC, *p \leq 0.0005; β -thalassemia BM EryA and EryB, *p<0.0005; EryC, *p=0.025. The increase in spleen EryA Bcl-x_L was significantly higher (p=0.023) in wild-type spleen than in wild-type β -thalassemia mice. For all statistical tests, two-tailed t-test with unequal variance was used.

Figure A1.8

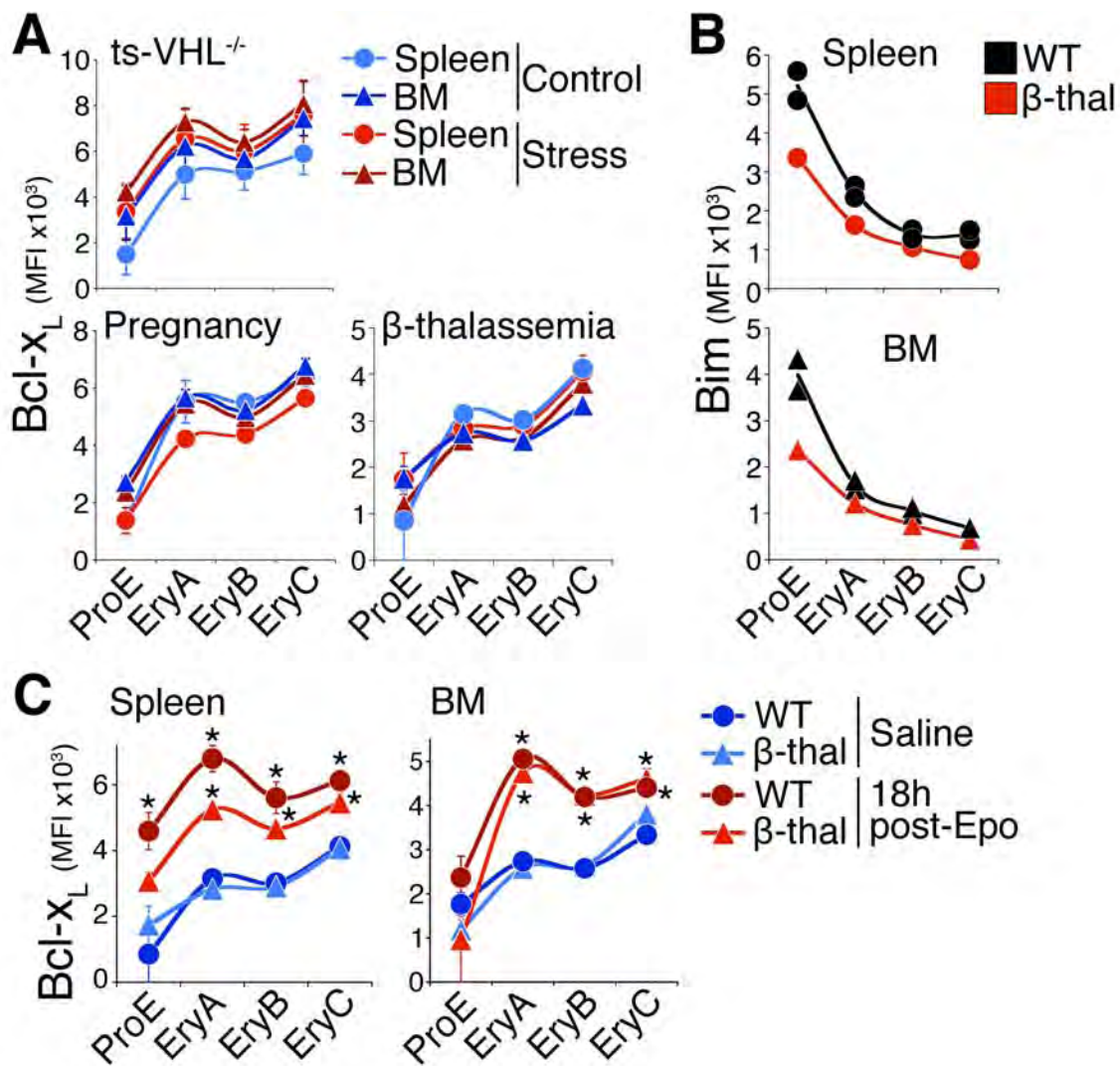


Figure A1.9 Plasma Epo measurements in mice with β -thalassemia and in ts-VHL^{-/-} mice.

For each mouse model, two independent ELISAs, each with similar results, were pooled together. Individual mouse data as well as mean \pm SEM are shown. Epo increase in β -thalassemia was significant at $p=0.002$ (two-tailed t-test, unequal variance).

Stat5 activation *in vivo* undergoes adaptation

We asked whether adaptation in the Bcl-x_L stress response is due to adaptation in Stat5, its upstream regulator. We first examined the time course of Stat5 activation *in vivo* following Epo injection (300 U/ 25g), using intracellular flow cytometry in freshly explanted spleen and bone-marrow at the indicated time points post-injection (Figure A1.10A). The number of ProE and EryA containing active, phosphorylated Stat5 (p-Stat5) increased rapidly following injection, peaking by 30 minutes, but declining rapidly to a lower level by 6 hours (Figure A1.10A). Of note, plasma Epo peaked at 6 hours (Figure A1.1A), suggesting the decline in p-Stat5 is intrinsic to the p-Stat5 response and is not due to declining Epo.

Signal adaptation may be due to negative feedback [295, 296]. p-Stat5-mediated transcriptional activation of SOCS family proteins results in their feedback inhibition of the Jak2 and Stat5 response [297]. This negative regulation in part depends on SOCS protein binding to phosphotyrosines on the activated EpoR cytoplasmic domain [210]. To investigate the possibility that Stat5-mediated negative feedback is responsible for adaptation in the p-Stat5 response, we investigated two ‘knock-in’ mouse models, expressing the EpoR mutants EpoR-H and EpoR-HM [46], both lacking the negative regulatory distal portion of the EpoR cytoplasmic domain containing 7 of its 8 phosphotyrosines, including SOCS family docking sites [210]. In EpoR-HM, the remaining Y343, a Stat5 docking site, is mutated to phenylalanine [46]. The EpoR-H mouse has a mildly elevated basal hematocrit. By contrast, the EpoR-HM mouse has only a mild anemia in the basal state but a deficient stress response [46].

We tested the response of freshly harvested fetal liver early erythroblasts derived from EpoR-H, EpoR-HM and wild-type embryos to continuous stimulation with Epo for up to 6 hours *in vitro*. The time course of response of wild-type erythroblasts was similar to that of adult erythroblasts *in vivo* (Figure A1.10A,B). The peak p-Stat5 response to Epo stimulation in EpoR-HM erythroblasts was 15% of the response in wild-type or EpoR-H mice, in agreement with previous results [25]. In EpoR-H erythroblasts, peak p-Stat5 was similar to that of the wild-type response, though baseline p-Stat5 was higher. In both EpoR-HM and EpoR-H, duration of the initial p-Stat5 peak was prolonged substantially (Figure A1.10B). These findings suggested that the distal EpoR cytoplasmic domain, likely through binding to Stat5-induced SOCS family proteins, is responsible for curtailing the p-Stat5 response.

Figure A1.10 Adaptation in the Bcl-x_L and p-Stat5 responses is dependent on the EpoR C-terminal cytoplasmic domain.

(A) The p-Stat5 response in spleen ProE and EryA *in vivo*, measured in freshly explanted spleen at the indicated time points following a single Epo injection (300 U/ 25g). Data is pooled from four independent experiments. Each time point is the mean \pm SEM of data from 2 to 4 mice.

(B) The p-Stat5 time course in response to Epo stimulation for the indicated periods. Freshly harvested fetal liver cells from EpoR-HM, EpoR-H and matched wild-type embryos at E13.5 were stimulated *in vitro* with 2 U/ml Epo. p-Stat5 in S1 cells is shown, expressed as median fluorescence intensity above background (isotype-control antibody). Representative of 3 similar experiments.

(C) The Bcl-x_L response in EpoR-H and EpoR-HM mice. Bcl-x_L was measured 18 hours following a single injection of either Epo or Saline, in freshly explanted spleen ProE and EryA of EpoR-H, EpoR-HM or wild-type controls. Data are mean \pm SEM of n=3 to 5 mice per bar. Significant Bcl-x_L increase from basal levels in spleen ProE and EryA was seen in Epo vs. Saline injected wild-type (black) and EpoR-H (red) mice (stars without brackets: WT ProE *p=0.003; EpoR-H ProE *p=0.012; WT EryA *p=0.00004; EpoR-H EryA *p=0.0001), but not in EpoR-HM mice. Bcl-x_L was reduced in basal state EpoR-HM spleen EryA (red star with red bracket, *p=0.027) compared with wild-type basal control. Bcl-x_L induction in wild-type spleen EryA was significantly above that of EpoR-HM EryA (black stars with brackets, *p=0.007, two-tailed t-test with unequal variance).

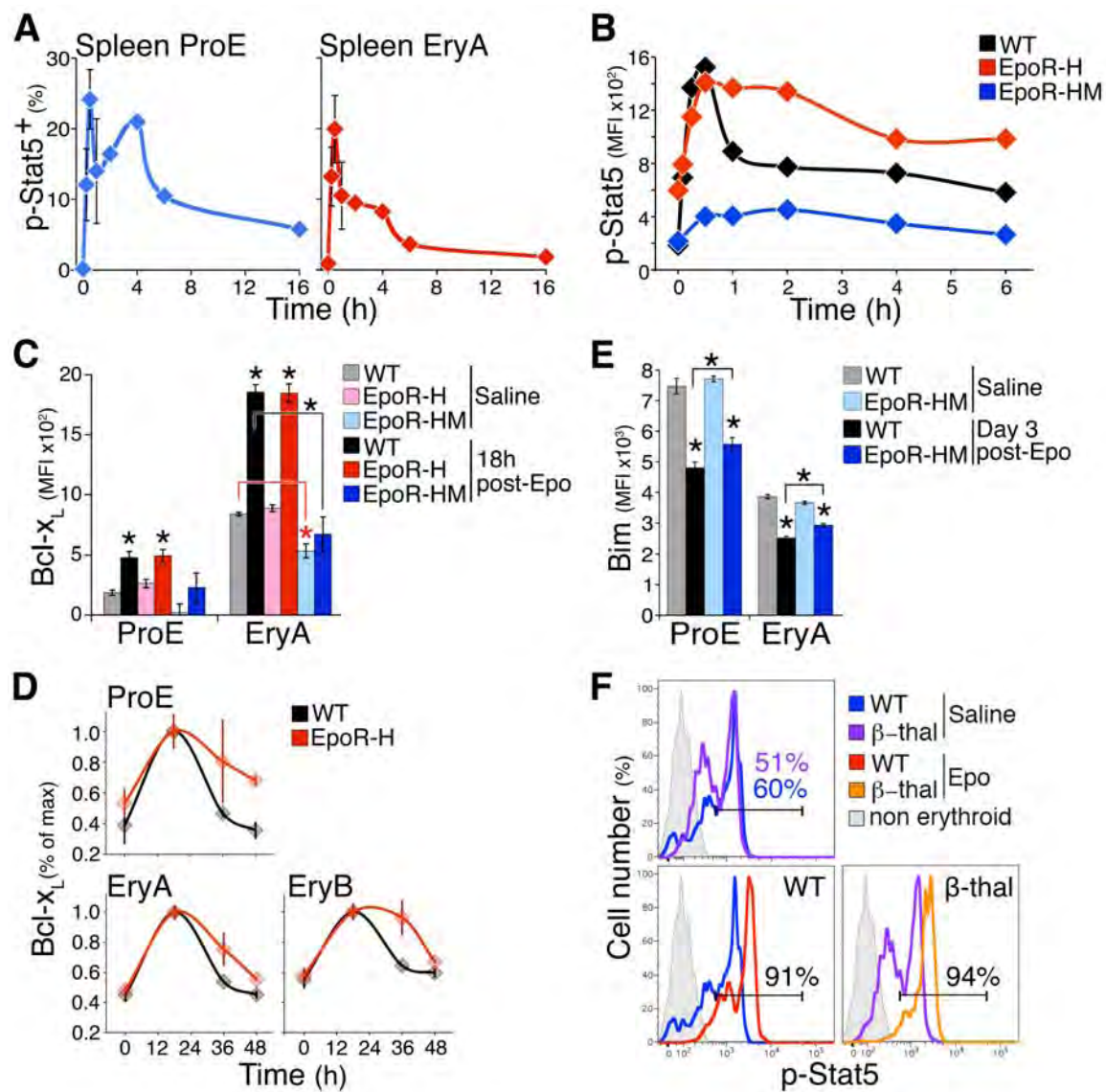
(D) Time course of the Bcl-x_L response in EpoR-H mice and in matched wild-type controls, following a single Epo injection (300 U/ 25g). Measurements were made in freshly explanted spleen at the indicated time points. Bcl-x_L is significantly higher in EpoR-H at 36 and 48 hours (p<0.005, paired t test on all subsets).

(E) Bim protein in spleen ProE and EryA of wild-type and EpoR-HM mice on day 3 following a single Epo injection (300 U/ 25 g). Data are mean \pm SEM of n=4 to 5 mice per bar. There was no significant difference in basal Bim between EpoR-HM and wild-

type control mice. Bim was significantly suppressed following Epo injection (* $p < 0.001$). Bim was suppressed by a significantly smaller extent in EpoR-HM ProE and EryA subsets (stars with brackets, * $p = 0.03$ and * $p = 0.001$, respectively, two-tailed t-test with unequal variance).

(F) The p-Stat5 histograms *in vivo* at peak response (30 minutes) following a single injection of either Epo (300U / 25g) or saline, in either β -thalassemia mice or in matched wild-type controls, measured in freshly explanted spleen ProE. The p-Stat5⁺ gate was drawn based on the non-erythroid population in spleen (grey histograms).

Figure A1.10



The Bcl-x_L and Bim stress responses in EpoR-H and EpoR-HM mice

The finding that the p-Stat5 signal undergoes adaptation (Figure A1.10A, B) suggests it may be responsible for the adaptation in the Bcl-x_L response. To test this, we asked whether failure of p-Stat5 adaptation in the EpoR-H mice (Figure A1.10B) would prevent adaptation of the Bcl-x_L response.

We therefore injected EpoR-H mice with Epo (300 U/ 25g) and examined the resulting induction in Bcl-x_L. The peak Bcl-x_L response was closely similar to that of matched wild-type control mice (Figures A1.10C, A1.11A). There was little increase in Bcl-x_L in EpoR-HM mice, consistent with p-Stat5 as the principal regulator of the Bcl-x_L stress response (Figures A1.10C, A1.11A). Importantly, there was a failure of adaptation of the Bcl-x_L response in EpoR-H mice. Bcl-x_L levels remained elevated well above their initial baseline at 36 and 48 hours post-injection in spleen ProE, and at 36 hours in EryA and EryB ($p < 0.005$, Figure A1.10D), even though Bcl-x_L levels in wild-type mice (Figure A1.10D) and serum Epo (Figure A1.4A) had returned to baseline. This strongly suggests that adaptation in the Bcl-x_L response requires the EpoR distal cytoplasmic domain and is most likely a result of adaptation in the p-Stat5 response, also dependent on this domain (Figure A1.10B).

Bim expression was suppressed in EpoR-HM mice in response to a single Epo injection (300 U/ 25 g). However, suppression was less efficient than in wild-type mice, by a small but statistically significant amount (Figures A1.10E, A1.11B, $p = 0.03$ and $p = 0.001$ in ProE and EryA, respectively). These results suggest that, in addition to Stat5, other pathways, likely ERK, regulate the EpoR-mediated Bim suppression [289].

Figure A1.11 The Bcl-x_L and Bim Epo responses in the EpoR-H and EpoR-HM mice.

Experiment and same mouse dataset as in Figure A1.10C, A1.10 E.

(A) Bcl-x_L expression in spleen (left) and bone-marrow (right) in erythroid subsets, 18 hours post- Epo or saline injection in wild-type, EpoR-H, and EpoR-HM mice. Experiment and same mouse dataset as in Figure A1.10C.

Left panel: Black stars without brackets indicate significant Bcl-x_L induction in spleen EryB and EryC subsets in Epo treated mice (*p<0.005). No significant Bcl-x_L induction was observed in EpoR-HM spleens (light blue vs. dark blue bars). EpoR-HM mice failed to increase Bcl-x_L to the level of EpoR-H or wild-type mice (black stars with brackets, *p<0.02). Basal Bcl-x_L levels in EpoR-HM EryB and EryC were also lower than in basal wild-type mice (red stars with red brackets, *p<0.05).

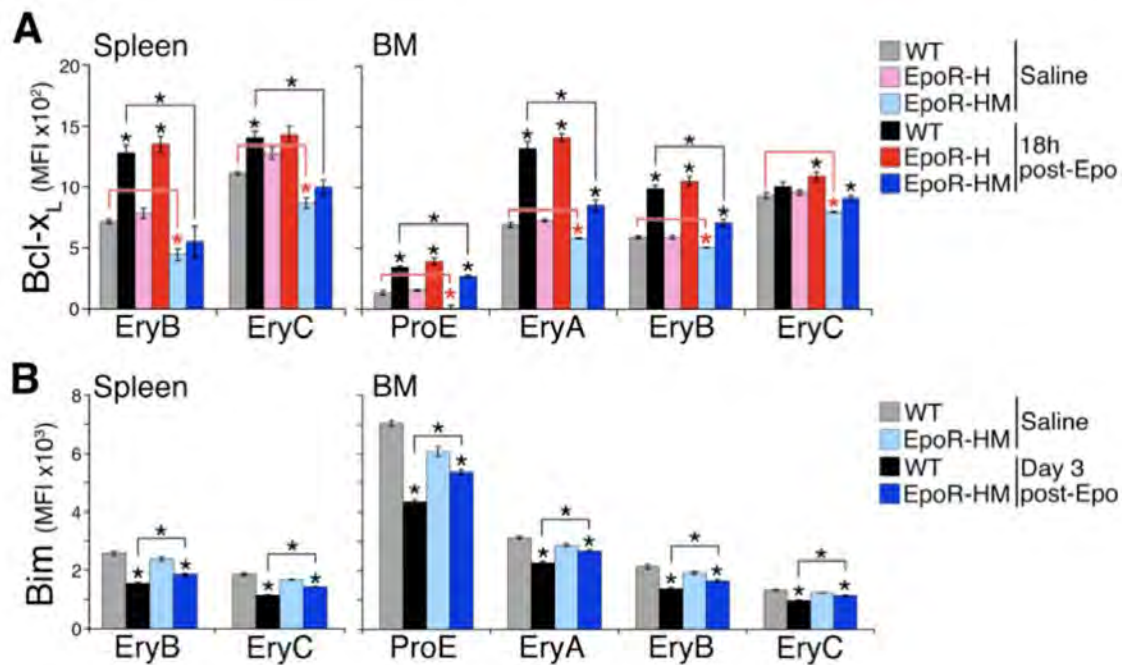
Right panel: Bcl-x_L induction in the bone-marrow erythroid subsets was observed for all three genotypes. Stars indicate significant differences. Wild-type Epo response vs. control: ProE, EryA and EryB, *p<0.0002. EpoR-H Epo response vs. control: ProE, EryA and EryB, *p<0.0001; EryC, *p=0.025. EpoR-HM Epo response vs. control: ProE, *p=0.003; EryA, EryB and EryC, *p<0.05. Magnitude of Bcl-x_L induction in EpoR-HM subsets was lower compared with wild-type induction (black stars with brackets, *p<0.006). Basal Bcl-x_L levels in EpoR-HM bone-marrow subsets were lower than in basal wild-type mice (red stars with red brackets, *p<0.02).

(B) Bim expression in spleen (left) and bone-marrow (right) in erythroid subsets, 3 days following Epo or saline injection in wild-type, EpoR-H, and EpoR-HM mice. Experiment and same mouse dataset as in Figure 3.6E. Data are mean ±SEM of n=4 to 5 mice per bar.

In both wild-type and EpoR-HM spleen EryB and EryC subsets, Bim was significantly suppressed below their respective basal levels with Epo (black stars, no brackets, *p<0.001). Similar findings were observed in the bone-marrow subsets (wild-type subsets: *p<0.0005; EpoR-HM subsets: *p<0.03). Magnitude of Bim suppression in EpoR-HM mice was lower than in the wild-type mice (black stars with brackets,

* $p < 0.005$). Some differences in basal Bim levels were observed between wild-type and EpoR-HM mice (gray bars *vs.* light blue bars, *not* indicated in plots: spleen EryB, $p = \text{NS}$; spleen EryC, * $p = 0.02$; BM ProE, * $p = 0.004$; BM EryA, * $p = 0.01$; BM EryB, $p = \text{NS}$; BM EryC, * $p = 0.03$).

Figure A1.11



The p-Stat5 response to an ‘acute on chronic’ stress stimulus

Although Bcl-x_L expression is not elevated in chronic stress, it is induced in response to an acute stimulus superimposed on the chronic stress stimulus (Figure A1.8C). Given the proposed role of Stat5 activation in Bcl-x_L induction, we similarly examined the p-Stat5 response to chronic and ‘acute on chronic’ stress stimuli. We found no increase in the level of p-Stat5 activation in ProE freshly isolated from β -thalassemic mice (Figure A1.10F, upper panel), in spite of the chronically elevated plasma Epo in these mice (Figure A1.9). A single injection of Epo (300 U/25 g) however, resulted in a rapid increase in p-Stat5 activation in both β -thalassemic mice and in matched control mice (Figure A1.10F, lower panels). Therefore, both the p-Stat5 and Bcl-x_L responses ‘reset’ during chronic stress, allowing them to respond afresh to an acute change in stress.

Discussion

We examined Bim suppression and Bcl-x_L induction, two EpoR-activated erythroblast survival pathways in fetal and adult basal and stress erythropoiesis. Their analysis *in vivo* revealed previously unsuspected functional specialization of EpoR-pathways to either the chronic or acute phases of the stress response. Bcl-x_L induction behaves like a classical sensory adapting pathway, being insensitive to the prevailing level of stress, and instead responding only to changes in stress level. Adaptation allows Bcl-x_L to provide a stop-gap at the onset of stress that rapidly rescues early erythroblasts from apoptosis, until slower but persistent stress pathways, such as Bim or Fas suppression, are activated. Mechanistically, we suggest that adaptation in the Bcl-x_L response is the result of adaptation in the response of p-Stat5, its upstream regulator.

Regulation of Bim and Bcl-x_L expression in early vs. late erythroblasts

We delineated the expression pattern of both Bim and Bcl-x_L proteins throughout erythroid maturation in adult and fetal hematopoietic tissue *in vivo*. The basal pattern observed in the absence of stress is one of low Bcl-x_L and high Bim in early erythroblasts, gradually inverting with differentiation so that in mature erythroblasts Bim levels are low, and Bcl-x_L levels are high (Figure A1.12A). These results are consistent with the previously reported increase in Bcl-x_L transcript and protein with erythroid differentiation *in vitro* [213, 281], and with the increase in Bcl-x_L and decrease in the pro-apoptotic Bid and Bax transcript with the transition from early to late erythroblasts in murine bone-marrow [271]. Together with our previous findings of high Fas and FasL co-expression in early, but not late, erythroblasts [14, 19, 206], a strong pattern emerges of apoptosis-

prone early erythroblasts, containing high levels of pro-apoptotic regulators and only low levels of anti-apoptotic proteins, gradually transitioning into apoptosis-resistant late erythroblasts in which anti-apoptotic proteins predominate. This underlying pattern explains why high levels of apoptosis are seen in early erythroblasts but not in late erythroblasts during normal fetal and basal adult erythropoiesis *in vivo* [14, 19, 206, 279] (Figure A1.1D, Figure A1.4E and A1.5B), and was recently suggested as being responsible for the sensitivity of early erythroblasts to irradiation [271].

Bcl-x_L expression is regulated by both GATA-1 and by EpoR-activated Stat5 [133]. Similarly, Bim suppression is regulated by both EpoR-activated ERK [289] and by GATA-1-induced LRF [290]. Here we find that in addition, Bim is regulated by EpoR-activated Stat5, as suggested by higher Bim levels in the Stat5^{-/-} fetal liver and to a lesser extent in the adult EpoR-HM mouse (Figure A1.1E, Figures A1.10E, A1.11B). Lower Bcl-x_L in the S1-S3 subsets of the Stat5^{-/-} fetal liver, and in EpoR-HM mice in the basal state, support older reports of the role of Stat5 in the induction of erythroid Bcl-x_L [130, 213, 275]. The role of Stat5 is especially notable, however, in the Bcl-x_L stress response, which is absent in the EpoR-HM mice (Figure A1.10C).

Based on their expression patterns, we propose that EpoR and GATA-1 -mediated regulation of Bim and Bcl-x_L are largely segregated into the early and late erythroblast compartments, respectively (Figure A1.12A). Specifically, the underlying, largely stress-insensitive gradual increase in Bcl-x_L and gradual suppression of Bim with differentiation, is likely to be mediated by GATA-1. Superimposed on this pattern are Epo-mediated, stress-dependent adjustments that accelerate Bcl-x_L induction and Bim

suppression in early erythroblasts (Figures A1.4 and A1.5 , Figure A1.12 A). Thus, only the apoptosis-prone CFU-e, proerythroblasts and early basophilic erythroblasts (=‘early erythroblast compartment’) are dependent on EpoR signaling for survival in the basal state. Further, during hypoxic stress, it is principally the early erythroblast compartment that is Epo-responsive, undergoing expansion as a result of a rapid drop in apoptosis [14, 19, 206, 279] (Figure A1.6E). The susceptibility of the early erythroblast compartment to apoptosis is precisely the characteristic that gives plasticity to the erythropoietic system, allowing the level of EpoR signaling to determine erythropoietic rate.

We previously showed that Epo-mediated suppression of early erythroblast apoptosis during stress is strongly correlated with suppression of early erythroblast Fas. Using Fas and FasL-mutant mice, we recently found that the Fas suppression pathway accounts for ~30% of the early erythroblast expansion in stress [279]. Bim suppression and Bcl-x_L induction are therefore likely to cooperate with Fas suppression, and potentially with as yet uncharacterized other anti-apoptotic pathways, in achieving the full expansion of the early erythroblast compartment during stress.

In late erythroblasts, Bim, Bcl-x_L and Fas expression are relatively unaffected by EpoR-stress signaling. Consistent with this, in Stat5^{-/-} embryos and in EpoR-HM mice, where EpoR-Stat5 signaling is deficient, Bcl-x_L levels are only modestly lower in late erythroblasts; the underlying pattern, likely GATA-1-mediated, of a gradual increase in Bcl-x_L and decline in Bim, is preserved.

Importantly, our results show that Stat5-regulated Bcl-x_L expression *in vivo* varies with differentiation stage, with embryonic day, and with the phase of the stress response.

These factors should therefore be considered in the interpretation of Bcl-x_L measurements *in vivo* and in models of this system *in vitro*.

Adaptation allows functional specialization of the Bcl-x_L response to the acute phase of stress

The acute and chronic phases of the stress response differ in their requirements. At the onset of stress the speed of the response is paramount, a property that is unimportant during the chronic, maintenance phase. Here we find that the Bcl-x_L response is significantly faster than Bim or Fas suppression. In addition, the Bcl-x_L response undergoes rapid adaptation, which makes it insensitive to the prevailing absolute level of stress. Like other classical sensory adapting mechanisms, though, it is re-activated as soon as a new change in stress takes place. In this way, the dynamic range of the Bcl-x_L response is extended, allowing a rapid response to changes in stress irrespective of the baseline stress levels. Our new data on the Bcl-x_L pathway shows that distinct molecular mechanisms regulate the acute and chronic phases of stress. The EpoR is therefore capable of generating at least two broad types of signal: persistent, giving rise to persistent suppression of Bim and Fas, and a rapidly adapting signal, responsible for the adaptation of the Bcl-x_L response (Figure A1.12B).

Mechanism of adaptation in the Bcl-x_L response

We identified adaptation in the p-Stat5 response in erythroblasts *in vivo* and suggest this to be the mechanism of adaptation in the Bcl-x_L response. Both p-Stat5 and Bcl-x_L respond similarly to an ‘acute on chronic’ stress stimulus, a response typical of other biological adapting systems like sensory adaptation or neutrophil chemotaxis.

Adaptation of both p-Stat5 and Bcl-x_L depends on the distal domain of the EpoR, a previously documented negative regulatory domain that contains docking sites for the Stat5-induced SOCS family of negative regulators [210] (Figure A1.12C). Negative feedback is a well-documented mechanism of adaptation in sensory systems [295, 296]. Stat5 transcriptionally activates SOCS inhibitors that feed back to limit Jak2 and Stat5 activation [297]. Though well-documented, the precise effect of this pathway on the p-Stat5 signal was not previously investigated. Here we found that in EpoR-H mice that lack this feedback inhibition, peak p-Stat5 signal intensity is not higher than in wild-type. However, the duration of the peak is prolonged (Figure A1.10D). Therefore, p-Stat5-mediated negative feedback is likely responsible for the adaptation of both the p-Stat5 and Bcl-x_L responses.

Implications for myeloproliferative disease mechanisms

The rapid adaptation of the Bcl-x_L response to stress raises the possibility that prolonged periods in which Bcl-x_L is elevated may be harmful. Indeed, persistently elevated levels of Bcl-x_L are characteristic of Polycythemia Vera and other myeloproliferative syndromes [284, 285, 298]. High Bcl-x_L was suggested as a cause of Epo-independent erythroid differentiation in Polycythemia Vera and of the apoptosis resistance of other myeloproliferative syndromes and neoplasms [284, 298, 299]. Our results, supported by recent reports of SOCS protein inactivation in myeloproliferative disease [300, 301], suggest that impairment of p-Stat5 and Bcl-x_L adaptation may contribute to their prolonged activation. Together these point to the importance of adaptation in the Bcl-x_L response as a homeostatic and tumor-suppressive mechanism.

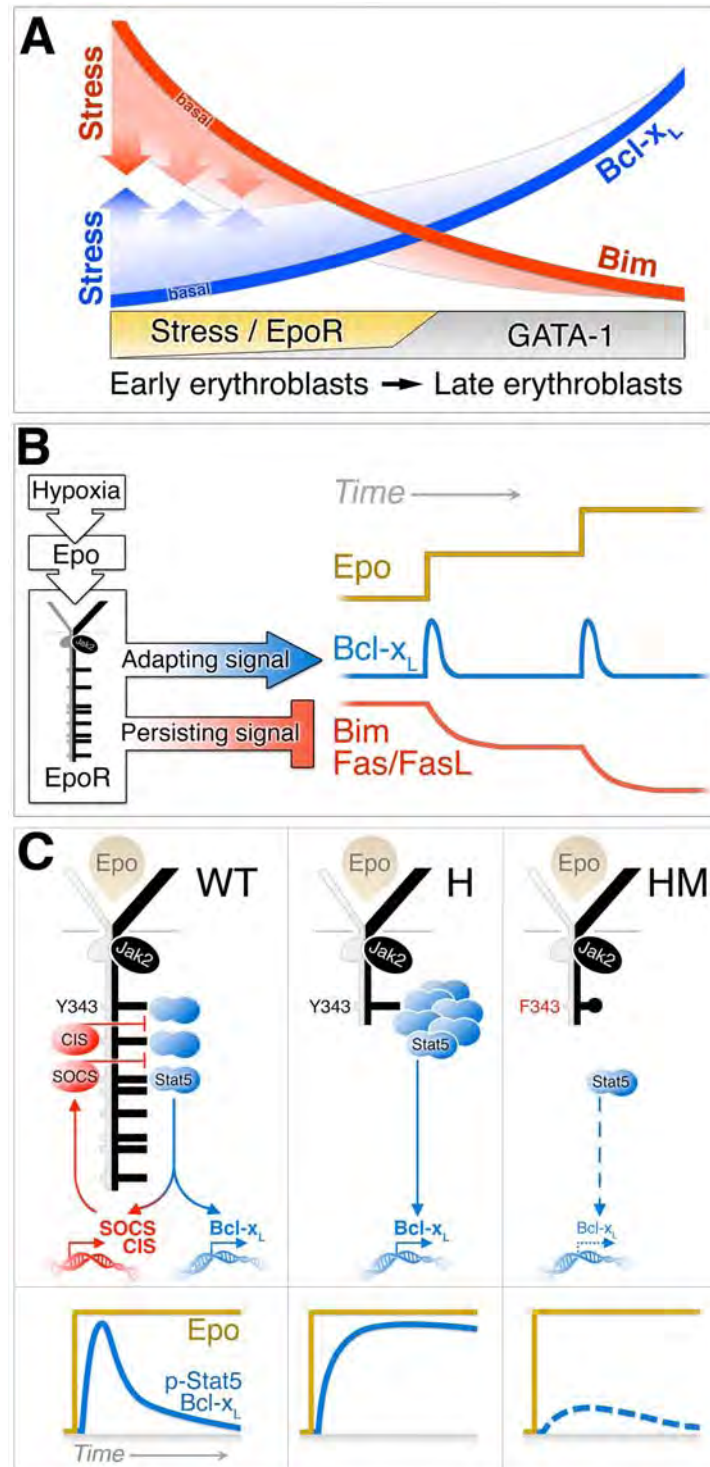
Figure A1.12 Regulation of Bcl-x_L and Bim expression in erythropoiesis.

(A) Model depicting expression of Bcl-x_L and Bim in the late and early erythroblast compartments, in basal erythropoiesis (solid lines) and during stress (fading shaded area). GATA-1 induces Bcl-x_L and suppresses Bim with differentiation, with maximal responses achieved in late erythroblasts. During stress, EpoR signaling operates principally in the early erythroblast compartment, accelerating both Bim suppression and Bcl-x_L induction.

(B) Contrasting dynamic stress responses of the Bcl-x_L, Bim and Fas pathways, both driven by the EpoR in the early erythroblast compartment. A sudden increase in stress drives a rapid, but transient adapting Bcl-x_L response. This response is re-activated with a further change in the stress level, but is insensitive to the absolute level of stress. Bim and Fas suppression in response to stress is slower but persistent and reflects the level of stress.

(C) Mechanism of adaptation in the Bcl-x_L response. EpoR-HM activation of both p-Stat5 and the Bcl-x_L is drastically attenuated, due to the absence of Stat5 phosphotyrosine docking sites on the EpoR-HM mutant receptor, in support of the role of p-Stat5 in the EpoR and stress-induced Bcl-x_L induction. In wild-type mice, the EpoR distal cytoplasmic domain binds p-Stat5-activated negative regulators of Jak2 and Stat5 such as SOCS3, SOCS2 and CIS, limiting the duration of both the p-Stat5 and the Bcl-x_L responses. In EpoR-H mice, absence of the distal EpoR domain results in a prolonged response and loss of adaptation.

Figure A1.12



Material and Methods

Mice

Stat5^{-/-} mice were obtained from Dr. Lothar Hennighausen, (NIDDK, Bethesda, MD). β -thalassemia mice and the ts-VHL^{-/-} mice were described previously [14]. Bim^{-/-} mice: B6.129S1-Bcl2l11^{tm1.1Ast}/J (stock #004525) were purchased from Jackson Laboratories (Bar Harbor, ME). EpoR-H and EpoR-HM mice were obtained from Dr. James Ihle, St. Jude Children's Research hospital, Memphis, TN [46]. In all experiments, mice were matched for the same background strain and embryonic age. For low oxygen chamber experiments, Balb/C male littermates of 6 to 11 weeks of age were used. All experiments were conducted in accordance with an animal protocol approved by the University of Massachusetts Medical School IACUC committee.

Erythropoietic stress

Recombinant human Epo (Epoetin alfa, Amgen, Thousand Oaks, CA) was injected subcutaneously in a total volume of 150 μ l in sterile isotonic saline. Reduced atmospheric oxygen treatment was conducted using the BioSpherix A-chamber (BioSpherix, Lacona, NY). Hypoxia was achieved by displacing oxygen with nitrogen at normal atmospheric pressure. Temperature, humidity and carbon dioxide readings were monitored.

Flow cytometry

Flow cytometry was performed on freshly explanted fetal liver, bone-marrow or spleen, as described [14, 19].

Live cell surface-staining (as described in Chapter III). Cells from freshly isolated

tissues were gently strained through 40- μ m strainer in the presence of cold phosphate-buffered saline and 5% fetal calf serum (PBS/5% FCS) or 0.2% bovine-serum albumin (BSA). Cells were immunostained for 20-45 minutes on ice in the presence of blocking rabbit IgG (Jackson ImmunoResearch, West Grove, PA), 2.5 μ g/mL fluorochrome-conjugated anti-Ter119 (BD Biosciences, San Diego, CA), and 2.5 μ g/mL fluorochrome-conjugated anti-CD71 (BD Biosciences). 7-AAD (BD Biosciences) or DAPI (Roche, Indianapolis, IN) was used to exclude dead cells. Staining for Fas or FasL was for 1 hour on ice with 5 μ g/mL biotin-conjugated anti-Fas (Jo2 clone, BD Biosciences) or 5 μ g/mL biotin-conjugated anti-FasL (MFL3 clone, BD Biosciences) and APC-conjugated streptavidin (Invitrogen). Annexin V staining was carried out according to the manufacturer's instructions (BD Biosciences).

Intracellular protein staining. To detect intracellular Bcl-x_L and Bim, cells were first stained with LIVE/DEAD fixable viability stain (Invitrogen), followed by surface-labeling for Ter119 and CD71 in the presence of blocking IgG. Next, cells were fixed with PBS solution containing 3% paraformaldehyde and 2% sucrose, and permeabilized with BD Cytotfix/CytopermTM Perm/Wash reagents, and stained in the Perm/Wash solution with anti-Ter119 (to maintain Ter119 signal in fixed cells) and with anti-Bcl-x_L antiserum (BD Biosciences 556361) or anti-Bim antibody (Cell Signaling, #2819), or isotype control. Isotype control for Bcl-x_L was Normal Rabbit Serum (Jackson Immunoresearch). Isotype control for Bim was Rabbit IgG (Jackson Immunoresearch). Primary Bcl-x_L or Bim staining was detected using secondary antibody (anti-Rabbit-APC, Invitrogen A-10931). Biological sample used for determining the isotype control's

background fluorescence consisted of a cell mix pooled from all mouse samples in a given experiment (isotype signal was similar across individual biological samples regardless of genotype or treatment).

Phospho-Stat5 staining. Cells were first stained with LIVE/DEAD viability dye, then resuspended in phosphowash (PBS, 1mM sodium orthovanadate, 1mM β -glycerol phosphate, 1 μ g/mL microcystin), fixed in 1.6% paraformaldehyde, permeabilized in 80% acetone and stored at -80°C. Thawed cells were stained in PBS/3% milk with AF647-conjugated anti-phospho-Stat5 antibody (BD Biosciences, 612599) and for Ter119 and CD71 as described previously. For all flow cytometry experiments, cells were analyzed on LSR II flow cytometer (BD Biosciences). Cell sorting was done on a DakoCytomation MoFlo (Fort Collins, CO).

Flow cytometry data analysis. Data were analyzed with FlowJo software (Tree Star, Ashland, OR) as described in Chapter IV [14, 208]. Singlets and live cells (based on DAPI, 7-AAD, or LIVE/DEAD stains) were selected, and subsets were gated based on Ter119, CD71 expression and forward scatter (FSC). Gating strategy for fetal liver and adult erythroblasts was performed as described in Chapter IV. For Fas surface stain, Fas-positive gate was drawn based on secondary-only control, as described. For Annexin V, positive gate was drawn based on the sample where Annexin V stain was omitted, as described. For each subset in each biological sample, non-specific isotype control's mean fluorescent intensity (MFI) signal was subtracted from the MFI of Bcl-x_L or Bim prior to plotting the data.

Quantitative real-time PCR

Total RNA was prepared from freshly sorted erythroblasts using the AllPrep DNA/RNA Micro Kit (Qiagen) with on column DNase treatment. Reverse-transcription was conducted using Superscript II (Invitrogen) with random hexamer primers. The ABI 7300 sequence detection system, TaqMan reagents and TagMan MGB probes (Applied Biosystems) were used and several dilutions of each template were used to ensure detection in the linear range of the assay. A 'no template' and 'no reverse-transcriptase' controls were included. The threshold cycle (Ct) for housekeeping genes GAPDH or β -actin were subtracted from the Ct for genes of interest to yield a relative expression value. The relative expression for each gene of interest in each sample was then normalized to expression in the S0 subset. QRT-PCR probes used: Gapdh (Mm99999915_g1), β -actin (Mm02619580_g1), β -globin (Mm01611268_g1). Bcl-x_L primers were CTGGGACACTTTTGTGGATCTCT and GAAGCGCTCCTGGCCTTT. Bim_{EL} primers were TCTTTTGACACAGACAGGAGC and AATCATTTGCAAACACCCTCC. Bim_L primers detected both Bim_{EL} and Bim_L isoforms, and were CTCAGTGCAATGGCTTCCATA and AATCATTTGCAAACACCCTCC.

CFU-e colony assay

Freshly isolated fetal liver cells were plated in M3231 Methocult® methylcellulose (StemCell Technologies, Vancouver, Canada) with the indicated dose of rh-Epo (Amgen). On day 3, plates were stained with 3,3'-Diaminobenzidine (Sigma-Aldrich) and scored for erythroid colonies.

Enzyme-linked Immunosorbent Assay (ELISA)

ELISA for endogenous mouse erythropoietin was performed according to the manufacturer's instructions (Quantikine ELISA, R&D Systems, Minneapolis, MN). EnVision 2102 Multilabel Reader (Perkin Elmer, Waltham, MA) was used to quantify fluorescence. Data was converted into mU/ml by multiplying pg/ml value by 129,000 IU/mg (International Standard for fully glycosylated Epo protein)[302].

Data analysis

Data analysis, including all statistical tests, was performed using Microsoft Excel Software (Redmond, WA), or GraphPad Prism Software (La Jolla, CA) where indicated.

Bibliography

1. Haase, V.H., *Hypoxic regulation of erythropoiesis and iron metabolism*. Am J Physiol Renal Physiol, 2010. **299**(1): p. F1-13.
2. Scortegagna, M., et al., *HIF-2alpha regulates murine hematopoietic development in an erythropoietin-dependent manner*. Blood, 2005. **105**(8): p. 3133-40.
3. Gruber, M., et al., *Acute postnatal ablation of Hif-2alpha results in anemia*. Proc Natl Acad Sci U S A, 2007. **104**(7): p. 2301-6.
4. Maxwell, P.H., et al., *The tumour suppressor protein VHL targets hypoxia-inducible factors for oxygen-dependent proteolysis*. Nature, 1999. **399**(6733): p. 271-5.
5. Ivan, M., et al., *HIFalpha targeted for VHL-mediated destruction by proline hydroxylation: implications for O2 sensing*. Science, 2001. **292**(5516): p. 464-8.
6. Ebert, B.L. and H.F. Bunn, *Regulation of the erythropoietin gene*. Blood, 1999. **94**(6): p. 1864-77.
7. Broudy, V.C., et al., *Interaction of stem cell factor and its receptor c-kit mediates lodgment and acute expansion of hematopoietic cells in the murine spleen*. Blood, 1996. **88**(1): p. 75-81.
8. Bauer, A., et al., *The glucocorticoid receptor is required for stress erythropoiesis*. Genes Dev, 1999. **13**(22): p. 2996-3002.
9. von Lindern, M., et al., *The glucocorticoid receptor cooperates with the erythropoietin receptor and c-Kit to enhance and sustain proliferation of erythroid progenitors in vitro*. Blood, 1999. **94**(2): p. 550-9.
10. Lenox, L.E., J.M. Perry, and R.F. Paulson, *BMP4 and Madh5 regulate the erythroid response to acute anemia*. Blood, 2005. **105**(7): p. 2741-8.
11. Iscove, N.N., F. Sieber, and K.H. Winterhalter, *Erythroid colony formation in cultures of mouse and human bone marrow: analysis of the requirement for erythropoietin by gel filtration and affinity chromatography on agarose-concanavalin A*. J Cell Physiol, 1974. **83**(2): p. 309-20.
12. Stephenson, J.R., et al., *Induction of colonies of hemoglobin-synthesizing cells by erythropoietin in vitro*. Proc Natl Acad Sci U S A, 1971. **68**(7): p. 1542-6.
13. Zhang, J., et al., *Role of Ras signaling in erythroid differentiation of mouse fetal liver cells: functional analysis by a flow cytometry-based novel culture system*. Blood, 2003. **102**(12): p. 3938-46.
14. Liu, Y., et al., *Suppression of Fas-FasL coexpression by erythropoietin mediates erythroblast expansion during the erythropoietic stress response in vivo*. Blood, 2006. **108**(1): p. 123-33.
15. Miyamoto, T., et al., *Myeloid or lymphoid promiscuity as a critical step in hematopoietic lineage commitment*. Dev Cell, 2002. **3**(1): p. 137-47.

16. Forsberg, E.C., et al., *New evidence supporting megakaryocyte-erythrocyte potential of flk2/flt3+ multipotent hematopoietic progenitors*. Cell, 2006. **126**(2): p. 415-26.
17. Wu, H., et al., *Generation of committed erythroid BFU-E and CFU-E progenitors does not require erythropoietin or the erythropoietin receptor*. Cell, 1995. **83**(1): p. 59-67.
18. Neubauer, H., et al., *Jak2 deficiency defines an essential developmental checkpoint in definitive hematopoiesis*. Cell, 1998. **93**(3): p. 397-409.
19. Socolovsky, M., *Molecular insights into stress erythropoiesis*. Curr Opin Hematol, 2007. **14**(3): p. 215-24.
20. D'Andrea, A.D., H.F. Lodish, and G.G. Wong, *Expression cloning of the murine erythropoietin receptor*. Cell, 1989. **57**(2): p. 277-85.
21. Remy, I., I.A. Wilson, and S.W. Michnick, *Erythropoietin receptor activation by a ligand-induced conformation change*. Science, 1999. **283**(5404): p. 990-3.
22. Livnah, O., et al., *Crystallographic evidence for preformed dimers of erythropoietin receptor before ligand activation*. Science, 1999. **283**(5404): p. 987-90.
23. Longmore, G.D. and H.F. Lodish, *An activating mutation in the murine erythropoietin receptor induces erythroleukemia in mice: a cytokine receptor superfamily oncogene*. Cell, 1991. **67**(6): p. 1089-102.
24. Damen, J.E., et al., *Tyrosine 343 in the erythropoietin receptor positively regulates erythropoietin-induced cell proliferation and Stat5 activation*. EMBO J, 1995. **14**(22): p. 5557-68.
25. Klingmuller, U., et al., *Multiple tyrosine residues in the cytosolic domain of the erythropoietin receptor promote activation of STAT5*. Proc Natl Acad Sci U S A, 1996. **93**(16): p. 8324-8.
26. Gobert, S., et al., *Identification of tyrosine residues within the intracellular domain of the erythropoietin receptor crucial for STAT5 activation*. EMBO J, 1996. **15**(10): p. 2434-41.
27. Miura, O., et al., *Erythropoietin-dependent association of phosphatidylinositol 3-kinase with tyrosine-phosphorylated erythropoietin receptor*. J Biol Chem, 1994. **269**(1): p. 614-20.
28. Miura, Y., et al., *Activation of the mitogen-activated protein kinase pathway by the erythropoietin receptor*. J Biol Chem, 1994. **269**(47): p. 29962-9.
29. Barber, D.L., et al., *Erythropoietin activates Raf1 by an Shc-independent pathway in CTLL-EPO-R cells*. Blood, 1997. **89**(1): p. 55-64.
30. Jacobs-Helber, S.M., J.J. Ryan, and S.T. Sawyer, *JNK and p38 are activated by erythropoietin (EPO) but are not induced in apoptosis following EPO withdrawal in EPO-dependent HCD57 cells*. Blood, 2000. **96**(3): p. 933-40.
31. Haq, R., et al., *Regulation of erythropoietin-induced STAT serine phosphorylation by distinct mitogen-activated protein kinases*. J Biol Chem, 2002. **277**(19): p. 17359-66.

32. Tamura, K., et al., *Requirement for p38alpha in erythropoietin expression: a role for stress kinases in erythropoiesis*. Cell, 2000. **102**(2): p. 221-31.
33. Uddin, S., et al., *Differentiation stage-specific activation of p38 mitogen-activated protein kinase isoforms in primary human erythroid cells*. Proc Natl Acad Sci U S A, 2004. **101**(1): p. 147-52.
34. Klingmuller, U., et al., *Specific recruitment of SH-PTP1 to the erythropoietin receptor causes inactivation of JAK2 and termination of proliferative signals*. Cell, 1995. **80**(5): p. 729-38.
35. Minoo, P., et al., *A novel SHP-1/Grb2-dependent mechanism of negative regulation of cytokine-receptor signaling: contribution of SHP-1 C-terminal tyrosines in cytokine signaling*. Blood, 2004. **103**(4): p. 1398-407.
36. Myers, M.P., et al., *TYK2 and JAK2 are substrates of protein-tyrosine phosphatase 1B*. J Biol Chem, 2001. **276**(51): p. 47771-4.
37. Irie-Sasaki, J., et al., *CD45 is a JAK phosphatase and negatively regulates cytokine receptor signalling*. Nature, 2001. **409**(6818): p. 349-54.
38. Mason, J.M., et al., *The SH2 inositol 5-phosphatase Ship1 is recruited in an SH2-dependent manner to the erythropoietin receptor*. J Biol Chem, 2000. **275**(6): p. 4398-406.
39. Hortner, M., et al., *A new high affinity binding site for suppressor of cytokine signaling-3 on the erythropoietin receptor*. Eur J Biochem, 2002. **269**(10): p. 2516-26.
40. Ketteler, R., et al., *The cytokine-inducible Scr homology domain-containing protein negatively regulates signaling by promoting apoptosis in erythroid progenitor cells*. J Biol Chem, 2003. **278**(4): p. 2654-60.
41. Sasaki, A., et al., *CIS3/SOCS-3 suppresses erythropoietin (EPO) signaling by binding the EPO receptor and JAK2*. J Biol Chem, 2000. **275**(38): p. 29338-47.
42. Ungureanu, D., et al., *Regulation of Jak2 through the ubiquitin-proteasome pathway involves phosphorylation of Jak2 on Y1007 and interaction with SOCS-1*. Mol Cell Biol, 2002. **22**(10): p. 3316-26.
43. Richmond, T.D., M. Chohan, and D.L. Barber, *Turning cells red: signal transduction mediated by erythropoietin*. Trends Cell Biol, 2005. **15**(3): p. 146-55.
44. Furukawa, T., et al., *Primary familial polycythaemia associated with a novel point mutation in the erythropoietin receptor*. Br J Haematol, 1997. **99**(1): p. 222-7.
45. Watowich, S.S., et al., *Erythropoietin receptor mutations associated with familial erythrocytosis cause hypersensitivity to erythropoietin in the heterozygous state*. Blood, 1999. **94**(7): p. 2530-2.
46. Zang, H., et al., *The distal region and receptor tyrosines of the Epo receptor are non-essential for in vivo erythropoiesis*. Embo J, 2001. **20**(12): p. 3156-66.
47. Menon, M.P., et al., *Signals for stress erythropoiesis are integrated via an erythropoietin receptor-phosphotyrosine-343-Stat5 axis*. J Clin Invest, 2006. **116**(3): p. 683-94.

48. Li, K., et al., *Attenuated signaling by a phosphotyrosine-null Epo receptor form in primary erythroid progenitor cells*. Blood, 2003. **102**(9): p. 3147-53.
49. Shuai, K., et al., *Activation of transcription by IFN-gamma: tyrosine phosphorylation of a 91-kD DNA binding protein*. Science, 1992. **258**(5089): p. 1808-12.
50. Schindler, C., et al., *Interferon-dependent tyrosine phosphorylation of a latent cytoplasmic transcription factor*. Science, 1992. **257**(5071): p. 809-13.
51. Shuai, K., et al., *A single phosphotyrosine residue of Stat91 required for gene activation by interferon-gamma*. Science, 1993. **261**(5129): p. 1744-6.
52. Leaman, D.W., et al., *Roles of JAKs in activation of STATs and stimulation of c-fos gene expression by epidermal growth factor*. Mol Cell Biol, 1996. **16**(1): p. 369-75.
53. Luchtefeld, M., H. Drexler, and B. Schieffer, *Role of G beta-subunit in angiotensin II-type 1 receptor signaling*. Biochem Biophys Res Commun, 2001. **280**(3): p. 756-60.
54. Kawata, T., et al., *SH2 signaling in a lower eukaryote: a STAT protein that regulates stalk cell differentiation in dictyostelium*. Cell, 1997. **89**(6): p. 909-16.
55. Hou, X.S., M.B. Melnick, and N. Perrimon, *Marelle acts downstream of the Drosophila HOP/JAK kinase and encodes a protein similar to the mammalian STATs*. Cell, 1996. **84**(3): p. 411-9.
56. Yan, R., et al., *Identification of a Stat gene that functions in Drosophila development*. Cell, 1996. **84**(3): p. 421-30.
57. Zeidler, M.P., N. Perrimon, and D.I. Strutt, *Polarity determination in the Drosophila eye: a novel role for unpaired and JAK/STAT signaling*. Genes Dev, 1999. **13**(10): p. 1342-53.
58. Sefton, L., et al., *An extracellular activator of the Drosophila JAK/STAT pathway is a sex-determination signal element*. Nature, 2000. **405**(6789): p. 970-3.
59. Jinks, T.M., et al., *The JAK/STAT signaling pathway is required for the initial choice of sexual identity in Drosophila melanogaster*. Mol Cell, 2000. **5**(3): p. 581-7.
60. Kiger, A.A., et al., *Stem cell self-renewal specified by JAK-STAT activation in response to a support cell cue*. Science, 2001. **294**(5551): p. 2542-5.
61. Tulina, N. and E. Matunis, *Control of stem cell self-renewal in Drosophila spermatogenesis by JAK-STAT signaling*. Science, 2001. **294**(5551): p. 2546-9.
62. Hou, S.X., et al., *The Jak/STAT pathway in model organisms: emerging roles in cell movement*. Dev Cell, 2002. **3**(6): p. 765-78.
63. Barillas-Mury, C., et al., *Anopheles gambiae Ag-STAT, a new insect member of the STAT family, is activated in response to bacterial infection*. EMBO J, 1999. **18**(4): p. 959-67.

64. Oates, A.C., et al., *Zebrafish stat3 is expressed in restricted tissues during embryogenesis and stat1 rescues cytokine signaling in a STAT1-deficient human cell line*. Dev Dyn, 1999. **215**(4): p. 352-70.
65. Pascal, A., et al., *Cloning and developmental expression of STAT5 in Xenopus laevis*. Mech Dev, 2001. **106**(1-2): p. 171-4.
66. Sung, S.C., et al., *Genomic structure, expression and characterization of a STAT5 homologue from pufferfish (Tetraodon fluviatilis)*. Eur J Biochem, 2003. **270**(2): p. 239-52.
67. Takeda, K., et al., *Targeted disruption of the mouse Stat3 gene leads to early embryonic lethality*. Proc Natl Acad Sci U S A, 1997. **94**(8): p. 3801-4.
68. Cui, Y., et al., *Inactivation of Stat5 in mouse mammary epithelium during pregnancy reveals distinct functions in cell proliferation, survival, and differentiation*. Mol Cell Biol, 2004. **24**(18): p. 8037-47.
69. Liu, X., et al., *Stat5a is mandatory for adult mammary gland development and lactogenesis*. Genes Dev, 1997. **11**(2): p. 179-86.
70. Udy, G.B., et al., *Requirement of STAT5b for sexual dimorphism of body growth rates and liver gene expression*. Proc Natl Acad Sci U S A, 1997. **94**(14): p. 7239-44.
71. Durbin, J.E., et al., *Targeted disruption of the mouse Stat1 gene results in compromised innate immunity to viral disease*. Cell, 1996. **84**(3): p. 443-50.
72. Meraz, M.A., et al., *Targeted disruption of the Stat1 gene in mice reveals unexpected physiologic specificity in the JAK-STAT signaling pathway*. Cell, 1996. **84**(3): p. 431-42.
73. Park, C., et al., *Immune response in Stat2 knockout mice*. Immunity, 2000. **13**(6): p. 795-804.
74. Kaplan, M.H., et al., *Impaired IL-12 responses and enhanced development of Th2 cells in Stat4-deficient mice*. Nature, 1996. **382**(6587): p. 174-7.
75. Takeda, K., et al., *Essential role of Stat6 in IL-4 signalling*. Nature, 1996. **380**(6575): p. 627-30.
76. Chen, X., et al., *Crystal structure of a tyrosine phosphorylated STAT-1 dimer bound to DNA*. Cell, 1998. **93**(5): p. 827-39.
77. Becker, S., B. Groner, and C.W. Muller, *Three-dimensional structure of the Stat3beta homodimer bound to DNA*. Nature, 1998. **394**(6689): p. 145-51.
78. Yu, H. and R. Jove, *The STATs of cancer--new molecular targets come of age*. Nat Rev Cancer, 2004. **4**(2): p. 97-105.
79. Vinkemeier, U., et al., *Structure of the amino-terminal protein interaction domain of STAT-4*. Science, 1998. **279**(5353): p. 1048-52.
80. Mao, X., et al., *Structural bases of unphosphorylated STAT1 association and receptor binding*. Mol Cell, 2005. **17**(6): p. 761-71.
81. O'Shea, J.J., M. Gadina, and R.D. Schreiber, *Cytokine signaling in 2002: new surprises in the Jak/Stat pathway*. Cell, 2002. **109 Suppl**: p. S121-31.
82. Cohen, G.B., R. Ren, and D. Baltimore, *Modular binding domains in signal transduction proteins*. Cell, 1995. **80**(2): p. 237-48.

83. Pawson, T., *Protein modules and signalling networks*. Nature, 1995. **373**(6515): p. 573-80.
84. Levy, D.E. and J.E. Darnell, Jr., *Stats: transcriptional control and biological impact*. Nat Rev Mol Cell Biol, 2002. **3**(9): p. 651-62.
85. Horvath, C.M., *STAT proteins and transcriptional responses to extracellular signals*. Trends Biochem Sci, 2000. **25**(10): p. 496-502.
86. Wang, D., et al., *A small amphipathic alpha-helical region is required for transcriptional activities and proteasome-dependent turnover of the tyrosine-phosphorylated Stat5*. EMBO J, 2000. **19**(3): p. 392-9.
87. ten Hoeve, J., et al., *Identification of a nuclear Stat1 protein tyrosine phosphatase*. Mol Cell Biol, 2002. **22**(16): p. 5662-8.
88. Chung, C.D., et al., *Specific inhibition of Stat3 signal transduction by PIAS3*. Science, 1997. **278**(5344): p. 1803-5.
89. Aoki, N. and T. Matsuda, *A cytosolic protein-tyrosine phosphatase PTP1B specifically dephosphorylates and deactivates prolactin-activated STAT5a and STAT5b*. J Biol Chem, 2000. **275**(50): p. 39718-26.
90. You, M., D.H. Yu, and G.S. Feng, *Shp-2 tyrosine phosphatase functions as a negative regulator of the interferon-stimulated Jak/STAT pathway*. Mol Cell Biol, 1999. **19**(3): p. 2416-24.
91. David, M., et al., *Differential regulation of the alpha/beta interferon-stimulated Jak/Stat pathway by the SH2 domain-containing tyrosine phosphatase SHPTP1*. Mol Cell Biol, 1995. **15**(12): p. 7050-8.
92. Krebs, D.L. and D.J. Hilton, *SOCS proteins: negative regulators of cytokine signaling*. Stem Cells, 2001. **19**(5): p. 378-87.
93. Yasukawa, H., et al., *The JAK-binding protein JAB inhibits Janus tyrosine kinase activity through binding in the activation loop*. EMBO J, 1999. **18**(5): p. 1309-20.
94. Endo, T.A., et al., *A new protein containing an SH2 domain that inhibits JAK kinases*. Nature, 1997. **387**(6636): p. 921-4.
95. Matsumoto, A., et al., *CIS, a cytokine inducible SH2 protein, is a target of the JAK-STAT5 pathway and modulates STAT5 activation*. Blood, 1997. **89**(9): p. 3148-54.
96. Yoshimura, A., et al., *A novel cytokine-inducible gene CIS encodes an SH2-containing protein that binds to tyrosine-phosphorylated interleukin 3 and erythropoietin receptors*. EMBO J, 1995. **14**(12): p. 2816-26.
97. Frantsve, J., et al., *Socs-1 inhibits TEL-JAK2-mediated transformation of hematopoietic cells through inhibition of JAK2 kinase activity and induction of proteasome-mediated degradation*. Mol Cell Biol, 2001. **21**(10): p. 3547-57.
98. Boyle, K., et al., *Deletion of the SOCS box of suppressor of cytokine signaling 3 (SOCS3) in embryonic stem cells reveals SOCS box-dependent regulation of JAK but not STAT phosphorylation*. Cell Signal, 2009. **21**(3): p. 394-404.

99. Callus, B.A. and B. Mathey-Prevot, *SOCS36E, a novel Drosophila SOCS protein, suppresses JAK/STAT and EGF-R signalling in the imaginal wing disc.* Oncogene, 2002. **21**(31): p. 4812-21.
100. Shuai, K., et al., *Interferon activation of the transcription factor Stat91 involves dimerization through SH2-phosphotyrosyl peptide interactions.* Cell, 1994. **76**(5): p. 821-8.
101. Novak, U., et al., *STAT3 forms stable homodimers in the presence of divalent cations prior to activation.* Biochem Biophys Res Commun, 1998. **247**(3): p. 558-63.
102. Ndubuisi, M.I., et al., *Cellular physiology of STAT3: Where's the cytoplasmic monomer?* J Biol Chem, 1999. **274**(36): p. 25499-509.
103. Stancato, L.F., et al., *Preassociation of STAT1 with STAT2 and STAT3 in separate signalling complexes prior to cytokine stimulation.* J Biol Chem, 1996. **271**(8): p. 4134-7.
104. Haan, S., et al., *Cytoplasmic STAT proteins associate prior to activation.* Biochem J, 2000. **345 Pt 3**: p. 417-21.
105. Braunstein, J., et al., *STATs dimerize in the absence of phosphorylation.* J Biol Chem, 2003. **278**(36): p. 34133-40.
106. Ota, N., et al., *N-domain-dependent nonphosphorylated STAT4 dimers required for cytokine-driven activation.* Nat Immunol, 2004. **5**(2): p. 208-15.
107. Baden, H.A., et al., *The amino-terminal domain of human STAT4. Overproduction, purification, and biophysical characterization.* J Biol Chem, 1998. **273**(27): p. 17109-14.
108. Chen, X., et al., *A reinterpretation of the dimerization interface of the N-terminal domains of STATs.* Protein Sci, 2003. **12**(2): p. 361-5.
109. Neculai, D., et al., *Structure of the unphosphorylated STAT5a dimer.* J Biol Chem, 2005. **280**(49): p. 40782-7.
110. Mertens, C., et al., *Dephosphorylation of phosphotyrosine on STAT1 dimers requires extensive spatial reorientation of the monomers facilitated by the N-terminal domain.* Genes Dev, 2006. **20**(24): p. 3372-81.
111. Zhong, M., et al., *Implications of an antiparallel dimeric structure of nonphosphorylated STAT1 for the activation-inactivation cycle.* Proc Natl Acad Sci U S A, 2005. **102**(11): p. 3966-71.
112. Shuai, K., J. Liao, and M.M. Song, *Enhancement of antiproliferative activity of gamma interferon by the specific inhibition of tyrosine dephosphorylation of Stat1.* Mol Cell Biol, 1996. **16**(9): p. 4932-41.
113. Strehlow, I. and C. Schindler, *Amino-terminal signal transducer and activator of transcription (STAT) domains regulate nuclear translocation and STAT deactivation.* J Biol Chem, 1998. **273**(43): p. 28049-56.
114. Wakao, H., F. Gouilleux, and B. Groner, *Mammary gland factor (MGF) is a novel member of the cytokine regulated transcription factor gene family and confers the prolactin response.* EMBO J, 1994. **13**(9): p. 2182-91.

115. Azam, M., et al., *Functionally distinct isoforms of STAT5 are generated by protein processing*. *Immunity*, 1997. **6**(6): p. 691-701.
116. Liu, X., et al., *Cloning and expression of Stat5 and an additional homologue (Stat5b) involved in prolactin signal transduction in mouse mammary tissue*. *Proc Natl Acad Sci U S A*, 1995. **92**(19): p. 8831-5.
117. Mui, A.L., et al., *Interleukin-3, granulocyte-macrophage colony-stimulating factor, and interleukin-5 transduce signals through two forms of STAT5*. *J Leukoc Biol*, 1995. **57**(5): p. 799-803.
118. Dai, X., et al., *Stat5 is essential for early B cell development but not for B cell maturation and function*. *J Immunol*, 2007. **179**(2): p. 1068-79.
119. Zhu, B.M., et al., *Hematopoietic-specific Stat5-null mice display microcytic hypochromic anemia associated with reduced transferrin receptor gene expression*. *Blood*, 2008. **112**(5): p. 2071-80.
120. Li, G., et al., *STAT5 requires the N-domain to maintain hematopoietic stem cell repopulating function and appropriate lymphoid-myeloid lineage output*. *Exp Hematol*, 2007. **35**(11): p. 1684-94.
121. Schepers, H., et al., *STAT5 is required for long-term maintenance of normal and leukemic human stem/progenitor cells*. *Blood*, 2007. **110**(8): p. 2880-8.
122. de Groot, R.P., et al., *STAT5 activation by BCR-Abl contributes to transformation of K562 leukemia cells*. *Blood*, 1999. **94**(3): p. 1108-12.
123. Spiekermann, K., et al., *Constitutive activation of STAT3 and STAT5 is induced by leukemic fusion proteins with protein tyrosine kinase activity and is sufficient for transformation of hematopoietic precursor cells*. *Exp Hematol*, 2002. **30**(3): p. 262-71.
124. Harir, N., et al., *Constitutive activation of Stat5 promotes its cytoplasmic localization and association with PI3-kinase in myeloid leukemias*. *Blood*, 2007. **109**(4): p. 1678-86.
125. Moriggl, R., et al., *Stat5 tetramer formation is associated with leukemogenesis*. *Cancer Cell*, 2005. **7**(1): p. 87-99.
126. Socolovsky, M., et al., *Fetal anemia and apoptosis of red cell progenitors in Stat5a^{-/-}5b^{-/-} mice: a direct role for Stat5 in bcl-X_L induction*. *Cell*, 1999. **98**: p. 181-191.
127. Socolovsky, M., et al., *Ineffective erythropoiesis in Stat5a(-/-)5b(-/-) mice due to decreased survival of early erythroblasts*. *Blood*, 2001. **98**(12): p. 3261-73.
128. Longmore, G.D., *A unique role for Stat5 in recovery from acute anemia*. *J Clin Invest*, 2006. **116**(3): p. 626-8.
129. Teglund, S., et al., *Stat5a and Stat5b proteins have essential and nonessential, or redundant, roles in cytokine responses*. *Cell*, 1998. **93**(5): p. 841-50.
130. Socolovsky, M., et al., *Fetal anemia and apoptosis of red cell progenitors in Stat5a^{-/-}5b^{-/-} mice: a direct role for Stat5 in Bcl-X(L) induction*. *Cell*, 1999. **98**(2): p. 181-91.
131. Motoyama, N., et al., *Massive cell death of immature hematopoietic cells and neurons in Bcl-x-deficient mice*. *Science*, 1995. **267**(5203): p. 1506-10.

132. Dolznig, H., et al., *Apoptosis protection by the Epo target Bcl-X(L) allows factor-independent differentiation of primary erythroblasts*. *Curr Biol*, 2002. **12**(13): p. 1076-85.
133. Gregory, T., et al., *GATA-1 and erythropoietin cooperate to promote erythroid cell survival by regulating bcl-xL expression*. *Blood*, 1999. **94**(1): p. 87-96.
134. Kerenyi, M.A., et al., *Stat5 regulates cellular iron uptake of erythroid cells via IRP-2 and TfR-1*. *Blood*, 2008. **112**(9): p. 3878-88.
135. Wakao, H., et al., *Interleukin 2 and erythropoietin activate STAT5/MGF via distinct pathways*. *EMBO J*, 1995. **14**(11): p. 2527-35.
136. Gouilleux, F., et al., *Prolactin, growth hormone, erythropoietin and granulocyte-macrophage colony stimulating factor induce MGF-Stat5 DNA binding activity*. *EMBO J*, 1995. **14**(9): p. 2005-13.
137. Bergelson, S., et al., *Tyrosine residues within the intracellular domain of the erythropoietin receptor mediate activation of AP-1 transcription factors*. *J Biol Chem*, 1998. **273**(4): p. 2396-401.
138. Quelle, F.W., et al., *Erythropoietin induces activation of Stat5 through association with specific tyrosines on the receptor that are not required for a mitogenic response*. *Mol Cell Biol*, 1996. **16**(4): p. 1622-31.
139. Huff, K., D. End, and G. Guroff, *Nerve growth factor-induced alteration in the response of PC12 pheochromocytoma cells to epidermal growth factor*. *J Cell Biol*, 1981. **88**(1): p. 189-98.
140. Greene, L.A. and A.S. Tischler, *Establishment of a noradrenergic clonal line of rat adrenal pheochromocytoma cells which respond to nerve growth factor*. *Proc Natl Acad Sci U S A*, 1976. **73**(7): p. 2424-8.
141. Huang, C.Y. and J.E. Ferrell, Jr., *Dependence of Mos-induced Cdc2 activation on MAP kinase function in a cell-free system*. *EMBO J*, 1996. **15**(9): p. 2169-73.
142. Ferrell, J.E., Jr., *MAP kinases in mitogenesis and development*. *Curr Top Dev Biol*, 1996. **33**: p. 1-60.
143. Heasley, L.E. and G.L. Johnson, *The beta-PDGF receptor induces neuronal differentiation of PC12 cells*. *Mol Biol Cell*, 1992. **3**(5): p. 545-53.
144. Traverse, S., et al., *Sustained activation of the mitogen-activated protein (MAP) kinase cascade may be required for differentiation of PC12 cells. Comparison of the effects of nerve growth factor and epidermal growth factor*. *Biochem J*, 1992. **288 (Pt 2)**: p. 351-5.
145. Nguyen, T.T., et al., *Co-regulation of the mitogen-activated protein kinase, extracellular signal-regulated kinase 1, and the 90-kDa ribosomal S6 kinase in PC12 cells. Distinct effects of the neurotrophic factor, nerve growth factor, and the mitogenic factor, epidermal growth factor*. *J Biol Chem*, 1993. **268**(13): p. 9803-10.
146. Ferrell, J.E., Jr., *Tripping the switch fantastic: how a protein kinase cascade can convert graded inputs into switch-like outputs*. *Trends Biochem Sci*, 1996. **21**(12): p. 460-6.

147. Koshland, D.E., Jr., A. Goldbeter, and J.B. Stock, *Amplification and adaptation in regulatory and sensory systems*. Science, 1982. **217**(4556): p. 220-5.
148. Ferrell, J.E., Jr., *How regulated protein translocation can produce switch-like responses*. Trends Biochem Sci, 1998. **23**(12): p. 461-5.
149. Ferrell, J.E., Jr., *Self-perpetuating states in signal transduction: positive feedback, double-negative feedback and bistability*. Curr Opin Cell Biol, 2002. **14**(2): p. 140-8.
150. Ferrell, J.E., Jr. and E.M. Machleder, *The biochemical basis of an all-or-none cell fate switch in Xenopus oocytes*. Science, 1998. **280**(5365): p. 895-8.
151. Sohaskey, M.L. and J.E. Ferrell, Jr., *Distinct, constitutively active MAPK phosphatases function in Xenopus oocytes: implications for p42 MAPK regulation In vivo*. Mol Biol Cell, 1999. **10**(11): p. 3729-43.
152. Guadagno, T.M. and J.E. Ferrell, Jr., *Requirement for MAPK activation for normal mitotic progression in Xenopus egg extracts*. Science, 1998. **282**(5392): p. 1312-5.
153. Huang, C.Y. and J.E. Ferrell, Jr., *Ultrasensitivity in the mitogen-activated protein kinase cascade*. Proc Natl Acad Sci U S A, 1996. **93**(19): p. 10078-83.
154. Yue, J., W. Xiong, and J.E. Ferrell, *B-Raf and C-Raf are required for Ras-stimulated p42 MAP kinase activation in Xenopus egg extracts*. Oncogene, 2006. **25**(23): p. 3307-15.
155. Yue, J. and J.E. Ferrell, Jr., *Mos mediates the mitotic activation of p42 MAPK in Xenopus egg extracts*. Curr Biol, 2004. **14**(17): p. 1581-6.
156. Xiong, W. and J.E. Ferrell, Jr., *A positive-feedback-based bistable 'memory module' that governs a cell fate decision*. Nature, 2003. **426**(6965): p. 460-5.
157. Sohaskey, M.L. and J.E. Ferrell, Jr., *Activation of p42 mitogen-activated protein kinase (MAPK), but not c-Jun NH(2)-terminal kinase, induces phosphorylation and stabilization of MAPK phosphatase XCL100 in Xenopus oocytes*. Mol Biol Cell, 2002. **13**(2): p. 454-68.
158. Roy, L.M., et al., *Mos proto-oncogene function during oocyte maturation in Xenopus*. Oncogene, 1996. **12**(10): p. 2203-11.
159. Matten, W.T., et al., *Positive feedback between MAP kinase and Mos during Xenopus oocyte maturation*. Dev Biol, 1996. **179**(2): p. 485-92.
160. Gotoh, Y., et al., *Initiation of Xenopus oocyte maturation by activation of the mitogen-activated protein kinase cascade*. J Biol Chem, 1995. **270**(43): p. 25898-904.
161. Howard, E.L., et al., *The mitogen-activated protein kinase signaling pathway stimulates mos mRNA cytoplasmic polyadenylation during Xenopus oocyte maturation*. Mol Cell Biol, 1999. **19**(3): p. 1990-9.
162. Ptashne, M., A.D. Johnson, and C.O. Pabo, *A genetic switch in a bacterial virus*. Sci Am, 1982. **247**(5): p. 128-30, 132, 134-40.
163. Ferrell, J.E., Jr., *Building a cellular switch: more lessons from a good egg*. Bioessays, 1999. **21**(10): p. 866-70.

164. Ferrell, J.E., Jr., *Xenopus oocyte maturation: new lessons from a good egg*. Bioessays, 1999. **21**(10): p. 833-42.
165. Irish, J.M., et al., *Single cell profiling of potentiated phospho-protein networks in cancer cells*. Cell, 2004. **118**(2): p. 217-28.
166. Krutzik, P.O., et al., *Analysis of protein phosphorylation and cellular signaling events by flow cytometry: techniques and clinical applications*. Clin Immunol, 2004. **110**(3): p. 206-21.
167. Perez, O.D., P.O. Krutzik, and G.P. Nolan, *Flow cytometric analysis of kinase signaling cascades*. Methods Mol Biol, 2004. **263**: p. 67-94.
168. Krutzik, P.O. and G.P. Nolan, *Intracellular phospho-protein staining techniques for flow cytometry: monitoring single cell signaling events*. Cytometry A, 2003. **55**(2): p. 61-70.
169. Krutzik, P.O., M.B. Hale, and G.P. Nolan, *Characterization of the murine immunological signaling network with phosphospecific flow cytometry*. J Immunol, 2005. **175**(4): p. 2366-73.
170. Krutzik, P.O., M.R. Clutter, and G.P. Nolan, *Coordinate analysis of murine immune cell surface markers and intracellular phosphoproteins by flow cytometry*. J Immunol, 2005. **175**(4): p. 2357-65.
171. Peck, A.R., et al., *Loss of nuclear localized and tyrosine phosphorylated stat5 in breast cancer predicts poor clinical outcome and increased risk of antiestrogen therapy failure*. J Clin Oncol. **29**(18): p. 2448-58.
172. Yamashita, H., et al., *Stat5 expression predicts response to endocrine therapy and improves survival in estrogen receptor-positive breast cancer*. Endocr Relat Cancer, 2006. **13**(3): p. 885-93.
173. Lai, S.Y., et al., *Erythropoietin-mediated activation of JAK-STAT signaling contributes to cellular invasion in head and neck squamous cell carcinoma*. Oncogene, 2005. **24**(27): p. 4442-9.
174. Leong, P.L., et al., *Differential function of STAT5 isoforms in head and neck cancer growth control*. Oncogene, 2002. **21**(18): p. 2846-53.
175. Chai, S.K., G.L. Nichols, and P. Rothman, *Constitutive activation of JAKs and STATs in BCR-Abl-expressing cell lines and peripheral blood cells derived from leukemic patients*. J Immunol, 1997. **159**(10): p. 4720-8.
176. Carlesso, N., D.A. Frank, and J.D. Griffin, *Tyrosyl phosphorylation and DNA binding activity of signal transducers and activators of transcription (STAT) proteins in hematopoietic cell lines transformed by Bcr/Abl*. J Exp Med, 1996. **183**(3): p. 811-20.
177. Shuai, K., et al., *Constitutive activation of STAT5 by the BCR-ABL oncogene in chronic myelogenous leukemia*. Oncogene, 1996. **13**(2): p. 247-54.
178. Weber-Nordt, R.M., et al., *Constitutive activation of STAT proteins in primary lymphoid and myeloid leukemia cells and in Epstein-Barr virus (EBV)-related lymphoma cell lines*. Blood, 1996. **88**(3): p. 809-16.
179. Schwaller, J., et al., *Stat5 is essential for the myelo- and lymphoproliferative disease induced by TEL/JAK2*. Mol Cell, 2000. **6**(3): p. 693-704.

180. Funakoshi-Tago, M., et al., *STAT5 activation is critical for the transformation mediated by myeloproliferative disorder-associated JAK2 V617F mutant*. J Biol Chem. **285**(8): p. 5296-307.
181. Takeda, Y., et al., *Direct activation of STAT5 by ETV6-LYN fusion protein promotes induction of myeloproliferative neoplasm with myelofibrosis*. Br J Haematol. **153**(5): p. 589-98.
182. Aboudola, S., et al., *Bone marrow phospho-STAT5 expression in non-CML chronic myeloproliferative disorders correlates with JAK2 V617F mutation and provides evidence of in vivo JAK2 activation*. Am J Surg Pathol, 2007. **31**(2): p. 233-9.
183. Shide, K., et al., *Development of ET, primary myelofibrosis and PV in mice expressing JAK2 V617F*. Leukemia, 2008. **22**(1): p. 87-95.
184. Chen, E., et al., *Distinct clinical phenotypes associated with JAK2V617F reflect differential STAT1 signaling*. Cancer Cell. **18**(5): p. 524-35.
185. James, C., et al., *A unique clonal JAK2 mutation leading to constitutive signalling causes polycythaemia vera*. Nature, 2005. **434**(7037): p. 1144-8.
186. Levine, R.L., et al., *Activating mutation in the tyrosine kinase JAK2 in polycythemia vera, essential thrombocythemia, and myeloid metaplasia with myelofibrosis*. Cancer Cell, 2005. **7**(4): p. 387-97.
187. Luo, H., W.P. Hanratty, and C.R. Dearolf, *An amino acid substitution in the Drosophila hopTum-1 Jak kinase causes leukemia-like hematopoietic defects*. EMBO J, 1995. **14**(7): p. 1412-20.
188. Harrison, D.A., et al., *Activation of a Drosophila Janus kinase (JAK) causes hematopoietic neoplasia and developmental defects*. EMBO J, 1995. **14**(12): p. 2857-65.
189. Luo, H., et al., *The Hopscotch Jak kinase requires the Raf pathway to promote blood cell activation and differentiation in Drosophila*. Mol Genet Genomics, 2002. **267**(1): p. 57-63.
190. Remillieux-Leschelle, N., P. Santamaria, and N.B. Randsholt, *Regulation of larval hematopoiesis in Drosophila melanogaster: a role for the multi sex combs gene*. Genetics, 2002. **162**(3): p. 1259-74.
191. Ilaria, R.L., Jr. and R.A. Van Etten, *P210 and P190(BCR/ABL) induce the tyrosine phosphorylation and DNA binding activity of multiple specific STAT family members*. J Biol Chem, 1996. **271**(49): p. 31704-10.
192. Sillaber, C., et al., *STAT5 activation contributes to growth and viability in Bcr/Abl-transformed cells*. Blood, 2000. **95**(6): p. 2118-25.
193. Daley, G.Q., R.A. Van Etten, and D. Baltimore, *Induction of chronic myelogenous leukemia in mice by the P210bcr/abl gene of the Philadelphia chromosome*. Science, 1990. **247**(4944): p. 824-30.
194. Ho, J.M., et al., *Fusion of the ets transcription factor TEL to Jak2 results in constitutive Jak-Stat signaling*. Blood, 1999. **93**(12): p. 4354-64.

195. Mizuki, M., et al., *Flt3 mutations from patients with acute myeloid leukemia induce transformation of 32D cells mediated by the Ras and STAT5 pathways*. Blood, 2000. **96**(12): p. 3907-14.
196. Levis, M., et al., *A FLT3-targeted tyrosine kinase inhibitor is cytotoxic to leukemia cells in vitro and in vivo*. Blood, 2002. **99**(11): p. 3885-91.
197. Hoelbl, A., et al., *Stat5 is indispensable for the maintenance of bcr/abl-positive leukaemia*. EMBO Mol Med. **2**(3): p. 98-110.
198. Ye, D., et al., *STAT5 signaling is required for the efficient induction and maintenance of CML in mice*. Blood, 2006. **107**(12): p. 4917-25.
199. Hoelbl, A., et al., *Clarifying the role of Stat5 in lymphoid development and Abelson-induced transformation*. Blood, 2006. **107**(12): p. 4898-906.
200. Nieborowska-Skorska, M., et al., *Signal transducer and activator of transcription (STAT)5 activation by BCR/ABL is dependent on intact Src homology (SH)3 and SH2 domains of BCR/ABL and is required for leukemogenesis*. J Exp Med, 1999. **189**(8): p. 1229-42.
201. Huang, M., et al., *Inhibition of Bcr-Abl kinase activity by PD180970 blocks constitutive activation of Stat5 and growth of CML cells*. Oncogene, 2002. **21**(57): p. 8804-16.
202. Constantinescu, S.N., S. Ghaffari, and H.F. Lodish, *The Erythropoietin receptor: structure, activation and intracellular signal transduction*. TEM, 1999. **10**(1): p. 18-23.
203. Schindler, C., D.E. Levy, and T. Decker, *JAK-STAT signaling: from interferons to cytokines*. J Biol Chem, 2007. **282**(28): p. 20059-63.
204. Marshall, C.J., *Specificity of receptor tyrosine kinase signaling: transient versus sustained extracellular signal-regulated kinase activation*. Cell, 1995. **80**(2): p. 179-85.
205. Das, J., et al., *Digital signaling and hysteresis characterize ras activation in lymphoid cells*. Cell, 2009. **136**(2): p. 337-51.
206. Socolovsky, M., et al., *Negative Autoregulation by FAS Mediates Robust Fetal Erythropoiesis*. PLoS Biol, 2007. **5**(10): p. e252.
207. Sachs, K., et al., *Causal protein-signaling networks derived from multiparameter single-cell data*. Science, 2005. **308**(5721): p. 523-9.
208. Pop, R., et al., *A key commitment step in erythropoiesis is synchronized with the cell cycle clock through mutual inhibition between PU.1 and S-phase progression*. PLoS Biol, 2010. **8**(9).
209. D'Andrea, A.D., et al., *The cytoplasmic region of the erythropoietin receptor contains nonoverlapping positive and negative growth-regulatory domains*. Mol Cell Biol, 1991. **11**(4): p. 1980-7.
210. Lodish, H.F., et al., *Intracellular signaling by the erythropoietin receptor, in Erythropoietins, Erythropoietic Factors, and Erythropoiesis: Molecular, Cellular, Preclinical, and Clinical Biology*, S.G. Elliott, M. Foote, and G. Molineux, Editors. 2009, Birkhäuser: Basel. p. 155-174.

211. Tzafriri, A.R., *Michaelis-Menten kinetics at high enzyme concentrations*. Bull Math Biol, 2003. **65**(6): p. 1111-29.
212. Rami Tzafriri, A. and E.R. Edelman, *Quasi-steady-state kinetics at enzyme and substrate concentrations in excess of the Michaelis-Menten constant*. J Theor Biol, 2007. **245**(4): p. 737-48.
213. Dolznig, H., et al., *Erythroid progenitor renewal versus differentiation: genetic evidence for cell autonomous, essential functions of EpoR, Stat5 and the GR*. Oncogene, 2006. **25**(20): p. 2890-900.
214. Hennighausen, L. and G.W. Robinson, *Interpretation of cytokine signaling through the transcription factors STAT5A and STAT5B*. Genes Dev, 2008. **22**(6): p. 711-21.
215. Tyson, J.J., K.C. Chen, and B. Novak, *Sniffers, buzzers, toggles and blinkers: dynamics of regulatory and signaling pathways in the cell*. Curr Opin Cell Biol, 2003. **15**(2): p. 221-31.
216. Pomerening, J.R., E.D. Sontag, and J.E. Ferrell, Jr., *Building a cell cycle oscillator: hysteresis and bistability in the activation of Cdc2*. Nat Cell Biol, 2003. **5**(4): p. 346-51.
217. Onishi, M., et al., *Identification and characterization of a constitutively active STAT5 mutant that promotes cell proliferation*. Mol. Cell. Biol., 1998. **18**(7): p. 3871-3879.
218. Steinfeld, J.I., J.S. Francisco, and W.L. Hase, *Autocatalysis and oscillating reactions*, in *Chemical Kinetics and Dynamics*. 1989, Prentice-Hall: New Jersey. p. 182-183.
219. Banks, R.B., *Growth and diffusion phenomena: mathematical frameworks and applications*. 1994, Berlin Heidelberg New York: Springer-Verlag.
220. John, S., et al., *The significance of tetramerization in promoter recruitment by Stat5*. Mol Cell Biol, 1999. **19**(3): p. 1910-8.
221. Biggar, S.R. and G.R. Crabtree, *Cell signaling can direct either binary or graded transcriptional responses*. Embo J, 2001. **20**(12): p. 3167-76.
222. Ozbudak, E.M., et al., *Multistability in the lactose utilization network of Escherichia coli*. Nature, 2004. **427**(6976): p. 737-40.
223. Ruf, F., et al., *Mixed analog/digital gonadotrope biosynthetic response to gonadotropin-releasing hormone*. J Biol Chem, 2006. **281**(41): p. 30967-78.
224. Thomas, R., *On the relation between the logical structure of systems and their ability to generate multiple steady states or sustained oscillations*, in *Ser. Synergetics*. 1981, Springer. p. 180-193.
225. Xu, X., Y.L. Sun, and T. Hoey, *Cooperative DNA binding and sequence-selective recognition conferred by the STAT amino-terminal domain*. Science, 1996. **273**(5276): p. 794-7.
226. Shorter, J. and S. Lindquist, *Prions as adaptive conduits of memory and inheritance*. Nat Rev Genet, 2005. **6**(6): p. 435-50.

227. Cohen, J., et al., *Phosphorylation of erythropoietin receptors in the endoplasmic reticulum by pervanadate-mediated inhibition of tyrosine phosphatases*. *Biochem J*, 1997. **327 (Pt 2)**: p. 391-7.
228. Guihard, S., et al., *The MAPK ERK1 is a negative regulator of the adult steady-state splenic erythropoiesis*. *Blood*, 2010. **115(18)**: p. 3686-94.
229. Yu, X., et al., *An erythroid chaperone that facilitates folding of alpha-globin subunits for hemoglobin synthesis*. *J Clin Invest*, 2007. **117(7)**: p. 1856-65.
230. Chen, M.L., et al., *Erythroid dysplasia, megaloblastic anemia, and impaired lymphopoiesis arising from mitochondrial dysfunction*. *Blood*, 2009. **114(19)**: p. 4045-53.
231. Chen, K., et al., *Resolving the distinct stages in erythroid differentiation based on dynamic changes in membrane protein expression during erythropoiesis*. *Proc Natl Acad Sci U S A*, 2009. **106(41)**: p. 17413-8.
232. McGrath, K.E., T.P. Bushnell, and J. Palis, *Multispectral imaging of hematopoietic cells: where flow meets morphology*. *J Immunol Methods*, 2008. **336(2)**: p. 91-7.
233. Borsook, H., et al., *Synthesis of haemoglobin in relation to the maturation of erythroid cells*. *Nature*, 1962. **196**: p. 347-50.
234. Wierenga, A.T., et al., *STAT5-induced self-renewal and impaired myelopoiesis of human hematopoietic stem/progenitor cells involves down-modulation of C/EBPalpha*. *Blood*, 2006. **107(11)**: p. 4326-33.
235. Wierenga, A.T., E. Vellenga, and J.J. Schuringa, *Maximal STAT5-induced proliferation and self-renewal at intermediate STAT5 activity levels*. *Mol Cell Biol*, 2008. **28(21)**: p. 6668-80.
236. Olthof, S.G., et al., *Downregulation of signal transducer and activator of transcription 5 (STAT5) in CD34+ cells promotes megakaryocytic development, whereas activation of STAT5 drives erythropoiesis*. *Stem Cells*, 2008. **26(7)**: p. 1732-42.
237. Yao, Z., et al., *Stat5a/b are essential for normal lymphoid development and differentiation*. *Proc Natl Acad Sci U S A*, 2006. **103(4)**: p. 1000-5.
238. Floyd, Z.E., et al., *Degradation of STAT5 proteins in 3T3-L1 adipocytes is induced by TNF- α and cycloheximide in a manner independent of STAT5A activation*. *Am J Physiol Endocrinol Metab*, 2007. **292(2)**: p. E461-8.
239. Chen, Y., et al., *Proteasome-dependent down-regulation of activated Stat5A in the nucleus*. *Blood*, 2006. **108(2)**: p. 566-74.
240. Dentelli, P., et al., *microRNA-222 controls neovascularization by regulating signal transducer and activator of transcription 5A expression*. *Arterioscler Thromb Vasc Biol*. **30(8)**: p. 1562-8.
241. Bruchova, H., et al., *Regulated expression of microRNAs in normal and polycythemia vera erythropoiesis*. *Exp Hematol*, 2007. **35(11)**: p. 1657-67.
242. Felli, N., et al., *MicroRNAs 221 and 222 inhibit normal erythropoiesis and erythroleukemic cell growth via kit receptor down-modulation*. *Proc Natl Acad Sci U S A*, 2005. **102(50)**: p. 18081-6.

243. Harding, A. and J.F. Hancock, *Ras nanoclusters: combining digital and analog signaling*. Cell Cycle, 2008. **7**(2): p. 127-34.
244. Chakraborty, A.K., et al., *Molecular origin and functional consequences of digital signaling and hysteresis during Ras activation in lymphocytes*. Sci Signal, 2009. **2**(66): p. pt2.
245. Verdier, F., et al., *Proteasomes regulate erythropoietin receptor and signal transducer and activator of transcription 5 (STAT5) activation. Possible involvement of the ubiquitinated Cis protein*. J Biol Chem, 1998. **273**(43): p. 28185-90.
246. Soldaini, E., et al., *DNA binding site selection of dimeric and tetrameric Stat5 proteins reveals a large repertoire of divergent tetrameric Stat5a binding sites*. Mol Cell Biol, 2000. **20**(1): p. 389-401.
247. Lerner, L., et al., *STAT3-dependent enhanceosome assembly and disassembly: synergy with GR for full transcriptional increase of the alpha 2-macroglobulin gene*. Genes Dev, 2003. **17**(20): p. 2564-77.
248. Kim, H.P. and W.J. Leonard, *The basis for TCR-mediated regulation of the IL-2 receptor alpha chain gene: role of widely separated regulatory elements*. EMBO J, 2002. **21**(12): p. 3051-9.
249. Droscher, M., et al., *Cytokine-induced paracrystals prolong the activity of signal transducers and activators of transcription (STAT) and provide a model for the regulation of protein solubility by small ubiquitin-like modifier (SUMO)*. J Biol Chem. **286**(21): p. 18731-46.
250. Wen, Z., Z. Zhong, and J.E. Darnell, Jr., *Maximal activation of transcription by Stat1 and Stat3 requires both tyrosine and serine phosphorylation*. Cell, 1995. **82**(2): p. 241-50.
251. Zhang, X., et al., *Requirement of serine phosphorylation for formation of STAT-promoter complexes*. Science, 1995. **267**(5206): p. 1990-4.
252. Decker, T. and P. Kovarik, *Serine phosphorylation of STATs*. Oncogene, 2000. **19**(21): p. 2628-37.
253. Chen, Y., et al., *Identification of Shp-2 as a Stat5A phosphatase*. J Biol Chem, 2003. **278**(19): p. 16520-7.
254. Wu, T.R., et al., *SHP-2 is a dual-specificity phosphatase involved in Stat1 dephosphorylation at both tyrosine and serine residues in nuclei*. J Biol Chem, 2002. **277**(49): p. 47572-80.
255. Rho, J., et al., *The arginine-1493 residue in QRRGRTGR1493G motif IV of the hepatitis C virus NS3 helicase domain is essential for NS3 protein methylation by the protein arginine methyltransferase 1*. J Virol, 2001. **75**(17): p. 8031-44.
256. Mowen, K.A., et al., *Arginine methylation of STAT1 modulates IFNalpha/beta-induced transcription*. Cell, 2001. **104**(5): p. 731-41.
257. Wang, R., P. Cherukuri, and J. Luo, *Activation of Stat3 sequence-specific DNA binding and transcription by p300/CREB-binding protein-mediated acetylation*. J Biol Chem, 2005. **280**(12): p. 11528-34.

258. Ungureanu, D., et al., *SUMO-1 conjugation selectively modulates STAT1-mediated gene responses*. Blood, 2005. **106**(1): p. 224-6.
259. Liu, B., et al., *Inhibition of Stat1-mediated gene activation by PIAS1*. Proc Natl Acad Sci U S A, 1998. **95**(18): p. 10626-31.
260. Rogers, R.S., C.M. Horvath, and M.J. Matunis, *SUMO modification of STAT1 and its role in PIAS-mediated inhibition of gene activation*. J Biol Chem, 2003. **278**(32): p. 30091-7.
261. Kim, T.K. and T. Maniatis, *Regulation of interferon-gamma-activated STAT1 by the ubiquitin-proteasome pathway*. Science, 1996. **273**(5282): p. 1717-9.
262. Shuai, K., et al., *Constitutive activation of STAT5 by the BCR-ABL oncogene in chronic myelogenous leukemia*. Oncogene, 1996. **13**(2): p. 247-254.
263. Birkenkamp, K.U., et al., *Regulation of constitutive STAT5 phosphorylation in acute myeloid leukemia blasts*. Leukemia, 2001. **15**(12): p. 1923-31.
264. Spiekermann, K., et al., *Overexpression and constitutive activation of FLT3 induces STAT5 activation in primary acute myeloid leukemia blast cells*. Clin Cancer Res, 2003. **9**(6): p. 2140-50.
265. Growney, J.D., et al., *Activation mutations of human c-KIT resistant to imatinib mesylate are sensitive to the tyrosine kinase inhibitor PKC412*. Blood, 2005. **106**(2): p. 721-4.
266. Cain, J.A., et al., *Myeloproliferative disease induced by TEL-PDGFRB displays dynamic range sensitivity to Stat5 gene dosage*. Blood, 2007. **109**(9): p. 3906-14.
267. Hexner, E.O., et al., *Lestaurtinib (CEP701) is a JAK2 inhibitor that suppresses JAK2/STAT5 signaling and the proliferation of primary erythroid cells from patients with myeloproliferative disorders*. Blood, 2008. **111**(12): p. 5663-71.
268. Erslev, A.J. and J. Caro, *Erythropoietin titers in response to anemia or hypoxia*. Blood Cells, 1987. **13**(1-2): p. 207-16.
269. Koury, M.J. and M.C. Bondurant, *The molecular mechanism of erythropoietin action*. Eur. J. Biochem., 1992. **210**: p. 649-663.
270. Koury, M.J. and M.C. Bondurant, *Erythropoietin retards DNA breakdown and prevents programmed death in erythroid progenitor cells*. Science, 1990. **248**: p. 378-381.
271. Peslak, S.A., et al., *Sublethal radiation injury uncovers a functional transition during erythroid maturation*. Exp Hematol. **39**(4): p. 434-45.
272. Wood, A.D., et al., *ID1 promotes expansion and survival of primary erythroid cells and is a target of JAK2V617F-STAT5 signaling*. Blood, 2009. **114**(9): p. 1820-30.
273. Sathyanarayana, P., et al., *EPO receptor circuits for primary erythroblast survival*. Blood, 2008. **111**(11): p. 5390-9.
274. Bouscary, D., et al., *Critical role for PI 3-kinase in the control of erythropoietin-induced erythroid progenitor proliferation*. Blood, 2003. **101**(9): p. 3436-43.
275. Socolovsky, M., et al., *Ineffective erythropoiesis in Stat5a(-/-)5b(-/-) mice due to decreased survival of early erythroblasts*. Blood, 2001. **98**(12): p. 3261-73.

276. Halupa, A., et al., *A novel role for STAT1 in regulating murine erythropoiesis: deletion of STAT1 results in overall reduction of erythroid progenitors and alters their distribution.* Blood, 2005. **105**(2): p. 552-61.
277. Wagner, K.U., et al., *Conditional deletion of the Bcl-x gene from erythroid cells results in hemolytic anemia and profound splenomegaly.* Development, 2000. **127**(22): p. 4949-58.
278. Koulis, M., et al., *Negative autoregulation by fas stabilizes adult erythropoiesis and accelerates its stress response.* PLoS One. **6**(7): p. e21192.
279. Koulis, M., et al., *Identification and analysis of mouse erythroid progenitors using the CD71/Ter119 Flow-cytometric assay.* JoVE, 2011.
280. Silva, C.M., H. Lu, and R.N. Day, *Characterization and cloning of STAT5 from IM-9 cells and its activation by growth hormone.* Mol Endocrinol, 1996. **10**(5): p. 508-18.
281. Gregoli, P.A. and M.C. Bondurant, *The roles of bcl-X and apopain in the control of erythropoiesis by erythropoietin.* Blood, 1997. **90**(2): p. 630-640.
282. Motoyama, N., et al., *bcl-x prevents apoptotic cell death of both primitive and definitive erythrocytes at the end of maturation.* J Exp Med, 1999. **189**(11): p. 1691-8.
283. Schweers, R.L., et al., *NIX is required for programmed mitochondrial clearance during reticulocyte maturation.* Proc Natl Acad Sci U S A, 2007. **104**(49): p. 19500-5.
284. Garcon, L., et al., *Constitutive activation of STAT5 and Bcl-xL overexpression can induce endogenous erythroid colony formation in human primary cells.* Blood, 2006. **108**(5): p. 1551-4.
285. Silva, M., et al., *Expression of Bcl-x in erythroid precursors from patients with polycythemia vera [see comments].* N Engl J Med, 1998. **338**(9): p. 564-71.
286. Green, D.R., *Life, death, BH3 profiles, and the salmon moussé.* Cancer Cell, 2007. **12**(2): p. 97-9.
287. Kuribara, R., et al., *Roles of Bim in apoptosis of normal and Bcr-Abl-expressing hematopoietic progenitors.* Mol Cell Biol, 2004. **24**(14): p. 6172-83.
288. Shinjyo, T., et al., *Downregulation of Bim, a proapoptotic relative of Bcl-2, is a pivotal step in cytokine-initiated survival signaling in murine hematopoietic progenitors.* Mol Cell Biol, 2001. **21**(3): p. 854-64.
289. Abutin, R.M., et al., *Erythropoietin-induced phosphorylation/degradation of BIM contributes to survival of erythroid cells.* Exp Hematol, 2009. **37**(2): p. 151-8.
290. Maeda, T., et al., *LRF is an essential downstream target of GATA1 in erythroid development and regulates BIM-dependent apoptosis.* Dev Cell, 2009. **17**(4): p. 527-40.
291. Pugh, L.G., *Blood Volume and Haemoglobin Concentration at Altitudes above 18,000 Ft. (5500 M).* J Physiol, 1964. **170**: p. 344-54.
292. Schmidt, W., *Effects of intermittent exposure to high altitude on blood volume and erythropoietic activity.* High Alt Med Biol, 2002. **3**(2): p. 167-76.

293. Yang, B., et al., *A mouse model for beta 0-thalassemia*. Proc Natl Acad Sci U S A, 1995. **92**(25): p. 11608-12.
294. Haase, V.H., et al., *Vascular tumors in livers with targeted inactivation of the von Hippel-Lindau tumor suppressor*. Proc Natl Acad Sci U S A, 2001. **98**(4): p. 1583-8.
295. Yi, T.M., et al., *Robust perfect adaptation in bacterial chemotaxis through integral feedback control*. Proc Natl Acad Sci U S A, 2000. **97**(9): p. 4649-53.
296. Kuhara, A., et al., *Negative regulation and gain control of sensory neurons by the C. elegans calcineurin TAX-6*. Neuron, 2002. **33**(5): p. 751-63.
297. Wormald, S. and D.J. Hilton, *Inhibitors of cytokine signal transduction*. J Biol Chem, 2004. **279**(2): p. 821-4.
298. Hsieh, P.P., et al., *The role of Janus Kinase 2 V617F mutation in extramedullary hematopoiesis of the spleen in neoplastic myeloid disorders*. Mod Pathol, 2007. **20**(9): p. 929-35.
299. Diaz, T., et al., *Lestaurtinib inhibition of the Jak/STAT signaling pathway in hodgkin lymphoma inhibits proliferation and induces apoptosis*. PLoS One. **6**(4): p. e18856.
300. Capello, D., et al., *Epigenetic inactivation of suppressors of cytokine signalling in Philadelphia-negative chronic myeloproliferative disorders*. Br J Haematol, 2008. **141**(4): p. 504-11.
301. Fernandez-Mercado, M., et al., *Methylation status of SOCS1 and SOCS3 in BCR-ABL negative and JAK2V617F negative chronic myeloproliferative neoplasms*. Leuk Res, 2008. **32**(10): p. 1638-40.
302. Jelkmann, W., *Molecular biology of erythropoietin*. Intern Med, 2004. **43**(8): p. 649-59.